TECHNISCHE UNIVERSITÄT WIEN

Energy Economics Group

Dissertation

Integrating heat pump flexibility in building stock modeling to support decarbonization through sector coupled energy systems

in fulfilment of the requirements for the degree of
Doktor der technischen Wissenschaften

submitted at the
Energy Economics Group
Faculty of Electrical Engineering and Information Technology
Technische Universität Wien

by

Dipl.-Ing. Philipp Mascherbauer

Supervisor:

Prof. Dr. Reinhard Haas
Technische Universität Wien

Reviewer and Examiner:

Prof. Dr. Martin Patel
Université de Genève

Prof. Dr. Mathias Haase
Züricher Hochschule für Angewandte Wissenschaften

Vienna, September 2025

Contents

Abbreviations

Abbreviation	Full name
AC	Air conditioner
CAPEX	Capital expenditures
COP	Coefficient of performance
DER	Distributed energy resources
DHW	Domestic hot water
DR	Demand response
EU	European Union
EV	Electric vehicle
GSC	Grid support coefficient
HEMS	Home energy management system
HP	Heat pump
HV	High voltage
HVAC	Heating, Ventilation, and Air Conditioning
LV	Low voltage
MFH	Multi family house
MPC	Model predictive control
MV	Medium voltage
O&M	Operation and maintenance
OPEX	Operational expenditures
OLTC	On-load tap-changing
PV	Photovoltaic
RNM	Reference Network Model
SFH	Single family house

Abstract

In a future decarbonized energy system, demand side flexibility will be crucial for maintaining electricity grid stability. Heat pumps will play a key role in decarbonizing the heating sector, and they can also offer an opportunity to shift electrical demand for short periods of time, even without any storage installations. This thesis investigates what the future potential of the residential building stock in the EU Member States is, to contribute to the future short-term demand side flexibility needs. To achieve this, heat pump flexibility is integrated into building stock modeling. Particularly, an optimization model was developed to be applied on the results of an existing building stock model. The model optimizes the demand-side flexibility of prosumagers—households that both produce and consume electricity, by minimizing their electricity costs considering hourly price signals. The model was validated by comparing it with a building simulation tool and via different optimization techniques. Following the validation, the model was applied to analyze demand response potential at the EU level for each Member State, providing insights into how national characteristics influence the overall flexibility contribution from residential buildings.

This dissertation is structured around five peer-reviewed publications addressing the following topics: 1) the potential for shifting electricity demand using thermal mass, 2) the influence of different hourly electricity price signals on demand side flexibility, and 3) the impact of prosumagers on electricity distribution grids in future scenarios.

Findings suggest that the thermal mass can significantly increase demand shifting abilities with at least one third of all demand shifted by prosumagers attributed to the thermal mass. The electricity price signal is highlighted as a driver for demand-side response, showing that rising electricity price volatility can double the amount of energy prosumagers would shift under a cost-minimization rationale. Results underscore the importance of appropriate price signals and reducing peak demand to limit additional stress on the electricity distribution grid. Together, the five papers provide a comprehensive overview of future demand flexibility potential within the residential building stock, highlighting key drivers, possible contributions to short-term flexibility, and challenges for electricity grids.

A need for future work is pointed out in regards to data availability for buildings at a spatially disaggregated level within the EU. Further, taking the flexibility at the distribution electricity grid level into account will be crucial for planning the future electricity system.

1 Introduction

1.1 Motivation

The building stock accounts for 36% of greenhouse gas emissions and 40% of energy consumption in the European Union (EU) (European Parliament 2024). One promising solution to reduce the carbon footprint of the building stock is by replacing fossil fueled boilers to electrified heating systems, especially heat pumps (HPs) (Bloess et al. 2018). Studies suggest that HPs will play an important role in a decarbonized building stock (Gaur et al. 2021) alongside district heating (Fallahnejad 2024) and, in some cases, biomass boilers. HPs are a cost-efficient technology for low-temperature heat generation, although they still face barriers when it comes to their implementation such as high investment costs (Y. Wang et al. 2022) compared to conventional boilers, aesthetics, noise, and the belief that they are inefficient (Cozza et al. 2022). The uptake of electrified heating systems is not only viewed as a challenge in its implementation from a social and policy perspective but also from a technical viewpoint regarding additional required electricity grid capacities. Together with the uptake of renewable generation, HPs bring both a new challenge for the electricity grid and also an opportunity to increase demand-side flexibility. To reduce possible grid stress and congestion, additional flexibility will be needed in the future (Gaur et al. 2021). The residential building stock could offer short-term flexibility through demand response (DR). Especially DR using the thermal mass of buildings seems promising as no additional investments are needed to use this potential. DR of HPs in single buildings has been studied extensively, and the general consensus is that HPs can provide flexibility without violating indoor comfort constraints.

Studies consistently evaluate the flexibility options for a future decarbonized electricity system (Khalili et al. 2025; Suna et al. 2022). These flexibility options can be distinguished based on the timescales over which they are provided. Time periods range from sub- and hourly fluctuations per day to daily, weekly and monthly fluctuations. Based on the ACER (2023) report, the daily flexibility need will more than double from 2021 to 2030, to a total of 362 TWh within the EU Member States (Figure 1.1). HPs in the residential building stock could contribute to achieving this flexibility need by shifting heating, cooling and hot water demand.

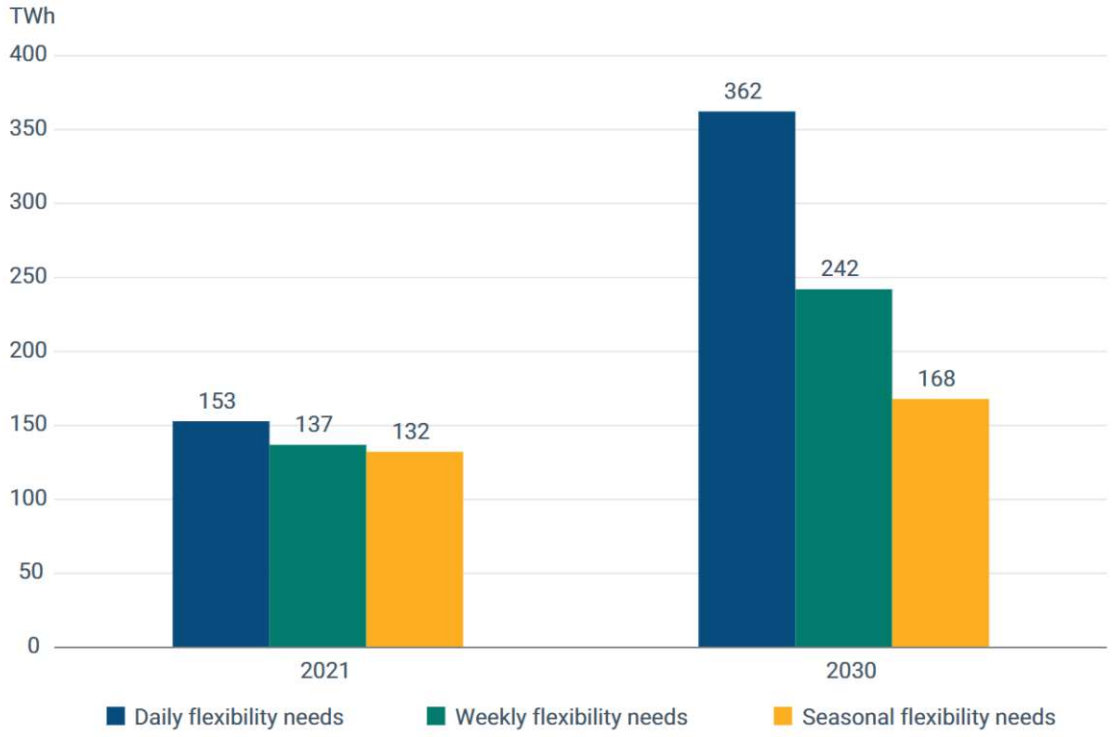

Figure 1.1: Daily, weekly and seasonal flexibility needs in Europe (ACER 2023).

One way to incentivize buildings with HP to shift loads is through a price signal (Romero Rodríguez et al. 2018). Changing price signals can be implemented through time-of-use tariffs or real-time prices, which then can further differ in their implementation (Paterakis et al. 2017). The operation of the HP can be optimized based on a variable retail electricity price either by an in-house home energy management system (HEMS) or a remote aggregator. The advantages of a remote aggregator are that the aggregator has information on the total system status and can control the DR of single consumers to achieve system-optimal operation. On the other hand, aggregation of multiple HPs requires advanced control strategies and can face barriers such as user acceptance. The implementation of HEMS is less complicated and allows individuals to decide how they want to participate in DR. This thesis focuses on in-house operations using a HEMS, implying that homeowners provide flexibility for their own benefit. Households with HEMS that consume, produce, and manage their own electricity will be referred to as prosumagers in this thesis. Prosumagers try to minimize their energy operation costs by adapting their consumption based on a price signal. The possibility of prosumagers to achieve energy cost reduction has been widely studied in the literature (e.g. Stute et al. (2024a)). This thesis relies on the following assumption: in prosumager households heating and cooling of the indoor environment together with storage operation, if available, is controlled automatically. DR with other controllable loads where human interaction would be needed, such as washing machines, are not considered in this thesis.

1.2 Research questions

While extensive research has quantified the potential of individual buildings equipped with HPs to shift electricity demand, there remains a research gap concerning aggregated potentials at larger scales, such as at the national or at EU level. This higher-level perspective is critical for informing strategic planning and grid management policies, especially considering the ongoing electrification of heating systems and the expansion of renewables. The following hypothesis will be evaluated further in this thesis: HPs will provide a relevant

contribution to short-term flexibility in the future and relieve the electricity grid as long as the electricity price sends the right signals. Specifically, this thesis presents a methodology to determine the flexibility potential of prosumagers in different countries. It is shown to what extent residential buildings, particularly those equipped with HPs, can effectively shift electricity load at large scales (national and EU level), and how factors such as the utilization of thermal mass and electricity price signals shape this potential. Additionally, it is discussed under which conditions prosumagers on a large scale are beneficial for the electricity system. In doing so, three main research questions are answered. The questions are answered by peer-reviewed articles published by the author as the first author. These three questions, alongside a short explanation, are presented in the following.

Research question 1: *How much electricity load can the residential building stock shift and what role can the thermal mass play in this potential?*

The core of this thesis is to model the upscale of the possible impact of prosumagers to building stock level to estimate how large the actual potential of the residential building stock could be to shift electric loads. The thermal mass is specifically focused on as it is available in each and every building as potential short-term storage. In Mascherbauer et al. (2024) the potential of the thermal mass is highlighted by a comparison of single buildings shifting loads with and without any additional storage. In both publications (Mascherbauer et al. 2022; Mascherbauer et al. 2024) the potential of the Austrian SFH building stock is assessed under different scenarios and with a different focus. Mascherbauer et al. (2022) focuses on the change in prosumagers electricity consumption with different appliances and ultimately estimates the impact of prosumagers on the electricity grid demand and photovoltaic (PV) self-consumption. In Mascherbauer et al. (2024) different price signals are analyzed, which serve as the main incentive for prosumagers to shift their electricity demand. Finally, Mascherbauer et al. (2025b) and Mascherbauer et al. (forthcoming) show the shifting potential on a EU level.

Research question 2: *How does the electricity price impact the potential to shift demand by prosumagers?*

Since prosumagers shift their demand based on an hourly price profile, the potential of every prosumager to shift demand is determined by the retail electricity price to some extent. Mascherbauer et al. (2024) investigates how different price profiles change the total shifted electricity demand of prosumagers at the Austrian building stock level, while Mascherbauer et al. (2025b) discusses how fixed grid tariffs can affect load shifting potentials on the EU level. The electricity price signal also determines how large potential cost savings are for prosumagers, which is one of the core questions answered in Mascherbauer et al. (2024).

The third research question shifts the focus away from the national building stock level to the local level and is answered in Mascherbauer et al. (2025a).

Research question 3: *How will the uptake of prosumagers impact future electricity distribution grid investments?*

While the previous research questions focused solely on the prosumagers themselves and their electricity demand, Mascherbauer et al. (2025a) connects the prosumagers with a detailed electricity distribution grid analysis. This analysis shows how much grid stress can be reduced by prosumagers at the local level and also connects electric vehicles (EVs) to future prosumaging buildings. Similar to HPs, EVs will play an increasingly important role in providing short-term flexibility. As EV penetration increases, their batteries rep-

resent a significant and growing source of flexible demand and potential storage capacity. By shifting charging times in response to price signals, or even discharging energy back to the grid (vehicle-to-grid), EVs can help balance supply and demand. This thesis shows how incentivizing EV charging through price signals could affect the distribution networks reinforcement needs.

In summary answering these three research questions will support or refute the hypothesis that HPs can provide a relevant contribution to short-term flexibility in the future and relieve the electricity grid as long as the retail electricity price sends the right signals. Figure 1.2 summarizes these three research questions and shows on which level of aggregation they are answered. As the approach taken in this thesis is a bottom up approach, economic benefits of prosumaging and DR actions on single building level are up-scaled to building stock level. The first and second research question are strongly interlinked through the electricity price signal. The third research question is linked to the other two through the change in electric load when DR is invoked.

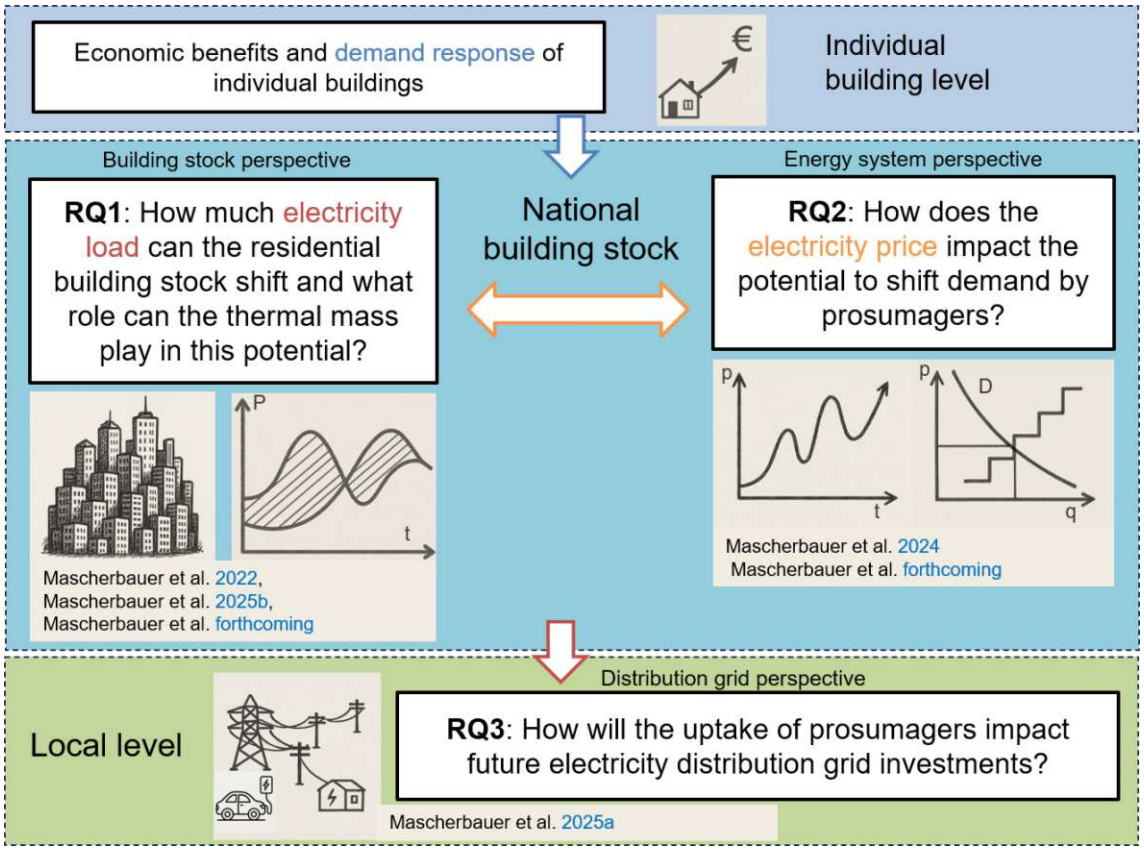

Figure 1.2: Graphic illustration of the research questions

The three research questions posed in this thesis are answered on different levels of spatial aggregation and are subject to four publications (one is still under review) and one peer reviewed conference paper. Table 1.1 provides an overview on which spatial level of aggregation the research questions answered in the different publications. The used technologies on building level are also provided, highlighting that EVs are only considered in the study on local level while the second research question was investigated focusing specifically on the potential of the thermal mass compared to also using thermal storage such as domestic hot water (DHW) and buffer tanks.

Table 1.1: Overview of the relation of each publication to the research questions, spatial level of aggregation and the technologies considered.

	Spatial level	Technologies	Paper
RQ1	EU27 Member State level and AUT	thermal mass, HP, heating and DHW tanks, battery, PV, air conditioner	Mascherbauer et al. (2022), "Investigating the impact of smart energy management system on the residential electricity consumption in Austria", https://doi.org/10.1016/j.energy.2022.123665 Mascherbauer et al. (2025b), "The Flexibility of Electrical Loads in the EU-27 Residential Building Stock", https://doi.org/10.1109/eem64765.2025.11050330 Mascherbauer et al. (forthcoming), "Future flexibility of the EU27 heat pump heated residential building stock", submitted to Energy - under review
RQ2	AUT	thermal mass, HP, heating and DHW tanks	Mascherbauer et al. (2024), "Impact of variable electricity price on heat pump operated buildings", https://doi.org/10.12688/openreseurope.15268.2
RQ3	Local (10 km2)	thermal mass, HP, thermal and DHW tanks, battery, PV, EVs, air conditioner	Mascherbauer et al. (2025a), "Analyzing the impact of heating electrification and prosumaging on the future distribution grid costs", https://doi.org/10.1016/j.apenergy.2025.125563

1.3 Structure of the thesis

The remainder of this thesis is structured as follows: First, the state of the art and the research gaps addressed by the author's publications are presented in Chapter 2. Chapter 3 describes the method used in this analysis. In Chapter 4, the results of the five publications are presented, followed by a discussion in Chapter 5 where the research questions are addressed directly. Finally, the conclusion is presented in Chapter 6, and the need for further research is identified.

2 State of the art and progress beyond

In this chapter, relevant literature regarding DR in buildings with HP is presented. The review is structured according to different aspects of DR in residential buildings. Section 2.1 gives a short overview of work that focuses on the optimization of single buildings. Section 2.1.2 focuses on papers that investigate the significance of the thermal mass to shift electricity demand in buildings, while Section 2.1.3 shows how the peak demand of buildings performing DR changes. In Section 2.1.4, the literature on the importance and effectiveness of the electricity price as an incentive to change DR behavior is reviewed. Next, Section 2.2 discusses how the term flexibility is used in the literature, Section 2.3 explains the connection between DR and electricity grid costs, and Section 2.4 reviews simulation methods for buildings. Finally, Section 2.5 explains how this thesis contributes to the current state of the art.

2.1 Demand response in residential buildings

2.1.1 Optimization of single residential buildings

Optimization models for household energy consumption have been developed for different research focuses, for example, the self-consumption rate of PV plus battery system (Klingler 2018), optimal size for PV and battery adoption (Kandler 2017), the impact of demand-side management measures on load shifting of households (Masy et al. 2015), among others. Correspondingly, the studies cover different energy demands and technologies and may even have different objective functions. To evaluate the diffusion of a PV plus battery system, Klingler (2018) developed an optimization model to maximize the self-consumption rate of PV generation based on the flexibility of an electric vehicle and an HP. The behavior of the households is represented by profiles of electricity consumption, EV charging hours, and heating demand. In this way, the study evaluated the market potential of PV plus battery systems in Germany. Usually, these studies aim to minimize overall costs. Angenendt et al. (2019) optimized a single-family house (SFH) to minimize the household's energy cost and to find the optimal system configuration with a two-stage optimization approach. They included thermal and battery storage, PV, and the respective investment costs. On the other hand, Kandler (2017) analyzed the optimal PV panel and battery size based on an optimization model that minimizes households' energy costs. The studies mentioned above include an optimization of the operation to analyze the costs focusing on sizing and selecting the optimal equipment for minimal cost. The following studies will focus more on the heating and cooling operation of single buildings and the potential to shift energy using the thermal mass.

2.1.2 Thermal mass for load shifting

DR in residential buildings has a high potential to shift electricity loads when heating systems are electrified. Multiple publications consider the thermal mass to have great potential in DR programs (Reynders et al. 2013; Lind et al. 2023; Le Dréau et al. 2016a; Golmohamadi 2021a; Sperber et al. 2020b), mainly because the investment costs are very low compared to any other storage technology (Zhang et al. 2021). Shakeri et al. (2020)

provide an overview of the current literature on DR management systems for single buildings. They emphasize that storage devices significantly affect the possibility of load shifting. Several of those studies also suggest that the potential of using thermal mass for load shifting is significant, and the interaction between the heating system and the thermal mass is an important factor (Wolisz et al. 2013; Reynders et al. 2013). In this regard, Wolisz et al. (2013) simulates a building made out of brick and shows that even without insulation, the heating demand after a pre-heating event of two hours can be reduced by 20% in the following hours. Floor heating systems and direct thermal activation are more effective in shifting loads using the thermal inertia than radiator systems. However, with the proper control strategy, HP peak loads can still be significantly reduced with a radiator heating system (Reynders et al. 2013). Masy et al. (2015) found that 3% to 14% of the load can be shifted by using the building's thermal mass with a well-insulated building. Their findings rely on a detailed simulation for a single building. Other studies indicate that electricity load can be effectively shifted by heating concrete slabs electrically (Olsthoorn et al. 2019). Their findings show that this approach is viable for shifting both morning and evening peaks in homes ranging from 80 m^2 to 200 m^2, with a slab thickness of 15 cm, in the Canadian building stock. J. Luo et al. (2020) extended this work by optimizing the parameters for electric heating in concrete slabs with respect to shifting potential, thermal comfort, and costs. They discovered that the thickness of insulation had the the greatest impact on achievable load shifting without compromising comfort. In fact, key constraints for using thermal mass are not the thermal mass itself, but rather the insulation and heat distribution system. Le Dréau et al. (2016b) modeled two different residential buildings and examined their potential for heat storage and heat conservation. The findings showed that the potential of thermal mass as heat storage depends on multiple factors. Again, the insulation is one of those factors, but the heat distribution system and seasonality also play important roles. On the other hand, the thermal mass also has a significant impact on the cooling needs. Kuczyński et al. (2020) conducted a case study comparing two nearly identical buildings, differing only in their external and internal walls. The results showed that the cooling demand for the building with concrete walls was reduced by 75% at a set temperature of 26°C, compared to the lightweight structure house. Using the building mass as thermal storage for load shifting can serve purposes such as reducing peak load, shifting demand to low-price hours, and improving system stability. One key incentive is to shift heating or cooling demand to off-peak hours, thereby reducing peak loads from a system perspective.

2.1.3 Peak load reduction through prosumagers

Using the thermal mass of buildings with electrified heating systems as short-term energy storage could lower peak demand at the system level (Heinen et al. 2017; Dong et al. 2023). Weiß et al. (2019a) focus on the peak shaving potential in the Austrian building stock through thermal inertia. They conclude that 50% of the heating peak loads could be shifted to off-peak hours for buildings built after 1980 by turning off the heating system until the indoor temperature is reduced from 22°C to 19°C in a typical winter week. Heinen et al. (2017) investigate how the utilization of thermal mass as storage can reduce the total system costs of residential heat electrification in Ireland. The researchers found that households with electrified heating systems could reduce their heating costs to be competitive with gas boilers by utilizing the thermal inertia of their building as a flexibility option. The profitability and the amount of stored energy depend primarily on the thermal insulation of the building. While a greater thermal capacity indicates a higher storage potential, a maximum exists where more thermal mass does not result in further storage potential as the heat transfer rate is too low (Chen et al. 2020). In Hedegaard et al. (2013), the operation of the HP installed in an individual household is optimized, along with the investment in heat storage. The model includes time-varying electricity prices and

illustrates the flexible operation of the HP combined with the use of thermal storage for load shifting. Several single-family households are considered to analyze the impact at the energy system level regarding the modification of the electricity load curve through peak load shaving. They conclude that, regardless of the heat storage options, the maximum HP capacity limits the flexibility potential on the peak day of the year, as HPs have to run on full power to cover the needed heat demand on cold days. In Dong et al. (2023), on the other hand, a control strategy is proposed to coordinate space heating across numerous residential buildings to reduce overall peak loads. Peak demand is reduced by 28% and costs by 14%. In C. Wang et al. (2024), the electricity costs can also be reduced by 14% and peak demand by 31% through DR. They did so by developing a predictive control model, optimizing the operation of the heating system without any thermal or electrical storage within the building except the building mass itself. Campillo et al. (2012) investigate the electricity consumption of households with ground-source HPs, and state that demand-side management and variable electricity tariffs will become a necessity to manage peak loads in the future. At the same time, Baeten et al. (2017) find that peak demand of 500 000 HP-heated dwellings in Belgium can be reduced by 11% using a multi-objective model predictive control strategy. They assess the impact of the size of space heating tanks on consumer costs and generation capacity. The reduction in peak demand comes with an increase in cost for the consumers. Lastly, Pena-Bello et al. (2021) analyze the impact of SFHs having PV, HPs, and storage installed on the grid. Their results show that retrofitting buildings with HPs can reduce the peak load of single buildings by up to 50%. Additionally, they found that capacity-based tariffs can reduce grid stress without having a negative influence on the cost savings for the prosumagers by reducing the peak load.

2.1.4 Effectiveness of electricity prices as incentive

The economic benefits of HP-heated buildings under variable price schemes are frequently discussed in the literature. Stute et al. (2024a) suggest that dynamic electricity price tariffs can significantly lower energy costs for end consumers, particularly when combined with an HP and an EV. They examine three different price signals, each with varying hourly price spreads. In the case of a high price spread (10.7 €/MWh standard deviation), 62% of the buildings studied benefit from investing in a HEMS. Conversely, Wilczynski et al. (2023) investigate the effectiveness of price-varying tariffs to shift heat consumption, but their results show that cost savings for efficient buildings are limited. They compare a time-of-use tariff with two dynamic tariffs. The first dynamic tariff is based on the spot price plus additional fixed charges, while the second one is a so-called HP dynamic price, defined in Rinaldi et al. (2021). In this case, the dynamic time-of-use tariff resulted in the lowest cost savings among the investigated tariff designs. Similarly, Sridhar et al. (2024) investigate five different buildings and three different electricity tariffs using HEMS in Finland. They report that a real-time price is more effective than a time-of-use tariff as an incentive to shift load. Additionally, well-insulated buildings achieved the highest cost savings. A similar result is found by Fitzpatrick et al. (2020) who compare three different electricity tariffs for DR in a single building. They observe that the building provides the highest flexibility when using a real-time price. Other pricing schemes evaluated include a two-level day/night tariff and critical peak pricing with three distinct price levels depending on the time of day. Østergaard et al. (2021) explore how electricity taxes influence the incentive to increase HP power and thermal energy storage. They also analyze the motivation for aligning HP operation with the dynamic needs of the electricity system in a district heating setup. Hourly variable taxes lead to a 20% increase in thermal energy storage in buildings, though they do not impact the HP capacity. Different electricity pricing schemes are not examined in their study. Bechtel et al. (2020) also consider the role of energy storage. They assess the impact of varying buffer heat storage sizes and HP power on the cost savings in HP-operated buildings under a variable price signal. Their findings

show that increasing the storage capacity significantly reduces the number of HP start-ups. With a 1500 L buffer storage in an SFH, operational costs can be reduced by up to 20%. However, taking into account the extra investment costs for a larger storage, a 200 L buffer tank is preferred. This study uses historical electricity prices from the German-Luxembourg market (EPEX Spot) and does not analyze different pricing schemes. Other studies compare real-time pricing with direct load control. Patteeuw et al. (2016) found that real-time pricing is less effective than direct load control in terms of CO_2 reductions and cost savings, particularly when residential HP penetration is high. They evaluate the potential of load shifting in highly energy-efficient HP buildings, considering two types of load shifting controls: 1) direct load control, where the HP load is managed by a third party, and 2) real-time pricing. Their analysis explores how load shifting with residential HPs can lower CO_2 emissions and identifies the most effective incentive to encourage homeowners to engage in load shifting.

In this thesis, real-time pricing is chosen from various variable electricity price mechanisms (such as critical peak pricing, day/night tariffs, or real-time pricing) for two main reasons: First, real-time pricing schemes for residential consumers are already in place and second, it provides a simple and effective way to encourage residents to shift their demand. Real-time pricing has been shown to outperform other pricing schemes in terms of effectiveness (Fitzpatrick et al. 2020; Katz et al. 2016). At the same time, direct control has been identified as a possible barrier to user acceptance (Klein et al. 2017). Additionally, Celik et al. (2017) highlight several issues that need to be addressed to effectively coordinate multiple smart homes (e.g., sociological aspects, network issues, delay in communication, accuracy of forecasts). Lastly, Y. Wang et al. (2022) states that the easiest way for end consumers to offer DR is through variable pricing schemes due to the high barriers (e.g., ramping rates, power capacity, response duration) for participating in electricity markets.

Other studies suggest that load shifting through variable electricity tariffs can lead to an overall increase in electricity demand (Miara et al. 2014; Nicolas Kelly et al. 2014). Miara et al. (2014) note that HP systems, when combined with buffer storage, offer promising DR potential. However, due to heat losses and the higher operating temperatures required for charging the buffer tank, electricity consumption rises by 20% when DR is fully utilized. Nicolas Kelly et al. (2014) attempt to shift all heating loads from peak to off-peak periods in a typical detached house in the UK. While a 1000 L hot water storage is sufficient to do so, the total electricity demand increases by 60%, and the charging peak demand for the tank is 50% higher than the average house demand during peak periods.

2.1.5 Prosumagers on building stock level

While there was a lot of research done on the load-shifting potential on a single building level, only a few focused on aggregating this potential to a district or even a country level. Sperber et al. (2020a) find that the maximum shiftable load in the German residential building stock is 57 GW_{el} by increasing the indoor temperature by 2°C. And Sperber et al. (2025) show that large-scale DR triggered by a single electricity price signal can lead to an "avalanche effect" at the country level. A so-called avalanche effect refers to an event that occurs if the simultaneous DR actions of many buildings create new peaks in electricity demand or prices. Large-scale DR could significantly impact the electricity market, an impact that is not captured by most existing studies. To address this issue, an iterative process is applied in which the flexibility provided by the HPs is fed back to the electricity market model, which in turn updates the day-ahead electricity price. The aim is to avoid any avalanche effects in the original demand and price data. Their results show that the DR of buildings by a unified price incentive (day-ahead price from 2019) does not reduce the peaks in the residual load. The two studies above look at the effect of prosumagers on

the system when incentivized by a single price profile. Conversely, the following studies look at prosumagers from a system perspective and identify how they could reduce overall system cost. Rieck et al. (2025) investigate how much the electricity consumption of the residential German building stock could be reduced by using HPs and the full PV roof potential, HEMS, and storage. Electricity demand for space heating could be reduced by 35% overall with SFHs reaching a self-sufficiency rate of up to 90%. The self-sufficiency rate decreases strongly with higher floor areas, as the rooftop area is smaller compared to the total floor area. While this study shows how much electricity grid demand could be reduced, Hoseinpoori et al. (2022) investigate how much more capacity the grid would need under different electrification strategies for hot water and space heating in buildings. They found that with a full electrification of all heating systems, the grid would need a 160% increase in capacity to cover the demand. However, through prosumagers with air source HPs and a thermal storage of 200 l per person, the peak demand could be reduced by around 20%. This result was achieved by implementing the DR of HPs into a system optimization, minimizing total system cost rather than single household cost. They also find that air-source HPs, together with thermal tanks, have a higher system value than ground-sourced HPs. Nick Kelly et al. (2021) assess the ability of the UK building stock to drop and pick up a load on short notice. They found that, on average, around 2 GW of load could be dropped while 4.7 GW additional load could be picked up. The numbers vary strongly based on the weather conditions. In their study, they used a randomly generated control signal to increase or decrease demand for up to 4 hours. Rinaldi et al. (2021) look at the optimal investment of residential rooftop PV and batteries and different renovation and HP adoption scenarios from a power sector perspective in Switzerland. They show that with a higher HP adoption, the adoption of PV will also go up due to the higher self-consumption rate. At the same time, retrofitting buildings that use HPs is important. Otherwise, the need for an increase in battery storage arises from a system perspective.

2.2 Definition and usage of the term "flexibility"

The term "flexibility" is defined and expressed in many different ways in the literature, some of which are compared in Hall et al. (2021). Yue et al. (2024) provide a comprehensive overview of building-related flexibility indicators and distinguish them into key performance indicators describing the interaction with the grid and the independence of a building. Reynders et al. (2017) define flexibility as the available capacity for active DR over a fixed time period. A similar definition of flexibility is used by Kathirgamanathan et al. (2020), but instead of using thermal power, they use electrical power. While this method is useful in lab settings but difficult to implement in transient simulations/optimizations, because DR event timing (charge/discharge windows) is ambiguous, since a discharging cycle could be interrupted by a new charging cycle at any given time. Klein et al. (2016) introduced a so-called grid support coefficient (GSC). They analyzed Germany using day-ahead prices, residual load, non-renewable cumulative energy use, and the share of variable renewables, illustrating their approach on a single building. They analyze the impact of all HPs in 2023 and 2030 on the residual load if they are operated 'grid-friendly'. Their results show that the residual peak loads are affected in a limited way. Le Dréau et al. (2016a) introduced a Flexibility Factor for the heating demand based on the hourly electricity price. They compare the amount of electricity consumed in the first and fourth price quartiles. Both the Flexibility Factor of Le Dréau et al. (2016a) and the GSC of Klein et al. (2016) have the advantage that they can be calculated based on a single load profile and a price profile. This way, any load and its corresponding price profile can be analyzed in terms of flexibility. In this thesis, both factors will be used, and their definition is provided in Section 3.2.

2.3 Demand response and electricity grid cost development

The studies already mentioned in this chapter indicate that load shifting and flexible operation of buildings with HPs can yield economic benefits for the individual end user. However, only a small share of studies investigating thermal mass as storage focus at the neighborhood or district level Lind et al. (2023). This raises the issue of how the distribution grid would be affected if numerous households in close proximity began shifting their load.

The following studies partly address the issue. Based on a load flow analysis in low voltage grids Stute et al. (2024b) investigate how dynamic grid tariffs impact grid reinforcement requirements in Germany. They map synthetic household load profiles to grid connection points to reflect load-shifting behavior. They find that a tariff with a capacity subscription component is most effective at minimizing grid reinforcement requirements as it effectively reduces peak demand. In McGarry et al. (2023), estimate impacts on secondary transformers in Scotland's distribution networks, using spatially linked socio-economic data to reflect electrification. This approach allows for obtaining cost estimates at a national level and also reduces the risk of misallocation of planning resources for grid reinforcements.

Probabilistic power flow assessments are widely used to evaluate the effects of increasing adoption of distributed energy resources (DERs) on distribution systems, including EVs and HPs (Hartvigsson et al. 2022; Navarro-Espinosa et al. 2014). Furthermore, various studies have examined the joint deployment of EVs with solar photovoltaics (PV) (Silva et al. 2022), as well as the integration of HPs with PV systems (Protopapadaki et al. 2017), and even full residential electrification retrofits that combine EVs, HPs, PV, and HEMS (Earle et al. 2023). Commonly used metrics in these probabilistic power flow analyses include the likelihood of exceeding grid operational limits, along with the frequency and intensity of violations related to both voltage and thermal constraints (Navarro-Espinosa et al. 2016). However, a notable limitation of these studies is that they do not account for the necessary grid reinforcements in scenarios with higher levels of electrification.

In fact, relatively few authors have estimated the cost of the network reinforcements required in future residential electrification scenarios. In Gupta et al. (2021), the required grid investments resulting from the uptake of EVs, HPs, and PV in 2035 and 2050 are analyzed for a representative case study encompassing 170 000 Swiss households. Their results show that PV has the highest impact on grid investments, and rural areas have higher investment needs than urban ones. The costs of distribution circuit and transformer upgrades for residential electric heating and EV charging in 2030, 2040, and 2050 for California have been estimated by Elmallah et al. (2022). Although the methodology employed in Elmallah et al. (2022) forecasts hourly profiles for EVs and HPs, it does not consider the response of prosumagers to price signals that incentivize them to shift their demand to off-peak hours (e.g., time-of-use tariffs).

2.4 Modeling methods for energy demand in buildings

There are three common kinds of models used to calculate the energy demand of buildings:

- First, there is software (e.g., TRNSYS, EnergyPlus) that calculates the heating and cooling demand of a building in detail and dynamically, e.g. at hourly resolution with the ability to distinguish between different thermal zones within a building. They

capture the transient thermodynamic behavior of building elements and model the effect of different heating distribution systems. Although software like EnergyPlus is based on physical principles and is open source, it functions as a compiled simulation engine without direct access to symbolic model equations. It solves highly nonlinear and coupled thermodynamic equations, involving time-dependent boundary conditions, radiative heat transfer, and system control logic. This complexity, along with the absence of gradient information and the long simulation runtimes, makes it very challenging to integrate such models into optimization frameworks. Therefore, while these tools offer high physical accuracy, their structure and computational cost limit their usage for optimization purposes.

- Second are simplified models where buildings are represented by resistances and capacities, referred to as "RC models". RC models are widely used in literature. Their simplicity and lower amount of needed building information make them more versatile in their application. RC models can be fitted to measured or simulated data from sophisticated software to achieve a similar but much less computationally expensive model of a building (Sperber et al. 2020b). They are also used in norms like the VDI 6007-1, DIN ISO 13790, and EN ISO 52016. Due to their simplicity, they can be easily implemented in optimization frameworks; this is the approach used in this thesis.

- Another strand of literature deals with neural networks, specifically physics-informed neural networks, to calculate the energy demand of buildings. The aim of these models is mainly to predict energy consumption to enable optimal control actions (Gokhale et al. 2022). Buildings can also be modeled using conventional neural networks (Lu et al. 2022). However, the amount of training data needed for physics-informed neural networks is lower, which makes them easier to apply in real-world controllers (Gokhale et al. 2022). Control mechanisms are not the focus of this thesis, and therefore, neural networks are not further considered in this thesis.

Specifically, the 5R1C approach described in DIN ISO 13790 is used to calculate the energy demand of a building in this work. A building is represented by five resistances and one capacity. The norm offers two basic procedures: (1) quasi-steady-state approach, which calculates the thermal loads of a building over a month; (2) simplified hourly approach, which calculates the heating and cooling demand at hourly resolution. Corrado et al. (2007) found that the quasi-steady approach is unreliable because it takes the mean outdoor temperature and a steady indoor temperature as input, then continuously calculates the operation of heating and cooling technologies. Bruno et al. (2016a) compared the simplified hourly approach to the results from TRNSYS. The heating demand calculated by the 5R1C model is similar to TRNSYS for single-family compact buildings, but not for large buildings and buildings with low thermal inertia. The cooling load shows significant variation for smaller buildings, but its accuracy improves for larger buildings. Kotzur (2018) indicates that the 5R1C approach delivers satisfactory results for heating on an hourly basis, but tends to overestimate cooling demand. This overestimation is partly due to the neglect of household behavior, as shading systems are typically closed during summer when solar irradiance is at its peak. Müller (2014) also tested the DIN ISO 13790 against the results from EnergyPlus and INVERT/EE-lab. Again, the results show that the hourly model overestimates cooling energy needs, especially in Mediterranean climates, but the energy needs for heating are in accordance. The comparison is made on a monthly basis, where the energy needs of the hourly calculations are added up. At last, Sperber et al. (2020a) compared a group of RC models, namely 1R1C, 2R2C, 3R2C, 4R3C, and 5R3C with the results from TRNSYS. Their findings show that adding a second capacity improved modeling significantly, especially for buildings that use low-temperature floor heating instead of radiators. However, they did not test the 5R1C approach described in DIN ISO 13790. The DIN ISO 13790 was replaced by the ISO 52016 in 2017, where the

number of resistances and capacities depends on the building geometry and features.

This thesis employs the previous standard (DIN ISO 13790) to model heating and cooling demand. Implementing the EN ISO 52016 standard would involve greater computational effort, particularly if the optimization needs to be integrated with other technologies. Additionally, the information needed for all building elements is not available as an output of the building stock model on which this work builds.

2.5 Novelties and advances beyond the state of the art

Based on the research questions posed earlier and on the literature presented, this thesis contributes to existing literature in the following areas.

Concerning the first research question, the novelty addressed by the author is the analysis of flexibility at an aggregated level. While some literature has investigated the DR potential of HPs on a large scale, these studies mostly assume the simultaneous control of all HPs by an aggregator or that they react simultaneously to a signal that specifies whether load should increase or decrease. In this thesis, prosumagers act in their own interest, incentivized by the hourly electricity price signal under a HEMS minimizing electricity cost. Furthermore, the model can be used for different future building stock scenarios at the national level. This way, the potential of the residential building stock to shift electricity usage using variable prices as an incentive can be analyzed under various scenarios, including the uptake of different storage technologies, PV, and different pricing schemes.

Regarding the second research question, the contribution to the literature lies in the analysis of different properties of the electricity price signal and how these affect the load shifting capabilities of HP-heated buildings. While studies have conducted research on different electricity price schemes to remunerate DR actions of HPs, they mostly compared different pricing schemes. In this thesis, a closer look is taken at the increase in peak pricing by increasing the CO_2 price, an increase in grid fees, and a change in the frequency of price changes. This enables recommendations on hourly price-signal design and their system-level impacts with widespread prosumager participation.

Concerning the third research question, the third publication (Mascherbauer et al. 2025a) addresses how prosumagers can affect the long-term planning of electricity distribution grids. Authorities nowadays are struggling with grid congestion, and the problem will increase when electric HPs and EVs are deployed more widely. Only a few studies examine the consequences for local electricity grids, although it might be an important barrier to a further transition to a decarbonized building stock. In this way, new insights are provided for potential grid-related costs that occur when heating systems are electrified, EVs and PVs are adopted, and households start actively shifting their electricity demand.

3 Method

Within this thesis, a simulation and optimization model was developed, named the FLEX model. This model calculates the differences in hourly energy consumption of buildings that are trying to minimize their energy costs by an automated control of the electrified heating system (optimization) and buildings that don't do that and satisfy their energy demand independent of the hourly price (simulation). The model was used in Mascherbauer et al. (2022), Mascherbauer et al. (2024), Mascherbauer et al. (2025a), and Mascherbauer et al. (2025b) and therefore this section is partly taken from these publications. The indoor temperature in the simulation is kept above a specific set temperature. In contrast, in the optimization, the indoor environment can be pre-heated and pre-cooled within comfort bounds, enabling the building to shift electricity demand through its thermal mass. Inputs to FLEX are summarized in Figure 3.1, and detailed in Section 3.3.

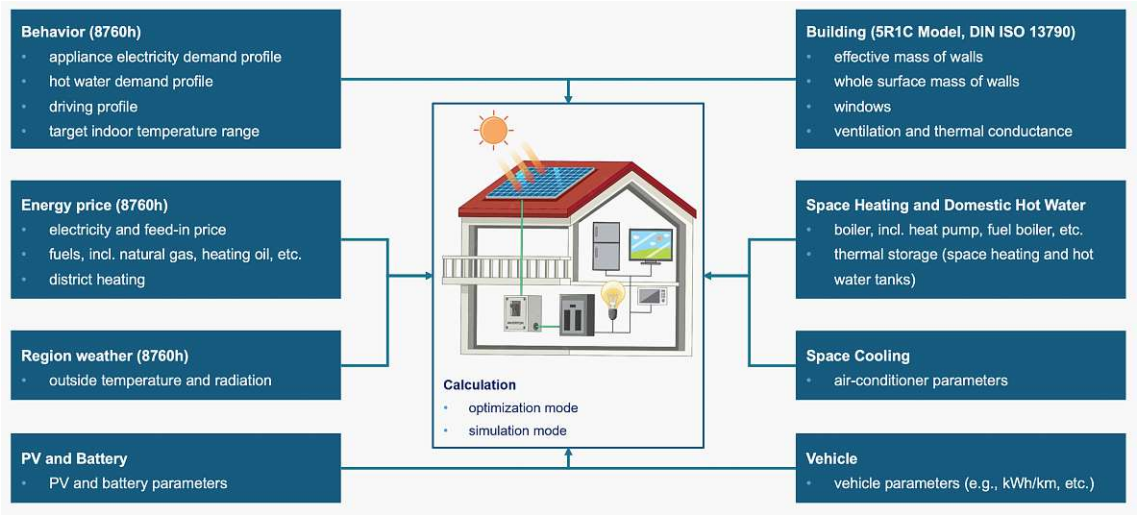

Figure 3.1: FLEX model

Within this chapter, the FLEX model together with other modeling approaches and data used in this thesis are explained. In particular, the modeling framework is presented in Section 3.1, and Section 3.2 provides an overview of the indicators used to describe the impact of prosumagers. The data used for modeling is explained in Section 3.3, while Section 3.4 introduces the application of the model at the local level. Finally, the limitations of the methodology, particularly of the modeling approach, are stated in Section 3.5.

3.1 Overview of the modeling framework

The FLEX model runs an hourly calculation for a building in two ways:

- The building's energy demand is simulated, representing buildings that are conventional consumers and prosumers nowadays, consuming and producing electricity without adapting the consumption behavior to an hourly electricity price. This mode will be called the "reference" mode in the following.

- The building's energy demand is optimized through an HEMS representing the consumption behavior of prosumagers who adapt their demand to an hourly electricity price.

In the reference mode, the input parameters are the same, but without optimization. Heating and cooling demand profiles are driven by outside temperature, radiation, indoor set temperature and internal gains. PV generation is assumed to satisfy the building's electricity consumption directly. The excess generation will first be stored in the battery and then used to charge the DHW tank before being sold to the grid. On the other hand, the battery and DHW tank are discharged immediately to cover internal demand if needed. In the reference mode, the thermal mass of the building is considered in the thermal dynamics (captured by the 5R1C model) but without being optimized, i.e., pre-heated or pre-cooled. Additionally, the heating buffer tank is not used in the reference mode for simplification. With the logic for the battery, the tank would always be charged in summer with excess PV electricity. However, it cannot be discharged because space heating is not needed. Ultimately, this results in high losses and a self-consumption rate of PV generation, which is unrealistic and disrupts the purpose of the 'reference mode,' i.e., serving as the lower benchmark for comparison. So, for simplification, using a hot water buffer tank in the reference mode is not considered.

In the optimization mode, the heating and cooling (if available) are controlled automatically, together with the valves of thermal tanks and the battery, if installed. The thermal mass of the building acts as a storage itself and can be pre-heated and pre-cooled by raising or lowering the indoor temperature within comfort bounds. Appliances like washing machines and dishwashers were not included in the optimization as their operation cannot be fully automated in real life, and their potential to shift electric energy is minimal compared to the amount of energy that could be shifted through the heating and cooling demand.

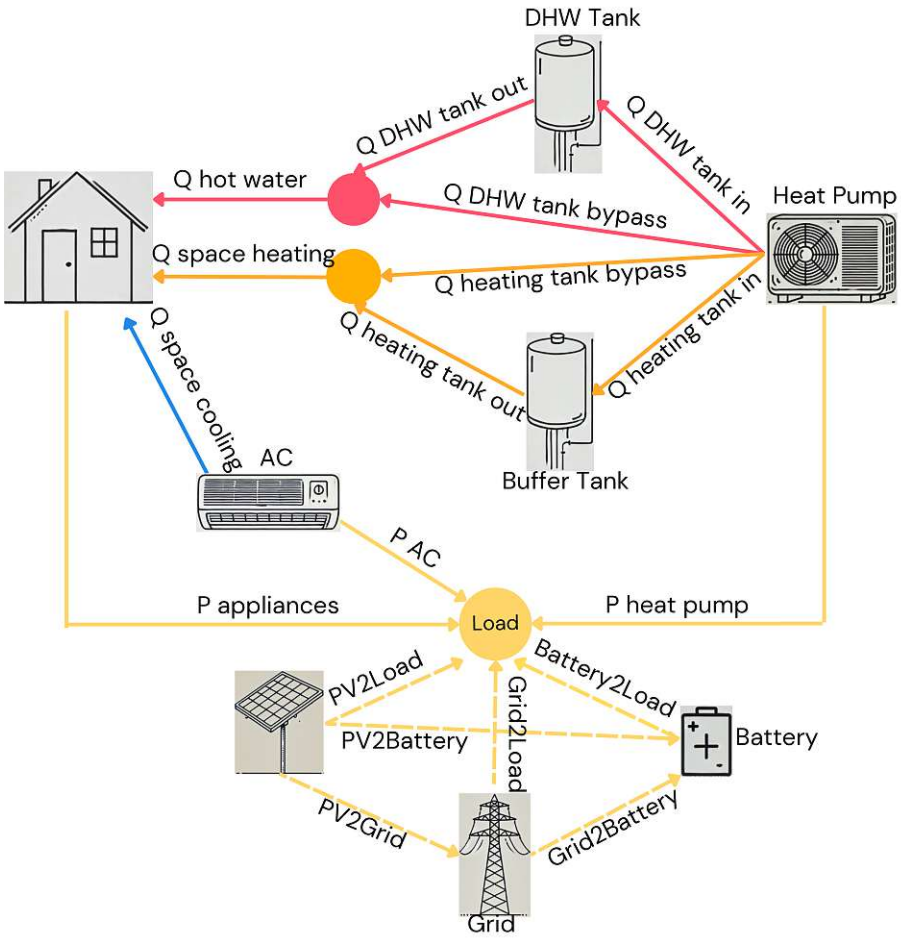

Figure 3.2: Sketch of the FLEX calculation

The energy and electricity flows for calculating the operation of the FLEX model are sketched in Figure 3.2, and in the following, the relationship between the different components is described mathematically. All symbols used in the mathematical formulation are provided in Table 3.1 at the end of this section. The table also provides information on whether a symbol is defined as a parameter or a variable within the optimization. The objective function (Equation 3.1) of the optimization is to minimize the yearly energy cost given a price signal (p) and a feed-in tariff ($p_{\text{feed in}}$). P_{Grid} represents the electric load drawn from the grid, and $P_{\text{feed in}}$ represents the electric load fed into the grid if the buildings have a PV system installed. The total load of a building (P_{Load}) is covered by the grid ($P_{Grid2Load}$), by the battery ($P_{Battery2Load}$) and the PV ($P_{PV2Load}$) (see Equation 3.2). The building load consists of the combined loads of all household appliances ($P_{appliances}$), the electricity demand of the HP (P_{HP}), and the AC (P_{AC}), described with Equation 3.4. Equation 3.5 describes how PV generation (P_{PV}) can be used to cover parts of the building load, charge the battery ($P_{PV2Battery}$), or be sold to the grid ($P_{PV2Grid}$).

$$\min \sum P_{\text{Grid,t}} \cdot p_t - P_{\text{PV2Grid,t}} \cdot p_{\text{feed in,t}} \quad t \in \{1, 2, \ldots, 8760\} \tag{3.1}$$

$$P_{\text{Grid, t}} = P_{\text{Grid2Load, t}} + P_{\text{Grid2Battery, t}} \tag{3.2}$$

$$P_{Load,t} = P_{\text{Grid2Load, t}} + P_{\text{PV2Load, t}} + P_{\text{Battery2Load, t}} \tag{3.3}$$

$$P_{Load,t} = P_{\text{appliances,t}} + P_{\text{HP},t} + P_{AC,t} \tag{3.4}$$

$$P_{PV,t} = P_{\text{PV2Load, t}} + P_{\text{PV2Battery, t}} + P_{\text{PV2Grid, t}} \tag{3.5}$$

The power of the HP (P_{HP}) is the sum of the power needed for space heating ($P_{\text{HP heating}}$) and DHW ($P_{\text{HP DHW}}$). Both $P_{\text{HP heating}}$ and $P_{\text{HP DHW}}$ are calculated through the respective

thermal energy demand for heating and DHW, as well as the storage. The COPs in Equations 3.8 and 3.9 for energy going into the tanks are different because of different supply temperatures. The total power of the HP is restricted by Equation 3.7. The coefficient of performance (COP) of the HP depends on the supply temperature (T_{supply}) and the source temperature (T_{src}), with an efficiency factor (η). The COPs for heat, hot water, and the respective tanks are differentiated due to their different supply temperatures. The tank supply temperature is 10°C higher than the maximum tank temperature, factoring in losses in the heat exchangers. The power needed by the AC (P_{AC}) is calculated with a fixed COP of 4 in Equation 3.11. The maximum power of the AC ($P_{\text{AC max}}$) was chosen to be sufficiently large to keep the indoor temperature of the building at a temperature of 27°C on the hottest day of the year.

$$P_{\text{HP},t} = P_{\text{HP heating,t}} + P_{\text{HP DHW,t}} \tag{3.6}$$

$$P_{\text{HP,t}} \leq P_{\text{HP, max}} \tag{3.7}$$

$$P_{\text{HP heating,t}} = \frac{Q_{\text{BufferTank bypass,t}}}{COP_{Room,t}} + \frac{Q_{\text{BufferTank in,t}}}{COP_{\text{BufferTank,t}}} \tag{3.8}$$

$$P_{\text{HP DHW,t}} = \frac{Q_{\text{DHWTank bypass},t}}{COP_{\text{DHW,t}}} + \frac{Q_{\text{DHWTank in,t}}}{COP_{\text{DHWTank,t}}} \tag{3.9}$$

$$COP_t = \eta \cdot \frac{T_{\text{supply},t}}{T_{\text{supply},t} - T_{\text{src},t}} \tag{3.10}$$

$$P_{AC,t} = \frac{Q_{SpaceCooling,t}}{4} \tag{3.11}$$

$$P_{AC,t} \leq P_{\text{AC max}} \tag{3.12}$$

In the optimization, the room temperature (Θ_{Room}) and the temperature of the thermal mass ($\Theta_{\text{thermal mass}}$) are decision variables bounded by the following constraints. Thermal energy used for heating the indoor environment is the sum of energy drawn from the buffer tank ($Q_{\text{BufferTank out}}$) and the energy bypassing the tank ($Q_{\text{BufferTank bypass}}$) (Equation 3.13). The same principle is used for satisfying the DHW demand in the Equation 3.14. Equations 3.15 to 3.20 describe how the room temperature (Θ_{room}) is calculated after DIN ISO 13790. All parameters named with H_{xx} describe building-specific parameters. How they are determined is described in Appendix A.2. Decision variables in this set of equations are $Q_{SpaceHeating}$ and $Q_{SpaceCooling}$, which are dependent variables of the room temperature (Θ_{room}) and the thermal mass temperature ($\Theta_{\text{thermal mass}}$). The maximum power ($P_{\text{HP max}}$) of every HP is sized by calculating the needed thermal power in the coldest hour of the year. The value is rounded up to the higher hundredth digit. This way, the feasibility of the optimization is ensured while also ensuring that HPs are not massively oversized.

$$Q_{SpaceHeating,t} = Q_{\text{BufferTank out,t}} + Q_{\text{BufferTank bypass,t}} \tag{3.13}$$

$$Q_{HotWaterDemand,t} = Q_{\text{DHWTank out},t} + Q_{\text{DHWTank bypass},t} \tag{3.14}$$

$$\Theta_{\text{m start},0} = \Theta_{\text{thermal mass start}} \tag{3.15}$$

$$\Theta_{\text{m start},t} = \Theta_{\text{thermal mass},t-1} \tag{3.16}$$

$$\phi_{st,t} = (1 - \frac{A_m}{A_{tot}} - \frac{H_{\text{trw}}}{9.1 \cdot A_{tot}}) \cdot (0.5 \cdot Q_i + Q_{solar,t}) \tag{3.17}$$

$$\Theta_{m,t} = \frac{\Theta_{\text{thermal mass},t} + \Theta_{\text{m start},t}}{2} \tag{3.18}$$

$$\Theta_{s,t} = H_{\text{trms}} \cdot \Theta_{m,t} + \phi_{st,t} + H_{\text{trw}} \cdot \Theta_{outside,t} + H_{\text{tr1}} \cdot \frac{\Theta_{outside,t} + (\Phi_{ia} + Q_{SpaceHeating,t} - Q_{SpaceCooling,t})/H_{ve}}{H_{\text{tr,ms}} + H_{\text{trw}} + H_{\text{tr1}}} \tag{3.19}$$

$$\Theta_{room,t} = \frac{H_{\text{tris}} \cdot \Theta_{s,t} + H_{ve} \cdot \Theta_{outside,t} + \Phi_{ia} + Q_{SpaceHeating,t} - Q_{SpaceCooling,t}}{H_{\text{tr,is}} + H_{ve}} \tag{3.20}$$

The following equations describe the dependence of heating and cooling on the thermal mass temperature. The thermal mass temperature is time-dependent. To initiate the thermal mass temperature at the start of each optimization ($\Theta_{\text{thermal mass start}}$), the building is simulated with a fixed indoor and outdoor temperature from the first hour of the optimization until the thermal mass temperature reaches a steady state. This value is then used as the start value for the thermal mass. H_{tr1}, H_{tr2} and H_{tr3} are auxiliary variables to shorten the equations and are described in the Appendix A.2 where the full formulation of the 5R1C model is provided.

$$\Phi_m = \frac{A_m}{A_{tot}} \cdot (0.5 \cdot Q_i + Q_{solar,t}) \tag{3.21}$$

$$\Phi_{mtot,t} = \Phi_m + H_{\text{trem}} \cdot \Theta_{outside,t} + H_{\text{tr3}} \cdot (\frac{\Phi_{ia} + Q_{SpaceHeating,t} - Q_{SpaceCooling,t}}{H_{ve}} + \Theta_{outside,t})/H_{\text{tr2}} \tag{3.22}$$

$$\Theta_{\text{thermal mass},t} = \frac{\Theta_{\text{m start},t} \cdot \frac{C_m}{3600} - 0.5 \cdot (H_{\text{tr3}} + H_{\text{trem}}) + \Phi_{mtot,t}}{\frac{C_m}{3600} + 0.5 \cdot (H_{\text{tr3}} + H_{\text{tr,em}})} \tag{3.23}$$

$$\tag{3.24}$$

The battery is modeled with the Equations 3.25 to 3.31. It can not be used to discharge electricity to the grid (3.26) and the maximum charging and discharging power is contained by Equations 3.27 and 3.28. The state of charge (SOC_{battery}) is described through Equation 3.29 with η_{charge} and $\eta_{\text{discharge}}$ describing the efficiency of the battery's charging and discharging process. At the start of the simulation, the battery is empty (Equation 3.31).

$$P_{BatteryCharge,t} = P_{PV2Battery,t} + P_{Grid2Battery,t} \tag{3.25}$$

$$P_{BatteryDischarge,t} = P_{Battery2Load,t} \tag{3.26}$$

$$0 \leq P_{BatteryCharge,t} \leq P_{\text{battery,max}} \tag{3.27}$$

$$0 \leq P_{BatteryDischarge,t} \leq min(P_{\text{Battery,max}}, SOC_{\text{battery,t}}) \tag{3.28}$$

$$SOC_{\text{Battery,t}} = SOC_{\text{Battery,(t-1)}} + P_{\text{BatteryCharge}} \cdot \eta_{\text{BatteryCharge}} - \frac{P_{\text{BatteryDischarge}}}{\eta_{\text{BatteryDischarge}}} \tag{3.29}$$

$$0 \leq SOC_{\text{Battery,t}} \leq SOC_{\text{Battery},max} \tag{3.30}$$

$$SOC_{\text{Battery,0}} = 0 \tag{3.31}$$

Equations 3.32 to 3.35 represent the physical limitations of the hot water tanks. Q_{tank} denotes the energy stored in a tank (Joule) at a particular hour, with m_{water} (kg) being the mass of the water and T_{tank} the current temperature inside the tank. $T_{\text{tank min}}$ is the minimum temperature inside the tank. $T_{\text{tank,0}}$ is the temperature inside the tank at the start of the simulation. For simplification, assumptions on the heat exchange inside the hot water tank are made so nonlinearities are not introduced into the optimization: (1) The temperature inside the hot water tank is homogeneous; (2) The temperature surrounding the tank is constant at 20°C; (3) The thermodynamic properties of the water - heat capacity (c_{water}), volume, and pressure - are constant. Both tanks have the same insulation with a heat transfer coefficient (Λ). The area (A_{tank}) of the tank is calculated by taking the minimum area of a cylinder with the respective volume[1]. $Q_{\text{tank loss}}$ describes

[1] A_{tank} is derived from the volume (V) of the tank by calculating the minimal surface area, i.e., $A_{tank} = 2\pi r^2 + \frac{2V}{r}$, with r being the radius, which is calculated by $r = \sqrt[3]{2 * \frac{V}{4\pi}}$.

the thermal losses of the storage through Equation 3.35 with the temperature surrounding the thermal tank $T_{\text{tank surrounding}}$.

$$Q_{\text{Tank},t} = m_{\text{water}} \cdot c_{\text{water}} \cdot (T_{\text{Tank},t} - T_{\text{Tank,min}}) \tag{3.32}$$

$$T_{\text{Tank},0} = T_{\text{Tank min}} \tag{3.33}$$

$$T_{\text{Tank min}} \leq T_{\text{tank},t} \leq T_{\text{tank max}} \tag{3.34}$$

$$Q_{\text{Tank loss}} = \Lambda \cdot A_{Tank} \cdot (T_{\text{Tank},t} - T_{\text{Tank,surrounding}}) \tag{3.35}$$

The optimization was developed in Python with Pyomo (Hart et al. 2017) and solved by Gurobi[2]. The source code can be found on GitHub[3].

Table 3.1: List of symbols with description for the FLEX model

Character	Unit	Type	Description
A_{Tank}	m^2	parameter	surface area of a thermal tank storage
A_f	m^2	parameter	heated floor area
A_m	m^2	parameter	effective mass related area
A_{tot}	m^2	parameter	total surface area of building
C_m	J/K	parameter	thermal capacity of a building
c_{water}	J/kgK	parameter	specific heat capacity of water
$H_{tr,em}$	W/K	parameter	transmission heat transfer coefficient between outside and the thermal mass node
H_{tris}	W/K	parameter	transmission heat transfer coefficient between the surface area node and indoor air temperature
H_{trms}	W/K	parameter	transmission heat transfer coefficient between the thermal mass node and the surface area node
$H_{tr,op}$	W/K	parameter	transmission heat transfer coefficient through opaque building elements
H_{ve}	W/K	parameter	transmission heat transfer coefficient of the ventilation
H_{trw}	W/K	parameter	transmission heat transfer coefficient through windows
m_{water}	kg	parameter	mass of water
p_t	EUR/kWh	parameter	retail electricity price
$p_{\text{feed in,t}}$	EUR/kWh	parameter	electricity feed in price
$P_{Load,t}$	W	variable	electrical power consumption of the household
$P_{appliances,t}$	W	parameter	electrical power consumption of the appliances in the house
$P_{\text{Grid,t}}$	W	variable	electrical power drawn from the electrical grid
$P_{Grid2Load,t}$	W	variable	electrical power from the grid into the household
$P_{Grid2Battery,t}$	W	variable	electrical power from the grid into the battery
$P_{PV,t}$	W	parameter	electrical generation of the PV system
$P_{PV2Load,t}$	W	variable	electrical power from the PV to the household
$P_{PV2Battery,t}$	W	variable	electrical power from the PV into the battery
$P_{PV2Grid,t}$	W	variable	electrical power from the PV fed to the grid
$P_{AC,t}$	W	variable	electrical power consumption of the AC
$P_{HP,t}$	W	variable	electrical power consumption of the HP
$P_{\text{HP heating,t}}$	W	variable	electrical power consumption used for heating

[2]Mathematical programming solver, https://www.gurobi.com/.
[3]FLEX model: https://github.com/H2020-newTRENDs/FLEX

Table 3.1: List of symbols with description for the FLEX model

Character	Unit	Type	Description
$P_{\text{HP DHW,t}}$	W	variable	electrical power consumption used for DHW generation
$P_{Battery2Load,t}$	W	variable	electrical power supplied from the battery to the household
$P_{BatteryCharge,t}$	W	variable	electrical power used to charge the battery
$P_{BatteryDischarge,t}$	W	variable	electrical power with which the battery is discharged
$SOC_{Battery,t}$	W	variable	State of charge of the battery
$\eta_{BatteryCharge}$	-	parameter	battery charging efficiency
$\eta_{BatteryDischarge}$	-	parameter	battery discharging efficiency
$COP_{DHW,t}$	$-$	parameter	coefficient of performance when generating DHW
$COP_{DHWTank,t}$	$-$	parameter	coefficient of performance when charging the DHW tank
$COP_{BufferTank,t}$	$-$	parameter	coefficient of performance when charging the buffer tank
$COP_{Room,t}$	$-$	parameter	coefficient of performance when heating the indoor environment
$T_{Tank,t}$	K	variable	temperature inside a tank
$T_{Tank,surrounding}$	K	parameter	temperature surrounding the thermal tank
$T_{supply,t}$	K	parameter	supply temperature
$T_{src,t}$	K	parameter	source temperature
$Q_{\text{Tank,t}}$	Wh	variable	thermal energy saved in a tank
$Q_{\text{Tank loss,t}}$	Wh	variable	thermal energy loss of a tank
$Q_{\text{BufferTank bypass,t}}$	Wh	variable	thermal energy bypassing the buffer tank
$Q_{\text{BufferTank in,t}}$	Wh	variable	thermal energy going into the buffer tank
$Q_{\text{BufferTank out,t}}$	Wh	variable	thermal energy discharged from the buffer tank
$Q_{\text{BufferTank,t}}$	Wh	variable	thermal energy saved in the buffer tank
$Q_{\text{HotWaterDemand,t}}$	Wh	parameter	thermal energy demand for hot water by the household
$Q_{\text{DHWTank in,t}}$	Wh	variable	thermal energy going into the DHW tank
$Q_{\text{DHWTank out,t}}$	Wh	variable	thermal energy discharged from the DHW tank
$Q_{\text{DHWTank bypass,t}}$	Wh	variable	thermal energy bypassing the DHW tank
$Q_{\text{SpaceHeating,t}}$	Wh	variable	thermal energy used for heating
$Q_{\text{SpaceCooling,t}}$	Wh	variable	thermal energy used for cooling
$Q_{\text{i,t}}$	Wh	parameter	internal gains
$Q_{\text{solar,t}}$	Wh	parameter	solar gains
$\theta_{outside,t}$	$^\circ C$	parameter	outside temperature
$\theta_{s,t}$	$^\circ C$	variable	temperature of the node s
$\theta_{m,t}$	$^\circ C$	variable	temperature of the node m
$\theta_{\text{thermal mass},t}$	$^\circ C$	variable	temperature of the thermal mass
$\theta_{room,t}$	$^\circ C$	variable	indoor temperature
$\theta_{\text{m start,t}}$	$^\circ C$	variable	temperature of the thermal mass in the previous timestep
$\phi_{\text{mtot,t}}$	W	variable	total heat flow to/from the thermal mass
$\phi_{\text{m,t}}$	W	parameter	heat flow to the thermal mass resulting from internal and solar gains
$\phi_{\text{ia,t}}$	W	parameter	heat flow to the indoor environment resulting from solar gains
$\phi_{\text{st,t}}$	W	parameter	heat flow to the node s resulting from solar and internal gains
Λ	W/m^2K	parameter	heat transfer coefficient of tank walls
r	m	parameter	radius
V	m^3	parameter	volume

3.2 Indicators used to assess results in terms of flexibility

The FLEX model was developed to assess the flexibility potential of the building stock in the publications (Mascherbauer et al. 2025a; Mascherbauer et al. 2024; Mascherbauer et al. 2022; Mascherbauer et al. 2025b). Because prosumagers shift their grid imports, the term *electricity demand* is often used. *Electricity demand* always denotes grid demand (imports). The electricity demand is analyzed both at an individual level and at an aggregated building stock level. At the building stock level the *total electricity demand*, refers to national electricity demand across all sectors. Finally, the *electricity demand of all prosumaging buildings* represents the sum of the grid demand of all prosumager buildings within a country or area. That said, the following indicators are often calculated for the electricity demand on different levels of aggregation.

Shifted electricity

The FLEX model aims to quantify the amount of shiftable electricity on a single building and building stock level. Similar to Fitzpatrick et al. (2020), shifted energy ($E_{shifted}$) in this thesis is defined as the difference between the electric power consumption profiles with and without DR:

$$E_{shifted} = \int P_{\text{simulation, t}} - P_{\text{HEMS, t}}\, dt \quad if \quad P_{\text{simulation, t}} > P_{\text{HEMS, t}} \tag{3.36}$$

$P_{\text{simulation, t}}$ denotes the electricity load from the grid in the simulation case, and $P_{\text{HEMS, t}}$ the load with a HEMS installed. If $P_{\text{HEMS, t}}$ is higher than $P_{\text{simulation, t}}$, the building is being pre-heated or storage is charged. Likewise the energy is shifted whenever $P_{\text{simulation, t}}$ is higher than $P_{\text{HEMS, t}}$. Naturally, the shifted electric energy ($E_{shifted}$) is lower than the energy used to charge storage and building mass due to thermal losses.

The average shifted electric energy share $\tilde{E}_{shifted}$ is the shifted electric energy ($E_{shifted}$) divided by the total electricity consumption over the year (reference case - $P_{simulation}$) to show how much electricity can be shifted as a percentage of the total electricity demand:

$$\tilde{E}_{shifted} = \frac{E_{shifted}}{\sum \int P_{\text{simulation, t}} dt} * 100 \tag{3.37}$$

PV self-consumption

By minimizing energy costs, prosumager tend to maximize PV self-consumption. Therefore, PV self-consumption is an indicator of the profitability or effectiveness of load shifting. In this thesis, the PV self-consumption is only calculated for buildings having PV. Electricity generated by the PV (E_{PV}) can either be used to cover the household load ($E_{PV2Load}$) or to charge the battery if available ($E_{PV2Battery}$). Excess PV electricity is sold to the grid.

$$\text{Self-consumption} = \frac{\sum_t (E_{\text{PV2Load, t}} + E_{\text{PV2Battery, t}})}{\sum_t E_{\text{PV, t}}} \tag{3.38}$$

Peak demand

The peak demand describes the highest electricity demand value within a year of a single building i or a sum of buildings if calculated on the building stock level.

$$\hat{P} = \max_{t \in [1,8760]} \sum_i P_{\text{Grid, i, t}} \tag{3.39}$$

Sperber et al. (2025) focus on residual load peaks in their work. To show how the peak demand can increase through prosumaging, like in Sperber et al. (2025), in this thesis,

the total grid demand on the national level was considered, including the demand of other sectors.

Additionally, in Mascherbauer et al. (2024), the daily peak-to-peak ($p2p$) values of both the electricity price and the electricity demand were analyzed. The daily $p2p$ serves as an indicator for the volatility of a profile.

$$p2p = \max_{t\in[1,24]}(P_{\text{Grid, d, t}}) - \min_{t\in[1,24]}(P_{\text{Grid, d, t}}), \quad \forall d \in [1, 365] \tag{3.40}$$

Total electricity demand

By analyzing the total difference in electricity demand (E_{total}) of households with and without HEMS, the demand increase or decrease through prosumagers in the building sector can be calculated. It shows if efficiency improvements, like the rise in PV self-consumption of prosumagers, offset losses that occur when demand is shifted.

$$E_{\text{total}} = \sum_i \int (P_{\text{HEMS, t,i}} - P_{\text{simulation, t,i}})dt \tag{3.41}$$

Flexibility Factor

Le Dréau et al. (2016a) introduced a Flexibility Factor for the heating demand based on the hourly price using the first and fourth price quartiles (low and high price time). A higher Flexibility Factor means that more energy is consumed at low prices. The Flexibility Factor provides information on how strongly a load profile adapts to changes in price. By comparing the Flexibility Factor of the consumer to prosumager demand profiles, the increased shift of electricity demand from higher to lower prices can be described in a single number.

$$\text{Flexibility Factor} = \frac{\int_{\text{low price}} P_t \quad dt - \int_{\text{high price}} P_t \quad dt}{\int_{\text{low price}} P_t \quad dt + \int_{\text{high price}} P_t \quad dt} \tag{3.42}$$

Grid support coefficient

Klein et al. (2016) introduced an absolute Grid Support Coefficient (GSC_{abs}) and a relative GSC (GSC_{rel}). The GSC_{abs} describes the grid friendliness of a certain consumption profile, while the GSC_{rel} is a rescaled version (between -100 and 100) of the GSC_{abs} to make it comparable between different profiles. GSC_{abs} is calculated by weighting the electricity consumption with the price and dividing it by the consumption times the average price ($\overline{p}$). The $GSC_{abs}(worstcase)$ and the $GSC_{abs}(bestcase)$ are calculated by assuming that the total electricity consumption within one day could be shifted to the full load hours with the lowest and highest price, respectively. The full load hours are defined by dividing the daily sum of electricity consumption by the maximum HP power ($P_{\text{HP, max}}$). Then the GSC_{abs} is calculated for these hours, with the total daily consumption shifted to the worst and best hours. The higher the GSC_{rel}, the more grid-supportive an electricity consumption profile is. The wholesale electricity price and the residual load are strongly correlated (Klein et al. 2016; Klein et al. 2017). In this thesis, the GSC_{rel} was calculated for the electricity demand of the HP-heated residential building stock with and without prosumagers on the EU member state level.

$$GSC_{abs} = \frac{\sum_{t=1}^{24} P_{\text{grid, t}} \cdot p_t}{\sum_{t=1}^{24} P_{\text{grid,t}} \cdot \overline{p}} \tag{3.43}$$

$$GSC_{rel} = 200 \cdot \frac{GSC_{abs}(\text{worst case}) - GSC_{abs}}{GSC_{abs}(\text{worst case}) - GSC_{abs}(\text{best case})} \tag{3.44}$$

Table 3.2: List of symbols for the indicators used to assess flexibility

Character	Unit	Description
$E_{shifted}$	Wh	electric energy shifted over a time period
$\tilde{E}$	%	electrical energy shifted as a
E_{total}	Wh	difference in electricity demand with and without HEMS
E_{PV}	Wh	total electrical energy produced by the PV
$E_{PV2Load}$	Wh	electrical energy provided by the PV to the household
$E_{PV2Battery}$	Wh	electrical energy provided by the PV to the battery
P_{HEMS}	W	electrical power demand of a prosumaging households
$P_{simulation}$	W	electrical power demand of a household without HEMS
$\hat{P}$	W	electrical peak power
Pr	EUR/kWh	Price prominence
$p2p$	W	peak-to-peak power
GSC_{abs}	-	absolute grid support coefficient
GSC_{rel}	-	relative grid support coefficient (normalized between -100 and 100)

3.3 Data

The FLEX model needs input data on buildings, energy prices and weather. The respective sources and assumptions for this data are described within this section.

3.3.1 Building stock data

The building stock of each country is described through a set of representative buildings, each of which is described by its building parameters. The building parameters describe the thermal properties of the building through 5 resistances and 1 capacity (5R1C). The resistances describe the insulation of different building elements, while the capacity describes the thermal mass of the building. Additionally, information on the ventilation system and the dimensions of the building are needed. Linking the FLEX model to the Invert/EE-LAB (Andreas Müller 2021) building stock model analysis of prosumagers on the building stock level for future scenarios is possible. Invert/EE-Lab is a techno-socio-economic bottom-up building stock model that simulates energy-related investment decisions in buildings, specifically focusing on space heating, hot water generation, and space cooling end-uses. The investment decisions for single buildings to improve energy efficiency measures or to switch heating systems are simulated through a combination of a discrete choice approach and technology diffusion theory, with additional constraints for each heating system and building type. The model calculates the useful energy demand (or energy needs) of the buildings and, thus, the building stock on a monthly basis. Investment decisions are made once a year. The model horizon of Invert/EE-Lab is usually 2050 (depending on the scenario). Since the minimal time resolution is on a monthly (energy demand) or yearly (investment decision) basis, the FLEX model was developed to enable the investigation of research questions that need a higher level of temporal resolution in future scenarios. Like the FLEX model, the Invert model uses the DIN ISO 13790 to calculate the energy demand of buildings. The building stock of each country is represented through archetypes. These archetypes represent buildings of a certain class (SFH, MFH, terraced houses, apartment blocks) built in a certain period (e.g., from 1991 to 2000). Within this classification, they are further distinguished by their renovation status. Every archetype has a number of different heating systems attributed to it, the number of installed PV systems, and the average size of these systems. In this thesis, the focus relies

on buildings using HPs to shift energy demand; thus, only buildings using air and ground source HPs are selected from the database. The number of archetypes in Invert increases from 2020 to 2050 as new buildings are built and old ones are renovated. The supply temperature depends on a building archetype's thermal insulation and heating system and is thus also an output of the Invert model. The Invert model was compared to other building stock models in the EU context under the same scenario assumption in (Awais et al. 2025).

Building stock data for Austria

In the first publication (Mascherbauer et al. 2022), the Austrian SFH building stock was analyzed in its current state. 11 different representative building types were selected. Every building type represents buildings built in a specific time period, starting from 1890 up to 2011. Based on available data from Statistik Austria[4] and Emhofer et al. (2014), the number of buildings in Austria equipped with HPs, PV, and thermal storage was estimated. Figure 3.3 shows the total number of buildings with an HP and a specific technological configuration: PV size with 0, 5, or 10 kWp; Battery (B) size with zero or 7 kWh; Hot water tank (T) size with 0 or 1500 L. Most buildings do not have a PV, and only 23 buildings have a 10 kWp PV and a hot water tank. Information on floor area and heating demand is provided in the Appendix A.1 in Table A.1.

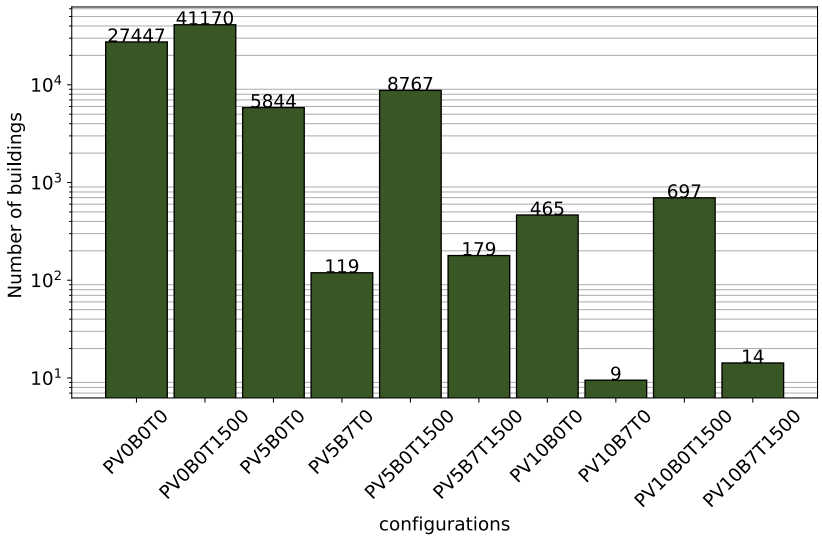

Figure 3.3: Number of SFH buildings in Austria with different technical configurations. (Mascherbauer et al. 2022)

In the second publication (Mascherbauer et al. 2024), the SFH building stock in Austria is represented by 36 building categories. Each category represents a typical SFH built in a certain time period and its overall thermal insulation properties. The different representative buildings and the installed number of HP in each category are presented in Figure A.2 in the Appendix A.1. Overall, Austria has around 1.55 million SFHs, of which 180 000 have a HP installed[5]. In 2023, the Austrian federal government implemented strong incentives for exchanging oil and gas boilers with HPs by subsidising installation costs up to 75%. Thus, it is expected that the share of SFHs with an HP will increase significantly within the next years[6]. The focus in Mascherbauer et al. (2024) was to investigate the

[4] https://www.statistik.at/

[5] Statistik Austria: https://www.statistik.at/

[6] https://www.oesterreich.gv.at/themen/umwelt_und_klima/energie_und_ressourcen_sparen/1/raus_aus_oel.html

impact of the electricity price signal on the load shifting potential. Therefore, the total amount of HP-operated buildings or the characteristics of the building stock itself were not changed from the status quo, except for the price signals. Otherwise, the resulting shifted electricity would be heavily dependent on the chosen building stock scenario and not on the electricity price itself. Information on the RC parameters of the building types is given in the Appendix A.1 in Table A.2.

Building stock data for EU27

To investigate the future load shifting potential of prosumagers in the EU building stock until 2050, the building stock was first modeled using the Invert model (Mascherbauer et al. 2025b). The Invert scenario chosen for the underlying building stock scenario is ambitious and aims to reach climate neutrality in the EU-27 in 2050. This goal is reached under the assumption of strong future electrification and high efficiency, which translates into high renovation rates (average 3.1% from 2019 to 2050). The average final energy demand for heating in the building sector will decrease by 39% by 2050 (Awais et al. 2025). The resulting average heating demand per square meter in the buildings heated with HPs is shown in Figure 3.4. A comparison of this scenario with other building stock scenarios and other building stock models was done within the ECEMF project (Awais et al. 2025).

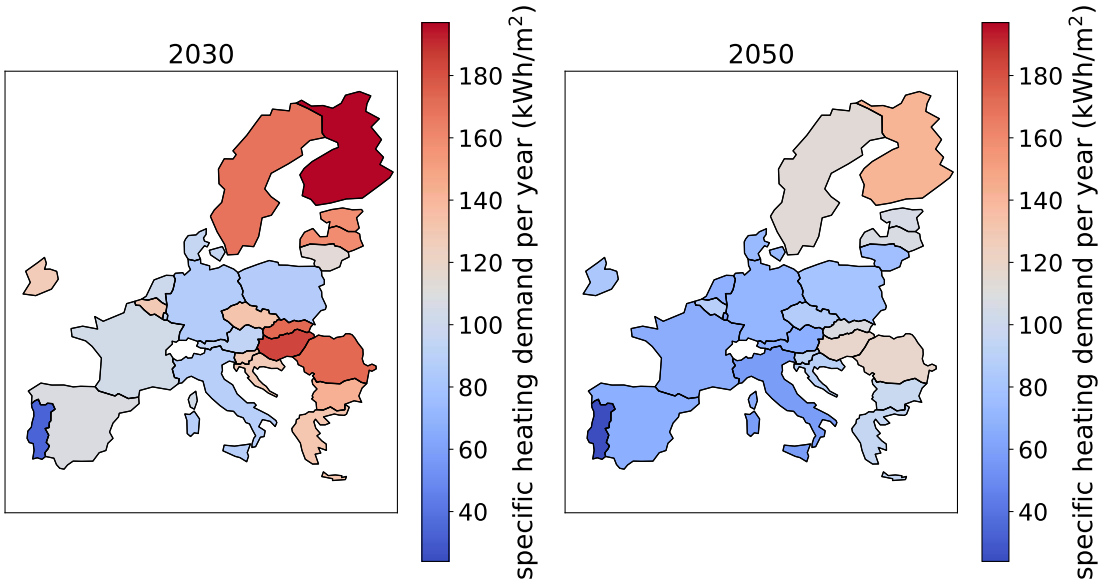

Figure 3.4: Average specific useful energy demand for heating in kWh/(m^2*yr) for the EU member states in 2030 and 2050.

3.3.2 Building technologies

In this section, the scenarios concerning the different building technologies used in the FLEX model are described. In each publication, different assumptions regarding the uptake of HPs, PV, battery, DHW, and heating tanks were made. For each of the technologies, the assumptions used are described in the following.

Heat pump

The efficiency of HPs is always modeled with Equation 3.10; however, the efficiency factor η is varied in different studies created within this thesis. In Mascherbauer et al. (2022), the efficiency factor was compared with data sheets from various HP producers and subsequently set to 0.35 for the air-source HP and 0.4 for the ground-source HP for the base

year. A comparison of the different COP values from manufacturers and the calculated COP is given in Figure 3.5. The manufacturer data are shown as box plots (Bosch n.d. Daikin n.d. Helios n.d. Ochsner 2021; Viessmann n.d.). In the scenarios until 2050, this factor was increased by 0.02 every 10 years to take an increase in efficiency into account. The source temperature for ground-sourced HPs was always assumed to be 10°C. The number of installed HPs per country varies strongly. Figure 3.6 shows the installed capacity in each country. With a high share of installed capacity compared to the overall electricity demand, DR through HPs can have a more pronounced impact on the electricity system. In 2050, Hungary and Croatia have the highest installed capacity in comparison to the average national grid load in this scenario.

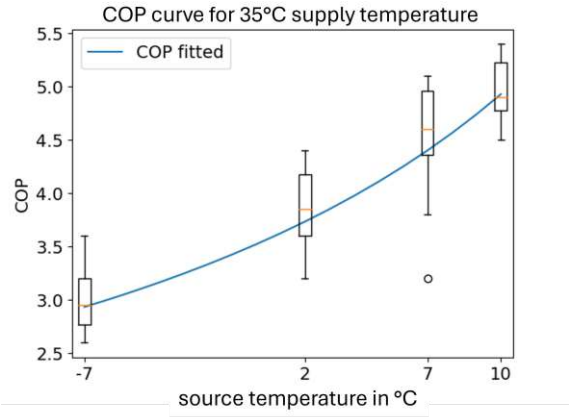

Figure 3.5: Fitted COP curve compared to manufacturer data (Bosch n.d. Daikin n.d. Helios n.d. Ochsner 2021; Viessmann n.d.). (Mascherbauer et al. 2022)

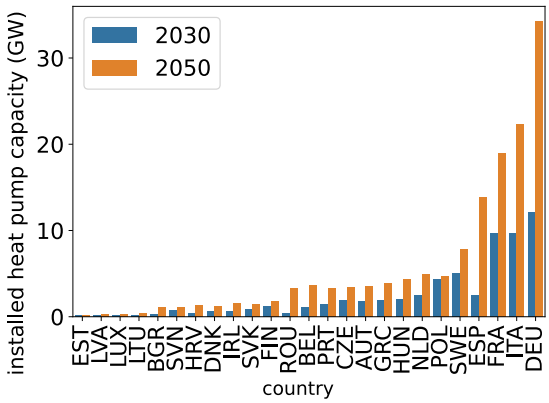

Figure 3.6: Installed HP capacity by EU-Member State in 2030 and 2050 in the selected scenario.

Domestic hot water- and heating tank

The maximum temperature inside the heating buffer tank was set to 45°C, and the DHW tank was set to 65°C. Although maximum temperatures in buffer or DHW tanks can be higher in reality, these values were chosen to limit the energy that can be stored within these tanks. Having higher temperatures would mean a much higher temperature difference that the HP has to overcome. This difference would have to be included in the corresponding COP, making the optimization non-linear. As a result, the feed temperature of the tanks was always 10°C higher than the building supply temperature in the case of the buffer tank or 75°C for the DHW tank. The tank walls' heat loss coefficient Λ is assumed to be 0.2 W/m^{2}K. The temperature surrounding the tanks is considered to be constant at 20°C to keep the problem linear. In the different studies, the tank size was differentiated. Sales data for small-scale thermal storage are not publicly reported in Austria. Most HPs have been installed in combination with a small domestic hot water storage. In the first publication Mascherbauer et al. (2022), 60% of all buildings with an HP are considered to have thermal storage in Austria. At EU Member State level, in Mascherbauer et al. (2025b) and Mascherbauer et al. (forthcoming) it was assumed that HPs are installed with a 30 L per kW$_{\text{th}}$ buffer tank and a 100 L DHW tank per person in the building.

Battery

The following assumptions were made regarding the batteries: (1) The input and output power is limited to 4.5 kW; (2) The efficiencies for charging and discharging are equal to 95%. According to Kebede et al. (2021), round-trip efficiency of stationary battery storage

is reported to be in the range between 78% and 98%. The estimated round-trip efficiency of 90.025% of this work is well within this range; (3) The battery is empty at the beginning of the simulation, and the capacity of the battery is 7 kWh in SFH and 15 kWh in MFHs. In Hernández et al. (2019), the optimal battery size for SFHs was calculated to be between 3.6 and 6.9 kWh. Leonhartsberger et al. (2021) also conducted a market analysis on battery storage in Austria and found that the average storage capacity is around 6.7 kWh. For large MFHs, a 15 kWh battery seems undersized. Still, the analysis in an urban area showed that the available rooftop area for large MFHs is usually too small to generate a large surplus of PV electricity, and only then would larger batteries be more profitable.

According to Leonhartsberger et al. (2021), a total number of 21 838 batteries were installed in Austria's residential homes in combination with a PV system since 2014. I estimate that around 67% of those are installed in newly built buildings (after 2014). No numbers are available before 2014, as batteries were too expensive and not established in the market. Thus, 2% of the buildings considered in the publication (Mascherbauer et al. 2022) have a battery installed in combination with a PV.

In the analysis at the EU member state level, batteries are not considered.

PV systems

For simplicity, the distribution of orientation of PV systems in each country was assumed to be 50% for maximal yield, 25% in the east, and 25% in the west direction with an optimal inclination angle. The PV type in all studies is a crystalline silicon type with a system loss of 14%[7].

PV systems in Austria

In Mascherbauer et al. (2022), around 375 000 SFHs were considered, of which 17.6% have 5 kWp installations and 1.4% 10 kWp installations. Hernández et al. (2019) analyzed the optimal PV and battery storage size, taking battery degradation into account, and found that the optimal PV size should be between 1.8 and 2.7 kWp. However, their buildings did not use an HP, which resulted in significantly lower electricity consumption, and they optimized for self-consumption and self-sufficiency. In this specific publication, the PV systems were all oriented for maximum yearly generation (Mascherbauer et al. 2022).

PV systems in the EU27

On the EU member state level (Mascherbauer et al. 2025b), the PV sizes per building archetype are derived from the Invert model. The size distribution over all of the EU member states, and the uptake of PV installations on HP-heated buildings in the used scenario in all countries are visualized in Figure 3.7 and 3.8 respectively. The total number of rooftop PV installations until 2050 on buildings with HPs is relatively low. The Invert model has strong restrictions on available rooftop areas, and thus, the proposed number and size of PV installations are not as high as expected in a complete decarbonization scenario. Also, uncertainties like vanishing feed-in tariffs or reduced subsidies on PV installations in the future might impact the overall roll-out.

[7]The estimated system losses are all the losses in the PV system, which cause the power actually delivered to be lower than the power produced by the PV modules. There are several causes for this loss, such as losses in cables, power inverters, dirt (sometimes snow) on the modules, and so on. Over the years, the modules also tend to lose a bit of their power. (European Commission Joint Research Centre 2024)

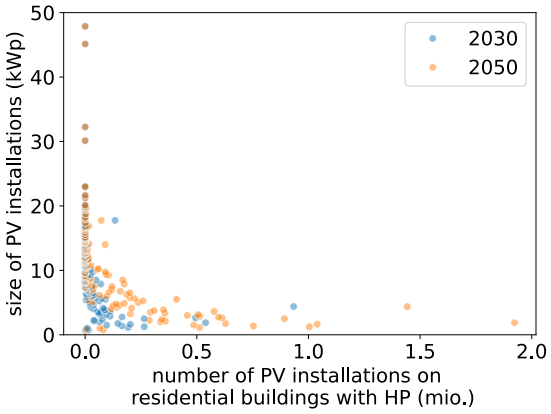

Figure 3.7: Distribution of PV sizes (nominal peak power - kWp) on HP heated residential buildings in the selected EU countries from 2020 to 2050

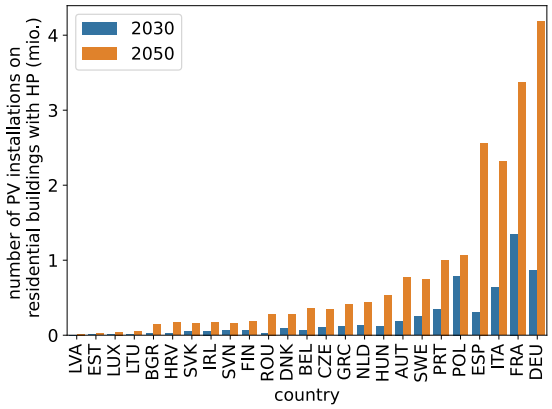

Figure 3.8: Number of rooftop PV installations on HP heated residential buildings.

3.3.3 Electricity prices

The electricity price signal is the main driver of the optimization problem. In the studies, hourly price profiles were either downloaded from the ENTSO-E platform for past price data or modeled using the Balmorel (*Balmorel Code* 2022) model for future price scenarios. From ENTSO-E, the wholesale day-ahead price is assumed to be the day-ahead price either with an additional fixed grid tariff (15 cent/kWh in Mascherbauer et al. (2022), and 20 cent/kWh in Mascherbauer et al. (2024) and Mascherbauer et al. (2025a)) or different grid fees to investigate the impact of negative prices on prosumager behavior (Mascherbauer et al. 2025b).

Balmorel model

Hourly electricity prices are needed to estimate the potential of load shifting in the future. These prices were modeled using the Balmorel model (*Balmorel Code* 2022; Wiese et al. 2018) in Mascherbauer et al. (2024) and the analysis on EU level (Mascherbauer et al. 2025b). Balmorel is a partial equilibrium model for the simultaneous optimization of generation, transmission, and consumption of electricity and heat. Within the system boundaries, electricity demand and supply are matched within a market model, considering supply costs following the merit order principle under the assumption of a perfectly competitive market. In a future decarbonized electricity system, a higher price variance on electricity spot markets is expected for systems with very high shares of renewable generation (Schöniger et al. 2022). This is because of more hours with spot prices close to zero due to very high shares of renewable generation with low variable generation costs. In times of low renewable generation and high load on the other side, flexibility options at higher costs like dispatchable generation units, storage discharge, or import set the marginal price, which results in relatively high spot prices. Within the system boundaries, electricity demand and supply are matched within a market model, considering supply costs following the merit order principle under the assumption of a perfectly competitive market. It is not determined specifically in which type of market the transactions take place economically. The marginal cost of supplying power demand are derived which can be interpreted as the geographically specific market price of power in the model output.

Electricity prices used to investigate the Austrian SFH building stock

In Mascherbauer et al. (2022), the variable electricity price was taken from EXAA[8] in 2016 for Austria. A fixed grid fee plus taxes of 15 cent/kWh was added to the variable price to make it a realistic price profile[9]. The flat price was set to the mean value of the variable price to get comparable results when using a flat price in the simulation. The feed-in tariff for electricity sold to the grid is constant at 7.67 cent/kWh (E-control 2017). These prices are shown in Figure 3.9.

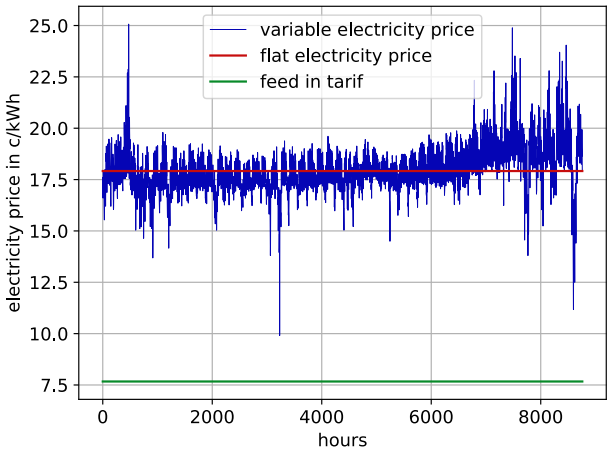

Figure 3.9: Variable and flat hourly electricity price from 2016 together with the feed-in tariff (EXAA 2016; E-control 2017) used for the analysis of the Austrian SFH building stock in Mascherbauer et al. (2022).

Electricity prices used to investigate the impact of the price on the load shifting potential

For the investigation of the potential in Austria to shift electricity via SFH HPs based on different electricity prices in Mascherbauer et al. (2024), the Austrian electricity system was modeled to reflect a decarbonized power system with higher price variance. In total, four prices were investigated; the first one was the actual electricity price from 2021, capturing extreme volatility in prices at the end of the year. The other three prices were modeled using the Balmorel model to see how, in a future electricity system, CO_2 prices and higher volatility in price changes affect the ability of residential buildings to shift electricity. Using Balmorel, the Austrian electricity and district heat system, as well as the neighboring countries, the Czech Republic, Germany, Hungary, Italy, and Slovenia, to capture export and import dynamics was modeled. Installed generation capacities, national electricity demand, and net transfer capacities were based on the Ten-Year Network Development Plan (TYNDP) 2020 National Trends scenario[10]. For Austria, the assumptions were based on the national energy and climate plan WAM scenario[11] and were refined to reflect the 100% renewable target (nationwide in annual balance terms) until 2030. That means that Austria meets its goals defined in the Renewable Expansion Act Nationalrat (2021) and becomes a net exporter of electricity. All electricity generated by natural gas is exported (on an annual balance). The model with input parameters has

[8] https://www.exaa.at/

[9] The statistical information on this price signal is as follows: mean, 17.9 cent/kWh; maximum, 25.1 cent/kWh; minimum, 9.9 cent/kWh; first quantile, 17.2 cent/kWh; third quantile, 18.5 cent/kWh; standard deviation, 1.2 cent/kWh; variance, 1.3cent/kWh.

[10] available under https://tyndp.entsoe.eu/, last visited: 29.06.2022

[11] Umweltbundesamt, last visited: 17.11.2022

been tested and validated in Hanke Marcel (2020) and Resch et al. (2022). The aim is to reflect various electricity market settings with different price patterns. In Mascherbauer et al. (2024), three price scenarios were analyzed to analyze sensitivities differing in the assumed CO_2 price. The CO_2 price influences the high-price hours when gas-fired units in this system define marginal costs. However, this could be any other flexibility option (e.g., hydro pump storage) at a high price level in a different market setting. It should be noted that the flexibility provided by the HPs in the building stock was not considered in the Balmorel calculation. The impact of HP flexibility on the wholesale electricity price was investigated in Schöniger et al. (2022). To every price profile, a hypothetical fixed grid fee plus taxes of 20 cents/kWh were also added in order to derive the retail electricity price. The resulting mean plus standard deviation for all price profiles is provided in Table 3.3. With an increasing CO_2 price, the price profile's mean value and volatility increase. All prices are depicted in Figure 3.10. The sharp increase in Price Scenario 1 is due to the gas shortage at the end of 2021.

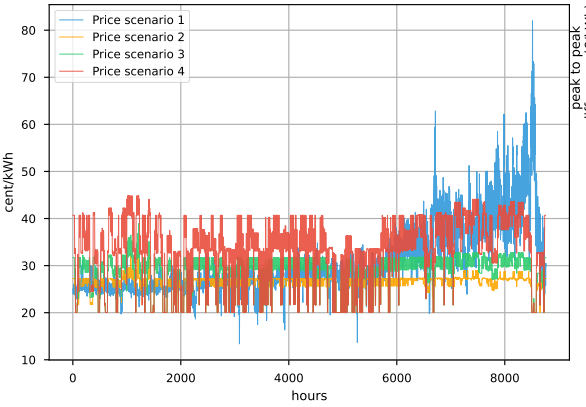

Figure 3.10: Electricity prices used to assess how the volatility influences load shifting behavior.

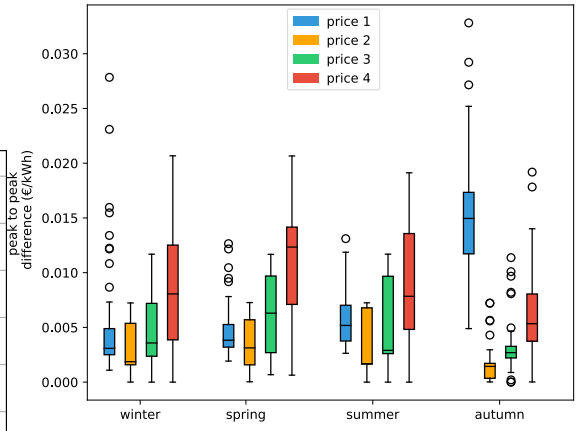

Figure 3.11: Box plots of the daily peak-to-peak amplitude of electricity prices used to examine the impact of prices on load-shifting behavior.

[a]

[a]Box plots show the median (horizontal line) and the interquartile range (IQR) (box outline). The whiskers extend from the hinge to the highest and lowest values within 1.5 × IQR of the hinge, and the points represent the outliers.

Figure 3.11 visualizes the daily peak-to-peak amplitude difference of all four prices. The peak-to-peak difference[12] in the day-ahead price from 2021 increases drastically throughout the year. In the modeled prices for 2030, incisive events, like energy shortages, were not considered; thus, the prices do not fluctuate that much throughout the year.

Another significant difference between the 2021 real-time and the simulated prices is the frequency of change. It is visible in Figure 3.10 that Price 1 is changing more frequently than the others. Table 3.3 shows the number of local maxima in the respective price profiles. The price from 2021 has about twice as many peaks as the prices from 2030 (prices 2, 3, and 4). In Mascherbauer et al. (2024), the focus was on volatility in terms of price spread. Structural price volatility in the form of higher frequency can also significantly impact the potential of load shifting. Studies showed that HPs could

[12]The maximum peak-to-peak difference is defined as the difference between the lowest and the highest value within a day.

participate in the intra-day and even the frequency regulation market (Meesenburg et al. 2020; Manner et al. 2020). But to participate in the regulation market, they must be pooled to reach the necessary capacity (Hülsmann et al. 2019). In this work, participation of residential HPs other than in the day-ahead market is not considered. Thus, price frequencies are limited to hourly changes. Although the thermal inertia of a building is slow, the high frequency of price change generally results in higher cost savings for HPs if they can react to the price signal.

Table 3.3: Mean and standard deviation of the price scenarios and CO_2 price as well as the number of local maxima in the profile. (Mascherbauer et al. 2024)

Price scenarios	mean (cent/kWh)	CO_2-price (EUR/tCO_2)	Number of local maxima
Price 1	30.69 ± 7.76	-	1225
Price 2	26.05 ± 2.27	53	621
Price 3	28.87 ± 3.52	106	646
Price 4	34.11 ± 6.35	212	618

Electricity prices used to analyze the flexibility potential for EU27

In line with the overall scenario narrative for a decarbonized EU in 2050, results of Balmorel are collected from a (Schöniger et al. 2023) with underlying CO_2 prices of 65 EUR/toCO_2 for 2030 and 500 EUR/toCO_2 for 2050 to model the electricity prices in all EU member states. In contrast to the analysis done only for Austria, the electricity grid was modeled using single nodes to represent a country. The weather data used to model renewable generation in Europe until 2050 is described in Section 3.3.4.

As shown in Mascherbauer et al. (2024), the load-shifting behavior heavily depends on both the frequency and absolute price change value. To capture these two statistics, first, we use the number of local electricity price peaks as an indicator to capture the frequency of price changes in all EU27 countries, as shown in Figure 3.12.

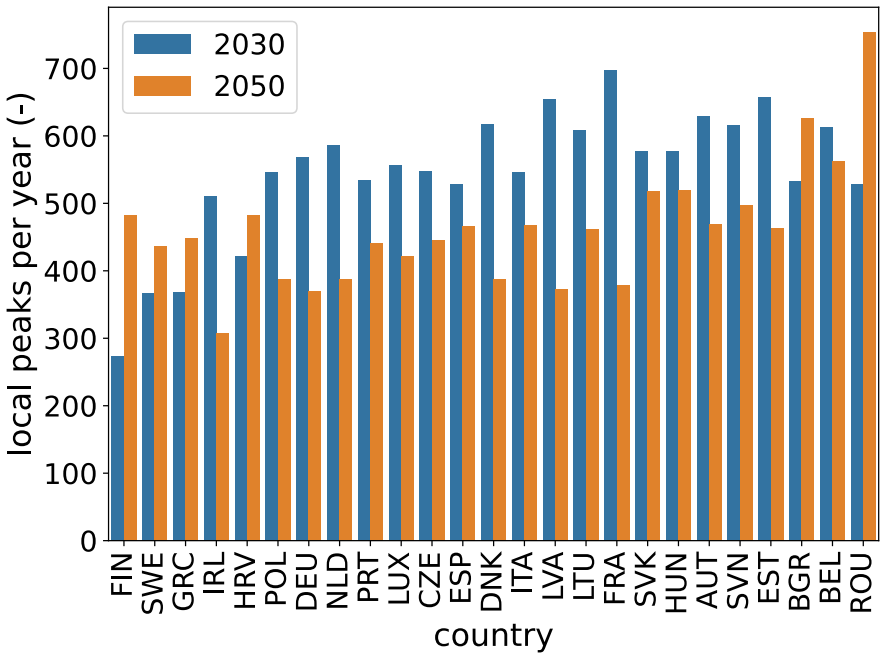

Figure 3.12: Number of local price peaks in each country for 2030 and 2050.

Second, the prominence of these electricity price peaks is calculated, as defined by Equation 3.45. The prominence for peak price at time t is represented by $Pr(t_p)$. It describes how much the local peak price (p_{t_p}) stands out compared to the higher local minimum to the right (p_{t_r}) and left (p_{t_l}) of the local peak with t_l and t_r being the nearest positions to the left and right of t_p where p_t rises again to at least p_{t_p} or ends.

$$Pr(t_p) = p_{t_p} - max(p_{t_l}, p_{t_r}) \tag{3.45}$$

With a high prominence, the effort to shift loads away from a peak increases. Due to the increase of renewable generation in the electricity mix from 2030 to 2050, expensive flexibilities in the power sector (like gas power plants) are not as often needed (Schöniger et al. 2022). Therefore, local price peaks are decreasing in most countries. Overall, the amount of local peaks decreases by 15%. On the other hand, the flexible power plants or storage systems have much higher marginal costs, leading to much higher average prominence of each local peak. At the same time, the average electricity price also increases in 2050 compared to 2030. Since the relative change in price compared to the absolute electricity price is crucial as an incentive for DR, the average prominence of all price peaks is divided by the mean electricity price for each country in Figure 3.13. This way, the indicator shows the load shifting incentive to some extent for each retail electricity price scenario. With a higher average prominence of price peaks over the mean electricity price, DR is more favorable for single prosumagers. In this work, the electricity price signals are distinguished into five scenarios: without grid fees (0 cent/kWh grid fees) and subsequently rising grid fees (5, 10, 20, and 40 cent/kWh grid fees). In the price scenario without grid fees, prices can go down to zero for the end consumers with the effect of an excessive increase in consumption in these hours. This scenario can be seen as an upper limit for the load shifting potential, as load shifting is limited only by physical limitations in these hours. By adding higher grid fees, the prominence of the price peaks is reduced, which has an impact on the incentive to shift electric loads.

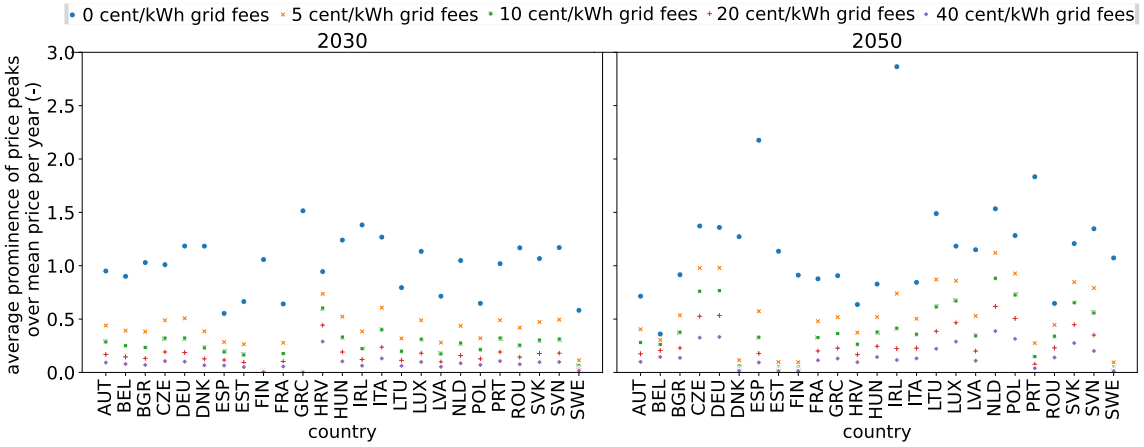

Figure 3.13: Peak price prominence divided by the mean electricity price for the price scenarios from 0 to 40 cent/kWh grid fees.

Figure 3.14 shows that the future electricity systems within the EU are modeled with a high share of PV as wholesale electricity prices tend to decrease between 9 am and 17 pm in almost every country. Additionally, average prices go up in 2050 compared to 2030.

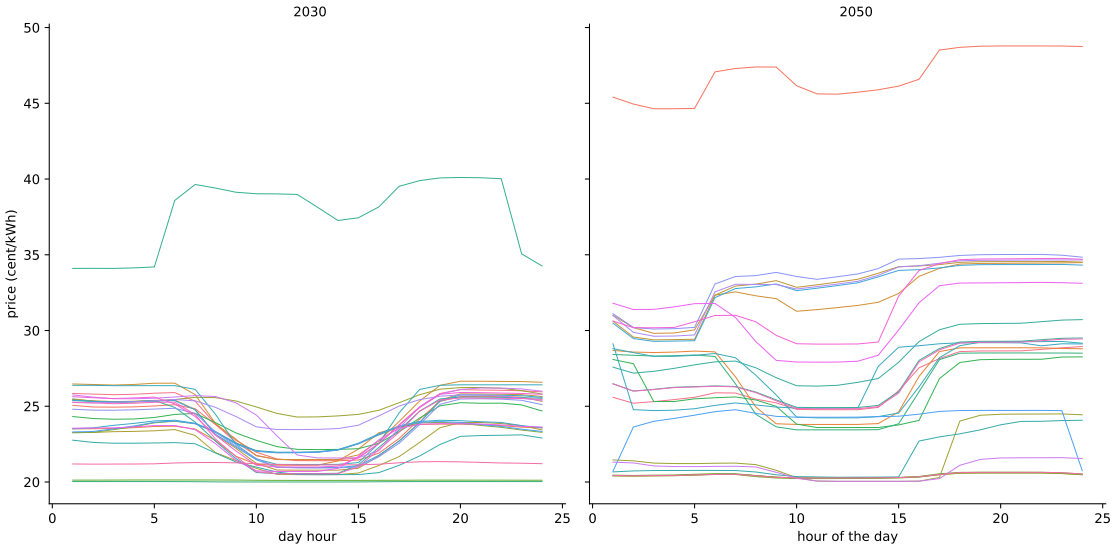

Figure 3.14: Daily mean electricity price for all analyzed EU member states in 2030 and 2050.

On top of the five price scenarios, we study the effect of a capacity-based price on the peak demand. In the EU, 14 countries currently include a capacity-based charge in their distribution grid fees according to the European Union Agency for the Cooperation of European Union Agency for the Cooperation of Energy Regulators et al. 2025. The assumption in the literature is that a capacity tariff can reduce peak loads. They are charged on the yearly or multi-year peak demand or under demand under peak conditions. The assumption in literature is that a capacity tariff can reduce peak loads (as in e.g. Pena-Bello et al. (2021)). To verify the assumption that a capacity component in the variable price can reduce peak demand, a capacity price of 50 EUR per kW peak per year is introduced into the objective function of the prosumagers. The objective function of the prosumager optimization is changed accordingly, as shown in Equation 3.46:

$$\min \sum_t (P_{\text{Grid,t}} \cdot p_t - P_{\text{PV2Grid,t}} \cdot p_{\text{feed in,t}}) + \max_t (P_{\text{Grid,t}}) \cdot p_{capacity} \quad t \in \{1, 2, \ldots, 8760\} \quad (3.46)$$

The capacity price ($p_{capacity}$) of 50 EUR is a representative value, which is certainly not a valid capacity tariff for all countries. Within Austria alone, capacity tariffs differ between 26 EUR and 67 EUR based on the location within the country (E-Control 2016). Still, introducing this tariff gives insights into how peak demand tariffs might influence the peak demand and shifted electricity.

3.3.4 Weather data

The FLEX model uses hourly outdoor temperature and radiation data. As there is no spatial allocation of buildings in each country, weather profiles are downloaded on the NUTS3 level from PV GIS (Huld et al. 2012) and averaged by weighting them with the regional heat demand. The information on regional heat demand is taken from the HOTMAPS Database (Ali Aydemir et al. 2020). The direct and indirect solar radiation is obtained in every celestial direction on a vertical plane, which will then be multiplied by the effective window area of the respective direction to calculate the solar gains.

Weather data for EU27

Weather data for future scenarios is available under (Formayer et al. 2023a) and described in (Formayer et al. 2023b; Schöniger et al. 2024). This work uses data from the Representative Concentration Pathways (RCP) scenario RCP4.5. The RCP4.5 scenario is a stabilization scenario, which means the radiative forcing level stabilizes at 4.5 W/m^2 before 2100 by deploying various technologies and strategies for reducing greenhouse gas emissions. According to this scenario, the cooling demand will rise by 129%, and the heating demand will decrease by 25% until 2100. Contrary to the weather data for Austria, the radiation and temperature data are aggregated by a population-weighted mean (Schöniger et al. 2023). According to this scenario, the average temperature in each country for 2030 and 2050 is visualized in Figure 3.15.

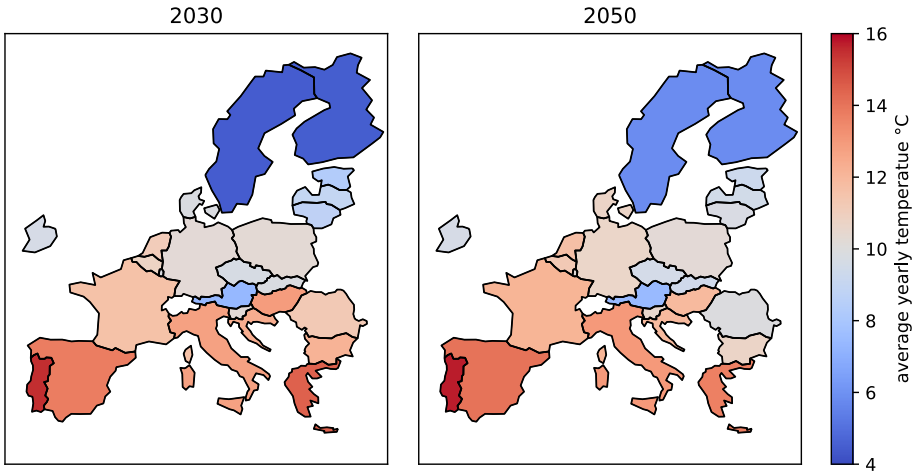

Figure 3.15: Average temperature in each country

3.3.5 Behavior

Finally, the model needs information on the behavior settings. For analysis on a country-level scale, the indoor set temperature is not varied by people being at home or not. For the electricity demand of appliances, an average demand profile (APCS 2019) is used, which is rescaled to the average electricity demand of a resident in each country using data from Eurostat (Eurostat 2024a; Eurostat 2024b). Taking an average profile ensures that no simultaneous behavior is up-scaled to the building stock level, and the optimization does not have information on high-demand events (e.g., cooking, showering), which, in reality, is almost impossible to predict. The same is done for the DHW usage. An average

synthetic profile from HotMaps (Ali Aydemir et al. 2020) is used for the DHW demand and rescaled to the average usage for hot water in each country. The natural temperature of the water is assumed to be 10°C and the supply temperature 55°C.

For the studies conducted on the Austrian building stock (Mascherbauer et al. 2022; Mascherbauer et al. 2024), the average indoor set temperature was assumed to be 20°C. In EU countries, however, the average indoor set temperature varies (Mascherbauer et al. 2025b; Mascherbauer et al. forthcoming). In southern countries, an average indoor set temperature of 20°C is often a strong overestimation. By comparing the heating demand on the country level from the 5R1C model to Eurostat in the year 2020 and also for the years 2030 and 2050 with the average set temperatures in Invert, the indoor set temperature was adjusted to the values in Figure 3.16. The set temperatures for Greece and Portugal are very low, which could be explained by a combination of the discrepancy between the actual building stock properties and the modeled ones, and that people often only heat specific rooms, which reduces the average temperature in the whole building significantly. At the same time, indoor set temperatures in Germany and Hungary are relatively high, which could also be because of heat losses, and with that, the reported energy consumption is higher than the modeled one. The model compensates for this by increasing the average set temperature. Set temperatures in 2050 are higher as the increased insulation and thermal comfort often also lead to an increase in indoor set temperature through the rebound effect (Hens et al. 2010).

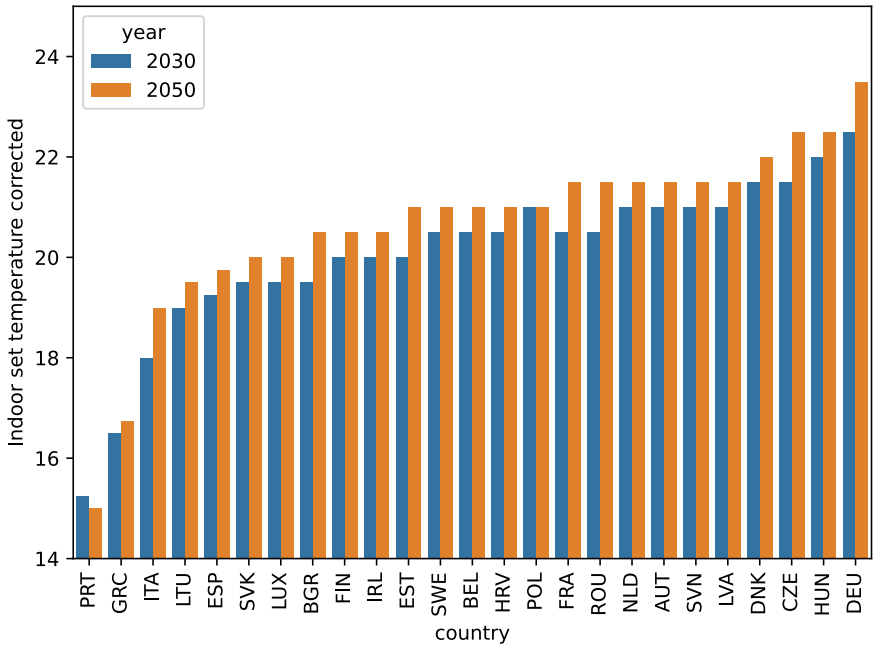

Figure 3.16: Average indoor set temperature in EU member states for 2030 and 2050.

3.4 Usage of the FLEX model on local level

In Mascherbauer et al. (2025a), the FLEX model was applied to two urban regions to assess how prosumaging could impact the electricity distribution grid reinforcement needs. Therefore, this section is based on Mascherbauer et al. (2025a). The rise in the adoption of electrified heating systems, mainly HPs, has been increasing the electricity demand of residential end users, which requires the reinforcement and expansion of the low-voltage distribution grids. This trend also interacts with the diffusion of several other technologies: decentralized PV systems, EVs, and HEMS. Compared with the high-voltage transmission lines, the monitoring and study of low-voltage distribution grids is less understood. It is

hard to predict the impact of multiple technology trends in buildings on the distribution grid. The question arises of how heavily the distribution grid will have to be reinforced in the future to handle the additional burden imposed by electrified heating systems, EV charging stations, and prosumagers. In Mascherbauer et al. (2025a), the grid reinforcement costs in two urban case studies under different scenarios concerning the uptake of electrified heating systems, storage systems, PV, building renovations, and prosumagers until 2050. To do so, the FLEX model is coupled with the Reference Network Model (RNM), a granular spatial model, to calculate the needed investment and operation costs of distribution grids. With this approach, a very high level of granularity and detail, which enables estimating possible future grid reinforcement needs in the distribution grid, was achieved. The two urban areas are located in the north and south of Europe. By linking the two models for the two case studies, the following research questions are answered: First, how are future investments in distribution grids impacted by the decarbonization efforts of the residential building stock? Second, can prosumagers lower these investment costs?

The following inputs for the FLEX model were altered compared to the usage on a building stock level:

- Indoor set temperature: average indoor set temperature is set to not fall below 20°C in heated buildings. Direct electric-heated buildings are an exception; here, the average indoor set temperature is set to 18°C when heating is activated (plugged in), otherwise, the indoor temperature has no lower bound. Direct electric heating systems in this thesis are considered to be plug-in heat ventilators with an efficiency of 1. People use them only at specific times and mostly over a certain period instead of keeping a certain minimum room temperature. I tried to mimic this behavior by not setting a minimum indoor set temperature when the heating is turned off. If heating is turned on, the average set temperature would be set to 18°C. The probability distribution of people using the direct electric heating systems was chosen so that the resulting summed load profiles resemble the shape of actual measured profiles (*esios (https://www.esios.ree.es/es)* 2024).

- Weather data: Air temperature and solar radiation were downloaded from JRC (European Commission Joint Research Centre 2024) for the respective cities on hourly granularity. 2019 was chosen for the weather data, as more recent data was unavailable.

- Electricity price: Day-ahead price for Leeuwarden was taken from the ENTSO-E (Transparency Platform 2024) platform as end consumer electricity prices for 2019 with additional hypothetical grid fees so that the minimum price was at 5 cent/kWh. For Murcia, the actual tariffs for residential consumers from 2019 (*esios (https://www.esios.ree.es/es)* 2024) for the "efficiency 2 periods tariff" of the active energy invoicing price to match the price data with the weather data were used.

Heating systems included in this work are: air source HP, ground source HP, direct electric heating, conventional boiler (including gas, fuel, coal, biomass, etc.), and no heating system at all. The resulting load profiles on a single building level were used as input for the RNM.

3.4.1 Combination with reference network model

The FLEX model was combined with the RNM to model the future grid investment needs in two specific urban case studies. The workflow of the modeling framework included three parts, as shown in Figure 3.17. First, by combining Open Street Maps (OSM) (OpenStreetMap contributors 2017) with other building databases, as well as the scenarios of building renovation and technology diffusion, the building stock map of the two case study regions for the four modeling years (2020, 2030, 2040, 2050) is created. Second, the energy demand of each individual building, as well as the electricity demand of EVs,

are calculated in hourly resolution. Third, taking the building stock map and the energy demand profiles as input, the RNM calculates the distribution grid needs. For 2020, the RNM follows a greenfield approach and generates a reference distribution grid for each case study. Then, for the years 2030-2050, the RNM calculates the enhancement needs of the distribution grid, taking the 2020 grid as a baseline.

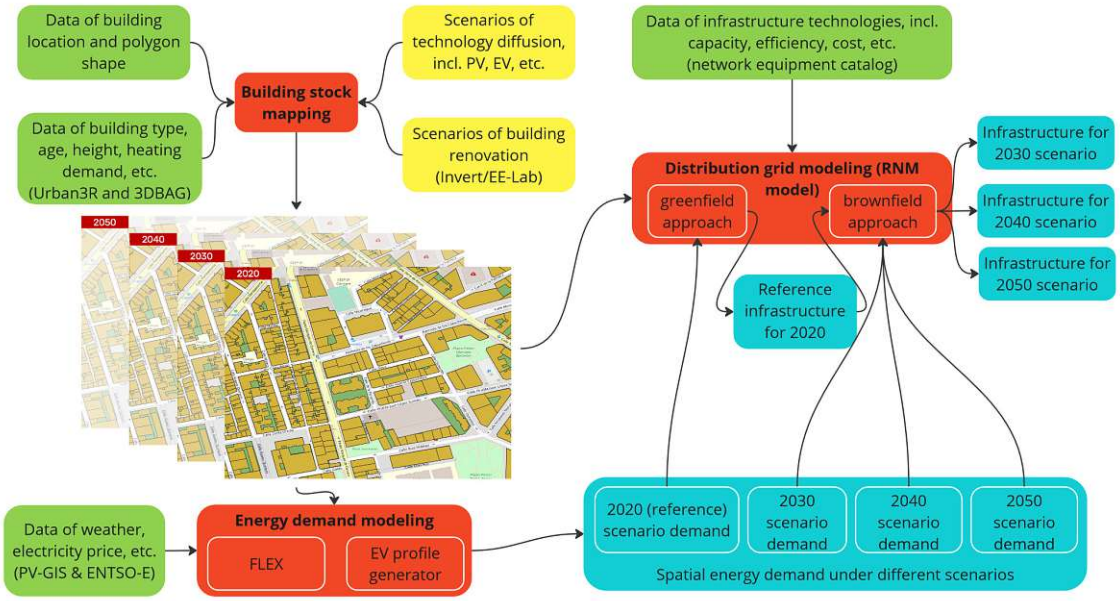

Figure 3.17: Modeling framework used in the publication Mascherbauer et al. (2025a) on local level.

Building stock mapping

Two regions which span over a 10 km^2 area in Murcia (Spain) and Leeuwarden (Netherlands) are selected to represent south and north European climate[13]. These two regions were selected based on the available data resources, their climatic conditions, and the shares of the installed heating systems. This way, results are transferable to similar regions in southern Europe, where buildings are not necessarily heated by gas boilers, and central and north-eastern Europe, where gas boilers dominate the residential heating sector. The building data of each individual building in the two areas are collected and processed as follows:

1. The construction period and other relevant building-related data, like the building age and height, are gathered from local databases (URBAN3R (*URBAN3R* 2025) for Murcia and 3DBAG (Peters et al. 2022) for Leeuwarden).

2. Building footprints were taken from OSM as Urban3R and 3DBag contain only rough estimations of the building shapes.

3. The polygon shapes from OSM are merged with the data from Urban3R and 3DBAG, and the ground area of the OSM shapes is considered as floor area. Non-residential buildings were filtered out if they were labeled as non-residential in one of the databases.

[13]Using EPSG 4326 the coordinates for selecting the areas are:
Leeuwarden: north: 53.2178674080337, south: 53.1932515262881, east: 5.82625369878255, west: 5.76735091362368
Murcia: north: 37.9988137604873, south: 37.9656536677982, east: -1.10710096876283, west: -1.13912542769010

4. Adjacent walls are calculated using a 21 cm overlapping factor. Further, "encapsulated" buildings are ignored. This way it is ensured that small yards, staircases, or rooftop terraces are not considered as small buildings within a building.

5. The number of persons per building was taken from URBAN3R and 3DBAG, respectively. If not available for specific buildings, it was chosen based on HotMaps data (The Hotmaps Team 2020). If the square meter per person in a house were below 20, the number of people for the building was recalculated using a factor of 42.5 m^2/person. This way, it was ensured that faulty data (a very high number of persons per building) would not distort the results.

6. Window areas are evenly distributed, which leads to an over- and underestimation of solar gains, depending on the actual orientation of the windows.

7. Buildings with faulty data (e.g. negative building height) were excluded.

8. At last, a manual inspection was done to exclude large buildings identified as non-residential via Google Maps. Additionally, buildings with a polygon area lower than 45 m^2 were also excluded. This way, small sheds, kiosks, etc. are not considered in the analysis.

As a result, 15 654 buildings in Leeuwarden and 4 447 buildings in Murcia were parameterized. The data was collected for 2019 and 2020 for the two regions since, for these years, all the needed data was available. The building type structure marks a significant difference in the two case studies, wherein in the selected area of Murcia, we have mainly MFHs. In Leeuwarden, most buildings are SFHs and row houses or tiny multi-family buildings (not more than two or three families). The attached wall area of each building to its neighbors was calculated using the polygon shapes. In further calculations, the heat transfer to neighboring buildings was neglected.

To develop the building stocks in future modeling years, data from Invert/EE-Lab (Müller 2015) was combined with open sources, as well as assumptions when data is unavailable. On the building level, only information on the average heat demand per square meter was available for the two regions. This heat demand together with the floor area, building type and construction period (if available) was used to find a the most similar representative building in the INVERT/EE-Lab database. With the U-values from the INVERT/EE-Lab and the dimensions from OSM, 3DBAG, and URBAN3R, the 5R1C parameters were calculated on the building level. Window areas were calculated based on the facade area and the window-to-wall ratio from the selected, most similar representative building.
For the years 2030, 2040 and 2050 random buildings are being renovated until the renovation targets for each building type (SFH, MFH) determined by building stock scenarios are met. The building stock scenarios are described in more detail in the following section 3.4.1. Demolishing and reconstruction of buildings is not considered. The penetration paths of different technologies for the two regions were developed based on open data and scenario assumptions.

Scenarios

For each case study, 12 scenarios were developed, which can be split into three scenario branches (Figure 3.18):

1. I distinguished between a *Strong policy* and a *Weak policy* scenario, which describes the building stock. In the strong policy scenario, climate neutrality within the building stock will be achieved in the year 2050, whereas in the weak policy scenario, policy implementations are left as they are right now, not leading to a climate-neutral building stock in 2050. The strong and weak policy scenarios influence the future

state of the buildings, meaning they determine the rate of renovation and needed heat demand, as well as the rate of installed HPs, PV, and battery adoption.

2. For each policy scenario, there is a scenario with *low*, *medium*, and *high* share of prosumagers. In this way, the impact of prosumagers on future reinforcements needs in the distribution grid is evaluated.

3. EV adoption was added to each scenario, meaning there were two scenarios, one *without EVs* and one *with EVs* (see section 3.4.1). This way, the strong impact of EVs on the electricity grid can be isolated.

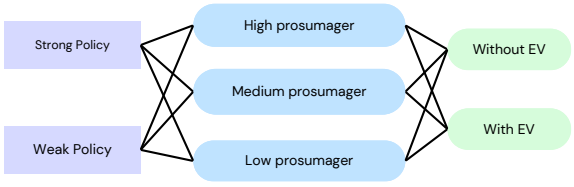

Figure 3.18: Integration of various policy, prosumager, and EV scenarios to form the final 12 scenarios analyzed. (Mascherbauer et al. 2025a)

Policy scenarios

As introduced in Section 3.4.1, two scenario results from Invert/EE-Lab were selected to parameterize the building stocks in the two regions from 2030 to 2050. In the strong policy scenario, it is assumed that more efficiency measures are implemented, and the heating and cooling demand of buildings is lower. Figure 3.19 shows the percentage of installed heating systems for the strong and weak policy scenarios. In both scenarios, the share of conventional heating systems is strongly reduced, and the share of electrified heating systems is increased. In Murcia, already 20% of buildings use air-sourced HPs in 2020. This is because summers are very hot in Murcia, and winters are mild. Many buildings have air-source HPs installed for cooling purposes in the summer. Additionally, a lot of direct electric heating systems (39%) in the base year are installed, which almost do not exist in the Leeuwarden region. In Leeuwarden, conventional heating systems dominated strongly in 2020 and were mainly replaced by HPs in the following years. In the strong policy scenario, the renovation rates (expressed as a percentage of renovated ground floor area per year) are much higher than in the weak policy scenario. 2.3% of all SFHs and 4.7% of all MFHs in Murcia are yearly renovated between 2019 and 2050. In Leeuwarden, the rates are 3.8% for SFH and 3% for MFH. On the contrary, in the weak policy scenario, these rates are 1.4% for SFH and MFH in Murcia and 1% and 0.8% in Leeuwarden. The renovation rates in Murcia are higher because fewer deep renovations and more light-investment renovations are undertaken (e.g., changing windows) because of the mild climate here. In both policy scenarios, the average final energy demand for heating (kWh/m^2) is reduced significantly from 2019 to 2050. In the strong policy scenario, the final energy demand is reduced by 71% in Murcia and by 59% in Leeuwarden. In the weak policy scenario, the heating demand is reduced by 68% in Murcia and 56% in Leeuwarden. Because of the high electrification of the building stock, even with existing policy measures, poorly insulated buildings will be refurbished in the future because it is more economical. This explains the slight difference in savings in heating demand between the strong and weak policy scenarios.

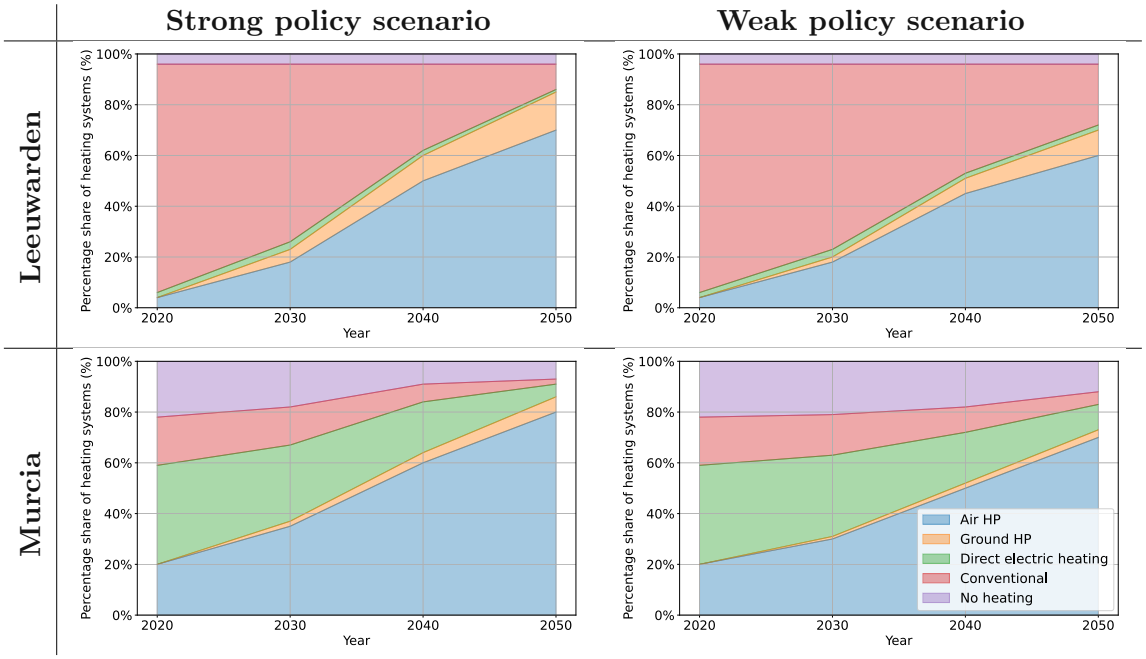

Figure 3.19: Comparison of heating systems for different policy scenarios in Leeuwarden and Murcia. (Mascherbauer et al. 2025a)

The possible options for additional installations in the buildings are shown in Table 3.4. Battery systems are only installed in buildings with PV and heating buffer tanks in buildings that utilize an HP. There is no correlation between the installations of HPs and PVs. The maximum power of the AC was not restricted, assuming that it is sufficiently strong to keep the indoor temperature below a specific set temperature (27°C).

Table 3.4: Possible additional installations for each building. (Mascherbauer et al. 2025a)

Building type	**PV**	**Battery**	**DHW-Tank**	**Heating buffer tank**	**AC**
SFH	0, 5 (kWp) + orientation: maximum yield, east, west	0, 7 (kWh)	0, 300 (l)	0, 700 (l)	Yes, No
MFH	0, 15 (kWp) + orientation: maximum yield, east, west	0, 15 (kWh)	0, 700 (l)	0, 1500 (l)	Yes, No

Table 3.5 shows the assumed distribution of all additional installations. Percentages in the table indicate how many buildings are equipped with the respective technology. Batteries are only installed in buildings with PV, thus the percentage of buildings with a battery refers to all buildings with a PV. The same applies to the buffer tank, which is only installed in buildings with HP. The number of installed PVs rises more in the strong policy scenario. In the weak policy scenarios, I estimated a higher percentage of AC than in the strong policy scenarios due to lower investments in building refurbishments and passive shading systems, increasing the need for active cooling. The percentage of installed PV systems is the same in both regions, whereas the AC adoption differs due to the different climate zones. Thermal and battery storage shares of all buildings are the same in both case studies. The percentage of installed battery systems varies slightly in the strong and weak policy scenarios.

Table 3.5: Building technology adoption in the scenarios. (Mascherbauer et al. 2025a)

	Leuuwarden / Murcia			
Building Technologies	2020	2030	2040	2050
AC (strong policy)	20% / 50%	30% / 60%	50% / 80%	70% / 90%
AC (weak policy)	20% / 50%	35% / 65%	60% / 80%	80% / 95%
PV (strong policy)	2% / 1.5%	15%	40%	60%

Table 3.5: Building technology adoption in the scenarios. (Mascherbauer et al. 2025a)

	Leuuwarden / Murcia			
PV (weak policy)	2% / 1.5%	10%	30%	50%
DHW tank	50%	55%	60%	65%
Buffer tank	0%	5%	15%	25%
Battery (weak policy)	10%	12%	16%	25%
Battery (strong policy)	10%	12%	20%	30%

Prosumager scenarios

Regarding the shares of prosumagers, the assumptions for the two regions are the same, as shown in Table 3.6.

Table 3.6: Share of prosumagers in the prosumager scenarios. (Mascherbauer et al. 2025a)

	Leuuwarden / Murcia			
Scenarios	2020	2030	2040	2050
Low	0%	5%	10%	20%
Medium	0%	10%	30%	50%
High	0%	15%	40%	80%

EV scenarios

Two types of input data are used to generate the EV load profiles in future scenarios with the methodology presented in Section 3.4.1:

- *Building data*: building coordinates, building type, and number of households per building from Section 3.4.1. In addition, the prosumager shares in Table 3.6 are considered.
- *Mobility data*: survey data on the number of cars per household, EV adoption targets, probability distribution of arrival times, and cumulative density function of daily distance driven.

The number of cars per household in Table 3.7 is determined based on car ownership survey data for Leeuwarden (Centraal Bureau voor de Statistiek 2024) and Murcia (Instituto Nacional de Estadística 2024). The penetration of EVs in 2030 has been set in accordance with national objectives for EVs outlined in National Climate and Energy Plans (European Commission 2024). In 2050, it is assumed that all light-duty vehicles will have zero emissions, and battery-electric vehicles will remain the dominant technology in this segment.

Table 3.7: Probability distribution of number of cars per household for Leeuwarden and Murcia. (Centraal Bureau voor de Statistiek 2024; Instituto Nacional de Estadística 2024)

Number of EVs per household	0	1	2	3+
Leeuwarden, NL	46%	33%	16%	5%
Murcia, ES	18%	46%	28%	8%

Each vehicle's arrival time and daily distance traveled are assigned based on probability distributions. Figure 3.20 illustrates the probability distribution of the times at which EV owners arrive home, based on public mobility data from cell phone terminals in Spain (Ministerio de Transportes y Movilidad Sostenible 2024) and a sample of private EV charging sessions in the Netherlands (Elaad Platform 2024). Figure 3.21 shows the cumulative density function of the distance Murcians traveled daily. This distribution is

derived from the number of daily trips and individual trip distances in Murcia (Ministerio de Transportes y Movilidad Sostenible 2024). In the absence of granular data for Leeuwarden, the same distribution is used as the average distance driven in a day is comparable for both regions.

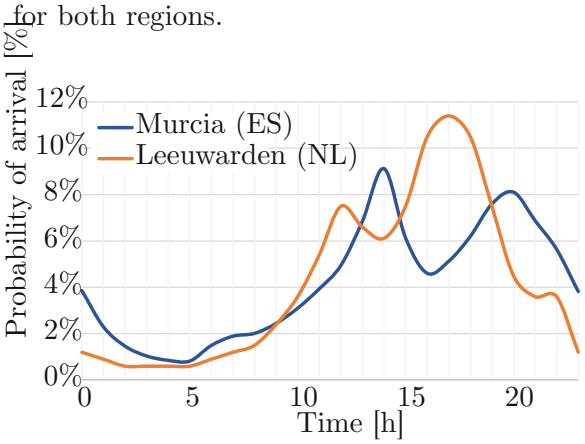

Figure 3.20: Probability distribution of arrival times. (Mascherbauer et al. 2025a)

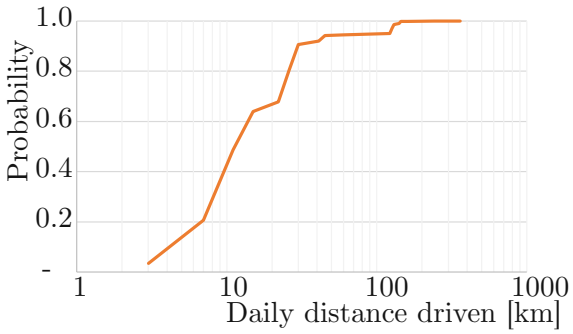

Figure 3.21: Cumulative density function of daily distance driven. (Mascherbauer et al. 2025a)

EV profiles generator

Currently, EVs represent the most viable option for decarbonizing light-duty vehicles. The main challenge for characterizing hourly EV residential charging profiles in future scenarios is that the availability of data on residential EV charging is scarce (Calearo et al. 2021). Although there are few datasets and studies for early-adopter regions, such as Norway (Å. L. Sørensen et al. 2021; Å. Sørensen et al. 2023), a stochastic profile generator for residential EV charging based on the available building and mobility data in the regions of interest was developed. This methodology also estimates future EV penetration levels and the locations of EVs within residential areas. Figure 3.22 presents the flowchart of the proposed methodology, which follows similar steps to (Unterluggauer et al. 2023; Sørensen et al. 2022; Fischer et al. 2019).

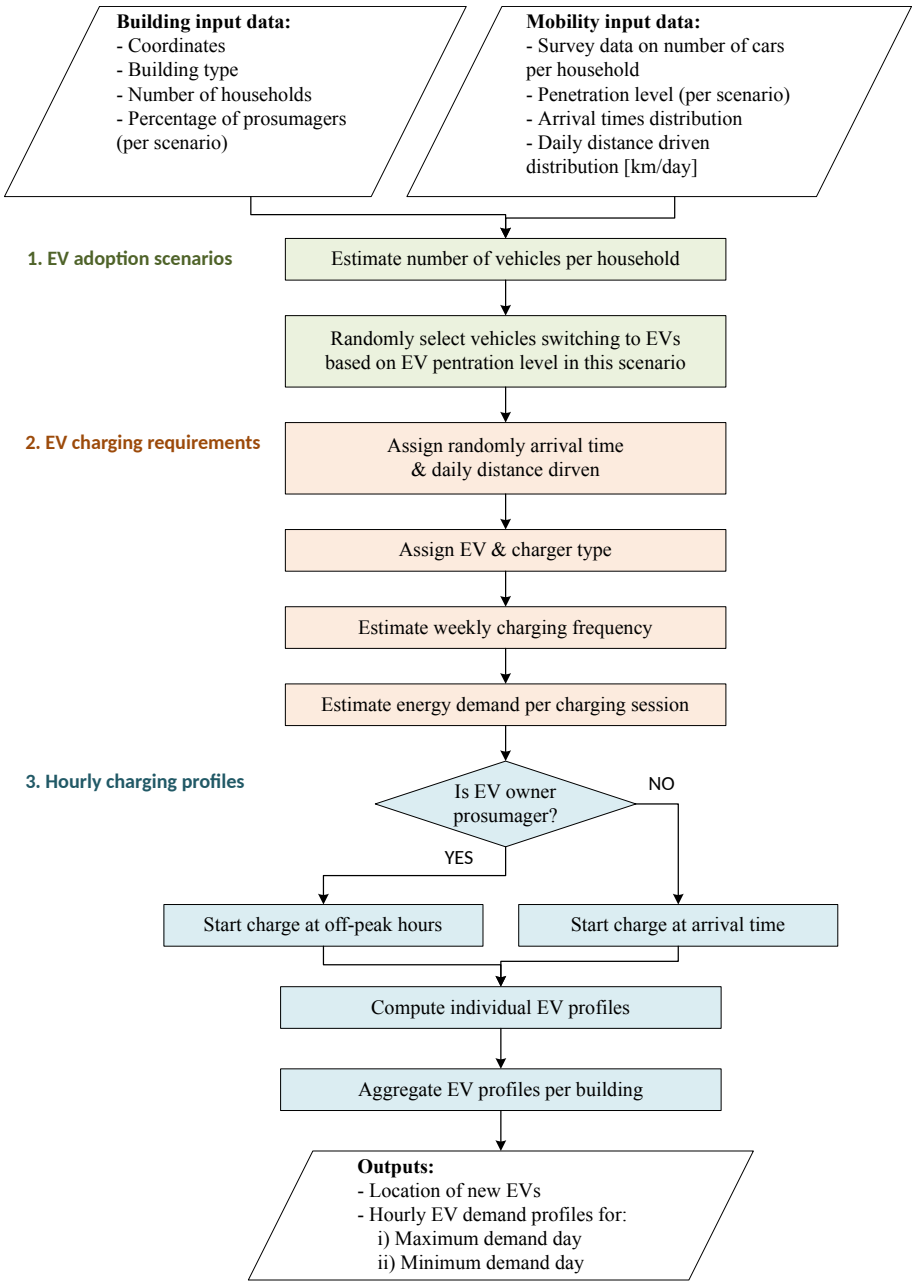

Figure 3.22: Flowchart of residential EV load profile generator model. (Mascherbauer et al. 2025a)

The model is structured into three stages:

1. *Modeling of EV adoption scenarios:*

   The first stage of the model determines the number of EVs and their location. The number of cars per household is estimated based on national surveys of car ownership per household. These surveys are used to characterize a probability distribution of the number of cars per household. Then, a random selection of car owners opting to transition from internal combustion engine vehicles to EVs is performed based on the projected EV penetration level for a specific year and scenario. EV adoption rates are estimated in accordance with objectives set by national authorities within the designated regions.

2. *Characterization of EV charging requirements:*

   The second step is to characterize the charging needs of each EV. In each scenario, each vehicle's arrival time and daily distance traveled are assigned based on proba-

bility distributions. Then, the type of charger and the weekly charging frequency are assigned following the methodology in Gonzalez Venegas et al. (2021), which employs the daily energy demand of each EV as the primary input. Three AC charging power levels are considered: 3.6 kW, 7.2 kW & 11 kW. The weekly charging frequency allows for the calculation of the energy that is charged per session. While the majority of their charging needs are met at home chargers, EVs may occasionally charge at public charging points. A factor representing the charging demand met at public charging stations is incorporated into the model. This factor is set to 20% in 2030 but is increased to 30% in 2050, reflecting that early adopters have more consistent access to residential chargers.

3. *Modeling of hourly charging profiles:*

   A question that has not been sufficiently addressed in other models (Unterluggauer et al. 2023; Sørensen et al. 2022; Fischer et al. 2019) is how to establish the scenarios with the highest and lowest electricity demand from residential EVs for planning the distribution grid. For instance, synchronization of EV charging could happen due to low end consumer electricity prices or the night before a national holiday (Unterluggauer et al. 2022). It is, therefore, assumed that, in the worst-case scenario, all EV owners will decide to charge on the same day. This does not imply that all EVs will charge simultaneously, as the diversity in the arrival times is still considered. On the other hand, for the scenario with the lowest EV demand, it is assumed that only EVs charging six or seven days per week will be charging that day, as they may be unable to postpone their charge to the next day.

   The last step is to compute the hourly demand profiles for the EVs. If the EV owner is a prosumager, it is assumed that its charger is capable of smart charging and can delay the charging session to off-peak hours with lower electricity tariffs. Otherwise, the EV will commence charging as soon as it is connected to the charger. Finally, the hourly demand profiles for EVs in the same building are aggregated.

3.4.2 Distribution grid modeling

The resulting load and feed-in profiles for every building computed with FLEX and EV profiles generator models are provided as input to the RNM to estimate the necessary electricity distribution grid investments in future decarbonization scenarios. Two representative days are considered to plan the distribution networks:

- Day with the highest electricity peak load (a winter day)
- Day with the highest peak feed to the grid (a spring day)

The RNM, introduced by Mateo et al. (2011), plans the layout of low voltage (LV), medium voltage (MV), and high voltage (HV) lines together with the positions and capacity of distribution transformers and substations. The objective is to minimize the distribution system costs while satisfying topological and quality of supply constraints. First, the RNM in greenfield mode obtains a synthetic model of the initial distribution grid for the base case (2020). Then, the RNM in brownfield mode reinforces this initial grid to accommodate the new loads (e.g., HPs, EVs, etc.) and PV installations in each future scenario.

Greenfield planning of "existing" distribution networks

In the base 2020 scenario, the RNM is employed to generate a synthetic model of the existing electricity distribution networks in the areas of interest. The greenfield planning functionality of the RNM allows for the design of a cost-effective distribution network to supply all consumers and distributed generators in a particular area while complying

with voltage and thermal limits and geographical and reliability constraints. This model has been utilized to develop European large-scale synthetic grids from scratch in Mateo et al. (2018a) and to plan the distribution network of new urban districts (De Rosa et al. 2024). Even though the complete distribution grid at the country level is not modeled, the analysis remains reliable and replicable, as the conditions of individual feeders are not solely considered, which is a common approach in this field.

The inputs to the RNM are the buildings' location and their load and generation profiles, the location and charging profile of EVs, the layout of street maps, a catalog of standard electrical equipment (e.g., power lines, distribution transformers, etc.), and general configuration parameters. The catalog of standard equipment considers reference unitary investment and operation and maintenance (O&M) costs for electricity distribution equipment in Spain (Boletín Oficial del Estado 2024b).

The objective of the greenfield RNM is to minimize investment, energy losses, and O&M costs throughout the network's lifespan. It employs a bottom-up methodology whereby LV, MV, and HV grids are planned sequentially. The initial step is to identify and size the supply points (e.g., MV/LV distribution transformers, HV/MV substations, etc.) for each voltage level. Subsequently, the routing and capacity of power lines are planned. The initial configuration of the power lines, a minimum spanning tree connecting all buildings to the supply points, is not always feasible. In such cases, the configuration is modified to comply with geographical and technical constraints. These constraints are primarily street layouts, voltage and thermal limits, and reliability indices. For the grid in Murcia, the load-based reliability indices used are the equivalent interruption time of installed power (known by its Spanish acronym: TIEPI) and the equivalent number of interruptions of installed power (known by its Spanish acronym: NIEPI) (Boletín Oficial del Estado 2024a), which are the Spanish equivalent to Average System Interruption Duration Index (ASIDI) and the Average System Interruption Frequency Index (ASIFI) defined in IEEE (2022).

The output of the greenfield RNM is the techno-economic parameters for each designated distribution network component and a detailed report of their cost by component type and voltage level. In addition, it provides geographic information system data for all network components, which can be used to represent these grids on a map (see Figure 3.23).

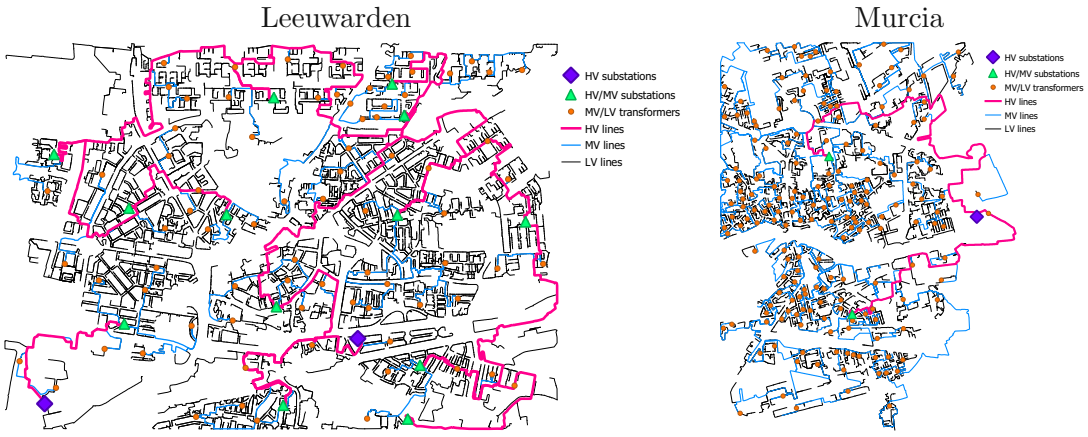

Figure 3.23: Greenfield grid in 2020 for Leeuwarden (left) and Murcia (right). (Mascherbauer et al. 2025a)

Brownfield planning of distribution networks under future policy scenarios

The initial grids for each area of interest obtained with the greenfield RNM serve as a reference for the brownfield RNM to plan cost-efficient distribution network reinforcements needed to accommodate the new demand and distributed generation expected in future scenarios. This methodology has been employed to assess the impacts of high penetrations of DERs on the distribution grids, including batteries (Mateo et al. 2016), solar PV self-consumption (Mateo et al. 2018b), and EVs (Martínez et al. 2021). However, this methodology has not previously been applied to assess the long-term impact of electrification policies (e.g., energy-efficient buildings, HPs, EVs, PV installations, etc.), nor to quantify the effect of an increasing share of prosumagers on the electricity grid infrastructure.

The brownfield functionality of the RNM proceeds similarly to the greenfield approach. The main difference is that an initial network is already provided to the brownfield RNM. Then, it connects new consumers and distributed generators to the initial network. The initial network configuration is improved using branch exchange to make it technically feasible at the minimum cost.

A limitation of the brownfield RNM is that while it optimally plans new locations of supply points (e.g., MV/LV distribution transformers) for new consumers, it can only increase the capacity of current elements to meet the additional demand of existing customers. This may lead to unrealistic numbers of parallel elements in long-term scenarios with very high demand and generation growth. This effect is seen in the 2040 and 2050 scenarios in Leeuwarden. Additional MV/LV distribution transformers were provided as input to the brownfield RNM to improve the results in these scenarios.

3.5 Limitations of the modeling approach

The FLEX model has been extensively tested to ensure that the 5R1C approach yields realistic results concerning the thermodynamic behavior of the model. Additionally, the impact of having perfect foresight of the model is analyzed and compared to a more realistic rolling horizon approach. All details are provided in the Appendix A.3.

Within Appendix A.3.1, it was shown that the 5R1C model does not adequately model buildings with floor heating systems, and thus, their potential to shift electricity demand is underestimated. In the European building stock, however, the majority of buildings are heated using radiators as heat distribution systems (ehi 2023) and most HPs in the EU so far have been installed in new and retrofitted buildings (JRC 2023). This is unlikely to change, as deep renovations, where the heating distribution system is changed, are very capital-intensive. The supply temperature for radiator heating systems can be lowered through adequate renovations to a degree where air-sourced HPs can sufficiently supply the building. In a high percentage of the current building stock, the supply temperature could already be lowered to 55°C or lower, according to Pothof et al. (2023), who measured flow temperatures in over 200 Dutch dwellings. Also in Cozza et al. (2022) it was shown that already 40% of buildings would be ready for a HP implementation in Switzerland. Thus, the author expects that in the future, existing buildings switching to HPs will, in most cases, keep their radiator heating system. It was also shown that the error of estimating the shifted energy is the highest in buildings that are the least likely to have HPs installed, namely buildings with low mass and bad insulation. By extending the 5R1C model to a 6R2C model in Appendix A.3.2 by adding a second capacity and a sixth resistance, the model's ability to simulate the thermal behavior of buildings with floor heating was improved. The results indicate that buildings with floor heating systems can shift 1.4 to 5.2 times more electricity than the 5R1C model predicted. At the same

time, shifted energy demand is slightly overestimated by the model, because it assumes a perfect forecast.

Using perfect foresight causes the FLEX model to overestimate cost savings and load shifting potentials. To address this, a rolling horizon approach was tested and compared to the perfect foresight in Appendix A.3.3. The results showed that incorporating the terminal cost for the thermal mass's state at the end of the horizon window was crucial for achieving better results with the rolling horizon approach. At the same time, it was not beneficial to include a terminal cost for thermal storage and batteries at the end of each horizon window. A 3-day rolling horizon approach showed that a longer forecast horizon could better manage the uncertainty in energy prices. It was shown that the optimization using a rolling horizon approach can achieve similar results as an optimization with a perfect forecast if implemented with sufficient large horizon windows. Additionally, terminal cost for storage need to be implemented if the storage is large enough to affect operation beyond the horizon window.

Other limitations apart from the model itself are the absence of grid capacities and the spatial distribution of loads at the country level. Both the Flexibility Factor and GSC are supposed to show "grid-friendliness"; however, without knowing the spatial distribution of the loads, possible grid congestion is not considered. Therefore, the author would describe the meaning of these factors as system friendliness because, regarding the grid, no well-founded statement can be made. Also, with this approach, the active DR is not factored into the electricity price. In Sperber et al. (2025), it was shown that the DR of residential HPs could impact the price. Similarly, since the FLEX model is not coupled directly to an electricity grid model, it remains unclear if a potential demand increase from a collective response of prosumagers can actually be supplied. The author trusts that the wholesale electricity price and the residual load are strongly correlated (correlation factor of 0.8) as shown in Klein et al. (2016) and Klein et al. (2017).

4 Results

In this chapter, the results of the FLEX model are separated into four sections. In the first Section 4.1, the results focus on the Austrian SFH building stock and are based on the publication Mascherbauer et al. (2024). It discusses the impact of higher volatility in hourly prices induced by higher CO_2 prices, and analyzes how this higher volatility reflects in yearly savings for single prosumagers and how much energy can be shifted by single prosumagers. The section mainly focuses on answering RQ2.

In Section 4.2, results from Mascherbauer et al. (2022) on the PV self-consumption and change of energy consumption of prosumagers are presented. This section mainly relates to RQ1.

While the first two sections focus on single prosumagers and an analysis of the Austrian case, in Section 4.3 the future potential of prosumagers at the EU Member State level is presented based on the publications Mascherbauer et al. (2025b) and Mascherbauer et al. (forthcoming). In this section, both RQ1 and RQ2 are addressed. It is shown how strongly the flexibility potential depends on grid tariffs, and the change in grid-related factors is presented. These factors include the Flexibility Factor, peak demand, and the GSC.

Finally, in Section 4.4, RQ3 is addressed by presenting the results of two local urban case studies and the impact of prosumagers on the electricity distribution grid based on Mascherbauer et al. (2025a). The future cost increase for reinforcing and operating the distribution grid is assessed under different scenarios with a focus on the question of whether prosumagers can lower these costs.

4.1 Impact of electricity prices on load shifting in Austria

The investigation on the hourly price to shift electricity is answered in the second publication Mascherbauer et al. (2024) of which the results are presented in this section. The analysis was done on a single building level (Section 4.1.1) and the Austrian SFH building stock (Section 4.1.2). At last, the economic viability of prosumagers under different price scenarios is analyzed in Section 4.1.3.

4.1.1 Analysis on single building level

First we look at a single SFH which is a typical modern SFH in the Austrian building stock built after 2010. The building has a floor area of 170 m^2 and a useful energy demand for space heating of 45 W/m^2. The thermal capacity of this building is low and the insulation level high compared to older buildings in the building stock. Then, the same building is simulated with a 400l DHW storage, and a 750l space heating buffer storage to show the difference in load shifting potential by implementing thermal storage. In Figure 4.1 the grid electricity demand for a building in the 12^{th} week is visualized for 4 different electricity prices. The prices are visualized and described in chapter 3.3.3. The three load profiles represent the load if: 1) no load shifting is happening (reference), 2) load shifting without any thermal storage (HEMS no storage) and 3) load shifting with a DHW and heating

buffer storage (HEMS with storage). On the right-hand y-axis, we see the electricity price profile. The 12th week is shown because during this period price 1 is similar to prices in the years prior to 2021.

Looking at the price scenarios 2, 3, and 4 we see that the higher price difference only increases the incentive to shift loads marginally when thermal storages are available. Without thermal storage, the peak loads during low energy price times are limited by the maximum indoor set temperature. With higher price volatility, the building is pre-heated to a greater extent if possible.

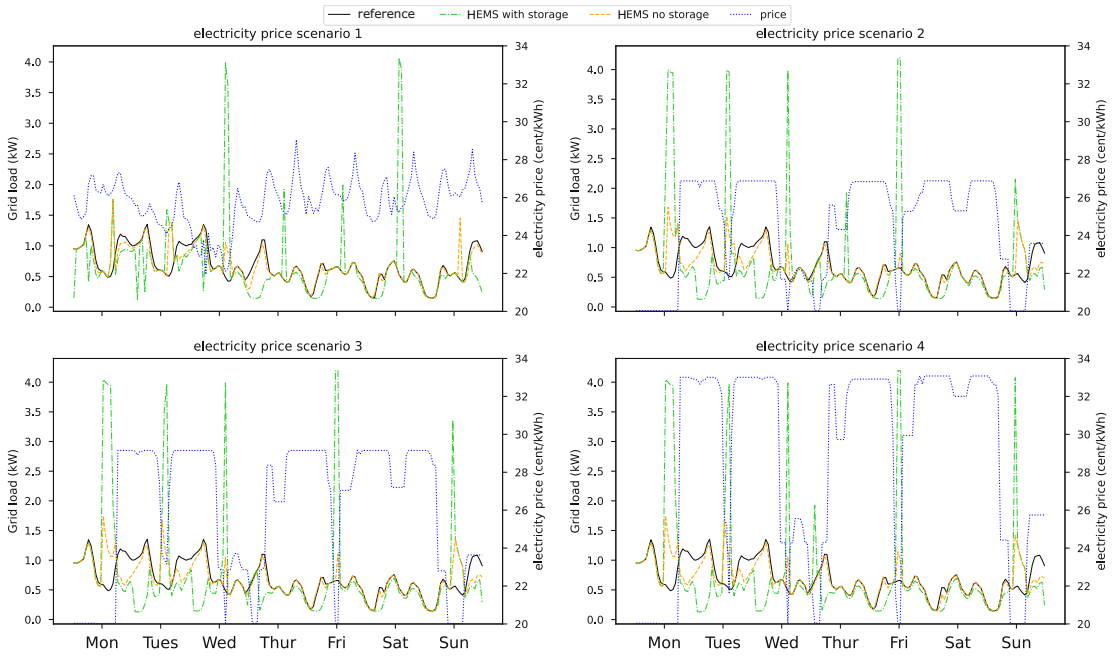

Figure 4.1: Electricity bought from the grid with and without HEMS in the 12th week of the year. The electricity price is visualized on the right-hand axis. Mascherbauer et al. (2024)

Figure 4.2 shows the amount of electricity bought at a specific price. In the reference case, electricity is bought independently of the price. But when the building is optimized, electricity is bought at lower prices and demand is reduced at higher prices. In price scenarios 2,3, and 4 the amount of electricity purchased from the grid when the price is at its lowest almost doubles when the building has the thermal storages implemented. Even without thermal storage, the increase in electricity consumption at lower prices and the decrease at higher prices are visible.

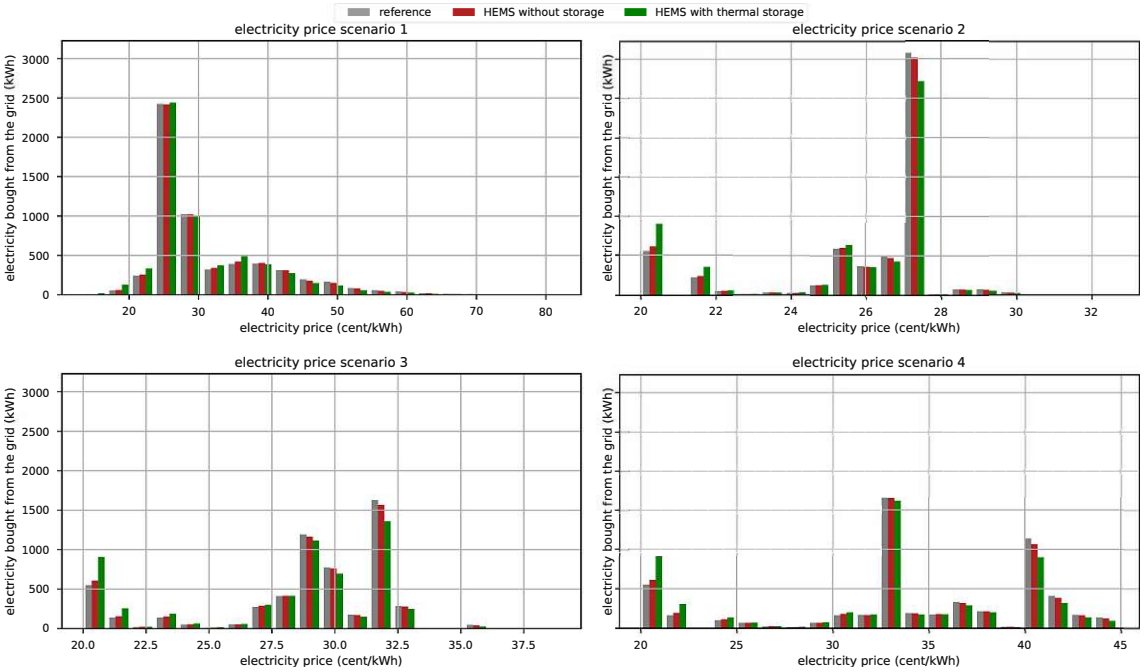

Figure 4.2: Electricity demand at certain prices in the reference case and with the implementation of HEMS. "With thermal storage" indicates that the house has a 750 l buffer storage, and a 400 l DHW storage. Mascherbauer et al. (2024)

The maximum average indoor set temperature was varied between 23, 25, and 27°C during winter to investigate the sensitivity of the allowed indoor set temperature bandwidth for pre-heating. Figure 4.3 shows that higher electricity price volatility increases the incentive to shift energy by pre-heating the building. Comparing the price scenarios 1 to 2,3 and 4, we see that price 1 creates a greater incentive to shift load than price 2 and 3. This is due to the nature of the price profiles. Price 1 is changing much more frequently than the other three prices. But with the implementation of thermal storage, shifted demand is much higher in the price scenarios 3 and 4. The thermal storages compensate for the lower frequency of price changes by storing much more energy over a longer period of time with lower losses. The correlation between the allowed indoor temperature bandwidth and the energy shifted by the optimization is not linear because of the increase in thermal losses with higher indoor temperatures.

If the building has installed thermal storages, the shifted energy rises to around 450 kWh/year in the first price scenario. This result is in line with Fitzpatrick et al. (2020) where a building with 310m^2 floor area, 2000l buffer storage, and 400l DHW storage shifts a maximum of 1370 kWh of electric energy. The allowed indoor temperature is still impacting the total amount of shifted load even though the load shifting is done predominantly by the storages. The amount of energy that is shifted with the implementation of thermal storages is by a multitude higher in this case. The absolute amount of shifted energy through thermal storages is almost independent of the building type. Buildings with higher thermal mass and higher energy demand can shift more electricity through the thermal mass. Thermal storages are prioritized for load shifting because the losses are smaller in most cases. Thus, any price change that would incentivize a house to pre-heat will give an even higher incentive to shift load via the thermal storage. Although thermal storages efficiently shift energy with minimal losses, using a building's existing thermal mass provides a low-cost way in terms of investment costs if storages are not already installed.

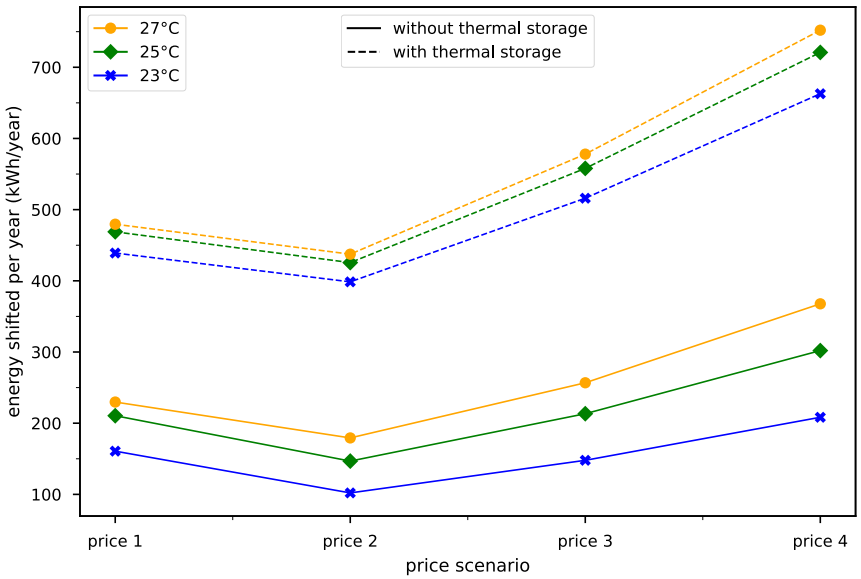

Figure 4.3: Energy shifted over one year in the building with no thermal storage and the building with DHW storage and buffer storage. The temperatures represent the maximum allowed indoor temperatures during winter. Mascherbauer et al. (2024)

4.1.2 Analysis on Austrian SFH building stock

In dependence of the four electricity price signals, the potential load shift for the whole SFH building stock in Austria is presented in the following. The total amount of electricity shifted over one year in each price scenario is visualized in Figure 4.4 on the left side. In this case only the thermal mass of the buildings is used for load shifting. The potential of the building stock to shift load via HPs is around 20 GWh when considering the price from 2021. This corresponds to approximately 1.5% of the electricity consumed by these buildings within the same time period. The increasing volatility in price scenarios 2, 3 and 4 leads to a significant increase in electricity being shifted showing that variable price profiles can give an increasing incentive to shift loads. On the right hand side of Figure 4.4 the maximum daily peak-to-peak difference of the aggregated load profiles of SFH with HP in the Austrian building stock is visualized. The reference case represents the peak-to-peak demand for the case of no DR. In literature, it is often mentioned that load shifting will result in an even higher peak demand (Nicolas Kelly et al. 2014). In the resulting aggregated load profiles, this effect is only marginally visible except in autumn. The electricity price in 2021 is becoming so volatile and high that daily peak-to-peak loads are significantly higher than the reference and all the other scenarios. The peak-to-peak difference of all HP heated SFH buildings in Austria reaches a maximum of 350 MW. The peak demand in the Austrian grid is in the magnitude of 80 GW. Therefore potential of the shifting electricity through the thermal mass of SFH is small but not neglectable.

As shown before, buildings with implemented storage capacities can shift a lot more electricity. To see how strongly storage capacities can influence the peak-to-peak difference on a daily basis and the overall shifted demand a scenario where every single building with an HP has a 750l heating buffer storage and a 400l DHW storage was generated. The real market penetration of hot water storage in HP-operated buildings in Austria is unknown. The following results serve as a benchmark. In Figure 4.5 we can see that the peak-to-peak difference is more than two-folding compared to the reference, reaching 700 MW. Also peak demand is reached throughout the year independent of the price scenario. However the occurrence of high peak-to-peak demands increases with increasing price volatility. The total amount of electricity shifted rises to 74 GWh in price scenario 1 which is almost four times higher than without thermal storage capacity.

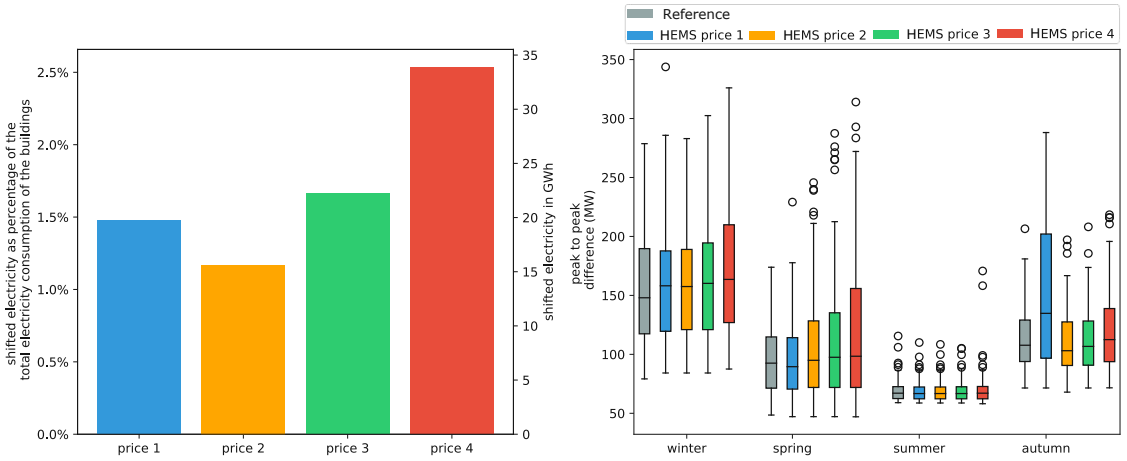

Figure 4.4: Left: Amount of electricity shifted throughout the year based on the different price scenarios in Austria. Right: Box plots of seasonal effect in grid demand, based on daily peak-to-peak amplitude difference. Mascherbauer et al. (2024)

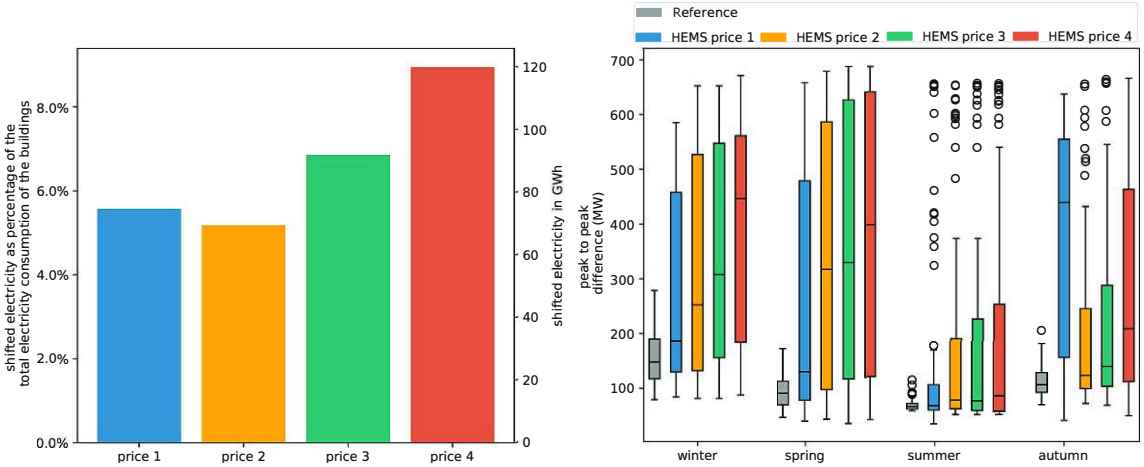

Figure 4.5: Left: Amount of electricity shifted throughout the year based on the different price scenarios with buildings having thermal storages in Austria. Right: Box plots of seasonal effect in grid demand, based on daily peak-to-peak amplitude difference. Mascherbauer et al. (2024)

The results show that HPs can effectively shift electricity through the thermal mass. Peak loads increase only marginally for buildings without any storage capacity. Thermal losses that occur and indoor set temperature constraints limit the maximum peak power when optimizing such buildings' heating demand. However, with available storage, the peak-to-peak demand can more than double. This is especially relevant when HP penetration in a certain region is very high, and HPs are operated with the same strategy. This problem can be avoided by providing different price incentives for users. It is therefore crucial that the price signal reflects electricity scarcity in such a system. Overall the results show that there is significant potential for DR in the residential building stock. This potential can increase even further in the future depending on decarbonisation ambitions and energy scarcity. Furthermore, the potential for the thermal mass is bigger if temporarily cooling down buildings to a certain temperature (e.g. 18°C) is considered as well.

4.1.3 Economic viability of prosumagers using the thermal mass

DR without any additional incentive is unlikely to be done by homeowners from an economic point of few as shown in Mascherbauer et al. (2024). The annual operation cost savings for SFHs using only the thermal mass to shift their demand is below 25€ per year. The four prices are the same as in the previous section and are described in Section 3.3.3. In Figure 4.6, the annual operation cost savings for each SFH building type in Austria are visualized without any thermal storage. With a higher volatility in price change, the economic optimization of HP becomes more lucrative. The optimization is less lucrative for modern buildings. These buildings are characterized by lower thermal mass and a higher degree of insulation. Thus, they have a much lower heat- and electricity demand. The same reason accounts for the difference between air source and ground source HP since the ground source HP is more efficient. Because of the high volatility in the 2021 price profile at the end of the year, the implementation of a HEMS is more lucrative in the buildings compared to the second price profile. A sensitivity analysis showed, that with prices prior to 2021, economic gains through prosumaging were always lower than in the second price scenario. The annual operation cost reductions are generally between 2 and 23€ depending on the price profile and the energy demand of the house. If these buildings had a 750 L heating buffer and a 400 L DHW storage, the cost reductions would rise between 5 and 95€ without taking any investment costs into account. Therefore, implementing a HEMS into buildings that would use only the thermal mass for demand shifting must be very cheap (between 10 and 100€, depending on the building type) to yield return of investments after, for example five years. Without additional monetary incentives, homeowners are unlikely to tap into the potential of load shifting through the thermal mass alone. This finding is in accordance with other studies that suggest that the additional investments by individual buildings will not be compensated by participating in DR (Härkönen et al. 2022).

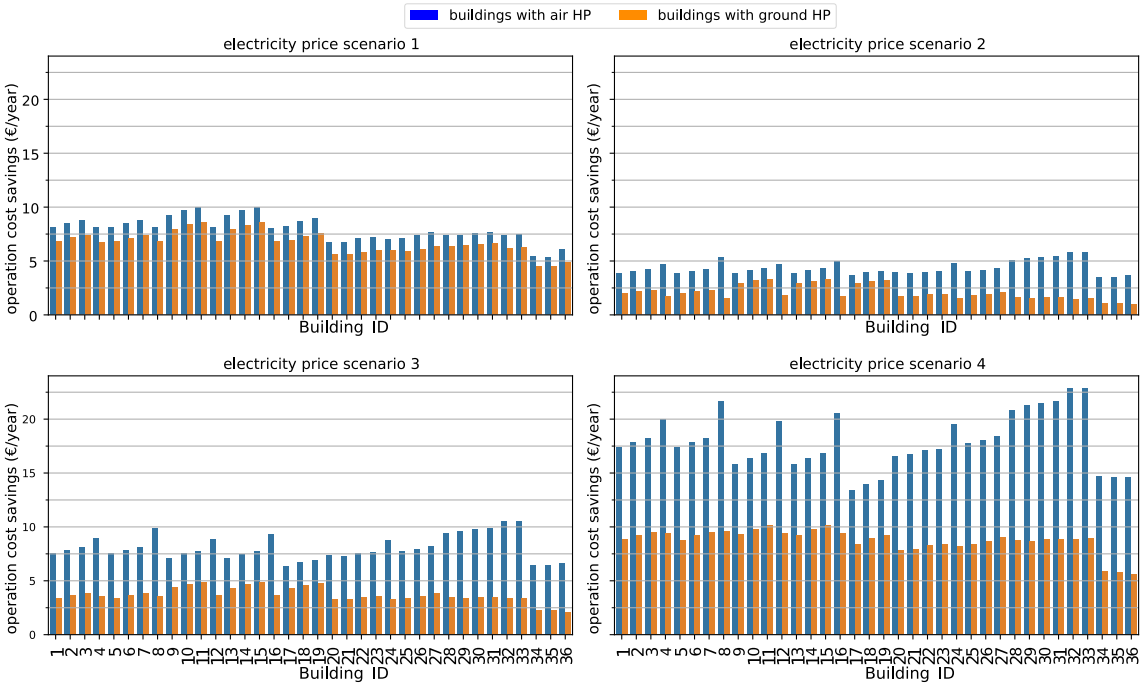

Figure 4.6: Operation cost savings per building type and HP type in all four electricity price scenarios. Mascherbauer et al. (2024)

Analysis for MFHs resulted in similar cost savings percentage wise, meaning for the single homeowners the annual savings are also small. In literature it is often suggested that DR using HPs could alleviate grid stress. However, to tap into this potential, prosumagers

will likely need an additional reimbursement. The potential impact of prosumagers on the distribution grid will be analyzed in section 4.4.

4.2 Change in grid- and PV self-consumption of prosumagers in Austria

In this section it is investigated how potential prosumagers change their PV self-consumption and grid demand. The results are taken from Mascherbauer et al. (2022). Two different price scenarios are investigated (see Section 3.3.3), a flat and a variable electricity price. Eleven representative SFH for Austria were modeled with different installations regarding PV, battery and buffer heating tank (Mascherbauer et al. 2022). Every building was modeled with each possible combination of hot water tank, PV and battery resulting in 528 simulations and optimizations for a specific price scenario. Figure 4.7 illustrates the PV self-consumption rate for these 528 simulations under reference and optimization modes with a flat price profile.
Buildings with PV increase their PV self-consumption as the optimization minimizes electricity bought from the grid. The increase in self-consumption is especially prevalent in buildings that do not have a battery installed which already increases self-consumption significantly without any optimization (see Figure 4.7 in the bottom right). The self-consumption rates for the SFHs with a 5 kWp and 10 kWp PV system without battery are around 32% and 22%, respectively. They will be increased to 47% and 31% when battery is available without optimizing the energy consumption. These results are in the range consistent with existing studies (Yildiz et al. 2021; Luthander et al. 2015). Obviously, the self-consumption rate is zero for all building configurations that do not have a PV system. With a 10 kWp PV, the overall consumption rate drops compared to the 5 kWp PV because electricity surplus can not be utilized. The impact of thermal storage on self-consumption rate is limited, similar to the battery. Results show that the self consumption rate is not heavily dependent on the building type and its energy demand although buildings with a higher heating and subsequently electricity demand naturally will have a higher self-consumption rate.

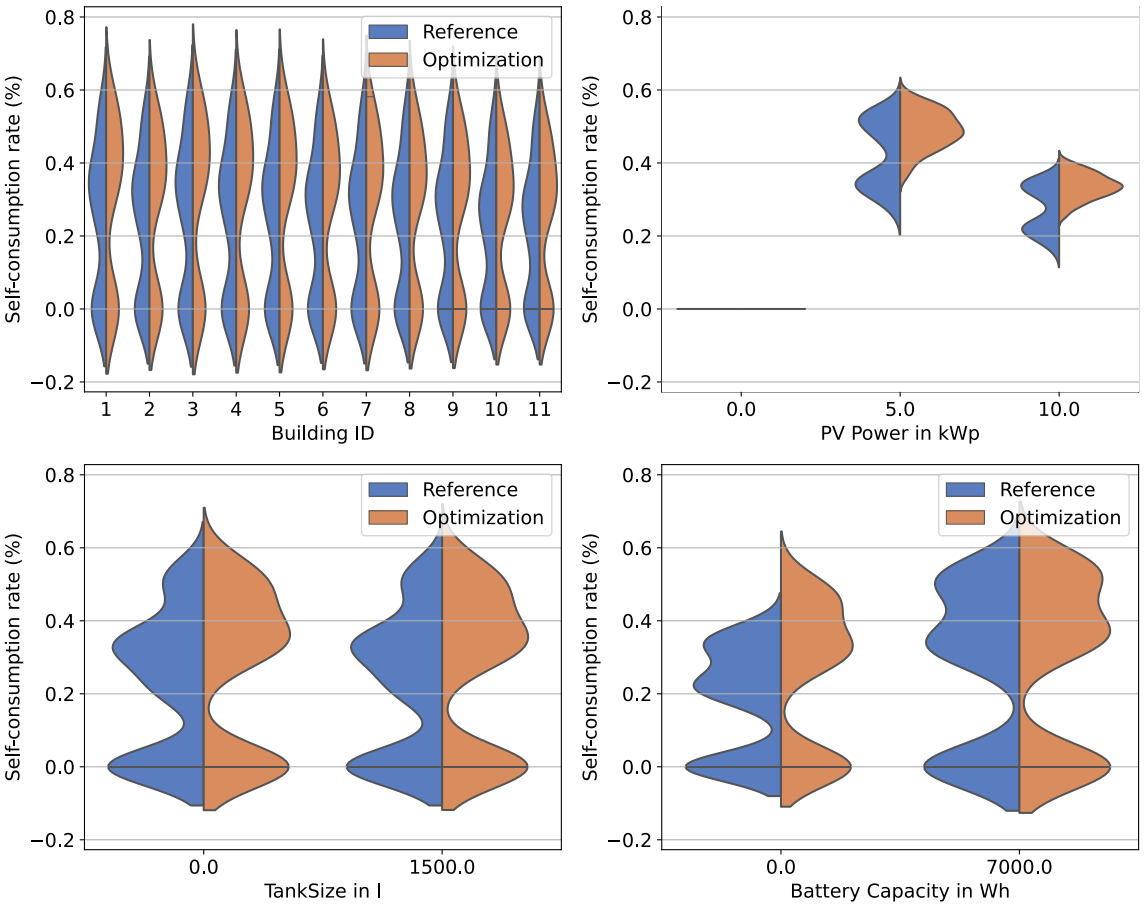

Figure 4.7: Impact of HEMS on PV self-consumption rate of individual SFH (flat price) in Austria (Mascherbauer et al. 2022)

Buildings having a PV and maximizing their self-consumption under a flat electricity price scenario naturally decrease their grid electricity consumption. Figure 4.8 shows the electricity demand of SFHs in Austria under a flat electricity price with different configurations. First, as shown in the top-left plot, buildings with better insulation demand less electricity from the grid, and optimization can further reduce this amount. The maximum annual decrease of grid-electricity consumption through the optimization is 40.69%, which is found for a well-insulated building (ID = 11) equipped with a 10 kWp PV (no battery), an AC, a ground source HP, and thermal storage. Second, the adoption of PV significantly reduces the grid-electricity consumption, and the larger size of PV leads to lower grid-electricity demand (up-right). Third, as shown in the left bottom plot, the thermal storage has limited impact on the optimization results. The key reason is that, when the PV generation is higher in summer, space heating is not needed, so the optimization will not save the excess PV-generation in the tank. The thermal tank is only used by the buildings with 10 kWp PV systems because they generate enough electricity to be stored in the tank in winter. The use of the battery (bottom right) results in much lower electricity demand in the reference mode for buildings with PV as most of the surplus electricity can be stored and used. In the optimization mode, the difference is not significantly visible because the optimization can also utilize other storage potentials (eg. pre-heat/cool the building) when no battery is available. If the optimization is performed on buildings without PV under a static electricity price, a minimum decrease in grid electricity consumption can be observed as air source HPs shift their consumption very slightly based on the hourly COP which varies based on the outside temperature.

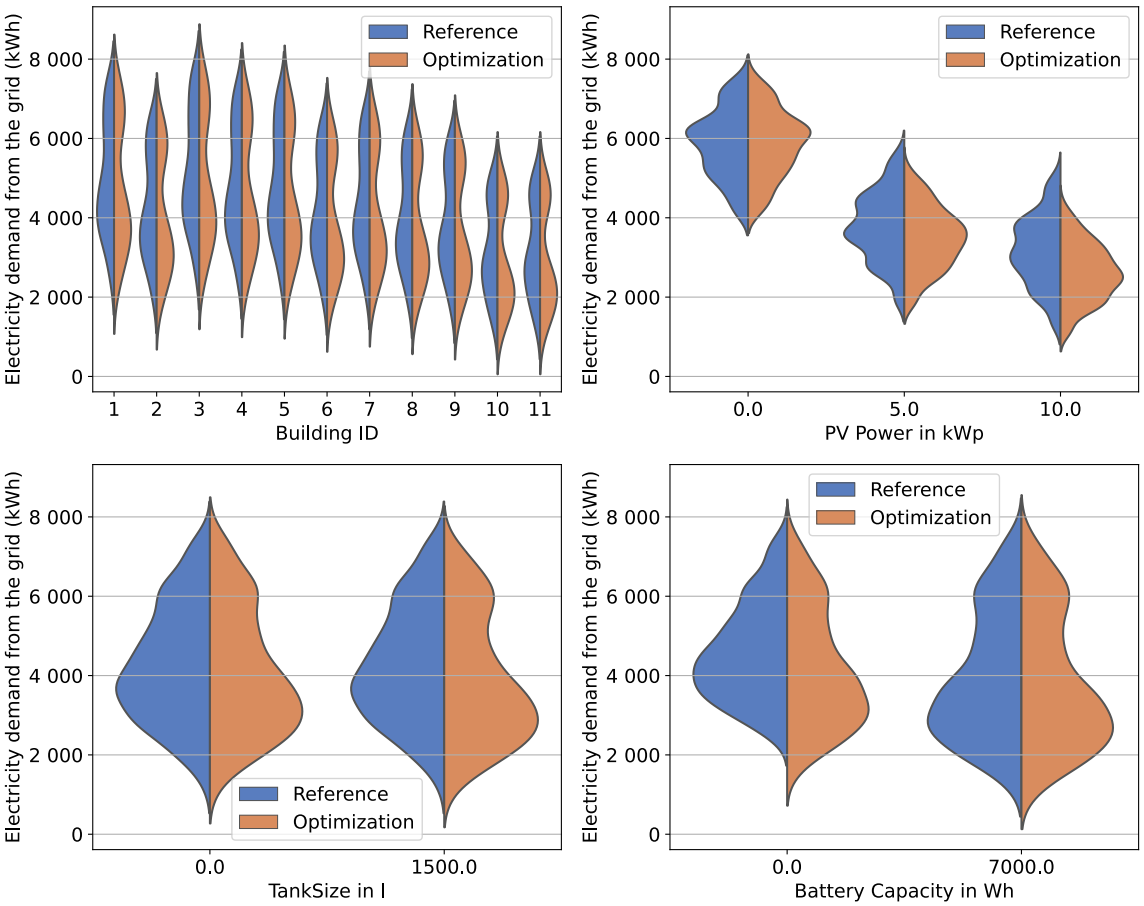

Figure 4.8: Impact of HEMS on grid-electricity consumption of individual buildings (flat price) in Austria.The height of the violin represents the distribution. The width represents the density of plotted results for different buildings. Mascherbauer et al. (2022)

The violin plots showed that the optimization impacts the total yearly energy consumption and increase the PV self-consumption rate depending on the installed appliances. In the following the Austrian SFH building stock was grouped into 10 groups defined in Chapter 3.3.1. Each group represents the Austrian SFH buildings stock with certain installations (PV, Battery (B), hot water tank (T)). The number of buildings with the specifications shown in Figure 3.3 are broken down by percentage into the individual building classes. Subsequently, the results are calculated for all building classes with the respective specifications in the optimization and reference mode. Tank sizes were either zero or 1500l, PV size zero, 5 and 10 kWp and the battery had a capacity of zero or 7 kWh. Table 4.1 shows these ten building configurations with the corresponding change in yearly energy demand if all buildings with this configurations were optimized with a flat or variable electricity tariff. Buildings with no PV don't change their consumption with a flat price signal optimization. But they increase their consumption by 1% with a variable price. The variable price used in this scenario is from 2016 and described in Section 3.3.3. The absolute values of changes in yearly grid electricity demand are very different within the different the number of buildings in each group varies strongly (see Figure 3.3). The resulting electricity demand is shown in Figure 4.9. The bars represent the total electricity demand from the grid on a logarithmic scale. The percentage change in grid-electricity consumption through the optimization of each configuration is shown on the right-hand axis for both price scenarios. The absolute values of these percentages are the ones presented in Table 4.1. The grid-electricity consumption is reduced by 7.4% and 17.9% for a 5 kWp PV and a 10 kWp PV (flat price) and by 7.2% and 17.8% (variable price), respectively, without any storage implemented. This highlights the potential of utilizing thermal mass as storage. The variable price leads to a higher utilization of

the thermal storage to bridge high prices and thus the percentage decrease of electricity consumption is less for those houses. In total, the optimization can lower the annual grid-electricity demand by 10.4 GWh or 6.8 GWh for the whole investigated building stock under the flat and variable price scenarios, respectively.

Table 4.1: Grid-electricity consumption increase and decrease for buildings with certain configurations (unit: MWh) in Austria

Building configuration	Flat [MWh]	Variable [MWh]	Building configuration	Flat [MWh]	Variable [MWh]
PV0B0T0	0	1451	PV0B0T1500	0	1796
PV5B0T0	-1587	-1551	PV5B7T0	-5	1
PV5B0T1500	-4275	-3946	PV5B7T1500	-32	-22
PV10B0T0	-270	-268	PV10B7T0	-1	-1
PV10B0T1500	-574	-555	PV10B7T1500	-4	-3

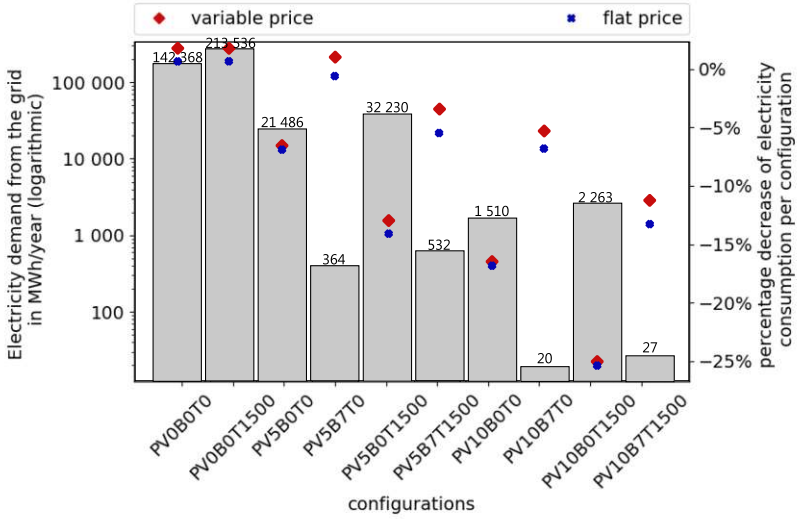

Figure 4.9: Impact of HEMS on grid-electricity consumption of the building stock in Austria. Mascherbauer et al. (2022)

The decrease in grid-electricity demand is solely due to the higher self-consumption of PV. Especially buildings without any kind of storage system increase their self-consumption when becoming prosumagers. Figure 4.10 shows the aggregated self-consumption rate of buildings with different configurations. The grey bars represent the results from the reference mode. In the reference mode thermal storage is not utilized, thus the buildings with a thermal storage show almost the same increase in self-consumption rate as buildings without a thermal storage. With larger PV sizes the self-consumption rate for buildings with buffer tanks would surpass the ones of buildings which shift their demand using the thermal mass. For buildings with a battery storage, the HEMS does not result in such a high increase in self-consumption because the battery already increases self-consumption significantly in the reference mode. The difference in self-consumption increase between the flat and the variable price signal is minimal and can be neglected as the feed in tariff is too low for the optimization to not maximize self-consumption.

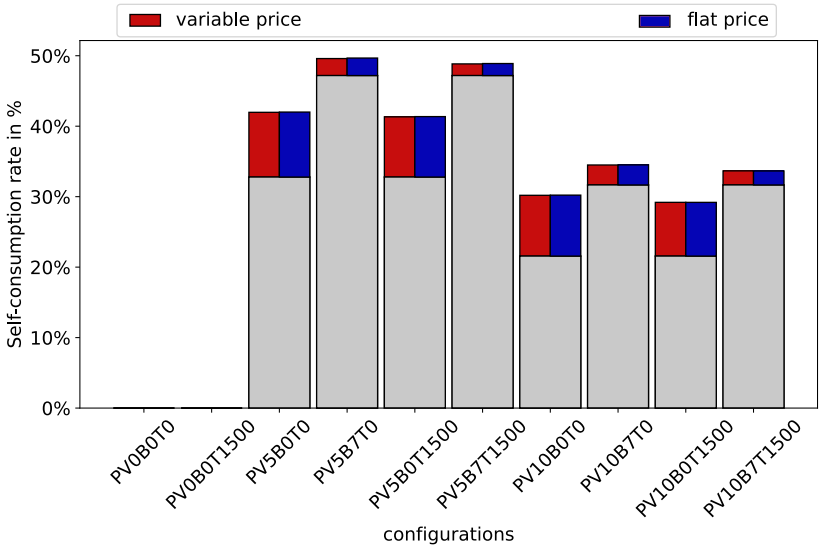

Figure 4.10: Impact of HEMS on PV self-consumption rate of the building stock in Austria. Mascherbauer et al. (2022)

The analysis of the single buildings showed that electricity demand reduction is only significant for buildings with PV installed and no battery. This also accounts for buildings that are optimized under an hourly electricity tariff. The total electricity consumption will rise through losses during load shifting, however the increase in PV self-consumption reduces the total annual demand for those buildings. Any building without PV will increase its electricity demand from the grid through DR. On SFH building stock level the total electricity demand reduction using optimization would be around 6.7 GWh and 3 GWh for flat and variable prices respectively. This is in the range of 0.8-1.5% of the total electricity demand of these buildings. DHW tanks were not considered in this analysis which would have a similar effect as the batteries. The self-consumption would not be increased as much through the optimization. That being said, the total possible reduction in energy demand through optimization of all HP operated SFH buildings in Austria is probably slightly overestimated because many buildings owning a HP will very likely also have a DHW storage installed.

4.3 Analysis on EU level

For the analysis of the EU member states, the building stock data was modeled with the model Invert/EE-Lab as described in Section 3.3.1, and prices were modeled using the Balmorel model (see Section 3.3.3). The following shows how prosumaging in the EU could affect specific grid friendliness indicators, the overall electricity demand, peak consumption, and how the flexibility potential changes throughout the year. In this evaluation, the electricity prices are distinguished into five scenarios: without grid fees (0 cent/kWh grid fees) and subsequently rising grid fees (5, 10, 20 and 40 cent/kWh grid fees). In the price scenario without grid fees, prices can go down to zero for the end consumers with the effect of excessive increase in consumption in these hours. This scenario can be seen as an upper limit for the load-shifting potential. Additionally the effect of a capacity price on the peak demand is investigated within this section. The results presented in this section are based on Mascherbauer et al. (2025b) and Mascherbauer et al. (forthcoming).

4.3.1 Shifted electricity demand

The shifted electric energy share (see Equation 3.37) through residential buildings visualized in Figure 4.11, is high in central Europe in countries with relatively high heat demand (Austria, Germany, Czech Republic) and high volatility in electricity prices. The northern countries exhibit a low amount of shifted energy share because their price spreads are low, and it is not lucrative for them to shift demand. Additionally, the shifted energy share is low due to the high heating demand. Portugal, on the other hand, shows a high shifted electric energy share despite low price volatility. This is because heating demand in Portugal is very low, hot-water production has high share of the total consumption and can be easily shifted throughout the year using DHW storage. Increasing grid fees decreases the share of shifted electric energy in the residential sector. With higher grid fees, the relative cost of thermal losses increases, and thus, the price spread has to be higher to offset these losses. The difference between the relative shifted electricity demand in 2030 and 2050 is counterintuitive since the heating demand declines overall due to the underlying climate change in the weather scenario and the better insulation of buildings. Also, the standard deviation of the prices increases from 2030 to 2050. However, the frequency of changes in price decreases in 2050 compared to 2030 by about 15%, which leaves less opportunity for the buildings to shift their demand. Additionally, the mean wholesale electricity price increases from 2030 to 2050, leading to the same effect observed when grid fees increase. However, what can not be observed in Figure 4.11 is that the absolute amount of shifted electricity in 2050 is higher than in 2030 (see Figure 4.16), depending on the scenario simply because a lot more buildings have HPs installed.

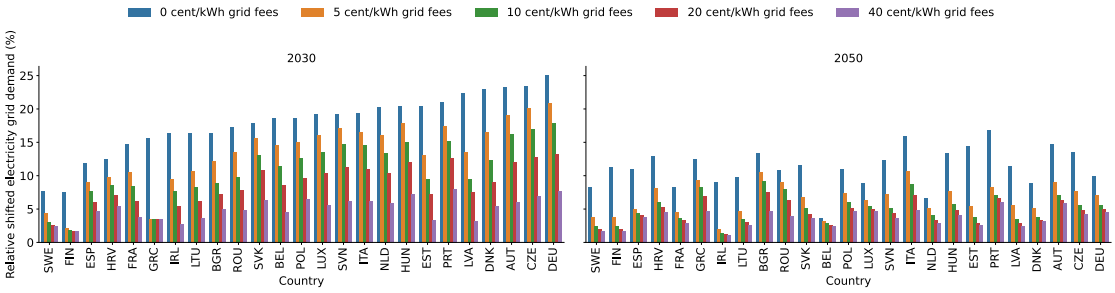

Figure 4.11: Shifted electric energy share of all buildings with HPs in each country in 2030 and 2050.

Looking at the average daily grid demand of prosumagers in Figure 4.12, it is evident that even though some buildings have a PV, the main consumption increase occurs at midday when PV production is at its peak. Electricity prices at this time are often low due to the surplus of PV production (see Figure 3.14). Therefore, prosumagers effectively increase the share of renewable energy, mainly PV, into the grid. This, of course, underlies the assumption that the grid constraints allow it to do so and that enough excess renewable production is available. Looking at the mean price over a day, it becomes clear that the electricity price will generally be higher in 2050, reducing the shifted demand. With higher grid fees, demand shifting is reduced, and the average normalized grid demand moves closer to the reference case.

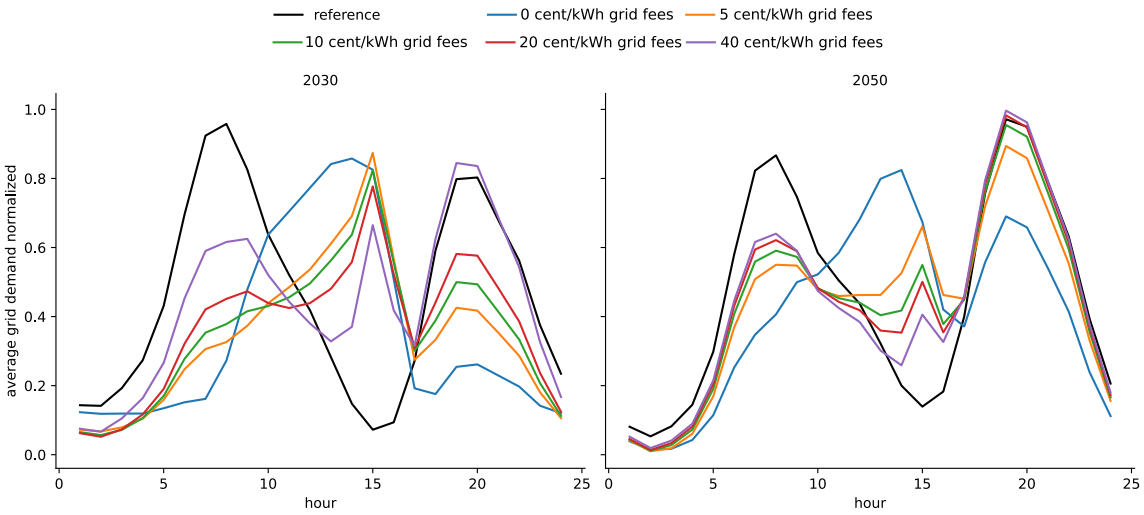

Figure 4.12: Daily average of the normalized grid demand comparison between residential consumers (reference) and prosumagers over all EU Member States.

For the 20 cent/kWh grid fee scenario, Figure 4.13 and 4.14 show how much demand is shifted daily, summed up over all the countries. The countries are color-coded after their average temperature, shown in the legend as a map. Positive values represent an increase in demand for prosumagers compared to their consumer counterpart at certain hours of the day. In contrast, negative values represent a decrease in demand in other hours. Note that the daily decrease and increase in demand are not equal because of losses and increased self-consumption of PV. In Figure 4.13, it is assumed that 10% of all prosumaging buildings have an AC installed. The shifted electricity is much lower in summer than in winter, as mainly DHW consumption can be shifted. If the share of cooled buildings is increased to 80% which is visualized in the shifted electricity is increased in Summer, with buildings shifting the cooling demand by pre-cooling the indoor environment. The cooling consumption overlaps well with PV generation, leading to a higher PV self-consumption rate in southern countries. However, the majority of electric energy is still shifted in winter due to the heating demand. Most cooling-induced demand is already covered by locally produced PV in the reference case, so increasing the share of cooled buildings has a limited effect.

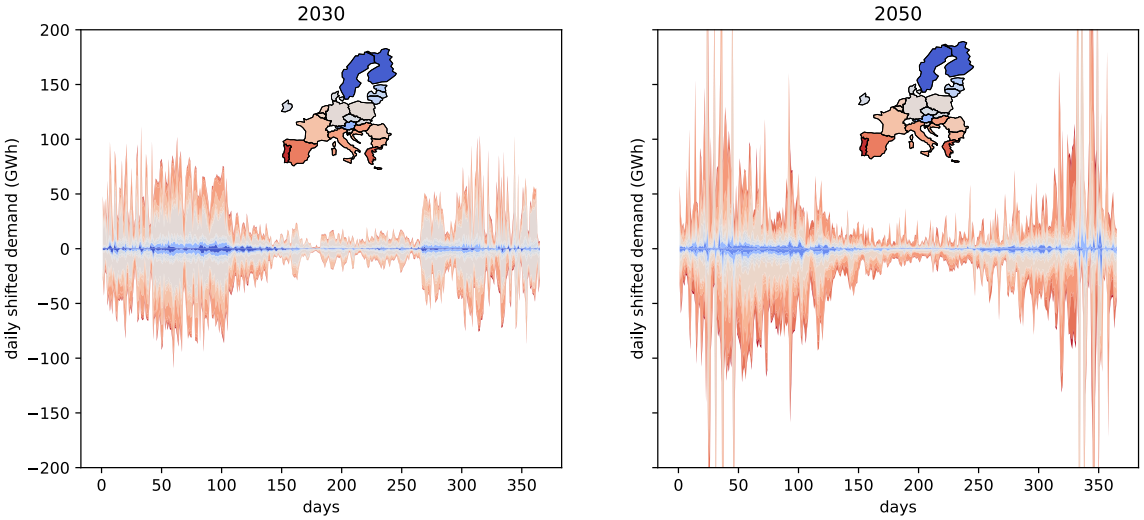

Figure 4.13: Daily shifted demand in the EU member states with **10%** of prosumagers using **AC** and 20 cent/kWh grid fees. Negative values represent the sum of daily demand that has been reduced in certain hours. In contrast, positive values represent the increase in demand in other hours during each day through prosumaging. The legend for the color codes is presented as a map, representing the average outdoor temperature in each country.

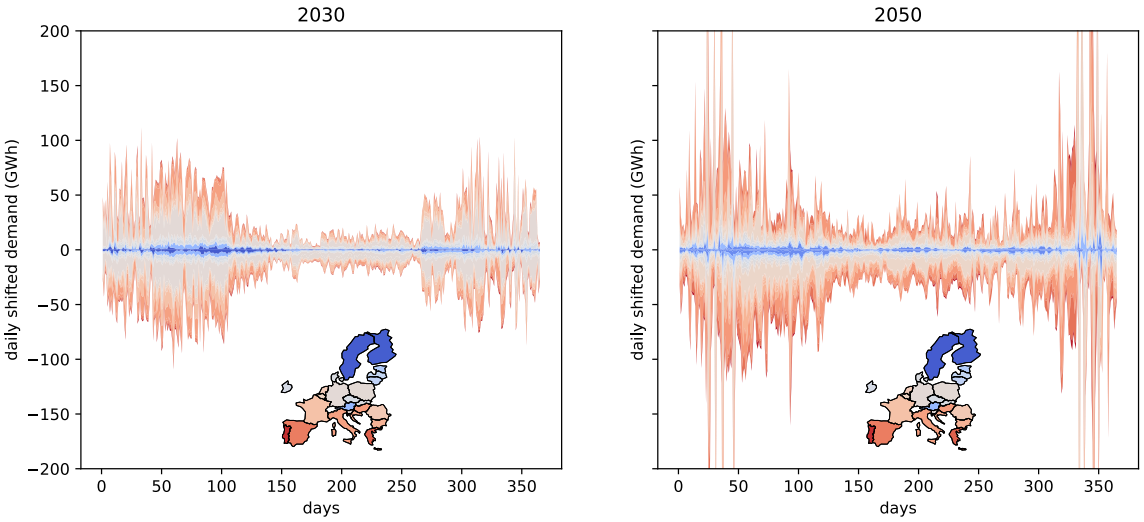

Figure 4.14: Daily shifted grid demand in the EU member states with **80%** of prosumagers using **AC** and 20 cent/kWh grid fees. Negative values represent the sum of daily demand that has been reduced in certain hours, while positive values represent the increase in demand in other hours during each day. The legend for the color codes is presented as a map, representing the average outdoor temperature in each country.

In previous results, it was often mentioned that the shiftable demand for buildings increases substantially when thermal storage is added. Figure 4.15 shows how much thermal demand is shifted throughout the year in 2030 and 2050 through the thermal mass distinguished by heating and cooling, DHW tanks, and heating tanks. The high winter spikes in 2050 are due to large electricity-price spikes. In summer, shifting is primarily due to hot-water demand. The slight increase in daily shifted demand for the heating tank in Summer is attributed to buildings partially filling their tanks with excess PV generation when feed-in tariffs are set to zero. In winter, a large part of the shifted demand can be attributed to the thermal mass of the buildings. In total, 30% to 40% of all the thermal demand shifted, was shifted through the thermal mass and 28% through DHW storage, and the remaining through the heating tanks with 20 cent/kWh grid fees. The shares

between these three options for thermal shifting change slightly in all other price scenarios or throughout the years. Without grid fees, more than double the amount of thermal energy is shifted in all countries collectively and the thermal mass shifts 42% of all the thermal energy in 2050. These numbers vary slightly when converting the thermal energy into electric energy. Because of the lower COP when charging a storage, the amount of electric energy shifted through the thermal mass is slightly lower while the DHW and heating tank contribute slightly more.

This result shows that the thermal mass, even when buffer heating tanks are available, is an economical option to shift electricity for short periods. It is often the preferred option to shift demand over short times, especially in efficient buildings because the efficiency of the HP is higher due to the lower supply temperature compared to the buffer tank. The thermal tanks were sized with 30 L/kW maximal thermal power of each HP, though in reality, actual tanks can be larger. At the same time, these buffer heating storage can be regarded as part of the heat distribution system in many cases, as they are used to ensure a smooth operation of the HP. Thus, they often do not require additional investment to tap the residential building stock's flexibility potential. In 2050, cumulative daily peaks for shifting thermal energy sum up to 1 TWh due to high price spreads.

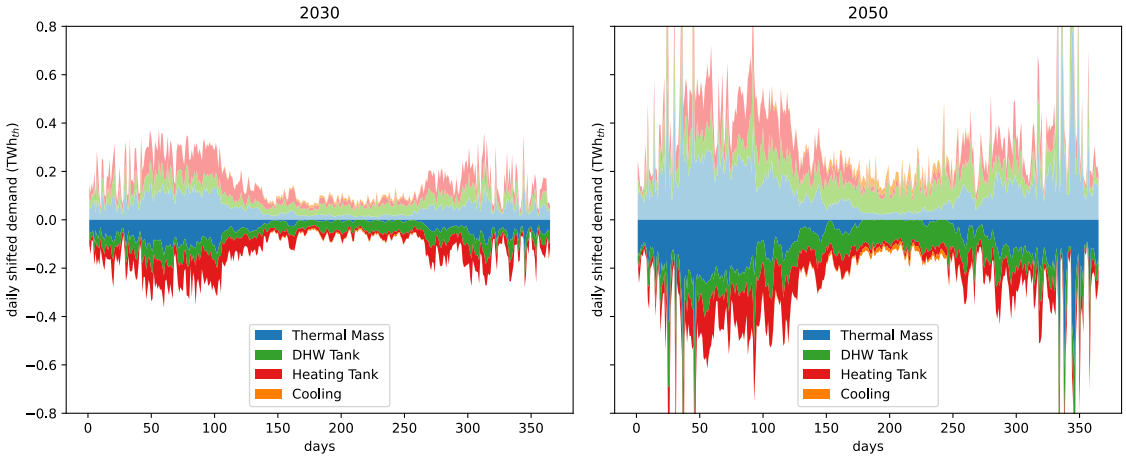

Figure 4.15: Daily thermal shifted demand distinguished between thermal mass, cooling, DHW and heating tank in the EU member states with 20 cents/kWh grid fees.

The analysis of Mascherbauer et al. (forthcoming) has shown that fixed grid fees have a pronounced impact on the potential of the residential building stock to shift electricity loads using HPs. Higher grid tariffs make load shifting less economically attractive. Figure 4.16 shows the total shifted electricity demand in the EU through HPs in the different scenarios with and without peak pricing. Higher grid fees reduce the shifted amount of energy because the relative costs of thermal losses increase, and thus, the price spread has to be higher to offset these losses. By adding a capacity component to the price, the total shifted demand is reduced, especially in scenarios with low grid fees. For high grid fees, the peak price does not have any effect. In 2050, adding the capacity price to the scenario with 40 cent/kWh grid fees increases the shifted electricity demand, as houses shift more electricity to reduce certain peaks. The difference between the relative shifted electricity demand in 2030 and 2050 is not intuitive since the heating demand declines overall due to the underlying climate change in the weather scenario and the better insulation of buildings. Also, the price volatility (standard deviation) increases from 2030 to 2050. However, the frequency of changes in price decreases in 2050 compared to 2030 by an average of 15%, which leaves less opportunity for the buildings to shift their demand. Additionally, the mean wholesale electricity price increases from 2030 to 2050, leading to

the same effect observed when grid fees increase. Still, the absolute shifted electricity in 2050 is higher than in 2030, because according to the modeled building stock scenario, a lot more buildings have HPs installed in 2050 than in 2030.

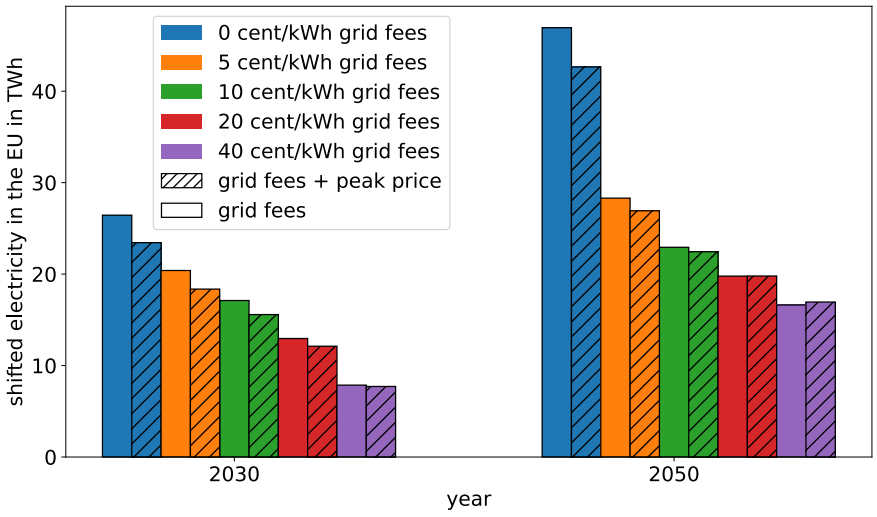

Figure 4.16: Shifted electricity demand in the EU through with different grid fees and a 50 EUR/kW peak price (shaded bars).

When comparing the results of shifted electricity in Figure 4.16 to the needed hourly flexibility of 362 TWh stated in the ACER (2023) report, it becomes evident that the building stock could offer around 2.5% to 8% of this needed short-term flexibility in 2030. The next section discusses how the peak electricity demand on a national level can change due to simultaneous load shifting.

4.3.2 Peak demand

In the previous analysis, we always considered the extreme comparison of all buildings heated with HPs becoming prosumagers or staying consumers. Having every building respond to hourly tariffs could affect the peak load on a national level. Therefore, Figure 4.17 shows how the electricity peak demand changes on a national level over the share of prosumagers. The lines represent the peak increase in overall grid demand for an individual country. This includes the demand of the residential sector and the complete non-residential sector. Without grid tariffs (0 cent/kWh), it is visible that some countries will increase their overall grid peak by almost 8% in 2030 and more than 10% in 2050 for a 100% share of prosumagers. Increasing the grid tariffs reduces this potential peak. Peak demand in 2050 is lower in most countries as the wholesale prices are higher on average. If the share of prosumagers stays below 25%, the peak demand increase is not expected to rise by more than 2% in any country. With higher grid fees, the peak demand in most countries even declines slightly (≈0.01%). Although not well visible in the graph, in some countries, an optimum share of prosumagers exists when it comes to reducing grid demand peaks. This optimal share depends on multiple factors, including prices, weather, renewable generation, the existing peak demand, available flexibilities from other sectors, and the ratio of available HP power compared to the overall grid demand. Countries that experience the highest peaks are those countries where electricity prices have high spikes and the ratio of installed heat pump capacity to overall grid demand is high.

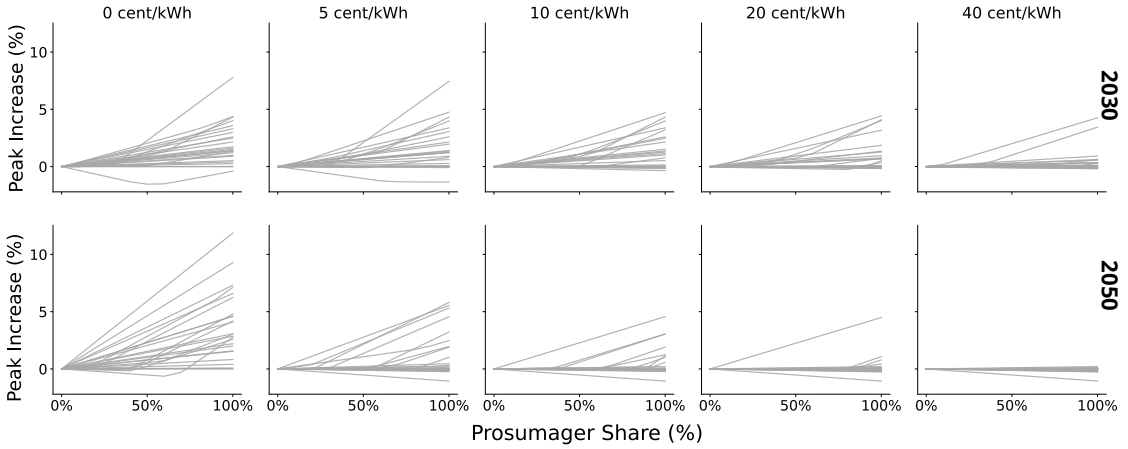

Figure 4.17: National peak demand increase for EU Member States over the share of prosumagers and different levels of grid fees in 2030 and 2050. Each country's peak demand is represented by a line over the prosumager share.

When introducing a capacity-based component of the grid fees, results show that, like reported in literature, the peak electricity load of all prosumagers on the country level is reduced significantly, which can be seen in Figure 4.18. The optimization even reduces the peak demand of prosumagers compared to their consumer counterparts, resulting in a negative peak demand increase. With the capacity pricing in place, the fixed grid fees do not play a relevant role for the peak demand on the prosumager household level. As a result, the peak electricity demand on a national level, shown in Figure 4.19, is also reduced in most cases by introducing the peak pricing. Especially for the scenarios without grid fees and 5 cent/kWh, maximum peaks are reduced significantly (from 12 to 6% in the worst case). However, this is not the case for all countries. In some countries, the reduction of prosumager peaks through peak pricing leads to an increase in national peak demand because the prosumagers no longer shift demand away from the original peak hour. For the scenario with 40 cent/kWh grid fees, the peak pricing has minimal influence, national peaks are hardly reduced or increased.

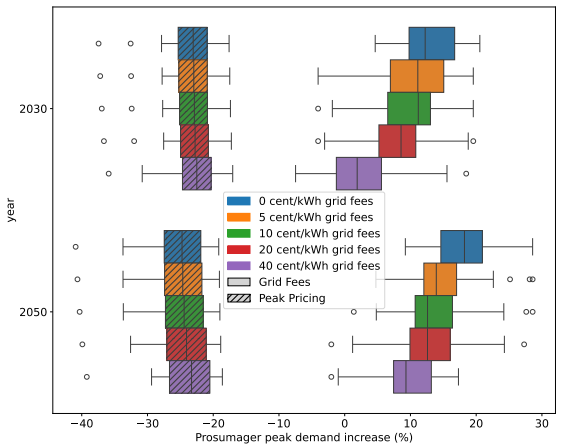

Figure 4.18: Peak electricity demand increase of all prosumagers compared to all consumers on the national level with and without peak pricing.

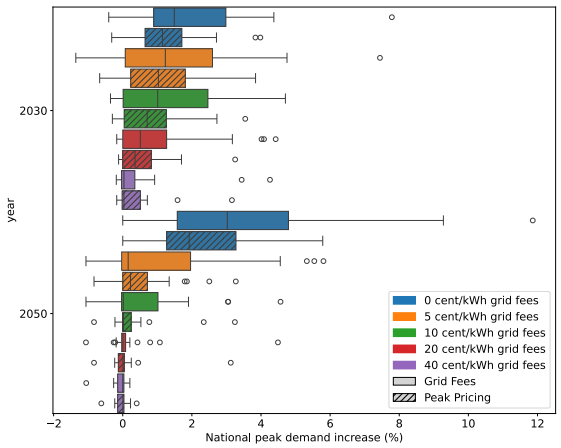

Figure 4.19: National increase in peak electricity demand because of prosumagers with and without peak pricing.

4.3.3 Change in total grid demand

Prosumagers have the potential to change the overall electricity demand. Through excessive load shifting and the accompanying losses, grid demand can rise. This is not necessarily a negative effect from a system perspective, as the additional grid demand stems from hours with low prices, which are often correlated to renewable generation. Figure 4.20 shows the change in electricity demand of residential buildings using HPs. As grid fees are increasing, and no PV feed-in tariff is considered in this thesis, PV self-consumption is maximized in every scenario, visible in Figure 4.21. Maximizing PV self-consumption can lead to a lower overall electricity grid demand at the country level. The average PV self-consumption is around 85%, which is due to the fact that rooftop area is strongly restricted in the building stock scenarios. Thus, many buildings have relatively small PV systems installed (1.25 to 3.5 kWp , see Figure 3.7 in Section 3.3.2), reaching self-consumption rates of nearly 100%. The "simulation" bar represents the PV self-consumption over all HP-heated buildings without optimization. In 2030, the optimization has a lower PV self-consumption with 0 cent/kWh grid fees because at times of PV generation, prices go down to zero, and the optimization uses electricity from the grid and sells PV, as it makes no difference. Figure 4.20 only shows the change in demand for these residential buildings with HPs. Due to lower overall electricity prices in 2030, the change in grid demand from HP-heated buildings operated by prosumagers is positive under both 5 and 10 cent/kWh grid fees, as more load is shifted and losses increase. By 2050, however, higher electricity prices together with the high PV self-consumption result in a reduction of grid demand even with a 5 cent/kWh grid fee. The total overall electricity demand change at the country level remains below 0.1% except for the scenario with zero grid fees, where it increases up to 0.4%.

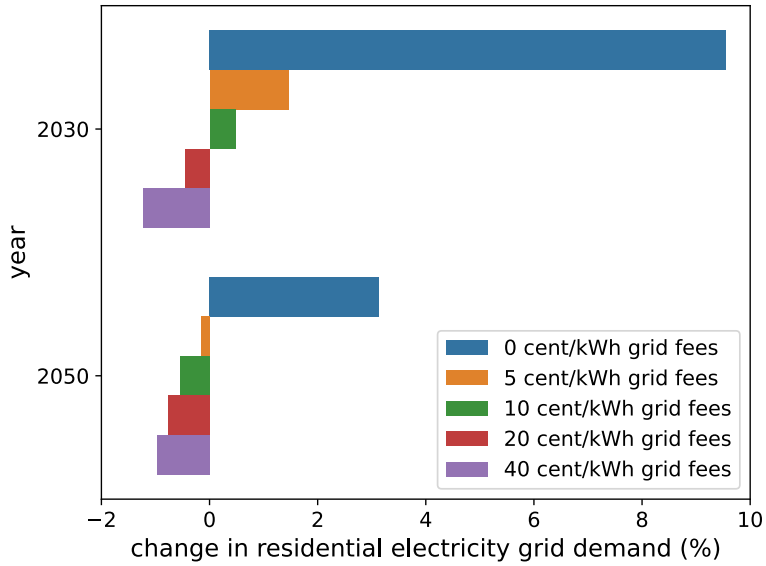

Figure 4.20: Change in residential grid demand in the EU through prosumaging over prices with different grid fees.

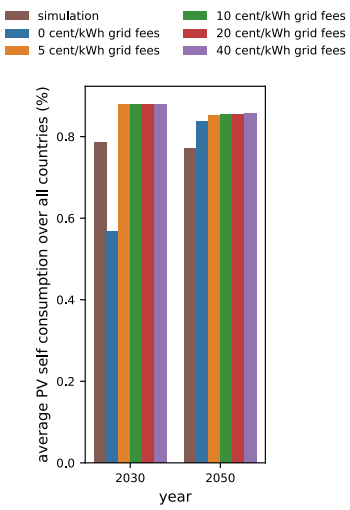

Figure 4.21: Mean PV self-consumption over all buildings with HP in the EU member states.

4.3.4 Flexibility factor

For the EU Member States (except Malta and Cyprus), the Flexibility Factor was calculated based on the grid demand of all potential consumers and prosumagers. The Flexibility Factor expresses how much electricity is used in the upper and lower price quartiles and is expressed within a range between -1 and 1. A high Flexibility Factor represents highly flexible demand, meaning that less electricity is used at high price times (4^{th} quartile) and

more at low price times (1st quartile). Figure 4.22 shows the Flexibility Factors for all EU countries as boxplots. The reference case refers to where prosumagers do not exist, and no load is shifted. Through prosumaging, the Flexibility Factor increases in every country. The lower increase in the Flexibility Factor in 2050 compared to 2030 is due to the lower amount of overall shifted electricity compared to the total consumed demand of the same buildings. In Figure 4.23, we see the total EU electricity demand change at high and low prices. With lower grid fees, the relative cost for load shifting is lower. Therefore, we see a higher demand increase at low prices (1st quartile) than the reduction at high time prices due to higher losses. With very low electricity grid fees, the change in demand on an average national level is already below 1%. However, it is increased around 10-75% in the first quartile and reduced up to 17% in the 4th price quartile for the buildings that perform the DR. Reducing the overall electricity demand at high prices could indicate a potential to reduce CO_2 emissions. At the same time, the increase in low prices would likely contribute to a higher share of renewable generation in the electricity mix or reduced curtailment of renewable generation. However, the question remains if renewables can completely cover this additional demand. A spatial analysis of the demand coupled with a grid model would be required to answer this question.

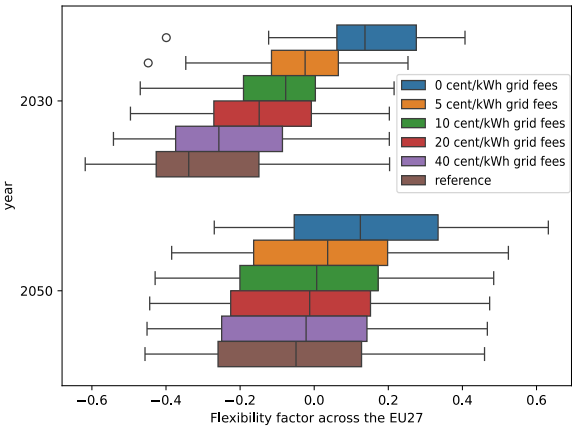

Figure 4.22: Flexibility factor over EU27.

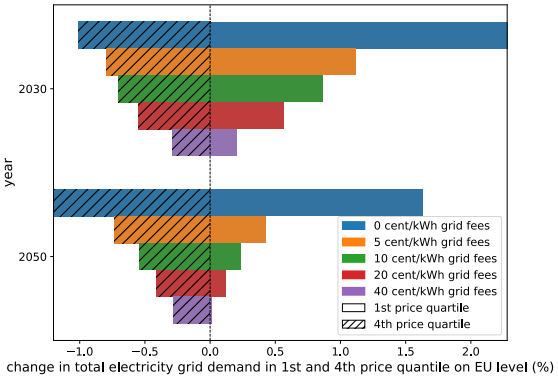

Figure 4.23: Average change in the total grid demand in the EU in the 1st and 4th price quartile.

4.3.5 Grid support coefficient

The GSC_{rel} shown in Figure 4.24 is lowered in every country by prosumagers, meaning that DR can be beneficial for the electricity grid. Interestingly, the GSC_{rel} drops even more when grid fees are increased in 2050. This means that even though more demand is shifted with lower grid fees, the resulting DR of prosumagers is less system-friendly. With zero prices, very inefficient DR actions are taken, which becomes evident when analyzing the change in total grid demand. The GSC_{rel} profits from the overall decrease in demand and increased PV self-consumption, which is why the scenario with the highest grid fees shows the best improvement in grid support through prosumagers in 2050. This observation cannot be made in 2030 for lower grid fees, although the scenario with the highest grid fees again results in the highest GSC_{rel}. Since the GSC is an indicator weighted by the price, in 2050, with overall higher prices and higher price prominence, minimizing the demand from the grid increases the GSC_{rel}. In 2030, the average prices are much lower (see Figure 3.14), thus the GSC_{rel} can also increase through excessive load shifting if the loads in high price hours can be reduced significantly at the same time. Between 10 and 20 cent/kWh grid fees, there seems to exist a minimum for the GSC_{rel} where the load is shifted to low-price hours. However, the additional losses outweigh the benefits because not enough load is shifted away from high price hours to increase the GSC_{rel}.

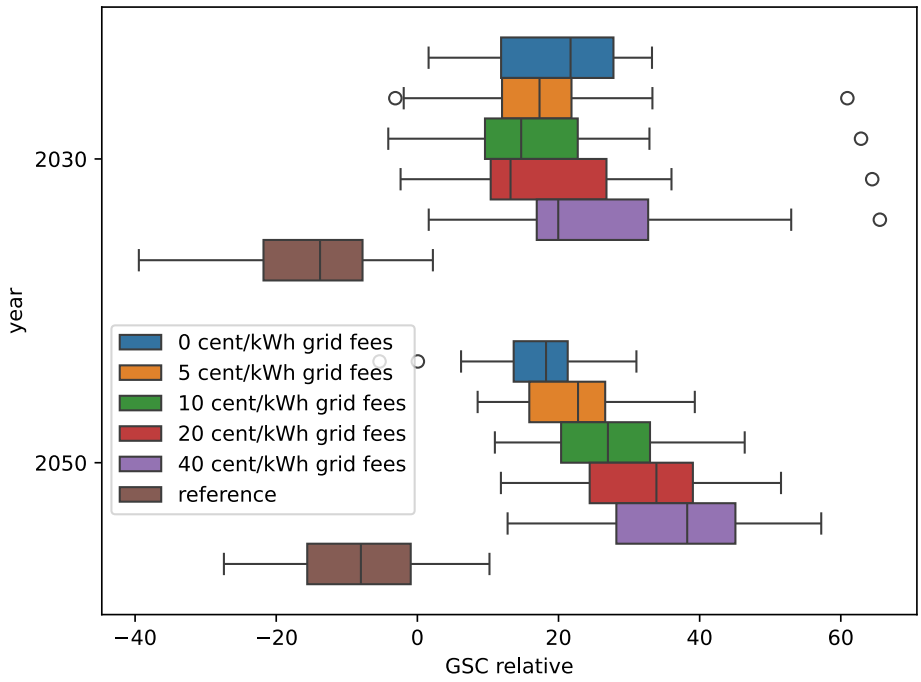

Figure 4.24: GSC_{rel} for all countries in the EU.

4.3.6 Resume

The analysis of this section has shown that fixed grid fees have a pronounced impact on the potential of the residential building stock to shift electric loads using HPs. Higher grid tariffs make load shifting less economically attractive. The difference in shifted electricity demand between the countries is determined mostly by the retail electricity price, the number of installed HPs, and the weather. Building stock characteristics have a minor effect. Load shifting is primarily done in winter, even in a scenario where 80% of the analyzed buildings have an AC installed. The countries shifting the most thermal demand and electricity using HPs are the central-eastern countries due to relatively high heating demand and volatile electricity prices. In the northern countries, prosumagers don't show a high willingness to shift demand due to their steady electricity prices. In contrast, in southern countries, the low heat demand limits the amount of demand that could be shifted. Even though buildings have hot water storage installed, the thermal mass is still used to a great extent for load shifting, underlying its potential as a short-term storage for HP-heated buildings. It should be noted that the building stock scenario used for the future prediction of the building stock status is quite ambitious, with a strong renovation rate and high uptake of electrified heating systems. Therefore, results on the total shiftable electricity demand might be an overestimation, being strongly dependent on the absolute number of HPs installed in the future and the uptake of Prosumagers so that HPs can actually respond to price signals. At the same time, batteries and EVs were neglected in this specific analysis, which can provide large additional flexibility depending on the uptake of EVs and battery storage.

This section also tried to analyze what impact prosumagers could have on the total grid demand and if prosumaging would benefit the electricity grid itself. Through higher PV self-consumption rates and if DR is done moderately, the overall grid demand can even be reduced annually. In this analysis, stationary batteries or electric vehicles were excluded, which could increase the PV self-consumption of many buildings without any optimization. When it comes to 'grid friendliness', the author used the Flexibility Factor and the GSC_{rel} to show how grid-friendly prosumagers are on a country-level basis. Both these factors provide information on the 'grid friendliness' based on the hourly electricity price.

The GSC in this analysis showed that the DR of prosumagers could be beneficial for the grid, even more so if grid fees are high and losses during load shifting are minimized. Since the actual grid is not taken into account in this approach, the author wants to point out that the 'Grid support coefficient' can be interpreted as a system support coefficient. The definition of the GSC (Klein et al. 2016) does not allow any interpretation of the status of the underlying electric grid. Since this modeling approach is not directly coupled to a grid model, such an analysis can not be made. To circumvent this problem, in literature, the correlation between the day-ahead price and the residual load is often used (Klein et al. 2016; Klein et al. 2017; Sperber et al. 2025). The Flexibility Factor shows that through DR of prosumagers, the overall electricity consumption in the EU could increase by more than 1% (depending on grid fees) at low price times and subsequently be decreased at high price times.

At the same time, excessive DR from HPs can lead to higher electricity demand peaks on a national level, which has also been reported in literature (Sperber et al. 2025). However, if grid fees are high enough (>10 cent/kWh), new load peaks created through prosumagers should not pose a problem. As shown in this analysis, the peak load only increases in countries with very high fluctuations in the electricity price signal and if prosumager shares go up to 100%. Realistically, prosumager shares in 2030 will be below 50%. For countries where the DR could significantly increase peak demand, a different approach should be taken to incentivize buildings to shift load, or a capacity price should be added to the grid fees. It was shown that a capacity-based price can reduce peak loads significantly while the amount of shifted electricity is only slightly reduced. Another option would be to introduce different hourly grid tariffs in the regions, better reflecting electricity scarcity and preventing the simultaneous reaction of too many prosumagers to the same price signal. This hypothesis, however, is subject to further research and can not be verified with the current approach. A more effective way to use the building stock's flexibility could also be through direct load control of the grid operator (Elma et al. 2022; Valovcin et al. 2022). At the same time, direct control has been identified as a possible barrier to user acceptance (Klein et al. 2017). The results presented above vary relatively highly within the different countries. A detailed analysis of each country with a spatial distribution of the loads to investigate the possibility of prosumagers reducing grid congestion should be subject to further research. To shed more light on the effect prosumagers can have on the electricity grid, the following section will analyze how prosumagers could affect future distribution grid investment needs on a local level.

4.4 Prosumagers and the distribution grid

One limitation of the FLEX model is that it is not connected to an electricity grid model, which makes it difficult to make assumptions about the feasibility of prosumagers. In this section, the possible impact of prosumagers on a detailed spatial granularity is analyzed, combining the FLEX model with the Reference Network Model (RNM) to model future investment needs for the distribution grid. This way, the impact of the simultaneous reaction of multiple prosumagers in close vicinity on the distribution grid is analyzed. The results presented in this section are taken from Mascherbauer et al. (2025a).

4.4.1 Peak demand

In Section 4.3.2, the peak demand did not change significantly as long as reasonable grid tariffs were applied. The share of prosumagers of HP-heated buildings did affect load peaks. We see a different effect in the detailed analysis of Leeuwarden and Murcia. Peak demand is not a result of many prosumagers shifting load with their HPs. Instead, it is defined by the coldest day of the year, electrification rates in an area, and the overall thermal insulation level of the buildings and EVs. Figure 4.25 shows the aggregated peak

demand of all buildings together in each region for 2030, 2040, and 2050. We can clearly see that on an aggregated level, the building-related peak demand (without EVs) decreases in Murcia due to the phasing out of direct electric heating systems. On the other hand, the building-related peak load strongly increases throughout the years in Leeuwarden due to the replacement of gas boilers with HPs. The strong policy scenario leads to a higher power consumption in 2040 due to higher adoption of HPs, but in 2050, the effect of better insulation counteracts, and we see lower peaks in the strong policy scenario in both case studies. Without electric vehicles, the share of prosumagers only marginally impacts the total peak demand (from 0-0.5% change in peak value). Prosumagers decrease the original peak demand significantly. However, by shifting demand, they create new peaks, leading to a similar overall peak demand occurring at a different hour.

Looking at the scenarios with electric vehicles, the difference between the prosumager scenarios is most visible. The simultaneous EV charging of prosumagers leads to massive power peaks. In Leeuwarden, the number of EVs is much higher than in Murcia, leading to a substantially higher peak load. This peak demand shows that simultaneous charging of EVs will most likely not be possible in the future and should not be incentivized by hourly prices for EVs in regions with high EV adoption. However, in Murcia, we can also see that the uptake of EVs overshadows the impact of electrified heating systems. Therefore, applying smart EV charging (like in Lotfi et al. (2022)) is crucial, which will need a different approach for coordinated charging.

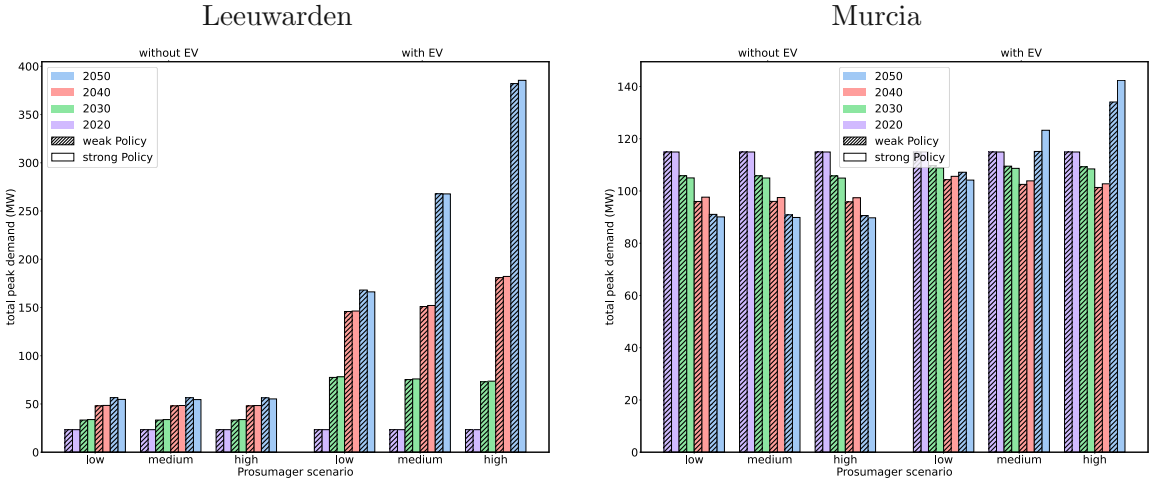

Figure 4.25: Peak grid load on the aggregated level on the peak demand day for different scenarios in Leeuwarden and Murcia. Mascherbauer et al. (2025a)

4.4.2 Peak feed in

In Section 4.2, it has been shown that prosumagers increase PV self-consumption through their energy optimization. Thus, locally, the maximum peak of PV generation fed to the grid is reduced with a higher share of prosumagers. Figure 4.26 shows the peak load fed to the grid on the day with the highest feed-in (a sunny day in Spring where neither heating nor cooling is needed). There is a clear difference in the two policy scenarios as more PV is adopted in the strong policy scenario. Since both areas are urban and the PV areas are not larger than 15 kWp per building, significant parts of the generation can be self-consumed or stored in thermal and electrical storage. Because the area in Murcia has more large MFHs, the maximum amount of electricity fed to the grid is smaller than in Leeuwarden, with a rising PV share. In the scenarios with EV, the total peak feed-in is reduced because some of the vehicles can be charged by the surplus of PV. However, the effect on EVs charging using excess PV generation at the hour of maximum feed-in is not

very pronounced because many cars aren't charging at this specific hour.

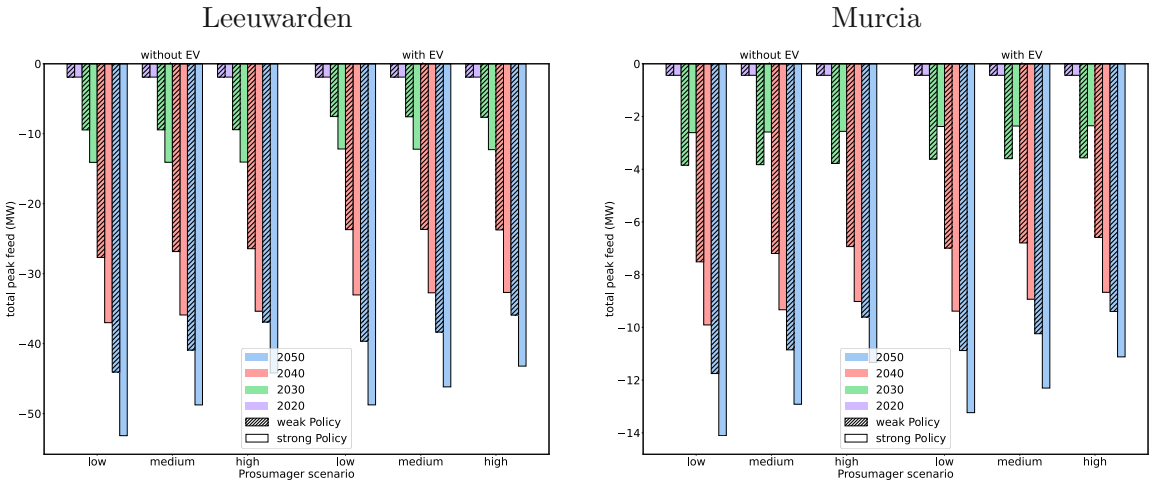

Figure 4.26: Peak feed into the grid on the peak feed-in day for different scenarios in Leeuwarden and Murcia. Mascherbauer et al. (2025a)

4.4.3 Distribution grid investment needs

This section analyzes and compares the techno-economic results of the distribution networks planned with the RNM model under the different policy and prosumaging scenarios. The results include the additional investment and O&M grid costs for each scenario and the increase in power losses for the peak demand day in each future scenario relative to the base case. The results for the base case grids in Murcia and Leeuwarden are presented in the Tables 4.2 to 4.5. Investments in network reinforcements are classified into three types of elements: low voltage (LV) power lines, medium to low voltage (MV/LV) distribution transformers, and medium voltage (MV) power lines. The results include the total length of overhead lines and underground cables for each voltage level. Note that in Leeuwarden, all LV and MV lines are underground, while in Murcia, there is a mix of underground and overhead lines (see Tables 4.2 and 4.4).

Similarly, Tables 4.3 and 4.5 show the costs for distribution transformers and substations in the initial grids. Murcia has a much higher initial installed capacity for distribution transformers. This can be attributed to Murcia's higher housing density and the prevalence of electric heating and cooling systems. The higher capacity and denser configuration of the MV grid in Murcia relative to Leeuwarden suggests that future reinforcement requirements will be lower. Moreover, these tables show the total CAPEX and O&M costs of power lines, distribution transformers, and substations for the initial 2020 grids. These values are the reference used to calculate the incremental costs for these distribution grids in future scenarios.

Table 4.2: Power lines data for the initial 2020 grid in Murcia, Spain. (Mascherbauer et al. 2025a)

	Overhead [km]	Underground [km]	CAPEX [mio. €]	O&M [€/yr.]
LV power lines	128.22	53.74	4.45	44 854
MV power lines	33.94	64.20	9.76	101 348
HV power lines	0.00	16.77	11.85	122 973

Table 4.3: Distribution transformers and substations data for the initial 2020 grid in Murcia, Spain. (Mascherbauer et al. 2025a)

	Quantity	Installed power [MVA]	CAPEX [mio. €]	O&M [€/yr.]
MV/LV Distribution Transformers	185	129.28	10.41	238 285
HV/MV Substations	2	160.00	4.15	223 223

Table 4.4: Power lines data for the initial 2020 grid in Leeuwarden, Netherlands. (Mascherbauer et al. 2025a)

	Overhead [km]	Underground [km]	CAPEX [mio. €]	O&M [€/yr.]
LV power lines	0.00	358.34	18.63	192 786
MV power lines	0.00	64.20	14.57	109 675
HV power lines	57.43	0.00	8.68	90 102

Table 4.5: Distribution transformers and substations data for the initial 2020 grid in Leeuwarden, Netherlands. (Mascherbauer et al. 2025a)

	Quantity	Installed power [MVA]	CAPEX [mio. €]	O&M [€/yr.]
MV/LV Distribution Transformers	90	30.6	4.83	110 537
HV/MV Substations	13	390	7.55	203 190

Figure 4.27 shows the total cost increase, including O&M and investment costs for the distribution grid under different scenarios. The results for Leeuwarden indicate a significantly higher requirement for grid reinforcements than in Murcia. This difference can be attributed to the high initial dependence on conventional heating systems in Leeuwarden (see Figure 3.19), whereas in Murcia, many households have already adopted electric heating in 2020. Additionally, Leeuwarden exhibits a lower urban density, comprising a greater proportion of single-family residences. This leads to a higher PV excess generation fed to the grid (see Figure 4.26), as there is a higher installed PV capacity per building and a lower demand in periods with high PV generation.

Generally, strong policy scenarios necessitate more grid reinforcements than weak ones, as the electrification level of buildings is higher and also the adoption rate of rooftop PV. The most notable distinction in Figure 4.27 is that in Murcia, grid reinforcement in strong policy scenarios is more pronounced in 2040, reflecting a faster adoption rate of EVs and HPs. Nevertheless, the incremental costs for 2050 remain similar across both strong and weak policy scenarios. Moreover, the decreasing investments in 2050 in Leeuwarden scenarios with no EVs when moving from low to high prosumager scenarios is attributed mainly to the higher PV self-consumption of prosumagers.

Including EV loads generally increases the peak demand, leading to a substantial increase in grid reinforcements. However, a comparison of the 2050 low prosumager scenarios for Leeuwarden with and without EVs in Figure 4.25 does not show this effect. This can be explained by the high PV penetration in Leeuwarden in 2050, which leads to reversed power flows and overvoltages at midday, resulting in high investment needs for LV lines (see Figure 4.28). The presence of new EVs charging during these hours reduces the peak PV feed-in (Figure 4.26), lowering reinforcement needs in low voltage lines, as illustrated in Figure 4.28.

Higher shares of prosumagers positively affect grid investment needs unless their controllable loads, particularly EVs, are synchronized at off-peak tariff periods. In 2050, the incremental cost increase is significantly lowered by prosumagers in Leeuwarden without EVs despite a very high share of prosumagers. However, the simultaneous charging of EVs leads to much higher peak demand at off-peak tariff periods (Figure 4.25) and higher grid

investments, especially in scenarios where prosumagers account for more than 40% of total customers. Thus, new economic incentives or demand response participation schemes should be implemented in the future to avoid synchronization of controllable loads at the hours with low tariffs, especially when it comes to EV charging.

The primary drivers for Leeuwarden's cost increase are investments for new MV/LV distribution transformers and the rollout of on-load tap-changing transformers (see Figure 4.30). These investments are necessary due to the significant voltage differences between high PV feed-in and peak demand hours throughout the year. Also, the LV power lines will need substantial investments (Figure 4.28).

On the other hand, the investment needed in distribution transformers is significantly smaller in Murcia (Figure 4.30). In Murcia, there is already a significant percentage of buildings with electric heating and more multi-family houses, so the initial MV grid in 2020 is stronger and denser. The main driver for additional costs in Murcia is the reinforcement need in LV lines (see Figure 4.28). Switching the remaining buildings to electrified heating systems requires a higher capacity in LV power lines connecting these houses. Prosumagers could significantly reduce the reinforcement in LV lines if EVs are charged in a grid-friendly way. Moreover, we can see that with an increase in building renovation (strong policy scenario without EVs), the grid will not need additional investments in 2050 compared to 2040.

PV adoption does not strongly impact Murcia because the available rooftop area is lower, and most of the PV generation is self-consumed. On the other hand, in Leeuwarden, the uptake of PV leads to increased costs. This could be reduced through prosumagers who try to maximize self-consumption and through additional local storage technologies (batteries, tanks), which can also be observed in the power losses (Figure 4.31). With a higher share of prosumagers, the power losses decrease. However, power losses can also be reduced due to higher grid reinforcements, which results in a higher power line capacity and lower resistance.

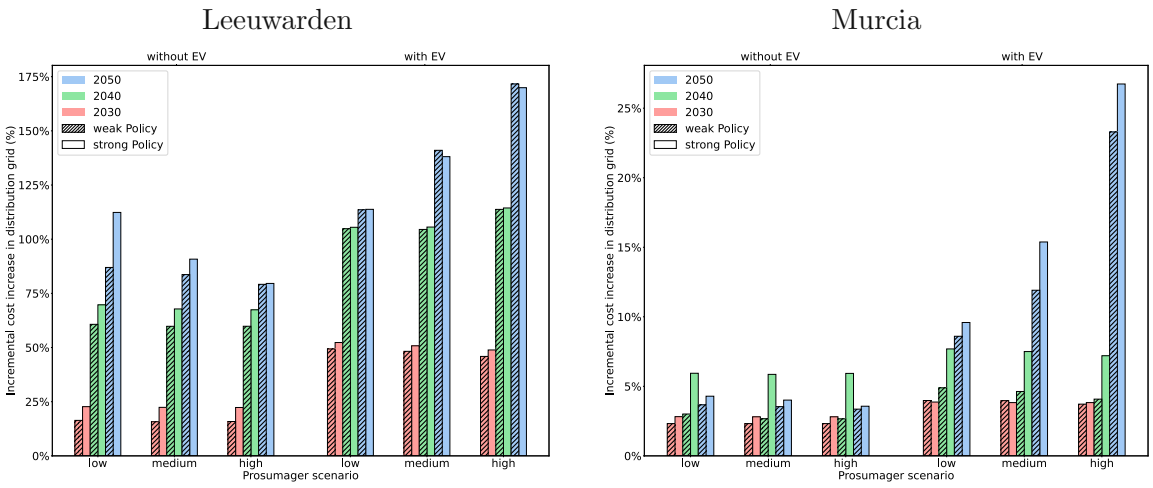

Figure 4.27: Distribution grid percentage cost increase in Leeuwarden and Murcia in different scenarios. (Mascherbauer et al. 2025a)

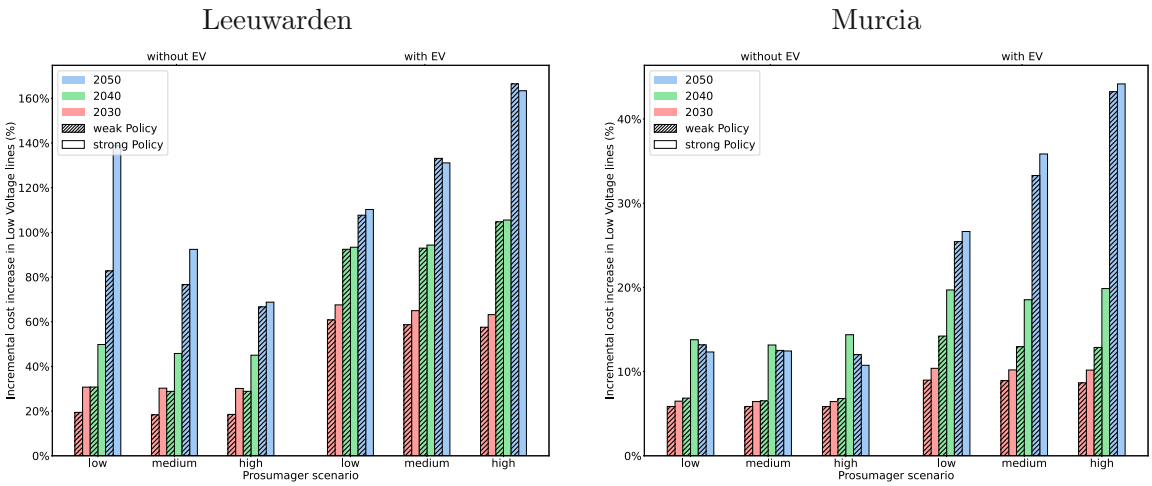

Figure 4.28: Low Voltage lines percentage cost increase in Leeuwarden and Murcia in different scenarios. (Mascherbauer et al. 2025a)

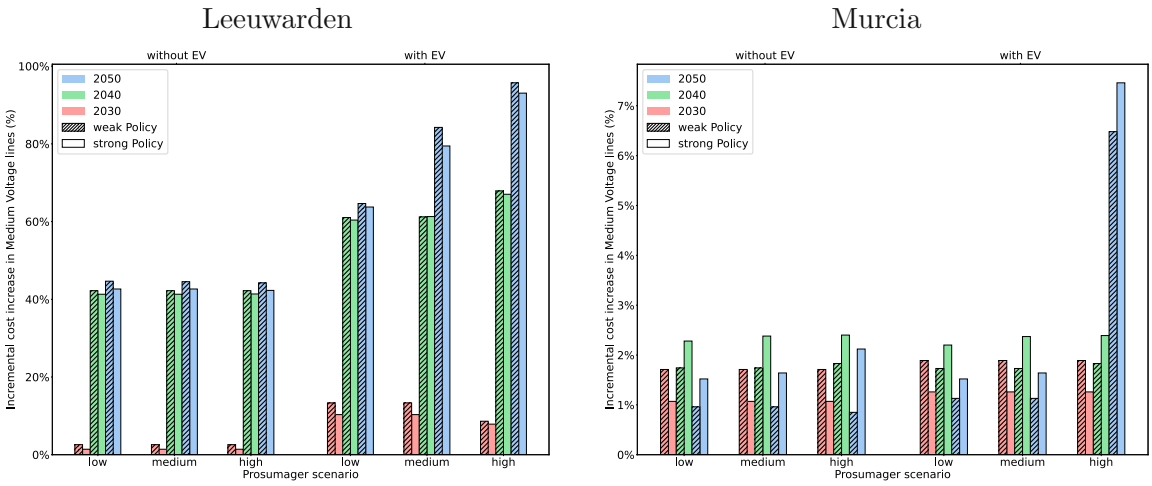

Figure 4.29: Medium Voltage lines percentage cost increase in Leeuwarden and Murcia in different scenarios. (Mascherbauer et al. 2025a)

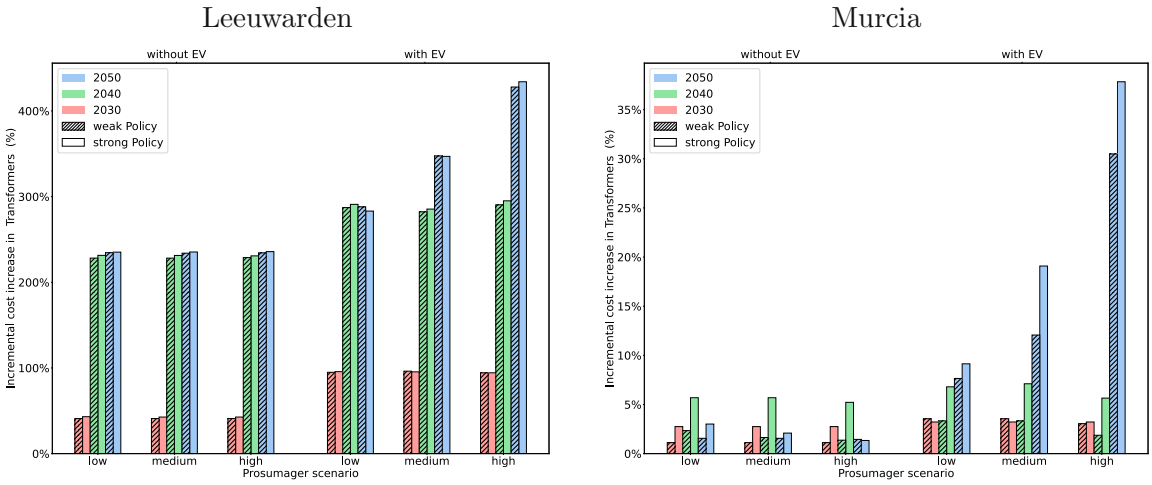

Figure 4.30: Transformer percentage cost increase in Leeuwarden and Murcia in different scenarios. (Mascherbauer et al. 2025a)

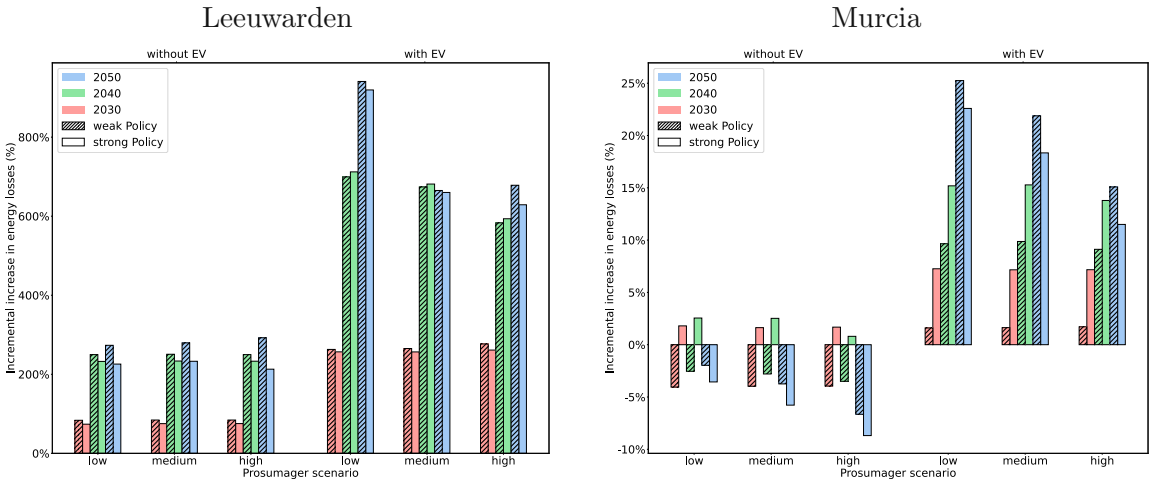

Figure 4.31: Percentage increase in power losses in Leeuwarden and Murcia for different scenarios. (Mascherbauer et al. 2025a)

4.4.4 Resume

The two case studies presented above from Mascherbauer et al. (2025a) provide insight into potential reinforcement needs for an urban location with a very high penetration of gas boilers in a colder climate as well as an urban location with a warm climate and an already high share of electric heating systems. It is anticipated that grid reinforcements will be required in both locations, although the extent of these investments and the underlying drivers are different. The aggregated peak load in both regions is expected to grow, with EV adoption being the largest factor. However, if new EV loads are not considered, the peak load on an aggregated level will rise in Leeuwarden but decline in Murcia. Investments in grid reinforcements are expected in all scenarios, even in those with lower aggregate peak loads. Note that the aggregated peak demand masks local peaks that can occur at individual feeders where the additional consumption of HPs is higher than the demand reduction achieved with increased energy efficiency and self-consumption. The long-term investment requirements for LV and MV grids in Leeuwarden are anticipated to be higher than in Murcia. This is due to a combination of factors, including the higher peak demand growth in Leeuwarden and the stronger initial distribution grid in Murcia, which already supplies a significant share of buildings with electric heating. Overall, it can be said that replacing heating systems will also be a driving factor for cost increases in European distribution grids.

Moreover, feed-in from solar PV generation is expected to increase, causing reversed power flows and overvoltage issues. This is especially significant in Leeuwarden, where the combination of a higher roof area available for PV and a higher share of conventional heating systems replaced by HPs can lead to needed medium to low voltage transformer investments 2-4 times the cost of the initial transformer capacity (Figure 4.30). This may be an overestimation since the model employs on-load tap-changing transformers to address the voltage difference between peak load and peak generation periods. While there may be other options for voltage control that could be considered, this result highlights the value of long-term planning for electricity grids in enabling decarbonization policies.

A limitation of Mascherbauer et al. (2025a) is that detailed data on the hosting capacity in Leeuwarden and Murcia to accommodate new demand and generation without reinforcement was not considered. Therefore, the need for grid extension in the first years might be lower than the study predicts. However, distribution grids in Leeuwarden currently have limited capacity for additional generation and queues for connecting new demand

(Netbeheer Nederland 2025). Besides, the long-term results would not be substantially different if the actual hosting capacity were considered to model the initial networks, as the hosting capacity is likely to be recuperated as distribution grids are reinforced. The increase in demand is many times higher than the initial hosting capacity.

Prosumagers can only lower these additional grid costs by shifting demand to off-peak hours and increasing self-consumption. Nevertheless, as illustrated in Figure 4.27, EV scenarios with a share of prosumagers beyond 40% result in higher incremental grid costs due to the synchronization of controllable loads. The necessary investments in grid reinforcement would require significant expenditures, particularly in Leeuwarden, due to the inadequate management of controllable loads. In the coming years, alternative solutions that consider the status of the distribution grid (e.g., smart charging strategies, local flexibility markets, alternative tariff incentives, etc.) are likely to be introduced. While the EV scenarios involving medium and high shares of prosumagers may possibly not materialize in 2050, the findings underscore the value of these alternatives. Future research should explore these alternatives to unlock the full potential of prosumagers to improve distribution network planning.

Not considering a correlation between HP and PV installations might result in slightly higher investments than needed. Mascherbauer et al. (2025a) did not consider the direct effects of climate change on weather profiles. An increase in active cooling systems is considered in this publication, but compared to heating, cooling does not drive the peak electricity demand. On the one hand, the temperature difference between the source and sink is lower for cooling purposes, making a typical compressor-driven HP more efficient for cooling than for heating. At the same time, cooling demand overlaps well with locally produced PV generation. Thus, the peak demand is expected to still occur on a winter day, especially considering that extreme weather events will increase.

5 Discussion and synthesis of results

In this chapter, the results of this thesis are discussed, and the formulated research questions are answered. The chapter is divided into three sections, one for each research question.

5.1 Research question 1

How much electricity load can the residential building stock shift and what role can the thermal mass play in this potential?

It was shown that approximately 10 to 20 GWh of electricity could be shifted by the current SFH stock in Austria per year using the thermal mass and not accounting additional systems such as DHW or heating buffers. 10 GWh would be shifted using day ahead prices from 2016, while almost 20 GWh is the potential with electricity prices from 2021. On the EU level, the electricity that could be flexibly used depends strongly on the uptake of HPs. With the simulated prices used in this thesis, prosumagers could shift from 2-8% of their yearly electricity usage in the worst case (Finland, Sweden) and up to 5-25% (Czech, Germany, Austria) in 2030. On the EU-level, this accounts for a total shifted electric energy of 9-28 TWh in 2030 and 20-45 TWh in 2050, depending also on the electricity price signal that is used. Increasing fixed grid fees reduces the peak demand created through prosumagers as the incentive to shift high amounts of electrical loads is reduced.

Although a simplified building model was used in this thesis, it was validated and shown to reasonably represent buildings with radiators as heating systems. Since deep renovations are costly and already a large share of buildings could be equipped with HPs without additional insulation or change of heating system, it is estimated that the majority of buildings that will switch to a HP in the future will still use radiators as a heating system. The additional thermal capacity of the heating system, which is especially important in floor-heated houses, is added with a buffer heating storage, which returns similar results in terms of shifted energy over the year.

Around 30% to 40% of the total electricity the building stock could shift is attributed solely to the thermal mass of buildings, not including the thermal capacity of the heating system itself. Therefore, shifting loads through the thermal mass of buildings not only has potential but is also economical even if the buildings have other possibilities to shift their demand (in this case, DHW tank and heating buffer tank). It should be noted that in summer, only DHW demand is shifted, which accounts for around 20-30% of total demand shifted by buildings that have both a DHW and a hot water storage. With lower average retail prices thermal storages are more utilized, while in 2050, because of overall higher retail electricity prices, the thermal mass is utilized more. It was investigated how an increase of AC to 80% of all HP-heated buildings would change the results. But the amount of cooling demand shifted is not as impactful as heating demand for two reasons. First, the temperature difference that cooling generators have to overcome is lower, making

cooling quite efficient compared to heating at low outside temperatures. Second, cooling demand in central and northern Europe occurs mainly during the day and can be covered well with PV-generated electricity. It was further shown that the central European countries have the highest load-shifting potential for two reasons. Their projected electricity prices in the future show high volatility, and their heating demand in winter is moderate to high. The building stock characteristics did not have a pronounced effect on the load shifting on the national level, although it was shown that well-insulated buildings can shift a higher percentage of their demand. At the same time, the author expects that HPs will mainly be installed in buildings where the supply temperature can be lowered to 55°C or lower. This can only be done in old buildings if they are renovated to some extent. The building stock scenario used for the future prediction of the building stock status is quite ambitious, with a strong renovation rate and high uptake of electrified heating systems. Therefore, results on the total shiftable electricity demand might be an overestimation, being strongly dependent on the absolute number of HPs installed in the future and the uptake of HEMS so that HPs can actually respond to price signals. At the same time, if renovation rates stay lower than anticipated in the used scenario and HPs are installed in buildings nevertheless, the shifting potential of the building stock will be even greater, as the average heating demand would increase in comparison to this scenario. Buildings with a higher energy demand have a higher absolute shifting potential, even though the shifted electric energy share will be lower compared to an efficient building.

Pre-heating a building leads to higher losses from the thermal mass, which means higher electricity consumption. The question arises of how electricity demand changes because of prosumagers. Within this thesis, optimizing HP operation to minimize cost has different effects on the electricity demand depending on what appliances (PV, battery, thermal tanks) are installed together with the HP. PV self-consumption is maximized by prosumagers, leading to a lower grid electricity demand from buildings that have PV installed. For buildings with a 5 kWp PV system and without any storage, HEMS can decrease the overall electricity demand from the grid by 1.5 to 1.6 GWh in Austria. The increase in self-consumption by installing a HEMS is small if a battery and DHW tank are already installed. The daily peak-to-peak demand of prosumagers increases substantially if thermal tanks are installed under a cost-minimization objective, given that no counteractive measures are taken. DHW tanks and batteries result in higher cost savings as they can utilize price differences or PV generation also in summer. In the study for Austria, battery systems were considered, while in the analysis on the EU level, only thermal storages were taken into account. Therefore, the total electricity demand reduction anticipated on the EU level through the increase in PV self-consumption could be considered to be slightly lower as batteries will increase self-consumption significantly even without a HEMS. For buildings without PV, though, the grid demand of prosumagers increases compared to that of their consumer counterparts. This increase, however, is strongly dependent on the electricity price signal as the driving factor of the optimization, which is why the impact of it was examined in this thesis through RQ2.

5.2 Research question 2

How does the price of electricity affect prosumagers' potential to shift demand?

Two properties of the retail electricity price influence the load-shifting potential of the residential building stock under the hypothesis that HP operation is being optimized to reduce electricity cost. The first property is the frequency of the price signal changing its value, and the second is the significance of these price changes. The frequency of price changes appears to have the most influence in this thesis, given the fact that the significance of each price change is often high enough to invoke a load-shifting behav-

ior. The significance of a price change can be described as the relative change in price from one hour to another. In this thesis, the significance of price change was altered by changing the marginal cost of flexible power generators in the electricity grid model (e.g., through higher CO_2 prices) or by adding fixed grid fees. Increasing grid fees reduces the significance of price changes, while higher CO_2 prices contribute to more prominent price peaks, thereby enhancing load-shifting behavior. An exact correlation between certain statistical values of the price profile and the load-shifting behavior at the building stock level was not established. For each building, a change in price has a different significance based on the installed appliances, insulation, weather, the current state of the building, storage levels, plus future states concerning price and weather. By using different prices from past years and modeling possible prices for the future, including certain sensitivities (e.g., CO_2 price), this thesis tries to give an estimation of how large the potential for load shifting through residential HPs is on a building stock level. With rising CO_2 prices, electricity price peaks are likely to rise in the future. With a CO_2 price of 212€/tCO_2 shifted electricity demand doubles in volume compared to a CO_2 price of 53€/tCO_2 in the scenarios calculated for 2030 in Austria. Apart from the CO_2 price increasing peak prices in the power sector, real-time pricing could be coupled with dynamic grid tariffs, thereby enhancing the possible yearly cost savings and making load shifting economically more attractive for prosumagers. Nevertheless, such measures would need to account for the risk of disproportionately affecting low-income households that lack access to smart HP technologies. Additionally, higher price volatility and the associated stronger response from prosumagers in terms of peak demand must be compatible with the supply networks.

Some studies suggest that HPs could also participate in the intra-day market or even in the frequency reserve market (Meesenburg et al. 2020; Manner et al. 2020), making load shifting much more lucrative. But to do so, HPs would have to be pooled to reach a certain minimum power capacity limit (Hülsmann et al. 2019). Additionally, accurate modeling of HP thermal dynamics is necessary to estimate the effectiveness of HPs in participating in the frequency regulation market (Song et al. 2025). Despite the technical challenges that have to be addressed for participating in intra-day or frequency regulation markets, for single prosumagers it could be more beneficial from an economic point of view.

Yearly cost savings of prosumagers shifting electricity demand through the thermal mass alone are very limited when using the day-ahead price. Even if the day-ahead price becomes more volatile. Buildings with high energy demand achieve higher absolute savings when becoming prosumagers. For large MFHs with central HP, the investment in a HEMS could be profitable if we assume the price for such a system is around 100€ and an expected payback period of less than five years. For buildings that already have a heating buffer tank and or a DHW tank installed, the economic incentive is much higher to become a prosumager. If storage is not installed, however, the upfront investment into a storage system will result in high payback times, depending on the energy consumption of the building. For low-energy consumption buildings with a high level of insulation, the economic incentive alone might not be enough to convince residents to become prosumagers. If increasing the number of prosumagers should be a goal in the future, additional incentives might be needed. Increasing the share of prosumagers could be achieved either through a regulatory framework or by subsidizing HPs that change consumption based on a price signal. Different grid tariffs for prosumagers and consumers could also be an effective tool for the increase in price peaks by adding time variable grid tariffs on top of already variable prices. However, in all these considerations, it should be ensured that energy justice is considered and high grid fees are not passed on to low-income households, which do not have the ability to shift loads.

While the thermal power output of HPs during pre-heating time is constrained by the

maximum indoor set temperature, with higher price peaks or zero pricing, pre-heating time is extended. Thus, the scenario where electricity price signals in all EU countries are without grid tariffs closely represents the physical limitation of the building stock to shift electricity throughout the year in most countries. In Germany and Austria, buildings with HPs would be able to shift 25% of their total electricity consumption from price peak to price off-peak hours. While prosumagers can shift a substantial amount of electric energy on a daily basis, the overall electricity demand of prosumagers increases due to additional losses. On the country level, however, this increase in demand on an annual level is minimal and depends on how actively demand is shifted. If retail electricity prices are high and the prominence of price change is lower, annual electricity demand consumed from the grid is reduced through prosumagers because of the increase in PV self-consumption. If electric loads are shifted excessively, for example, because of zero end consumer electricity prices in certain hours, the annual demand can increase by up to 10% in 2030 and 3.5% in 2050 over the whole EU. However, a sole increase in annual electricity demand is not necessarily a bad sign, as the increase in demand stems from hours with very low wholesale electricity prices, which are usually correlated to a negative residual load or overproduction of renewable generation units. Results have shown that the electricity demand at the EU-level can be increased by up to 2.1% in 2030 in low price times and at the same time reduced by 0.3 to 1% in times where the electricity price signal is within the 4^{th} price quantile.

5.3 Research question 3

How will the uptake of prosumagers impact future electricity distribution grid investments?

Future distribution networks will need to be reinforced to cope with additional loads of electrified heating systems and EVs. Nevertheless, a comprehensive simulation of the impacts across the entire distribution grid at a continental level would be impractical in terms of the computational resources required. Although this is a limitation of Mascherbauer et al. (2025a), insights into potential reinforcement needs for a location with a very high penetration of gas boilers in a colder climate, as well as a location with a warm climate and an already high share of electric heating systems, are provided. With this in mind, the methodology and the insights of the results are transferable to other regions with similar building and heating system characteristics. It is anticipated that grid reinforcements will be required in both locations, although the extent of these investments and the underlying drivers are different.

The peak load for HP-heated buildings is often determined through the coldest day of the year. At the national level, the yearly peak demand could be reduced by less than 0.1% through prosumagers. At the local level, results also showed no significant decrease in peak demand. Prosumagers proved beneficial for the distribution grid by increasing PV self-consumption, which reduces the peak PV generation fed into the grid and thus lowers reinforcement needs. This manifested especially in the needed investments in LV lines. MV lines and transformers are hardly impacted by prosumagers. On a local level, the impact of prosumagers does not only depend on the prosumagers themselves but also on other power consumers connected to the same grid. In Mascherbauer et al. (2025a), only the electricity demand of the residential buildings is considered. If the shift in power by prosumagers overlaps with medium-sized consumers (e.g., small enterprises), the effect on the grid could be different. A really important factor when it comes to the distribution grid reinforcements will be the uptake of EVs. If EVs are considered in the context of prosumagers, it is important that smart charging is not done over areas using the same price profile as an incentive to shift charging cycles. This would lead to a massive increase

in local peak load. These peaks can be high enough to trigger additional investment needs into transformers and MV lines in 2050.

On the other hand, a capacity-based tariff has been shown to be effective in reducing peak demand of prosumagers while reducing the total shifted electric energy only to a limited amount. At the national level, it was shown that an increase in peak demand due to simultaneous DR of many prosumagers can be reduced significantly by introducing a peak price on top of the variable retail electricity price. This reduction of peak demand at the prosumager level could be beneficial in the future for distribution grids.

The findings of the two case studies demonstrate the importance of long-term planning for grid investments and the need for future work to explore how local grid services (e.g., proposed Network Code on Demand Response) can enhance the positive impacts of prosumagers on distribution network planning. The lower reinforcement needs in Murcia compared to Leeuwarden are primarily due to the higher proportion of electric heating already in place in Murcia, which lessens the future load increase from HP adoption. Murcia exhibits a higher prevalence of multi-family residential buildings with comparatively reduced rooftop area per household, which can be allocated to solar PV installations. The results for Leeuwarden indicate that the grid will require extensive reinforcements by 2040, due to both the high demand growth from HPs and EVs and the wide voltage fluctuations observed between the lowest and highest voltages achieved on the peak demand and feed-in day, respectively. It may be necessary to incorporate unconventional planning practices, such as on-load tap-changing transformers or voltage regulators, in order to address the technological challenges of future long-term scenarios. Furthermore, it may be beneficial to engage in long-term planning for electricity distribution networks, given the potential challenges associated with identifying suitable locations for additional distribution transformers, particularly in urban areas.

In the case of Murcia and Leeuwarden, two policy scenarios were analyzed that reflect the renovation rate of the buildings and uptake of PV, AC, HP, and storage technologies. Distribution grid investments were almost always slightly higher for the strong policy scenario, even though buildings have a higher renovation rate in this scenario. The reason for this is simply the higher share of electrified heating and PV systems. Only in Leeuwarden in 2050, considering EVs, the strong policy scenario shows slightly lower costs, which is due to the fact that the higher PV penetration can soften the peak demand of the EVs. In general, the needed future investments of the distribution grid are very case-specific and will be driven by the uptake of EVs and HPs. Depending on the case, prosumagers can lower the needed investments.

6 Conclusion and Outlook

6.1 Conclusion

Decarbonizing the building sector represents a significant challenge. The shift towards electric heating systems, such as HPs, which are used to replace fossil fuel-powered heating systems, introduces new demands on the electricity grid, but also opens up valuable possibilities. On one hand, the growing use of electricity for heating coincides with a rising share of variable renewable electricity generation. The higher share of fluctuating electricity generation, together with the overall higher electricity demand, creates additional challenges for the power system on the transmission and distribution side. Furthermore, the potential mismatch between generation and demand requires additional flexibility. Buildings equipped with HPs could become a vital source of flexibility to match generation and demand. This thesis explores the future potential of such buildings across the EU to support the energy system by providing the needed flexibility.

The findings from this thesis support the hypothesis that HPs can contribute to short-term flexibility and relieve the electricity grid, particularly when the electricity price sends appropriate price signals. Real-time pricing can be an effective tool to change the electricity consumption patterns of heating and cooling devices. The operational cost savings largely depend on a building's energy demand and the electricity prices. Residential buildings, especially in Central Europe, have a significant potential for load shifting through the use of thermal mass, particularly during winter and transition seasons. At the EU-level 9-28 TWh of electric energy could be shifted through HP-operated residential buildings in 2030, of which around 40% is shifted by pre-heating the thermal mass of buildings.

The impact of electricity price volatility is crucial; with a higher marginal cost of flexible power plants, the flexibility potential of HPs increases, and prosumagers can shift more demand. However, this flexibility is not without its limitations, as high DR also correlates to higher total electricity consumption due to increased losses. The grid demand of prosumaging buildings in the EU could rise by up to 9% in 2030 and 3.5% in 2050. Even though this would decrease the EU's electricity consumption at high prices by up to 1%, the increase in consumption at low price times can be more than 2% of the total EU electricity consumption. Therefore, it will be important that retail electricity prices reflect actual electricity scarcity on a local level.

The electrification of residential energy uses, such as heating and transport, will challenge future electricity grid development plans, especially in colder regions where fossil-fueled heating systems currently dominate. Analyzing this requires looking at the problem at the lowest spatial level because the location of new loads and PV installations plays an important role. The stress on the local distribution grid can be lowered by incentivizing consumers to shift load to off-peak hours. In future scenarios, which are characterized by a high percentage of prosumagers and involve EVs, however, the stress on the local distribution grid could increase. The findings of this thesis indicate that very high shares of prosumagers with electricity prices, which do not reflect the distribution grid's status, will create new load peaks due to the simultaneous activation of controllable loads. Therefore,

very high shares of prosumagers will significantly increase the distribution grid's stress and require substantially higher investments unless demand response mechanisms considering the local distribution grid's status are implemented. From the standpoint of managing the burden on grid infrastructure, the introduction of real-time pricing should avoid negative or zero electricity prices for prosumagers, as these could otherwise result in substantial increases in peak demand. Encouraging self-consumption of PV energy should remain a key objective for prosumagers, given its potential to lower distribution grid expansion costs. One very effective method to reduce the peak demand of prosumagers is adding a capacity price to the electricity cost. Results of this thesis showed that this measure could reduce the yearly peak demand of HP-heated buildings compared to their consumer counterparts and could be an effective tool in the future to reduce congestion in distribution grids.

In conclusion, while HPs can provide valuable short-term flexibility, appropriate price signals and grid strategies will be essential for realizing their full potential without excessive reinforcement needs for the grid or negative side effects. The contribution of HPs is expected to grow, but they will need to be integrated with complementary technologies like HEMS to be able to automatically react to price changes. To avoid excessive distribution grid investments, PV self-consumption should be encouraged, and local electricity price design is crucial to avoid increased peak demand.

6.2 Future work

This final chapter points out the need for further research on top of what has been presented within this thesis. Given the conclusions derived in this thesis, several key areas for further research emerge. Addressing these areas will enhance the understanding of electricity demand flexibility in the residential building stock, optimize grid integration, and support Europe's ambitious decarbonization goals.

Firstly, additional research at the distribution grid level is necessary to comprehensively explore how different pricing incentives could impact prosumagers' behavior. Specifically, detailed investigations are required to develop tariff structures that accurately reflect local electricity scarcity or grid overload conditions. Such dynamic, localized tariffs could help prevent load synchronization, thereby reducing the risk of creating new demand peaks that exacerbate distribution grid stress. Furthermore, research is necessary to explore how variable electricity prices could be effectively coupled with dynamic grid tariffs reflecting real-time local electricity availability and network constraints. This approach could lead to different local electricity prices for end consumers in different regions, more accurately reflecting the specific needs and availability of electricity generation and grid infrastructure in each area.

Secondly, despite existing efforts at the EU level through the funding of various projects (MODERATE[1], BuiltHUB[2], ReLIFE[3], DigiBUILD[4] Building stock observatory[5]), research gaps remain concerning the detailed characteristics of the actual building stock in individual EU Member States. Country-specific investigations and comprehensive building databases are crucial to accurately quantify demand flexibility potentials and implement appropriate policies. These efforts would benefit from close cooperation with ongoing EU

[1]MODERATE project: https://moderate-project.eu/, Horizon Europe under grant agreement No 101069834

[2]BuiltHub project: https://builthub.eu/, European Union's Horizon 2020 programme under grant agreement N 957026

[3]ReLIFE project: https://relife-project.eu/, Life project co-funded by the European Union

[4]DigiBUILD project: https://digibuild-project.eu/

[5]BSO-EU Building Stock Observatory https://building-stock-observatory.energy.ec.europa.eu/database/

projects to ensure consistency, complementarity, and comprehensive coverage, also in regard to the spatial coverage of data. So far, data at the regional and country level is usually only available in an aggregated database without information on the location. Although some countries work on mapping the building stock with geographical information system (e.g. *URBAN3R* (2025) in Spain) comprehensive data is usually not available on larger scales. Having information on individual buildings' energy consumption and location is crucial when trying to understand how much flexibility is available, also considering electricity grid constraints.

Thirdly, the validation of existing theoretical and simulation-based models demands real-world data from individual buildings as well as comprehensive building stock data. Empirical studies and extensive measurement campaigns would significantly enhance the accuracy and reliability of demand flexibility models, enabling stakeholders to develop more precise forecasts and effective strategies.

Finally, research is needed to assess and quantify the precise impacts prosumagers have at various levels of the electricity grid—ranging from local distribution grids to regional and national transmission systems. In-depth analysis should explore how electricity generation, grid infrastructure at multiple levels, and diverse building stocks interplay. This holistic understanding is crucial to ensure the effective integration of prosumagers and to realize their potential in supporting a robust, sustainable, and economically viable energy system.

6.3 List of papers

Main publications during my PhD:

- **Philipp Mascherbauer**, Lukas Kranzl, Songmin Yu, Thomas Haupt (2022). "Investigating the impact of smart energy management system on the residential electricity consumption in Austria". en. In: Energy 249, p. 123665. DOI: https://doi.org/10.1016/j.energy.2022.123665.

- **Philipp Mascherbauer**, Franziska Schöniger, Lukas Kranzl, Songmin Yu (2024). "Impact of variable electricity price on heat pump operated buildings". In: Open Research Europe 2. Publisher: F1000 Research Ltd, p. 135. DOI: https://doi.org/10.12688/openreseurope.15268.2

- **Philipp Mascherbauer**, Miguel Martínez, Carlos Mateo, Songmin Yu, Lukas Kranzl (2025). "Analyzing the impact of heating electrification and prosumaging on the future distribution grid costs". In: Applied Energy 387, p. 125563. DOI: https://doi.org/10.1016/j.apenergy.2025.125563

- **Philipp Mascherbauer**, Lukas Kranzl, Florian Hasengst (2025). "The Flexibility of Electrical Loads in the EU-27 Residential Building Stock". In: 2025 21st International Conference on the European Energy Market (EEM). 2025 21st International Conference on the European Energy Market (EEM). Lisbon, Portugal: IEEE, pp. 1–6. DOI: https://doi.org/10.1109/eem64765.2025.11050330

- **Philipp Mascherbauer**, Ece Özer, Lukas Kranzl, Songmin Yu (forthcoming). "Future flexibility of the EU27 heat pump heated residential building stock". In: Submitted to Energy.

Complimentary publications during my PhD as co-author:

- Songmin Yu, **Philipp Mascherbauer**, Thomas Haupt, Kevan Skorna, Hannah Rickmann, Maksymilian Kochanski, Lukas Kranzl (2025). "Modeling households' behavior, energy system operation, and interaction in the energy community". In: Energy, p. 136338. DOI: https://doi.org/10.1016/j.energy.2025.136338

- Franziska Schöniger, **Philipp Mascherbauer**, Gustav Resch, Lukas Kranzl, Reinhard Haas (2024). "The potential of decentral heat pumps as flexibility option for decarbonised energy systems". en. In: Energy Efficiency 17.4, p. 26. DOI: https://doi.org/10.1007/s12053-024-10206-z

- Daniel Heidenthaler, Yingwen Deng, Markus Leeb, Michael Grobbauer, Lukas Kranzl, Lena Seiwald, **Philipp Mascherbauer**, Patricia Reindl, Thomas Bednar (2023). "Automated energy performance certificate based urban building energy modelling approach for predicting heat load profiles of districts". In: Energy 278, p. 128024. DOI: https://doi.org/10.1016/j.energy.2023.128024

Bibliography

Abdufattokhov, Shokhjakon et al. (2021). "Learning Convex Terminal Costs for Complexity Reduction in MPC". In: *2021 60th IEEE Conference on Decision and Control (CDC)*, pp. 2163–2168. DOI: 10.1109/CDC45484.2021.9683069.

ACER (Sept. 2023). *Flexibility solutions to support a decarbonised and secure EU electricity system*. EEA/ACER Report 09/2023. European Environment Agency, ACER.

Ali Aydemir et al. (2020). *Hotmaps Toolbox*.

Andreas Müller (2021). *Energy demand scenarios in buildings until the year 2050 - scenarios with refurbishment rate (maintenance + thermal renovation) of 0.5%, 1%, 2% and 3% (Version 1) [Data set]*. DOI: 10.5281/ZENODO.4687105.

Angenendt, Georg et al. (Jan. 2019). "Optimization and operation of integrated homes with photovoltaic battery energy storage systems and power-to-heat coupling". en. In: *Energy Conversion and Management: X* 1, p. 100005. DOI: 10.1016/j.ecmx.2019.100005.

APCS, ed. (2019). *Synthetische Lastprofile*.

Awais, Muhammad et al. (Apr. 30, 2025). *European Climate + Energy Modeling Forum (ECEMF), D2.3 – Synthesis Report on Energy Demand Modelling Comparison*. Deliverable, p. 83.

Baeten, Brecht et al. (June 2017). "Reduction of heat pump induced peak electricity use and required generation capacity through thermal energy storage and demand response". In: *Applied Energy* 195, pp. 184–195. DOI: 10.1016/j.apenergy.2017.03.055.

Balmorel Code (2022). https://github.com/balmorelcommunity/Balmorel.

Bechtel, Steffen et al. (2020). "Influence of thermal energy storage and heat pump parametrization for demand-side-management in a nearly-zero-energy-building using model predictive control". In: *Energy and Buildings* 226, p. 110364. DOI: 10.1016/j.enbuild.2020.110364.

Bloess, Andreas et al. (Feb. 2018). "Power-to-heat for renewable energy integration: A review of technologies, modeling approaches, and flexibility potentials". In: *Applied Energy* 212, pp. 1611–1626. DOI: 10.1016/j.apenergy.2017.12.073.

Boletín Oficial del Estado (2024a). *BOE-A-2000-24019 (https://www.boe.es/eli/es/rd/2000/12/01/1955/con)*. (Visited on 10/27/2024).

— (2024b). *BOE-A-2015-13488 (https://www.boe.es/eli/es/o/2015/12/11/iet2660)*. (Visited on 10/27/2024).

Bosch, ed. (n.d.). *Wärmepumpen von Bosch*.

Bruno, Roberto et al. (2016a). "The Prediction of Thermal Loads in Building by Means of the EN ISO 13790 Dynamic Model: A Comparison with TRNSYS". In: *Energy Procedia* 101, pp. 192–199. DOI: 10.1016/j.egypro.2016.11.025.

— (2016b). "The Prediction of Thermal Loads in Building by Means of the EN ISO 13790 Dynamic Model: A Comparison with TRNSYS". In: *Energy Procedia* 101, pp. 192–199. DOI: https://doi.org/10.1016/j.egypro.2016.11.025.

Calearo, Lisa et al. (2021). "A review of data sources for electric vehicle integration studies". In: *Renewable and Sustainable Energy Reviews* 151, p. 111518. DOI: https://doi.org/10.1016/j.rser.2021.111518.

Campillo, J. et al. (Oct. 2012). "Electricity demand impact from increased use of ground sourced heat pumps". In: *2012 3rd IEEE PES Innovative Smart Grid Technologies Europe (ISGT Europe)*. Berlin, Germany: IEEE, pp. 1–7. DOI: 10.1109/ISGTEurope.2012.6465876.

Celik, Berk et al. (Dec. 2017). "Electric energy management in residential areas through coordination of multiple smart homes". en. In: *Renewable and Sustainable Energy Reviews* 80, pp. 260–275. DOI: 10.1016/j.rser.2017.05.118.

Centraal Bureau voor de Statistiek (2024). *Car ownership per household January 1, 2023 (https://www.cbs.nl/nl-nl/maatwerk/2024/08/autobezit-per-huishouden-1-januari-2023)*. (Visited on 07/04/2024).

Chen, Yongbao et al. (2020). "Experimental investigation of demand response potential of buildings: Combined passive thermal mass and active storage". In: *Applied Energy* 280, p. 115956. DOI: 10.1016/j.apenergy.2020.115956.

Cholewa, Tomasz et al. (Nov. 2013). "On the heat transfer coefficients between heated/cooled radiant floor and room". In: *Energy and Buildings* 66, pp. 599–606. DOI: 10.1016/j.enbuild.2013.07.065.

Cirrincione, Laura et al. (2019). "The European standards for energy efficiency in buildings: An analysis of the evolution with reference to a case study". In: *74TH ATI NATIONAL CONGRESS: Energy Conversion: Research, Innovation and Development for Industry and Territories*. Vol. 2191. Erode, India, p. 020049. DOI: 10.1063/1.5138782.

Corrado, Vincenzo et al. (2007). "Assessment of building cooling energy need through a quasi-steady state model: Simplified correlation for gain-loss mismatch". In: *Energy and Buildings* 39.5, pp. 569–579. DOI: 10.1016/j.enbuild.2006.09.012.

Cozza, Stefano et al. (Nov. 2022). "Decarbonizing residential buildings with heat pumps: Transferability of front-runner experiences from Swiss Cantons". In: *Energy Reports* 8, pp. 14048–14060. DOI: 10.1016/j.egyr.2022.09.141.

Daikin, ed. (n.d.). *Daikin altherma technical data sheet*.

De Rosa, Luca et al. (2024). "Design and assessment of energy infrastructure in new decarbonized urban districts: A Spanish case study". In: *Energy Reports* 11, pp. 4631–4641. DOI: https://doi.org/10.1016/j.egyr.2024.04.037.

Dong, Zihang et al. (Jan. 2023). "Values of coordinated residential space heating in demand response provision". en. In: *Applied Energy* 330, p. 120353. DOI: 10.1016/j.apenergy.2022.120353.

E-Control (Jan. 1, 2016). *Verordnung der Regulierungskommission der E-Control, mit der die Entgelte für die Systemnutzung bestimmt werden (Systemnutzungsentgelte-Verordnung 2012, SNE-VO 2012)*.

E-control, ed. (2017). *Ökostrom-Einspeisetaifverordnung 2018*.

Earle, Lieko et al. (2023). "The impact of energy-efficiency upgrades and other distributed energy resources on a residential neighborhood-scale electrification retrofit". In: *Applied Energy* 329, p. 120256. DOI: https://doi.org/10.1016/j.apenergy.2022.120256.

ehi (2023). *Heating market report 2023*. European Heating Industry, p. 37.

Elaad Platform (2024). *ElaadNL Open Datasets for Electric Mobility Research | Update April 2020 (https://platform.elaad.io/analyses/ElaadNL_opendata.php)*. (Visited on 07/04/2024).

Elma, Onur et al. (Aug. 9, 2022). "A Smart Direct Load Control Approach Using Dynamic Voltage Control for Demand Response Programs". In: *Electric Power Components and Systems* 50.13, pp. 738–750. DOI: 10.1080/15325008.2022.2139869.

Elmallah, Salma et al. (Nov. 2022). "Can distribution grid infrastructure accommodate residential electrification and electric vehicle adoption in Northern California?" In: *Environmental Research: Infrastructure and Sustainability* 2.4, p. 045005. DOI: 10.1088/2634-4505/ac949c.

Emhofer, Johann et al. (2014). *HPP Annex 43: Country report Austria*. URL: %5Curl%7Bhttps://nachhaltigwirtschaften.at/resources/iea_pdf/hpt-annex-43-country_report_austria-2016.pdf%7D (visited on 11/28/2021).

esios (https://www.esios.ree.es/es) (2024). (Visited on 10/27/2024).

European Commission (2024). *National energy and climate plans (https://energy.ec.europa.eu/topics/energy-strategy/national-energy-and-climate-plans-necps_en)*. (Visited on 07/04/2024).

European Commission Joint Research Centre (2024). *PHOTOVOLTAIC GEOGRAPHICAL INFORMATION SYSTEM (https://re.jrc.ec.europa.eu/pvg_tools/en/)*. (Visited on 10/27/2024).

European Parliament, Council of the European Union (2024). *Directive (EU) 2024/1275 of the European Parliament and of the Council of 24 April 2024 on the energy performance of buildings*.

European Union Agency for the Cooperation of Energy Regulators et al. (2025). *Getting the signals right: Electricity network tariff methodolo- gies in Europe. 2025*.

Eurostat (2024a). *nrg-d-hhq (https://doi.org/10.2908/NRG_D_HHQ)*. (Visited on 10/27/2024).

— (2024b). *tps00001 (https://doi.org/10.2908/TPS00001)*. (Visited on 10/27/2024).

EXAA, ed. (2016). *EXAA Energy Exchange Austria*.

Fallahnejad, Mostafa (2024). "Economic assessment of district heating grid infrastructure". PhD thesis. TU Wien. DOI: 10.34726/HSS.2024.125102.

Fischer, David et al. (2019). "Electric vehicles' impacts on residential electric local profiles – A stochastic modelling approach considering socio-economic, behavioural and spatial factors". In: *Applied Energy* 233-234, pp. 644–658. DOI: https://doi.org/10.1016/j.apenergy.2018.10.010.

Fitzpatrick, Peter et al. (Sept. 2020). "Influence of electricity prices on energy flexibility of integrated hybrid heat pump and thermal storage systems in a residential building". en. In: *Energy and Buildings* 223, p. 110142. DOI: 10.1016/j.enbuild.2020.110142.

Formayer, Herbert et al. (2023a). *SECURES-Met - A European wide meteorological data set suitable for electricity modelling (supply and demand) for historical climate and climate change projections*. DOI: 10.5281/ZENODO.7907883.

Formayer, Herbert et al. (Sept. 7, 2023b). "SECURES-Met: A European meteorological data set suitable for electricity modelling applications". In: *Scientific Data* 10.1, p. 590. DOI: 10.1038/s41597-023-02494-4.

Gaur, Ankita Singh et al. (Jan. 2021). "Heat pumps and our low-carbon future: A comprehensive review". In: *Energy Research & Social Science* 71, p. 101764. DOI: 10.1016/j.erss.2020.101764.

Gokhale, Gargya et al. (May 2022). "Physics informed neural networks for control oriented thermal modeling of buildings". In: *Applied Energy* 314, p. 118852. DOI: 10.1016/j.apenergy.2022.118852.

Golmohamadi, Hessam (2021a). "Stochastic energy optimization of residential heat pumps in uncertain electricity markets". In: *Applied Energy* 303, p. 117629. DOI: https://doi.org/10.1016/j.apenergy.2021.117629.

— (2021b). "Stochastic energy optimization of residential heat pumps in uncertain electricity markets". In: *Applied Energy* 303, p. 117629. DOI: 10.1016/j.apenergy.2021.117629.

Gonzalez Venegas, Felipe et al. (2021). "Plug-in behavior of electric vehicles users: Insights from a large-scale trial and impacts for grid integration studies". In: *eTransportation* 10, p. 100131. DOI: https://doi.org/10.1016/j.etran.2021.100131.

Gupta, Ruchi et al. (2021). "Spatial analysis of distribution grid capacity and costs to enable massive deployment of PV, electric mobility and electric heating". In: *Applied Energy* 287, p. 116504. DOI: https://doi.org/10.1016/j.apenergy.2021.116504.

Hall, Monika et al. (Dec. 2021). "Comparison of Flexibility Factors and Introduction of A Flexibility Classification Using Advanced Heat Pump Control". en. In: *Energies* 14.24, p. 8391. DOI: 10.3390/en14248391.

Hanke Marcel (2020). *Modellierung von Strommarkterlösen. Entwicklung eines adäquaten modellhaften Abbilds des konventionellen Kraftwerksparks ausgewählter Länder Europas*. DOI: 10.34726/hss.2020.64208.

Härkönen, Kalevi et al. (2022). "Assessing the electric demand-side management potential of Helsinki's public service building stock in ancillary markets". In: *Sustainable Cities and Society* 76, p. 103460. DOI: 10.1016/j.scs.2021.103460.

Hart, William E. et al. (2017). *Pyomo — Optimization Modeling in Python*. Vol. 67. Cham: Springer International Publishing. DOI: 10.1007/978-3-319-58821-6.

Hartvigsson, Elias et al. (2022). "A large-scale high-resolution geographic analysis of impacts of electric vehicle charging on low-voltage grids". In: *Energy* 261, p. 125180. DOI: https://doi.org/10.1016/j.energy.2022.125180.

Hedegaard, Karsten et al. (Dec. 2013). "Energy system investment model incorporating heat pumps with thermal storage in buildings and buffer tanks". en. In: *Energy* 63, pp. 356–365. DOI: 10.1016/j.energy.2013.09.061.

Heinen, Steve et al. (May 2017). "Electrification of residential space heating considering coincidental weather events and building thermal inertia: A system-wide planning analysis". en. In: *Energy* 127, pp. 136–154. DOI: 10.1016/j.energy.2017.03.102.

Helios, ed. (n.d.). *Heliotherm: Die Wärmepumpe*.

Hens, Hugo et al. (Jan. 2010). "Energy consumption for heating and rebound effects". In: *Energy and Buildings* 42.1, pp. 105–110. DOI: 10.1016/j.enbuild.2009.07.017.

Hernández, J. C. et al. (2019). "Design criteria for the optimal sizing of a hybrid energy storage system in PV household-prosumers to maximize self-consumption and self-sufficiency". In: *Energy* 186, p. 115827. DOI: 10.1016/j.energy.2019.07.157.

Hoseinpoori, Pooya et al. (Sept. 2022). "A whole-system approach for quantifying the value of smart electrification for decarbonising heating in buildings". en. In: *Energy Conversion and Management* 268, p. 115952. DOI: 10.1016/j.enconman.2022.115952.

Hu, Maomao et al. (May 2019). "Price-responsive model predictive control of floor heating systems for demand response using building thermal mass". en. In: *Applied Thermal Engineering* 153, pp. 316–329. DOI: 10.1016/j.applthermaleng.2019.02.107.

Huld, Thomas et al. (2012). "A new solar radiation database for estimating PV performance in Europe and Africa". In: *Solar Energy* 86.6, pp. 1803–1815. DOI: 10.1016/j.solener.2012.03.006.

Hülsmann, Jonas et al. (2019). "Balancing power potential of pools of small-scale units". In: *2019 16th International Conference on the European Energy Market (EEM)*, pp. 1–6. DOI: 10.1109/EEM.2019.8916477.

IEEE (2022). "IEEE Guide for Electric Power Distribution Reliability Indices". In: *IEEE Std 1366-2022 (Revision of IEEE Std 1366-2012)*, pp. 1–44. DOI: 10.1109/IEEESTD.2022.9955492.

Instituto Nacional de Estadística (2024). *Survey on Essential Characteristics of Population and Housing. Year 2021 (https://www.ine.es/dyngs/INEbase/en/operacion.htm?c=Estadistica_C&cid=1254736177092&menu=ultiDatos&idp=1254735572981)*. (Visited on 07/04/2024).

JRC (2023). *Heat pumps in the European Union, Status report on technology, trends, value chains & markets*. EUR 31699EN. Joint Research Center, p. 65.

Kandler, Christian (2017). *Modellierung von Zeitnutzungs-, Mobilitäts- und Energieprofilen zur Bestimmung der Potentiale von Energiemanagementsystemen: Dissertation*. Technische Universität München. DOI: 10.13140/RG.2.2.17638.73281.

Kathirgamanathan, Anjukan et al. (2020). "Towards standardising market-independent indicators for quantifying energy flexibility in buildings". In: *Energy and Buildings* 220, p. 110027. DOI: https://doi.org/10.1016/j.enbuild.2020.110027.

Katz, Jonas et al. (Nov. 2016). "Load-shift incentives for household demand response: Evaluation of hourly dynamic pricing and rebate schemes in a wind-based electricity system". en. In: *Energy* 115, pp. 1602–1616. DOI: 10.1016/j.energy.2016.07.084.

Kebede, Abraham Alem et al. (2021). "Techno-economic analysis of lithium-ion and lead-acid batteries in stationary energy storage application". In: *Journal of Energy Storage* 40, p. 102748. DOI: 10.1016/j.est.2021.102748.

Kelly, Nick et al. (Dec. 2021). "Assessing the ability of electrified domestic heating in the UK to provide unplanned, short-term responsive demand". In: *Energy and Buildings* 252, p. 111430. DOI: 10.1016/j.enbuild.2021.111430.

Kelly, Nicolas et al. (2014). "Performance assessment of tariff-based air source heat pump load shifting in a UK detached dwelling featuring phase change-enhanced buffering". In: *Applied Thermal Engineering* 71.2, pp. 809–820. DOI: 10.1016/j.applthermaleng.2013.12.019.

Khalili, Siavash et al. (Apr. 2025). "Role and trends of flexibility options in 100% renewable energy system analyses towards the Power-to-X Economy". In: *Renewable and Sustainable Energy Reviews* 212, p. 115383. DOI: 10.1016/j.rser.2025.115383.

Klein, Konstantin et al. (Jan. 2016). "Grid support coefficients for electricity-based heating and cooling and field data analysis of present-day installations in Germany". en. In: *Applied Energy* 162, pp. 853–867. DOI: 10.1016/j.apenergy.2015.10.107.

Klein, Konstantin et al. (Oct. 2017). "Load shifting using the heating and cooling system of an office building: Quantitative potential evaluation for different flexibility and storage options". en. In: *Applied Energy* 203, pp. 917–937. DOI: 10.1016/j.apenergy.2017.06.073.

Klingler, Anna-Lena (2018). "The effect of electric vehicles and heat pumps on the market potential of PV + battery systems". In: *Energy* 161, pp. 1064–1073. DOI: 10.1016/j.energy.2018.07.210.

Kotzur, Leander (2018). "Future Grid Load of the Residential Building Sector". In: *Energie & Umwelt/Energy & Environmen*.

Kuczyński, T. et al. (2020). "Experimental study of the influence of thermal mass on thermal comfort and cooling energy demand in residential buildings". In: *Energy* 195, p. 116984. DOI: 10.1016/j.energy.2020.116984.

Laguna, Gerard et al. (Nov. 2022). "Dynamic horizon selection methodology for model predictive control in buildings". en. In: *Energy Reports* 8, pp. 10193–10202. DOI: 10.1016/j.egyr.2022.08.015.

Lauster, M. et al. (Mar. 2014). "Low order thermal network models for dynamic simulations of buildings on city district scale". en. In: *Building and Environment* 73, pp. 223–231. DOI: 10.1016/j.buildenv.2013.12.016.

Le Dréau, J. et al. (Sept. 2016a). "Energy flexibility of residential buildings using short term heat storage in the thermal mass". en. In: *Energy* 111, pp. 991–1002. DOI: 10.1016/j.energy.2016.05.076.

— (2016b). "Energy flexibility of residential buildings using short term heat storage in the thermal mass". In: *Energy* 111, pp. 991–1002. DOI: 10.1016/j.energy.2016.05.076.

Leonhartsberger, K. et al. (2021). "Analyse der Marktentwicklung von PV-Heimspeichersystemen in Österreich". In.

Lind, Johan et al. (Dec. 2023). "Energy flexibility using the thermal mass of residential buildings". en. In: *Energy and Buildings* 301, p. 113698. DOI: 10.1016/j.enbuild.2023.113698.

Lotfi, Mohamed et al. (Feb. 2022). "Coordinating energy management systems in smart cities with electric vehicles". en. In: *Applied Energy* 307, p. 118241. DOI: 10.1016/j.apenergy.2021.118241.

Lu, Chujie et al. (May 2022). "Building energy prediction using artificial neural networks: A literature survey". In: *Energy and Buildings* 262, p. 111718. DOI: 10.1016/j.enbuild.2021.111718.

Luo, Jianing et al. (2020). "Parametric study to maximize the peak load shifting and thermal comfort in residential buildings located in cold climates". In: *Journal of Energy Storage* 30, p. 101560. DOI: 10.1016/j.est.2020.101560.

Luo, X.J. et al. (May 2019). "Development of integrated demand and supply side management strategy of multi-energy system for residential building application". en. In: *Applied Energy* 242, pp. 570–587. DOI: 10.1016/j.apenergy.2019.03.149.

Luthander, Rasmus et al. (2015). "Photovoltaic self-consumption in buildings: A review". In: *Applied Energy* 142, pp. 80–94.

Manner, Pekka et al. (2020). "Domestic heat pumps as a source of primary frequency control reserve". In: *2020 17th International Conference on the European Energy Market (EEM)*, pp. 1–5. DOI: 10.1109/EEM49802.2020.9221902.

Martínez, Miguel et al. (2021). "Assessment of the impact of a fully electrified postal fleet for urban freight transportation". In: *International Journal of Electrical Power & Energy Systems* 129, p. 106770. DOI: https://doi.org/10.1016/j.ijepes.2021.106770.

Mascherbauer, Philipp et al. (June 2022). "Investigating the impact of smart energy management system on the residential electricity consumption in Austria". en. In: *Energy* 249, p. 123665. DOI: 10.1016/j.energy.2022.123665.

Mascherbauer, Philipp et al. (Sept. 6, 2024). "Impact of variable electricity price on heat pump operated buildings". In: *Open Research Europe* 2. Publisher: F1000 Research Ltd, p. 135. DOI: 10.12688/openreseurope.15268.2.

Mascherbauer, Philipp et al. (June 2025a). "Analyzing the impact of heating electrification and prosumaging on the future distribution grid costs". In: *Applied Energy* 387, p. 125563. DOI: 10.1016/j.apenergy.2025.125563.

Mascherbauer, Philipp et al. (May 27, 2025b). "The Flexibility of Electrical Loads in the EU-27 Residential Building Stock". In: *2025 21st International Conference on the European Energy Market (EEM)*. 2025 21st International Conference on the European Energy Market (EEM). Lisbon, Portugal: IEEE, pp. 1–6. DOI: 10.1109/eem64765.2025.11050330.

Mascherbauer, Philipp et al. (forthcoming). "Future flexibility of the EU27 heat pump heated residential building stock". In: *Submitted to Energy*. DOI: underreview.

Masy, Gabrielle et al. (Aug. 18, 2015). "Smart grid energy flexible buildings through the use of heat pumps and building thermal mass as energy storage in the Belgian context". In: *Science and Technology for the Built Environment* 21.6, pp. 800–811. DOI: 10.1080/23744731.2015.1035590.

Mateo, Carlos et al. (2011). "A Reference Network Model for Large-Scale Distribution Planning With Automatic Street Map Generation". In: *IEEE Transactions on Power Systems* 26.1, pp. 190–197. DOI: 10.1109/TPWRS.2010.2052077.

Mateo, Carlos et al. (2016). "Cost–benefit analysis of battery storage in medium-voltage distribution networks". In: *IET Generation, Transmission & Distribution* 10.3, pp. 815–821. DOI: doi:10.1049/iet-gtd.2015.0389. eprint: https://ietresearch.onlinelibrary.wiley.com/doi/pdf/10.1049/iet-gtd.2015.0389.

Mateo, Carlos et al. (2018a). "European representative electricity distribution networks". In: *International Journal of Electrical Power & Energy Systems* 99, pp. 273–280. DOI: https://doi.org/10.1016/j.ijepes.2018.01.027.

Mateo, Carlos et al. (2018b). "Impact of solar PV self-consumption policies on distribution networks and regulatory implications". In: *Solar Energy* 176, pp. 62–72. DOI: https://doi.org/10.1016/j.solener.2018.10.015.

McGarry, Connor et al. (2023). "A high-resolution geospatial and socio-technical methodology for assessing the impact of electrified heat and transport on distribution network

infrastructure". In: *Sustainable Energy, Grids and Networks* 35, p. 101118. DOI: https://doi.org/10.1016/j.segan.2023.101118.

Meesenburg, Wiebke et al. (2020). "Combined provision of primary frequency regulation from Vehicle-to-Grid (V2G) capable electric vehicles and community-scale heat pump". In: *Sustainable Energy, Grids and Networks* 23, p. 100382. DOI: 10.1016/j.segan.2020.100382.

Miara, Marek et al. (2014). "Simulation of an Air-to-Water Heat Pump System to Evaluate the Impact of Demand-Side-Management Measures on Efficiency and Load-Shifting Potential". In: *Energy Technology* 2.1, pp. 90–99. DOI: 10.1002/ente.201300087.

Michalak, Piotr (Oct. 2014). "The simple hourly method of EN ISO 13790 standard in Matlab/Simulink: A comparative study for the climatic conditions of Poland". en. In: *Energy* 75, pp. 568–578. DOI: 10.1016/j.energy.2014.08.019.

Ministerio de Transportes y Movilidad Sostenible (2024). *Mobility Open Data (https://data.mitma.gob.es/public/mov-municipal)*. (Visited on 07/04/2024).

Müller, Andreas (2014). *Heating and cooling energy demand and loads for building types in different countries of the EU: D2.3 of WP2 of the Entranze Project*.

— (2015). *Energy Demand Assessment for Space Conditioning and Domestic Hot Water: A Case Study for the Austrian Building Stock*. en. TU Wien, p. 285.

Nationalrat (2021). *Bundesgesetz über den Ausbau von Energie aus erneuerbaren Quellen: EAG*.

Navarro-Espinosa, Alejandro et al. (2014). "Probabilistic modeling and assessment of the impact of electric heat pumps on low voltage distribution networks". In: *Applied Energy* 127, pp. 249–266. DOI: https://doi.org/10.1016/j.apenergy.2014.04.026.

Navarro-Espinosa, Alejandro et al. (2016). "Probabilistic Impact Assessment of Low Carbon Technologies in LV Distribution Systems". In: *IEEE Transactions on Power Systems* 31.3, pp. 2192–2203. DOI: 10.1109/TPWRS.2015.2448663.

Netbeheer Nederland (2025). *Capaciteitskaart*. (Visited on 01/08/2025).

Ochsner, ed. (2021). *Ochsner Wärmepumpen*.

Olsthoorn, Dave et al. (2019). "Integration of electrically activated concrete slab for peak shifting in a light-weight residential building—Determining key parameters". In: *Journal of Energy Storage* 23, pp. 329–343. DOI: 10.1016/j.est.2019.03.023.

OpenStreetMap contributors (2017). *Open Street Maps (https://www.openstreetmap.org)*. (Visited on 10/27/2024).

Østergaard, Poul Alberg et al. (2021). "Variable taxes promoting district heating heat pump flexibility". In: *Energy* 221, p. 119839. DOI: 10.1016/j.energy.2021.119839.

Oviedo-Cepeda, Juan C. et al. (Oct. 2021). "Model Predictive Control Horizon Impact Over the Flexibility of a Net Zero Energy Building". In: *IECON 2021 – 47th Annual Conference of the IEEE Industrial Electronics Society*. Toronto, ON, Canada: IEEE, pp. 1–6. DOI: 10.1109/IECON48115.2021.9589828.

Park, Seho et al. (2021). "Model Predictive Control With Stochastically Approximated Cost-to-Go for Battery Cooling System of Electric Vehicles". In: *IEEE Transactions on Vehicular Technology* 70.5, pp. 4312–4323. DOI: 10.1109/TVT.2021.3073126.

Paterakis, Nikolaos G. et al. (Mar. 2017). "An overview of Demand Response: Key-elements and international experience". In: *Renewable and Sustainable Energy Reviews* 69, pp. 871–891. DOI: 10.1016/j.rser.2016.11.167.

Patteeuw, Dieter et al. (2016). "Comparison of load shifting incentives for low-energy buildings with heat pumps to attain grid flexibility benefits". In: *Applied Energy* 167, pp. 80–92. DOI: 10.1016/j.apenergy.2016.01.036.

Pena-Bello, Alejandro et al. (July 2021). "Decarbonizing heat with PV-coupled heat pumps supported by electricity and heat storage: Impacts and trade-offs for prosumers and the grid". In: *Energy Conversion and Management* 240, p. 114220. DOI: 10.1016/j.enconman.2021.114220.

Peters, Ravi et al. (2022). "Automated 3D reconstruction of LoD2 and LoD1 models for all 10 million buildings of the Netherlands". English. In: *Photogrammetric Engineering and Remote Sensing* 88.3, pp. 165–170. DOI: 10.14358/PERS.21-00032R2.

Pothof, I. et al. (Dec. 2023). "Data-driven method for optimized supply temperatures in residential buildings". In: *Energy* 284, p. 129183. DOI: 10.1016/j.energy.2023.129183.

Prat, Eléa et al. (Nov. 2024). "How long is long enough? Finite-horizon approximation of energy storage scheduling problems". In: *xrXiv*. arXiv:2411.17463 [math]. DOI: 10.48550/arXiv.2411.17463.

Protopapadaki, Christina et al. (2017). "Heat pump and PV impact on residential low-voltage distribution grids as a function of building and district properties". In: *Applied Energy* 192, pp. 268–281. DOI: https://doi.org/10.1016/j.apenergy.2016.11.103.

Resch et al. (2022). *Technical Report on the Modelling of RES auctions: Key insights on the model-based analyses conducted in the course of the AURES II project.*

Reynders, Glenn et al. (June 2013). "Potential of structural thermal mass for demand-side management in dwellings". en. In: *Building and Environment* 64, pp. 187–199. DOI: 10.1016/j.buildenv.2013.03.010.

Reynders, Glenn et al. (July 2017). "Generic characterization method for energy flexibility: Applied to structural thermal storage in residential buildings". en. In: *Applied Energy* 198, pp. 192–202. DOI: 10.1016/j.apenergy.2017.04.061.

Rieck, Katharina et al. (Jan. 2025). "Large-scale quantification of the future self-covered heat demand using a nationwide residential building database". en. In: *Energy*, p. 134622. DOI: 10.1016/j.energy.2025.134622.

Rinaldi, Arthur et al. (Jan. 2021). "Decarbonising heat with optimal PV and storage investments: A detailed sector coupling modelling framework with flexible heat pump operation". In: *Applied Energy* 282, p. 116110. DOI: 10.1016/j.apenergy.2020.116110.

Romero Rodríguez, Laura et al. (2018). "Contributions of heat pumps to demand response: A case study of a plus-energy dwelling". In: *Applied Energy* 214, pp. 191–204. DOI: 10.1016/j.apenergy.2018.01.086.

Schöniger, Franziska et al. (July 2022). "What comes down must go up: Why fluctuating renewable energy does not necessarily increase electricity spot price variance in Europe". en. In: *Energy Economics* 111, p. 106069. DOI: 10.1016/j.eneco.2022.106069.

Schöniger, Franziska et al. (2023). *Securing Austria's Electricity Supply in times of Climate Change; Final report of the ACRP12 project SECURES (2020-2023).* P. 48.

Schöniger, Franziska et al. (2024). *The Impact of Climate Change on Electricity Demand and Supply Profiles in Europe Until 2100.* DOI: 10.2139/ssrn.4978968.

Shakeri, Mohammad et al. (June 2020). "An Overview of the Building Energy Management System Considering the Demand Response Programs, Smart Strategies and Smart Grid". en. In: *Energies* 13.13, p. 3299. DOI: 10.3390/en13133299.

Silva, Luiz Eduardo Sales et al. (2022). "Combined PV-PEV Hosting Capacity Analysis in Low-Voltage Distribution Networks". In: *Electric Power Systems Research* 206, p. 107829. DOI: https://doi.org/10.1016/j.epsr.2022.107829.

Song, Ruihao et al. (Jan. 2025). "Integrating Air-Source Heat Pumps into the Demand-Side Fast Frequency Response Service: A Study Based on Thermal Dynamic Uncertainty". In: *IEEE Transactions on Sustainable Energy* 16.1, pp. 323–335. DOI: 10.1109/TSTE.2024.3456068.

Sørensen, Å.L. et al. (2023). "A method for generating complete EV charging datasets and analysis of residential charging behaviour in a large Norwegian case study". In: *Sustainable Energy, Grids and Networks* 36, p. 101195. DOI: https://doi.org/10.1016/j.segan.2023.101195.

Sørensen, Åse Lekang et al. (2021). "Residential electric vehicle charging datasets from apartment buildings". In: *Data in Brief* 36, p. 107105. DOI: https://doi.org/10.1016/j.dib.2021.107105.

Sørensen, Åse Lekang et al. (Aug. 2022). "Stochastic load profile generator for residential EV charging". In: *E3S Web of Conferences*. Vol. 362. E3S Web of Conferences, 03005, p. 03005. DOI: 10.1051/e3sconf/202236203005.

Sperber, Evelyn et al. (2020a). "Reduced-order models for assessing demand response with heat pumps – Insights from the German energy system". In: *Energy and Buildings* 223, p. 110144. DOI: 10.1016/j.enbuild.2020.110144.

— (Sept. 2020b). "Reduced-order models for assessing demand response with heat pumps – Insights from the German energy system". en. In: *Energy and Buildings* 223, p. 110144. DOI: 10.1016/j.enbuild.2020.110144.

Sperber, Evelyn et al. (June 2025). "Aligning heat pump operation with market signals: A win-win scenario for the electricity market and its actors?" en. In: *Energy Reports* 13, pp. 491–513. DOI: 10.1016/j.egyr.2024.12.028.

Sridhar, Araavind et al. (June 2024). "A data-driven approach with dynamic load control for efficient demand-side management in residential household across multiple devices". en. In: *Energy Reports* 11, pp. 5963–5977. DOI: 10.1016/j.egyr.2024.05.023.

Stute, Judith et al. (2024a). "Assessing the conditions for economic viability of dynamic electricity retail tariffs for households". In: *Advances in Applied Energy* 14, p. 100174. DOI: https://doi.org/10.1016/j.adapen.2024.100174.

Stute, Judith et al. (June 2024b). "How do dynamic electricity tariffs and different grid charge designs interact? - Implications for residential consumers and grid reinforcement requirements". en. In: *Energy Policy* 189, p. 114062. DOI: 10.1016/j.enpol.2024.114062.

Suna, Demet et al. (May 2022). "Assessment of flexibility needs and options for a 100% renewable electricity system by 2030 in Austria". In: *Smart Energy* 6, p. 100077. DOI: 10.1016/j.segy.2022.100077.

The Hotmaps Team (2020). *Hotmaps (https://www.hotmaps.eu/map)*. (Visited on 10/27/2024).

Transparency Platform (2024). *ENTSO-E (https://transparency.entsoe.eu/)*. (Visited on 10/27/2024).

Unterluggauer, Tim et al. (2022). "Impact of Electric Vehicle Charging Synchronization on the Urban Medium Voltage Power Distribution Network of Frederiksberg". In: *World Electric Vehicle Journal* 13.10. DOI: 10.3390/wevj13100182.

Unterluggauer, Tim et al. (2023). "Impact of cost-based smart electric vehicle charging on urban low voltage power distribution networks". In: *Sustainable Energy, Grids and Networks* 35, p. 101085. DOI: https://doi.org/10.1016/j.segan.2023.101085.

URBAN3R (2025). *Plataforma de datos abiertos para impulsar la regeneración urbana en España*. Promovida por la Dirección General de Agenda Urbana y Arquitectura (MITMA); desarrollada por Cíclica [space·community·ecology]. URL: https://urban3r.es/ (visited on 08/11/2025).

Valovcin, Sarah et al. (2022). "Using Smart Meter Data to Estimate Demand Reductions from Residential Direct Load Control Programs". In: *2022 IEEE International Smart Cities Conference (ISC2)*, pp. 1–6. DOI: 10.1109/ISC255366.2022.9922481.

Viessmann, ed. (n.d.). *Viessmann Vitocal A series*.

Wang, Cuiling et al. (2024). "Demand response for residential buildings using hierarchical nonlinear model predictive control for plug-and-play". In: *Applied Energy* 369, p. 123581. DOI: https://doi.org/10.1016/j.apenergy.2024.123581.

Wang, Huilong et al. (June 2023). "An XGBoost-Based predictive control strategy for HVAC systems in providing day-ahead demand response". en. In: *Building and Environment* 238, p. 110350. DOI: 10.1016/j.buildenv.2023.110350.

Wang, Y. et al. (Feb. 2022). "Development of efficient, flexible and affordable heat pumps for supporting heat and power decarbonisation in the UK and beyond: Review and perspectives". In: *Renewable and Sustainable Energy Reviews* 154, p. 111747. DOI: 10.1016/j.rser.2021.111747.

Weiß, Tobias et al. (2019a). "Energy flexibility of domestic thermal loads – a building typology approach of the residential building stock in Austria". In: *Advances in Building Energy Research* 13.1, pp. 122–137. DOI: 10.1080/17512549.2017.1420606.

— (Jan. 2019b). "Energy flexibility of domestic thermal loads – a building typology approach of the residential building stock in Austria". en. In: *Advances in Building Energy Research* 13.1, pp. 122–137. DOI: 10.1080/17512549.2017.1420606.

Wiese, Frauke et al. (2018). "Balmorel open source energy system model". In: *Energy Strategy Reviews* 20, pp. 26–34. DOI: 10.1016/j.esr.2018.01.003.

Wilczynski, Eric John et al. (Sept. 2023). "Assessment of the thermal energy flexibility of residential buildings with heat pumps under various electric tariff designs". In: *Energy and Buildings* 294, p. 113257. DOI: 10.1016/j.enbuild.2023.113257.

Wolisz, Henryk et al. (Aug. 28, 2013). "Dynamic Simulation Of Thermal Capacity And Charging/ Discharging Performance For Sensible Heat Storage In Building Wall Mass". In: DOI: 10.26868/25222708.2013.1371.

Yildiz, Baran et al. (2021). "Analysis of electricity consumption and thermal storage of domestic electric water heating systems to utilize excess PV generation". In: *Energy* 235, p. 121325. DOI: 10.1016/j.energy.2021.121325.

Yue, Lu et al. (June 2024). "A three-dimensional evaluation method for building energy systems to guide power grid-friendly interactions during the planning and operational stages". en. In: *Journal of Building Engineering* 86, p. 108816. DOI: 10.1016/j.jobe.2024.108816.

Zhang, Yichi et al. (Dec. 2021). "Techno-economic assessment of thermal energy storage technologies for demand-side management in low-temperature individual heating systems". en. In: *Energy* 236, p. 121496. DOI: 10.1016/j.energy.2021.121496.

A Appendix

A.1 Building information for the case of Austria

In Mascherbauer et al. (2022), only the SFHs from the Austrian building stock were analysed on their potential to shift electricity demand. The SFH building stock of Austria is represented by 11 representative buildings. Figure A.1 illustrates the number of buildings of all 11 categories and the share of buildings using a HP for heating.

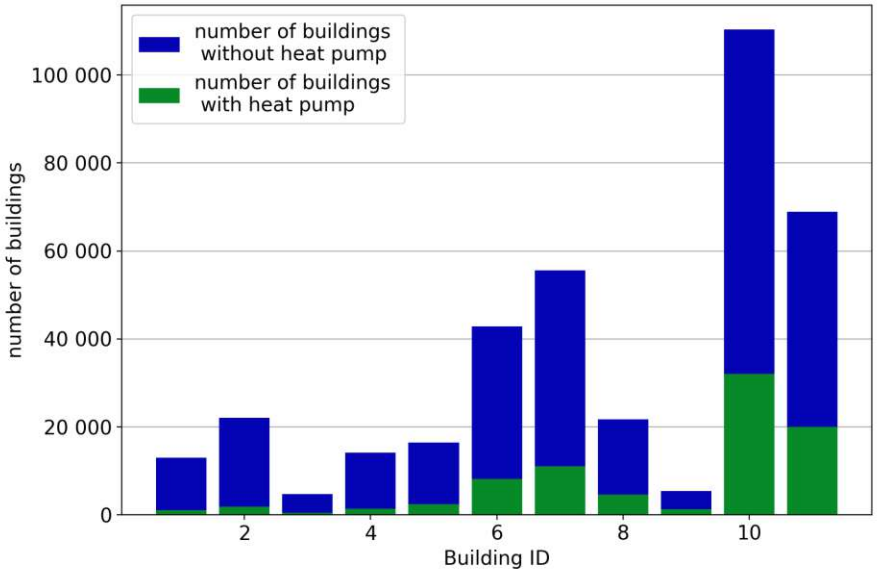

Figure A.1: Number of selected SFH in this study from the Austrian building stock (Andreas Müller 2021)

All building parameters are selected from the INVERT/EE-Lab Database (Andreas Müller 2021). Every building type represents buildings built in a specific time period, starting from 1890 up to 2011. For buildings built up to 1980, only those buildings that have been refurbished since then are considered. It is unlikely to install HPs in old buildings with insufficient insulation and an old heat distribution system. Information on each building category is provided in Table A.1.

Table A.1: Building IDs with average floor area (A_f) and useful energy demand for space heating (Mascherbauer et al. 2022)

ID	Type	Age Class	A_f (m^2)	Useful energy demand for space heating (W/m^2)
1	SFH	1890-1918	129	161.8
2	SFH	1890-1918	129	132.1
3	SFH	1919-1944	136	160.2
4	SFH	1919-1944	136	146.2
5	SFH	1945-1960	144	136.1
6	SFH	1961-1970	154	105.9
7	SFH	1971-1980	163	105.9
8	SFH	1981-1990	166	93.4
9	SFH	1991-2000	170	88.9
10	SFH	2001-2008	170	69.1
11	SFH	2009-2011	170	69.1

In the publication Mascherbauer et al. (2024), the SFH building stock in Austria is represented by 36 building types. Information about the buildings is provided in Table A.2. The appendix "mon" indicates that the buildings are under protection. Gen2, gen3, and gen4 indicate that these buildings have undergone a certain renovation, with higher numbers representing more recent renovations. Figure A.2 shows that most HPs have been installed in modern buildings.

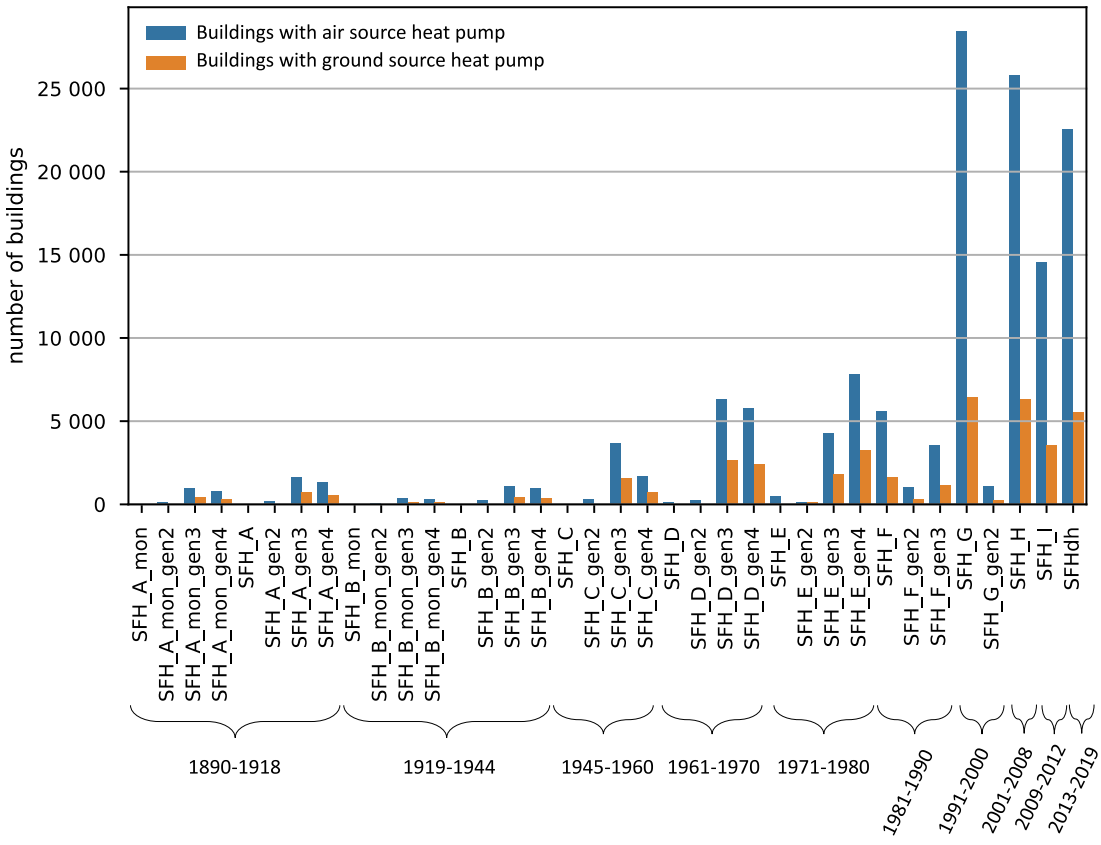

Figure A.2: Number of buildings with HPs in the Austrian SFH building stock (Andreas Müller 2021; Mascherbauer et al. 2024).

Table A.2: Building IDs with 5R1C parameters (Mascherbauer et al. 2024)

ID	Name	Generation of renovation	Age class	A_f (m^2)	H_{ve}	H_{op}	$H_{tr,w}$	C_m (mio. J/K)
1	SFH A mon	-	1890-1918	129	36	229	101	53
2		1				242	87	
3		2				250	78	
4		3				198	76	
5	SFH A	-	1890-1918	129	36	227	101	53
6		1				241	87	
7		2				250	78	
8		3				164	67	
9	SFH B mon	-	1919-1944	136	38	290	116	46
10		1				306	100	
11		2				316	89	
12		3				206	78	
13	SFH B	-	1919-1944	136	38	288	117	46
14		1				305	100	
15		2				316	89	
16		3				189	74	
17	SFH C	-	1945-1960	144	41	278	116	31
18		1				295	99	
19		2				304	89	
20		3				183	70	
21	SFH D	-	1961-1970	154	44	193	95	33
22		1				206	82	
23		2				212	77	
24		3				150	68	
25	SFH E	-	1971-1980	163	46	204	101	35
26		1				214	90	
27		2				226	79	
28		3				159	71	
29	SFH F	-	1981-1990	166	46	141	79	35
30		1				149	71	
31		2				142	69	
32	SFH G	-	1991-2000	170	48	120	71	31
33		1				122	68	
34	SFH H	-	2001-2008	170	48	90	59	19
35	SFH I	-	2009-2012	170	48	87	62	19
36	SFH dh	-	2012-2019	170	48	59	47	19

A.2 5R1C formulation

In this part of the appendix, the formulation of the 5R1C model as described in DIN ISO 13790 is described. Additional symbols used for the equations are presented in Table A.3.

Table A.3: Additional list of symbols used for the mathematical formulation of the 5R1C and 6R2C model.

Character	Unit	Description
U	W/m^2K	heat transfer coefficient
ψ	W/mK	heat transfer coefficient for thermal bridges
l	m	length
χ	W/K	heat transfer coefficient through punctual thermal bridge
$H_{tr,1}$	W/K	transmission heat transfer coefficient
$H_{tr,2}$	W/K	transmission heat transfer coefficient
$H_{tr,3}$	W/K	transmission heat transfer coefficient
h_{ms}	W/K	transmission heat transfer coefficient between the outside air and the surface area node
b_{tr}	-	heat transfer adjustment factor

Table A.3: Additional list of symbols used for the mathematical formulation of the 5R1C and 6R2C model.

Character	Unit	Description
b_{ve}	-	temperature adjustment factor for airflow
q_{ve}	m^3/s	air volume flow
k	J/m^2K	specific thermal capacity of building element
H_D	W/K	transmission heat transfer coefficient for direct heat transmission to the external environment
H_g	W/K	transmission heat transfer coefficient to the ground
H_U	W/K	transmission heat transfer coefficient to unconditioned rooms
H_A	W/K	transmission heat transfer coefficient to adjacent buildings
Λ_{at}	-	dimensionless ratio between the surface area of all surfaces facing into the room and the usable area
θ_{air}	$^\circ C$	Indoor air temperature
$\theta_{outside}$	$^\circ C$	Outdoor air temperature
θ_{sup}	$^\circ C$	Supply air temperature
θ_s	$^\circ C$	Temperature of the surface node
θ_m	$^\circ C$	Temperature of the thermal mass
$\theta_{m,avg}$	$^\circ C$	Average temperature of the thermal mass
θ_{floor}	$^\circ C$	Temperature of the floor heating system
ϕ_{HC}	W	Heating or cooling demand
ϕ_{ia}	W	Heat gains to the air node
ϕ_{int}	W/m^2	Internal heat gains
ϕ_{sol}	W/m^2	Solar gains
ϕ_{st}	W	Heat gains to the surface node
ϕ_m	W	Heat gains to the thermal mass
$\phi_{m,tot}$	W	Total heat flow into the thermal mass
$Q_{heating}$	W	Heat input from floor heating
C_m	J/K	Thermal capacity of the building mass
C_f	J/K	Thermal capacity of the floor heating system
H_{ve}	W/K	Ventilation heat transfer coefficient
H_{is}	W/K	Heat transfer between air and surface node
H_{ms}	W/K	Heat transfer between mass and surface node
H_{em}	W/K	Heat transfer from mass to exterior
H_w	W/K	Heat transfer through windows
H_f	W/K	Heat transfer from floor heating to indoor air
A_f	m^2	Heated floor area
A_{tot}	m^2	Total surface area of the building
A_m	m^2	Effective mass-related area
A_j	m^2	Surface area of building element j

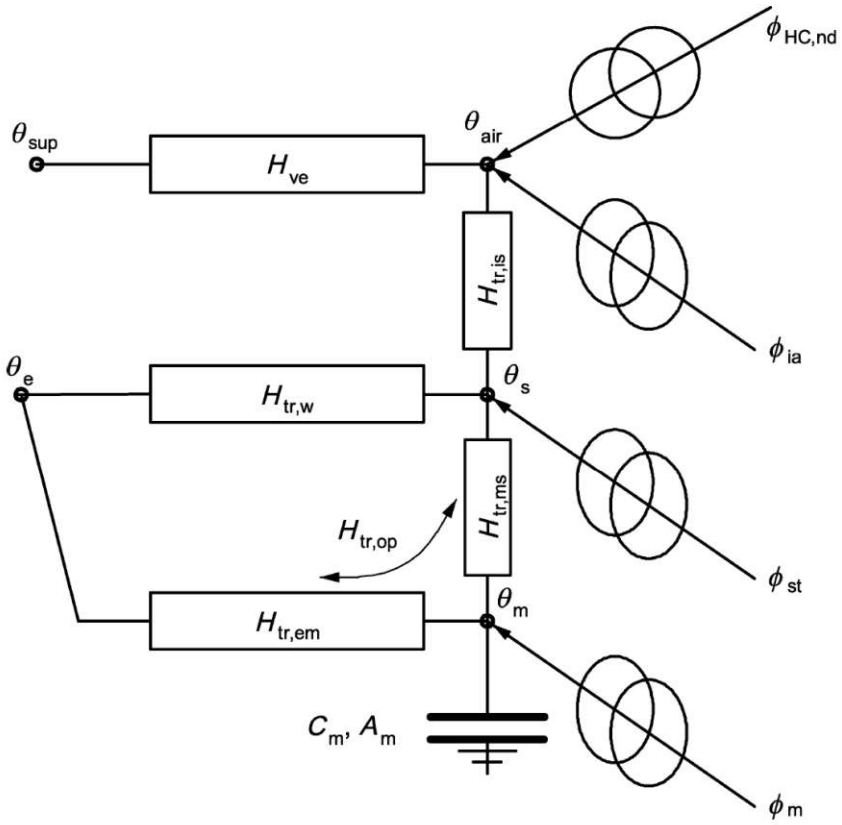

Figure A.3: 5R1C circuit representation

Figure A.3 shows the circuit representation of the 5R1C model described in the DIN ISO 13790. The relation between outside temperature ($\theta_{outside}$), indoor temperature (θ_{air}) and heating demand (ϕ_{HC}) is provided by the following equations. A detailed description of the calculation methodology can be found in DIN ISO 13790. In the following equations, ϕ represents any kind of heat flow in W and θ is used to describe temperatures in $°C$.

$$\theta_{air,t} = \frac{H_{is} \times \theta_{s,t} + H_{ve} \times \theta_{sup,t} + \phi_{ia} + \phi_{HC,t}}{H_{is} + H_{ve}} \tag{A.1}$$

θ_{sup} describes the air temperature from the ventilation system. If no ventilation system with heat exchangers is adopted θ_{sup} is set to $\theta_{outside}$. In this study, ventilation systems are neglected.

$$\phi_{ia} = 0.5 \times \phi_{int} \tag{A.2}$$

ϕ_{int} describe the internal heat gains in W/m^2. For simplification, the internal gains (ϕ_{int}) are kept constant, although in reality they can change every hour.

The node temperature θ_s is calculated throughthe following equation:

$$\theta_{s,t} = \frac{H_{ms} \times \theta_{m_{avg},t} + \phi_{st,t} + H_w \times \theta_{outside,t} + H_{tr1} \times (\theta_{sup,t} + \frac{\phi_{ia}+\phi_{HC,t}}{H_{ve}})}{H_{ms} + H_w + H_{tr1}} \tag{A.3}$$

The average temperature of the thermal mass ($\theta_{m_{avg},t}$) in each timestep is calculated as follows:

$$\theta_{m_{avg},t} = \frac{\theta_{m,t} + \theta_{m,t-1}}{2} \tag{A.4}$$

$\theta_{m,t}$ and $\theta_{m,t-1}$ represent the temperature of the thermal mass in the current and in the previous timestep and have to be calculated for each timestep individually:

$$\theta_{m,t} = \frac{\theta_{m,t-1} \times (\frac{C_m}{3600} - 0.5 \times (H_{tr3} + H_{em})) + \phi_{m_{tot},t}}{\frac{C_m}{3600} + 0.5 \times (H_{tr3} + H_{em})} \tag{A.5}$$

with

$$\phi_{m_{tot},,t} = \phi_{m,t} + H_{em} \times \theta_{outside,t} + H_{tr3} \times (\phi_{st,t} + H_w \times \theta_{outside,t} + \frac{H_{tr1}}{H_{tr2}} \times (\frac{\phi_{ia} + \phi_{HC,t}}{H_{ve}} + \theta_{sup,t})) \tag{A.6}$$

$$\phi_{st,t} = (1 - \frac{A_m}{A_t} - \frac{H_w}{9.1 \times A_t}) \times (0.5 \times \phi_{int} + \phi_{sol,t}) \tag{A.7}$$

with ϕ_{sol} describing the solar gains.

$$\phi_{m,t} = \frac{A_m}{A_t} \times (0.5 \times \phi_{int} + \phi_{sol,t}) \tag{A.8}$$

Every parameter described with an H represents a transmission heat transfer coefficient and is given in W/K. All building-specific parameters are described in the following equations:

$$H_{tr1} = \frac{1}{1/H_{ve} + 1/H_{is}} \tag{A.9}$$

with H_{ve} being the ventilation transfer coefficient.

$$H_{tr2} = H_{tr1} + H_w \tag{A.10}$$

$$H_{tr3} = \frac{1}{1/H_{tr2} + 1/H_{ms}} \tag{A.11}$$

$$H_{is} = h_{is} \times A_{tot} \tag{A.12}$$

with h_{is} being the heat transfer coefficient between the air node θ_{air} and the surface node θ_s which equals to $3.45 W/m^2K$. A_{tot} denotes the total surface area of the building in m^2.

$$A_{tot} = \Lambda_{at} \times A_f \tag{A.13}$$

where A_f is the effectively used floor area in m^2 and Λ_{at} represents the dimensionless ratio between the surface area of all surfaces that face into the space and the effective area. Λ_{at} is set to 4.5.

$$H_{em} = 1/(\frac{1}{H_{op}} - \frac{1}{H_{ms}}) \tag{A.14}$$

H_{ms} is provided in W/K:

$$H_{ms} = h_{ms} \times A_m \tag{A.15}$$

h_{ms} denotes the heat transfer coefficient between the nodes m and s and is fixed with $9.1 W/m^2K$. A_m is the effective mass-related area in m^2 and is calculated with following formula:

$$A_m = \frac{C_m^2}{\sum(A_j \times k_j^2)} \tag{A.16}$$

A_j represents the surface area of the building element j in m^2 and k_j represents the specific thermal capacity of a building element j in J/m^2K. C_m is provided in J/K and denotes the total thermal capacity of the building mass:

$$C_m = \sum(k_j \times A_j) \tag{A.17}$$

$$H_{op} = H_D + H_g + H_U + H_A \tag{A.18}$$

H_D, H_g, H_U, and H_A represent the transmission heat transfer coefficients for direct heat transmission to the external environment (H_D), for the steady-state heat transmission to the ground (H_g), through unconditioned rooms (H_U), and to adjacent buildings (H_A). The calculation of these four parameters is described in the DIN ISO 13789. In the following equation H_X stands for either H_D, H_g, H_U, H_A:

$$H_X = b_{tr,x} \times (\sum_i A_i \times U_i + \sum_k l_k \times \psi_k + \sum_j \chi_j) \tag{A.19}$$

with U_i being the heat transfer coefficient in W/m^2K for the respective building element i.
ψ... linear heat transfer coefficient for a thermal bridge
l... length of a thermal bridge
χ... heat transfer coefficient for a punctual thermal bridge
$b_{tr,x}$... adjustment factor if the temperature on the other side of the component is not equal to the temperature of the external environment

The total ventilation heat transfer coefficient (H_{ve}) is calculated as follows:

$$H_{ve} = \rho_a \times c_a \times (\sum_k b_{ve,k} \times q_{ve,k}) \tag{A.20}$$

$\rho_a \times c_a$... volume-related heat storage capacity of the air in J/m^3K
q_{ve}... the time-averaged air volume flow
b_{ve}... the temperature adjustment factor for airflow element k. If the supply air temperature is not equal to the temperature of the external environment, $b_{ve} \neq 1$.

A.3 Validation of the model

In this section, the developed FLEX model is critically questioned, and the strengths and limitations of the approach are provided and discussed. In the first part, the optimization framework and the dynamic behavior of buildings are compared to IDA ICE, a known building simulation tool. In literature, the 5R1C approach has been investigated and compared to other models. Lauster et al. (2014) used the 5R1C model to verify their implementation of the VDI 6007-1. Cirrincione et al. (2019) compared both the 5R1C approach from DIN ISO 13790 and the newer version of the calculation from EN ISO 52016 to results from Energy Plus. Both methods show a good estimation of the heating demand at a monthly level, however the EN ISO 52016 overestimated cooling needs even more than the 5R1C approach. In Michalak (2014), the 5R1C approach is also compared to Energy Plus for 10 different Polish cases. Results show that the calculated heating demand is realistic. However, the dynamic thermal behavior was not investigated. A comparison of the dynamic thermal behavior of the 5R1C model is done in Bruno et al. (2016b) with TRYNSIS. Results show that with very high thermal mass, the 5R1C does not predict the dynamic behavior accurately when it comes to heating; with moderate thermal mass, the predictions are good. For cooling, the dynamic behavior differs significantly from the TRYNSIS calculation.

None of the above-mentioned studies focused on DR using the 5R1C model. If the indoor set temperature is constantly changed through optimization, the predicted energy demand could deviate strongly from the real one. Thus, the following questions are formulated: Can the thermodynamic behavior of a building equipped with an HP and controlled with a HEMS using the 5R1C approach be accurately modeled? Will an optimization using the 5R1C approach also lower its electricity cost when calculated with a building dynamic simulation tool? To answer these questions, the HP operation is optimized for nine buildings located in Salzburg, Austria, using the FLEX model. The resulting optimized indoor set temperatures are then provided to the IDA ICE model, which calculates the energy demand for the exact same buildings. This way, it is shown whether the proposed control strategy of the FLEX model would work based on the results of a more sophisticated building simulation model.

Another limitation of the model is that it uses perfect foresight over the year. This may lead to an overestimation of the possible cost savings and load-shifting potentials. In the second part of this chapter (A.3.3), a rolling horizon approach is therefore tested against the existing model. It is shown that in order to achieve good results with a rolling horizon approach, the state of the thermal mass capacity within the building has to be monetized at the end of the horizon window.

A.3.1 Comparison of FLEX with IDA ICE

This section analyzes how the control strategy of the optimized 5R1C model would affect the results if implemented in IDA ICE regarding cost reductions and the potential of shifted energy. The model runs in IDA ICE are conducted with two different heating systems: once with an optimal heating system, meaning the heat is distributed without losses in the houses, and once with a floor heating system. The analysis is done for nine representative buildings located in Salzburg, Austria. Five of the buildings are SFHs, and four are MFHs. The thermal mass and the insulation level determine the thermodynamic behavior of the buildings. In Figure A.4, the properties of these nine buildings are visualized. The exact values used for the 5R1C model are presented in Table A.4. Detailed information that was used to model these buildings in IDA ICE, from which also the RC parameters were derived, is provided in the Appendix A.5.

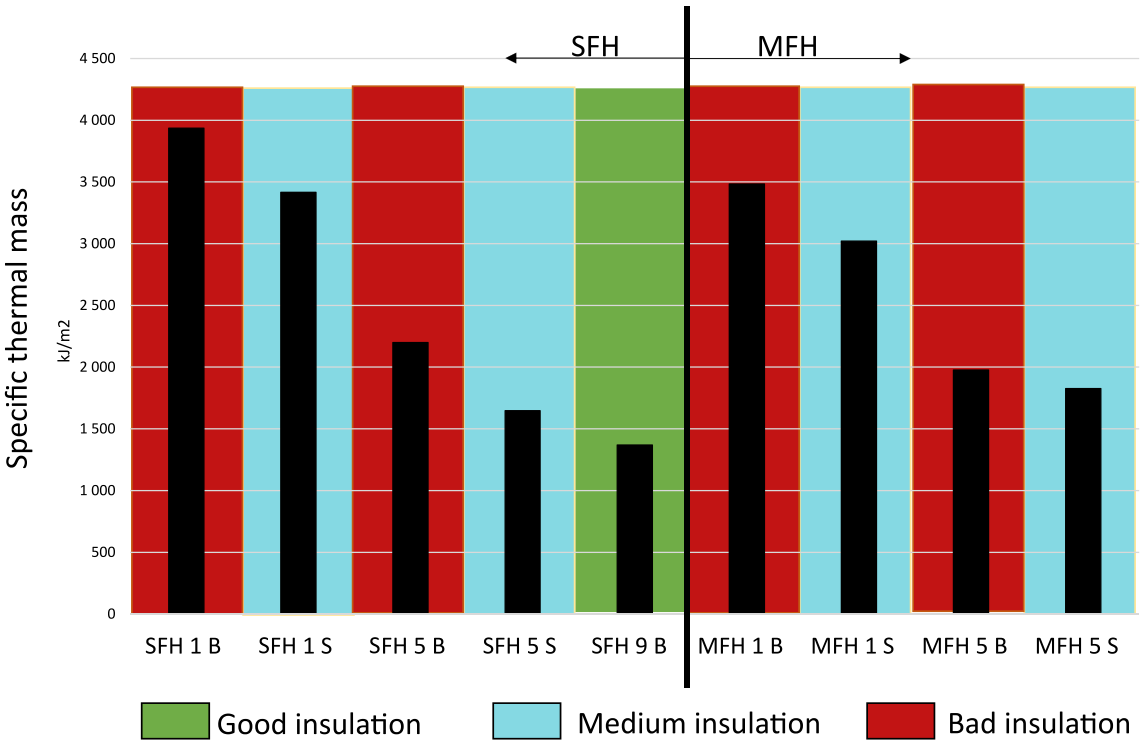

Figure A.4: Building properties of the buildings used to validate the model.

Table A.4: Properties of the buildings modeled with FLEX and IDA ICE

Building	Af (m^2)	Hop	Htr_w	Hve	CM factor	Am factor	internal gains (W/m^2)
SFH 1 B	221.4	469.3	37.8	63.5	3 934 822	4.0	4.1
SFH 1 S	221.4	191.6	22.0	63.6	3 415 854	4.2	4.1
SFH 5 B	221.6	315.1	46.8	59.7	2 198 880	4.1	4.1
SFH 5 S	221.6	165.1	24.5	60.9	1 647 301	3.8	4.1
SFH 9 B	188.7	79.6	21.1	51.0	1 369 608	4.2	4.1
MFH 1 B	390.8	715.5	77.4	177.8	3 482 782	3.6	4.1
MFH 1 S	390.8	363.4	50.3	178.0	3 020 247	3.7	4.1
MFH 5 B	526.5	545.9	110.4	195.0	1 976 692	3.2	4.1
MFH 5 S	526.5	311.6	73.9	192.8	1 825 799	3.3	4.1

The following approach was taken to test if optimization of the HP in a building using the 5R1C approach yields satisfactory results regarding cost minimization and shiftable electricity demand. The heating system operation of the nine above-described buildings is optimized using the 5R1C model. This optimization's resulting indoor set temperature is used as input for the IDA ICE model. The resulting energy demand curves and costs from both models are compared with each other. This is done with the day-ahead price profile from 2019[1] with an added grid fee of 20 cent/kWh, depicted in Figure A.5.

[1] https://www.entsoe.eu/

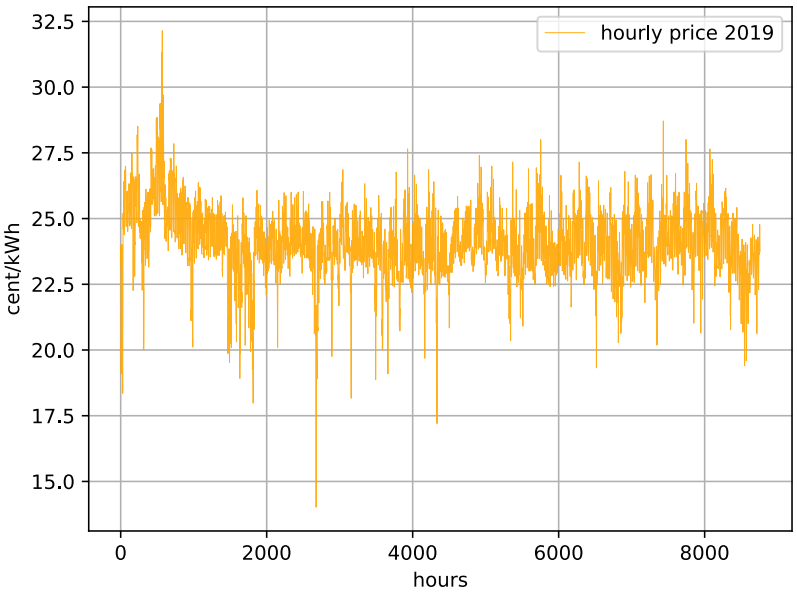

Figure A.5: Electricity price from Austria in 2019[1] used for the comparison between the 5R1C and the IDA ICE model.

According to literature and tests done within this thesis, the hourly 5R1C model simulates the heat demand best for buildings that are medium to poorly insulated with a high specific thermal mass. The 5R1C model is not as accurate for well-insulated and lightweight buildings. The analysis showed that especially buildings with floor heating systems can not be modeled to a satisfying accuracy with the 5R1C approach, which is also a common finding in literature (Sperber et al. 2020a). Therefore, the 5R1C model was extended by a second capacity and a sixth resistance to mimic the transient thermal behavior of the floor heating system.

A.3.2 Improving 5R1C approach to a 6R2C model

Simply increasing the thermal mass of a building with floor heating to change the transient behavior does not work. The literature mentions that RC models need at least two capacities to accurately represent the dynamic behavior of the building mass for buildings with floor heating (Sperber et al. 2020a). Thus, a second capacity was added to the existing 5R1C model as presented in Figure A.6.

The new 6R2C model has two undefined parameters: the capacity of the floor (C_f) and the heat transfer coefficient between the floor node and the air temperature (H_F). These values can not be integrated into the optimization as variables without introducing nonlinearity to the problem. Therefore, a combination of values was used in the optimization for the 6R2C model, with the indoor temperature being constrained to the temperature from the IDA ICE model in optimization mode. The resulting heating demand was then compared to the heating demand of the IDA ICE model using the mean squared error and the parameter combination between H_f and C_f with the smallest error. For H_F, values ranging from 2 to 11 W/m^{2}K were tried. The heat transfer coefficient in floor heating systems should range between 8 and 11 W/m^{2}K according to Cholewa et al. (2013) depending on the temperature difference between operational and room temperature. For C_f, it was assumed that the total thermal mass remains the same, and therefore, the value of C_f was subtracted from the thermal mass C_m. C_f per square meter was changed in

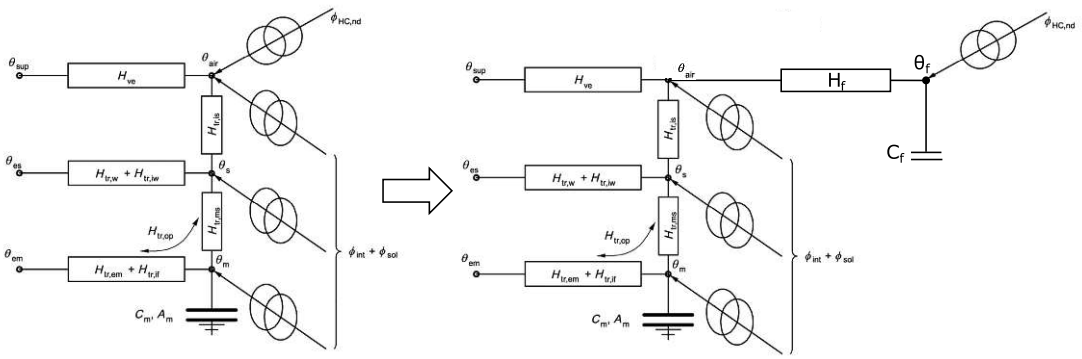

Figure A.6: Adding a second capacity for the floor heating system to the 5R1C model, making it a 6R2C model.

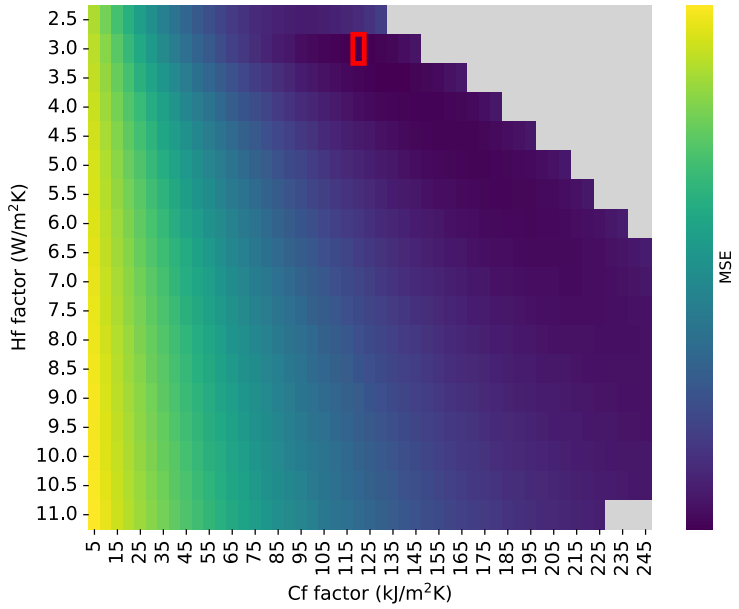

Figure A.7: Heatmap of the mean squared error for different C_f and H_f combinations. The red-marked result shows the C_f, H_f combination with the minimum error satisfying the maximum heating power constraints. Combinations in Grey proved to be infeasible.

steps 5 kJ/m^{2}K, ranging from a minimum of 5 to a maximum of 250 kJ/m^{2}K. To have a comparable value of the shifted electricity to the 5R1C model, the boundary conditions for the maximum heating power, both on the electrical and thermal side, are restricted by the maximum heating powers (electrical and thermal) of the 5R1C model. Allowing the 6R2C model to have a higher thermal power output would result in significantly higher shifted energy demand, showing that the floor heating system could shift much more electricity without violating indoor temperature constraints. The maximum power constraints make the model infeasible in cases where C_f is either too high or H_f is too low. As an example, the optimum feasible combination for one of the buildings is shown in Figure A.7. The full mathematical formulation of the 6R2C model is provided in Appendix A.4.

The resulting best combination for C_f and H_f to mimic the behavior of IDA ICE is shown in Table A.5. When considering the temperature difference between operational and air temperature, the H_f values are in the upper range of values described in Cholewa et al. (2013). The number of investigated buildings is too low to predict the C_f and H_f

values reliably[2]. Further research with a lot more buildings needs to be conducted to estimate the capacity of the floor reliably and the heat transfer coefficient between the floor and indoor air based on available RC parameters.

Table A.5: Overview of chosen C_f (kJ/m^{2}K) and H_f values (W/m^2).

Building	C_f factor [kJ/m^{2}K]	H_f [W/m^2]
SFH 1 B	65	4
SFH 1 S	155	5.5
SFH 5 B	120	3
SFH 5 S	105	3.5
SFH 9 B	35	2
MFH 1 B	35	4
MFH 1 S	150	5.5
MFH 5 B	145	5.5
MFH 5 S	130	5.5

With the values from Table A.5, the 6R2C model was compared to the 5R1C and IDA ICE models. On a yearly basis, the change in heat demand is insignificant between the 5R1C and the 6R2C model (Figure A.8), which is expected as the resistances of the building envelope are identical. The 5R1C model approximates the yearly heating demand for each building well, which is in accordance with results from Cirrincione et al. (2019) and Michalak (2014). Note that the heating demand for the IDA ICE model runs with an ideal heating system, ignoring heating system distribution losses, which is why there is a higher heating demand for floor heating. Only the heating demand of the SFH 9 B (well-insulated and lightweight) is strongly underestimated by the 5R1C model. In the following, we will use this building to analyze the hourly thermodynamic behavior as it represents the worst case for the model.

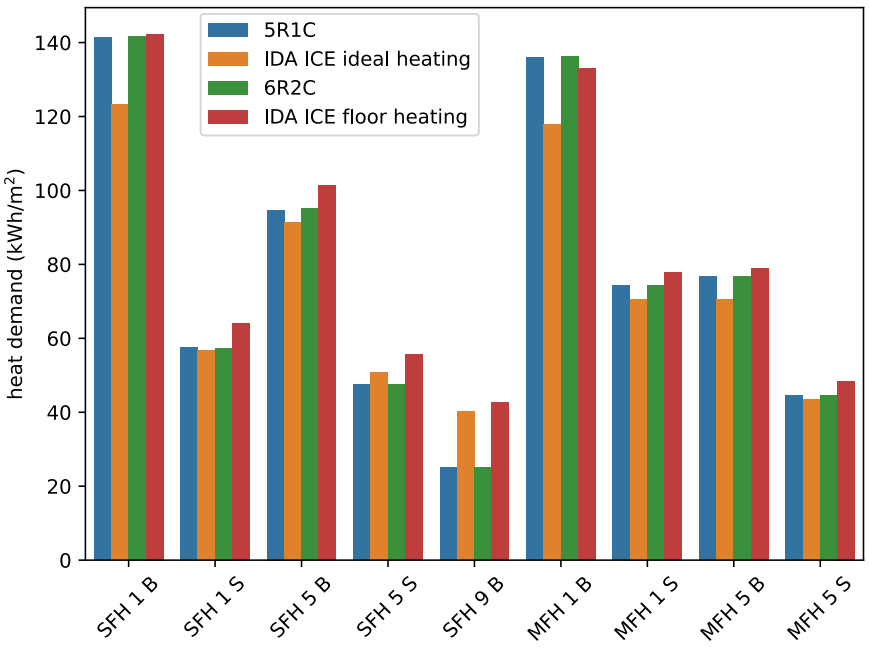

Figure A.8: Yearly heat demand comparison between the 5R1C model and IDA ICE.

[2]Random Forest regression attempt resulted in R^2 values of 0.13 and 0.5 for the prediction of H_f and C_f respectively.

When looking at the thermodynamic behavior in detail, we can see in Figure A.9 that the hourly heating demand and the indoor temperature align well between the 5R1C and IDA ICE. This means buildings with radiators as heating systems can be sufficiently well represented, and the thermal load-shifting behavior can be adequately modeled. The only discrepancy is the overall higher needed heating demand, which is due to the underestimation of the 5R1C approach for this specific building. Suppose this building is equipped with a floor heating system instead of radiators. In that case, the thermal response of the building can not be adequately represented by the 5R1C model anymore, as shown in Figure A.10. Figure A.10 depicts the heating demand and indoor temperature of the IDA ICE, 5R1C, and 6R2C models. The IDA ICE model uses the 5R1C indoor temperature as the set temperature. It is visible that when the 5R1C model pre-heats to 23°C, the IDA ICE model, using floor heating, can not reach this indoor set temperature within the pre-heating period due to the much higher thermal inertia. At the same time, the indoor temperature decreases more slowly, leading to higher losses than anticipated by the 5R1C model. The '6R2C following set temperature' model is bound to the same indoor temperature as the IDA ICE model. The mean squared error between the heating demand of the '6R2C following set temperature' and the IDA ICE model was used to determine the best parameters for C_f and H_f. It is visible that the 6R2C model follows the pattern of the IDA ICE model, however, the magnitude can not be reached. This would be impossible without changing the other RC parameters to precisely match the two models' heating demands. Finally, the '6R2C optimized' shows how the new 6R2C model would behave if it were to minimize electricity costs. We can see a clear difference in the indoor temperatures of the 5R1C and 6R2C models. Because of the inertia in the heating system, the 6R2C model uses smaller price deviations to pre-heat the building. On Saturday and Sunday, the indoor temperature in the 6R2C model behaves more realistically as the floor heating saves thermal energy over prolonged periods.

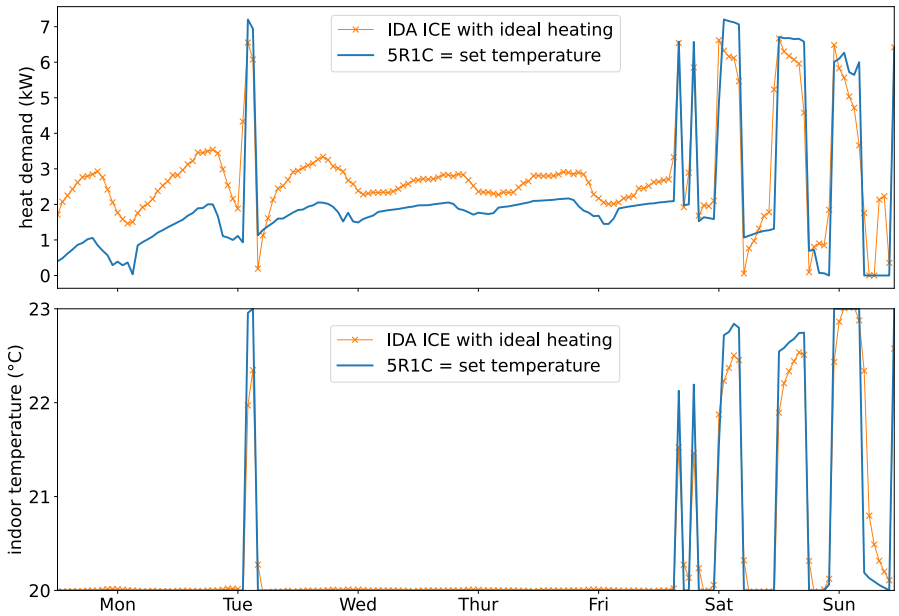

Figure A.9: Hourly comparison of the heat demand between the 5R1C model and IDA ICE over one week for house SFH 9 B **with radiator heating**.

To quantify how much the load shifting potential is underestimated by the FLEX model for buildings with floor heating systems, we use the definition provided in Section 3.2 for $\tilde{E}_{shifted}$. For buildings with radiators, the difference in shifted electricity between IDA ICE with an ideal heating system and the 5R1C model is low. It is partly attributed to the ignored heat distribution losses of the ideal heating system. The relative electricity de-

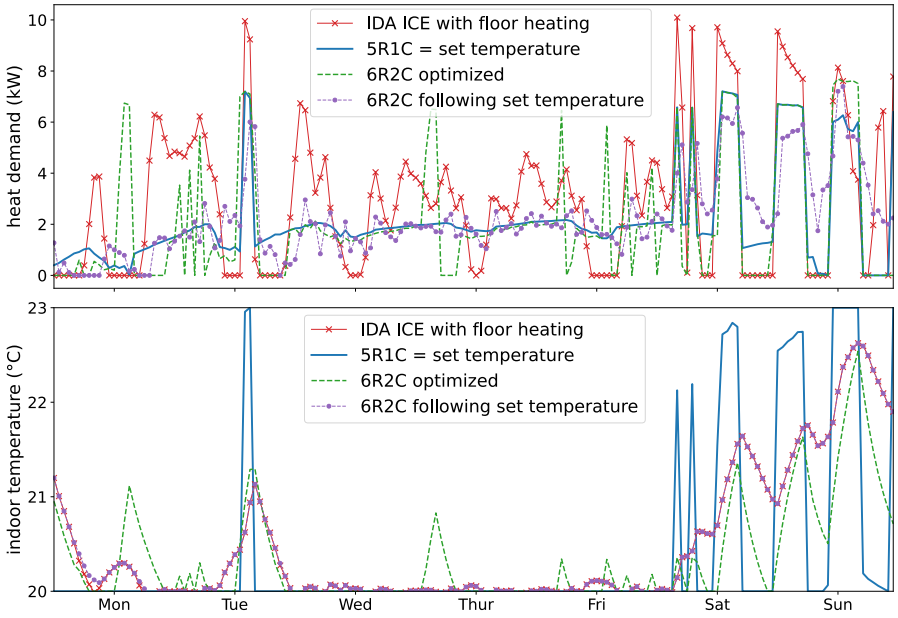

Figure A.10: Hourly comparison of the heat demand and the indoor temperature between the 5R1C, 6R2C, and IDA ICE model over one week for house SFH 9 B **with floor heating**.

mand shifted by IDA ICE, with floor heating, on the other hand, exceeds the calculated shifted demand of the 5R1C model in every building except in SFH 9 B (Figure A.11 and A.12). In the SFH 9 B building, the 5R1C model underestimates the heating demand. Buildings with low heating demand have a higher relative shifting potential. On the other hand, the IDA ICE calculations with an ideal heating system depict a lower amount of shifted electricity, which is also attributed to the overall lower heating demand shown in Figure A.8. At the same time, the high inertia of the floor heating system necessitates an early reactivation of the HP so as not to let the indoor temperature fall below 20°C in the subsequent hours. This lowers the calculated shifted electricity. The 6R2C model ('6R2C following set temperatures') compares much better in terms of shifted electricity demand both in absolute and relative values to the buildings using a floor heating system (in Figure A.12 and A.11). Only in the SFH 9 B building is the relative shifted electricity demand much higher than IDA ICE anticipated (Figure A.11). Again, this is attributed to the underestimation of the heating demand and evens out when looking at the absolute shifted demand in kWh (Figure A.12).

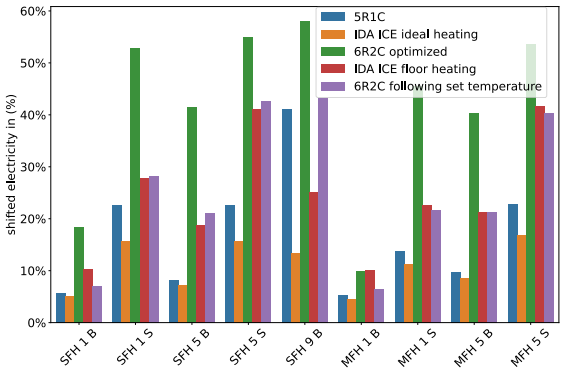

Figure A.11: Relative amount of shifted electricity in % with different models over one year.

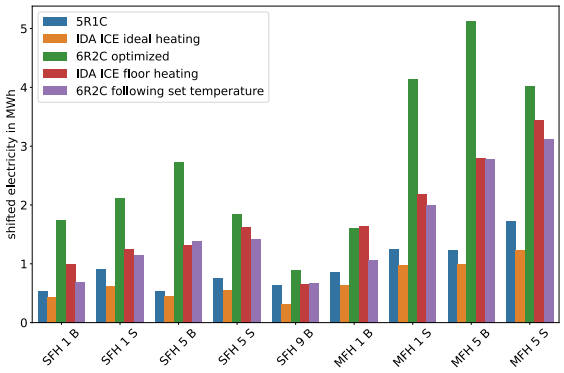

Figure A.12: Absolute amount of shifted electricity in kWh with different models over one year.

Using the 6R2C model in a normal optimization mode for buildings with a floor heating system results in a much higher shifted electricity than using the 5R1C model. Since the thermodynamic behavior is now considered in the optimization, demand is shifted more efficiently, minimizing losses. If the heat losses are correctly estimated by the RC components of the 5R1C and 6R2C models, the 6R2C model represents buildings with floor heating systems much better. The error made in estimating the shifted electricity as an absolute percentage is provided in Table A.6. Buildings with floor heating systems would shift 1.4 to 5.2 times more electricity than estimated by the 5R1C model. The shifting potential seems to be underestimated the most for badly insulated buildings with a relatively low thermal mass (SFH 5 B and MFH 5 B). On the other hand, the extension of the floor heating system without a direct connection to the outdoor temperature or surface temperature node will delay heat losses when the floor is heated up. The optimization uses this delay to its advantage.

Table A.6: Error when estimating the shifted electricity with the 5R1C model if the building uses a floor heating system. The error represents how much more electricity is shifted by the 6R2C model when optimized compared to the 5R1C model for the same building.

Building	Error (%)
SFH 1 B	326
SFH 1 S	234
SFH 5 B	512
SFH 5 S	242
SFH 9 B	141
MFH 1 B	186
MFH 1 S	329
MFH 5 B	415
MFH 5 S	234

Generally, it can be said that the shifted amount of electricity calculated with the 5R1C model is most realistic for heavy-weight buildings with low insulation and a radiator heating system. For well-insulated buildings, the shiftable amount of heating demand is overestimated in relative terms for radiator-heated buildings with differences between 0.1% and 39% and heavily underestimated for buildings with a floor heating system. For buildings with poor insulation and low thermal mass the shifted heating demand is underestimated the most. However, this kind of building rarely has a floor heating system installed. For buildings with better insulation, the error is much smaller. This difference can be further minimized if a heating buffer tank is included. Therefore, using the 6R2C model will not affect the accuracy at the country level within the existing uncertainties concerning the accuracy of building stock data.

The high inertia of the heating system impacts the achievable cost reductions. In Figure A.13, the change in operation cost if the FLEX model optimizes the heating operation is shown. Since the optimization is done with the 5R1C model, it always results in a cost reduction. However, for buildings with higher thermal inertia due to high insulation levels, we see that the indoor set temperatures provided by the FLEX model can result in an increase in operation cost for the IDA ICE model. The effect of the increased thermal inertia due to the floor heating system shows a higher change in costs than with the ideal heating system, as more energy is shifted. For the highly efficient building SFH 9 B, the costs drastically increase because the losses are much higher than anticipated by the 5R1C model due to the higher indoor temperature (see Figure A.10). For lightweight buildings with a high insulation level, the 5R1C model does not represent the transient thermo-

dynamic behavior accurately enough to reduce the operation costs by optimizing the HP operation. The change to the 6R2C model shows that almost all buildings have a higher potential for cost savings due to the higher possible shiftable energy. However, the cost savings are not as strongly underestimated as the shifted energy is overestimated. Cost savings are not as high because, with the additional capacity, demand is shifted at much lower price spreads, resulting in small additional cost advantages. In conclusion, possible cost savings for buildings with floor heating systems optimized through a 5R1C approach are slightly underestimated.

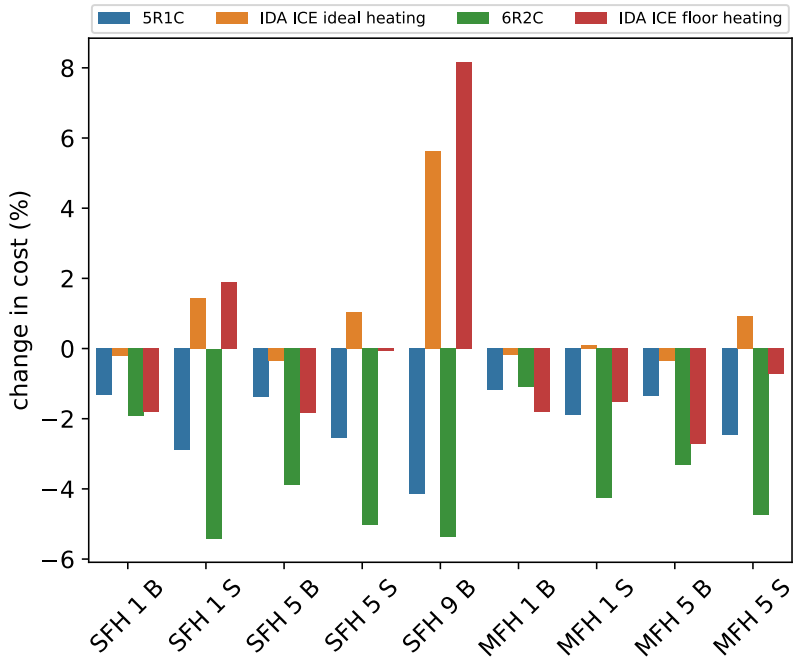

Figure A.13: Change in operation cost for the IDA ICE simulation if the FLEX optimization operates the building's heating system.

The results in this section showed that the transient thermodynamic behavior of heavyweight buildings with poor to medium insulation is represented well by the 5R1C model. Their costs can be decreased by optimizing the HP operation through the 5R1C model. On the other hand, lightweight buildings and floor heating systems are poorly represented, which can lead to increased costs if these buildings are optimized with a 5R1C approach. For buildings with radiator heating systems, the 5R1C approach slightly overestimates the potential of shifting electricity, and for buildings with floor heating systems, the shift-able electricity is strongly underestimated. Especially for badly insulated, lightweight buildings with floor heating systems, the model needs an adaptation to estimate load shifting and cost reduction potentials accurately. To do so, a second capacity and a sixth resistance were introduced to the model, imitating the floor heating system's thermodynamic behavior. With the developed 6R2C model, it was shown that buildings with floor heating systems can shift 1.4 to 5 times more electricity than anticipated by the 5R1C model. This is equivalent to the increase in load shifting potential when a thermal hot water storage for heating is implemented into the 5R1C model (explained in Section 4.1 and Mascherbauer et al. (2024)). Since not enough buildings were simulated to find a strong correlation between the RC parameters and the new C_f and H_f values, the 6R2C model is not used for analysis at the country level. However, to compensate for lost flexibility due to the missing thermal capacity, small thermal storage was added to buildings, which are usually added to HPs to enable a smoother operation of the HP. Adding a thermal storage to the 6R2C model does not result in significantly higher shifted electricity or operation cost

reduction because the HP in every building is limited in its thermal power. An increased shifting potential, however, would be more visible in scenarios where the electricity price signal changes with low frequency, offering long periods to pre-heat all available storage plus the thermal mass of the heating system and building together.

A.3.3 Perfect forecast vs. rolling horizon

Studies investigating the optimal sizes for building appliances or heating systems often use an optimization approach with perfect forecasting. When using this approach, uncertainties in forecasts for an optimal operation controller are neglected. Golmohamadi (2021b) creates a stochastic model predictive controller for HP buildings, focusing on thermal inertia and heat storage in the building. They find that ambient temperature and electricity price uncertainty have a more significant impact on the economic analysis than the domestic hot water consumption uncertainties. This section investigates how large the error is by assuming a perfect forecast horizon compared to a rolling horizon approach.

Sridhar et al. (2024) identified a gap in the literature when it comes to modeling single houses with HEMS over the whole year with a rolling horizon approach and different electricity prices. They use a rolling horizon approach over the whole year but do not monetize storage levels at the end of each modeling horizon. Monetization of the SOC of any storage is also referred to as "cost to go" (Park et al. 2021) or "terminal cost" (Abdufattokhov et al. 2021) of storage. Few studies focus on the cost to go for the thermal mass of a building. In Sridhar et al. (2024), the thermal mass is not modeled, only the thermal capacity of the indoor air. Modeling the thermal mass without monetizing the state of the thermal mass in the last timestep affects the results of an optimization significantly. The effects of preheating the thermal mass on the heating demand can last for more than 48 hours (Weiß et al. 2019b). Prat et al. (2024) investigate the optimal forecast horizon for different storage and show that the efficiency of a storage significantly impacts the needed forecast horizon. Also, the results deteriorate if no forecasting horizon is chosen, and instead, a fixed value for the storage has to be met at the end of each iteration. They also state that the optimal forecast window for each storage type changes over time.

A practical approach usually taken to model and control heating systems in buildings is model predictive control (MPC). For example, in H. Wang et al. (2023), an XGBoost-based predictive control is created for a commercial building with a heating, ventilation, and air conditioning (HVAC) system. Their results show that through DR, the operation cost can be effectively reduced by up to 27%, but the optimization was only done until 9 pm in the evening when the building closes. Thus, the thermal mass of the building is not monetized at the end of the optimization and does not impact the results. In X. Luo et al. (2019) an HVAC for a MFH is optimized using an MPC with the goal of making the building operation grid-friendly. Peak demand could be reduced to 44% of the original peak. An MPC can provide an optimal solution for the considered forecast window. However, under certain circumstances, an MPC can lead to a sub-optimal control strategy if, for example, future input variables or boundary conditions change significantly. Building controls are usually optimized using an MPC for a certain time horizon for which sufficiently good forecasts exist. With a larger time horizon, MPCs generate better results, but the uncertainty in forecasts increases drastically. Laguna et al. (2022) created a methodology to dynamically determine the optimal size of the rolling horizon windows based on the capacity of the thermal mass. They state that the optimization window has to be large enough to use the full potential of the thermal mass to shift loads. However, forecasts for weather and price data are usually not reliable enough for such long time periods. Oviedo-Cepeda et al. (2021) use MPC to optimize a building's energy management with a PV, geothermal HP, and floor heating. They use forecast intervals of 1, 3, and 5 days. The MPC using a rolling

horizon for the optimization improved significantly when increasing the horizon window from 1 to 5 days. Hu et al. (2019) developed an MPC controller for a building with floor heating, minimizing the electricity cost of a HP. The prediction horizon in this study is set to 12h, and the horizon is updated every hour with a sampling time of 30 minutes. Results show that daily electricity costs were reduced by 1.8-18% compared to a conventional on-off controller. In none of the studies are the results from the MPC-controlled building compared to those of a scenario where the building operator has perfect foresight.

The following analysis shows the difference between a perfect foresight optimization and a rolling horizon approach. It is shown that introducing terminal costs for the thermal mass at the end of the horizon can influence the optimal solution significantly. All symbols used within this section are provided in Table A.7.

The rolling horizon approach was implemented as follows: Every day at 12 o'clock, the algorithm received the new day ahead prices for the next day. Thus, the optimization is solved for 36 hours (12 remaining hours of the current day plus the whole next day) as demonstrated in Figure A.14. However, only the first 24 hours are used for building controls. To incentivize the optimization to keep energy in the storage, terminal costs (Γ) were calculated using the average dual variables (ξ_{avg}) from the previous day. The effect of using the dual variables of the prior day can be well observed in Figure A.15, where the rolling horizon lags behind the perfect forecast for 24 hours.

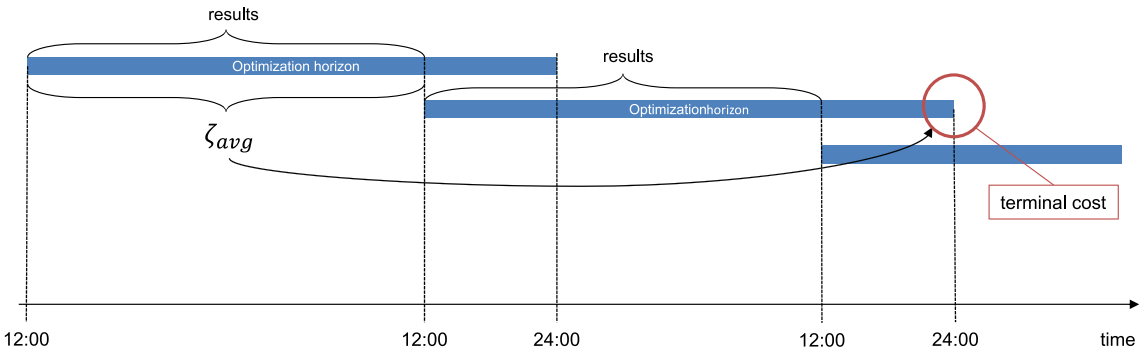

Figure A.14: Rolling Horizon Approach

$$\Gamma = SOC \cdot \xi_{avg} \tag{A.21}$$

Terminal cost of the thermal mass

Calculating the terminal cost (Γ) for the SOC of the thermal mass was done by using the dual variable $\xi_{building}$ of the corresponding constraint in the optimization model. The dual variable represents the cost needed to pre-heat the thermal mass by one degree. It is not possible to use the dual variable of the same time horizon to estimate the value of the storage at the end of the horizon without making the problem non-linear. Therefore, the mean value of the hourly dual values from the previous day was taken. As this dual variable goes to zero at the end of each horizon, only the first 24 values of each time horizon are used instead of all 36 to prevent distortion of the mean.

$$\Gamma_{\text{thermal mass}} = \Delta T_{\text{building mass}} \cdot \xi_{\text{building avg}} \cdot \beta_{\text{heat demand}} \tag{A.22}$$

$$\xi_{\text{building avg}} = \frac{1}{24} \sum \xi_{building,t} \quad t \leq 24 \tag{A.23}$$

The equations for ϕ_{st}, ϕ_m and ϕ_{mtot} (A.7, A.8 and A.6) are used as constraint for the thermal mass temperature in the optimization model. As mentioned, $\xi_{building}$ represents the dual variable of this constraint. The thermal mass temperature difference

$\Delta T_{\text{building mass}}$ is the difference between the thermal mass temperature the building would have if no demand response is used and the thermal mass temperature at the last step of the horizon. The binary parameter $\beta_{\text{heat demand}}$ ensures that $\Gamma_{\text{thermal mass}}$ is zero if no heating is required in the respective period. Since $\xi_{\text{building avg}}$ is from the previous day, with rising temperatures in Spring, the values for $\xi_{\text{building avg}}$ might be strongly overestimated if no heating is required anymore. The same accounts for Autumn, however, here no solution to the problem was found. The effect is shown in Figure A.15, where it is clearly visible that the value of the dual variable for the rolling horizon is significantly different from day 250 to 320. The binary parameter $\beta_{\text{heat demand}}$ fixes this problem for Spring, where a similar difference would be observed. Future research needs to be done to tackle this problem and to ensure a better approximation of the terminal cost in Autumn.

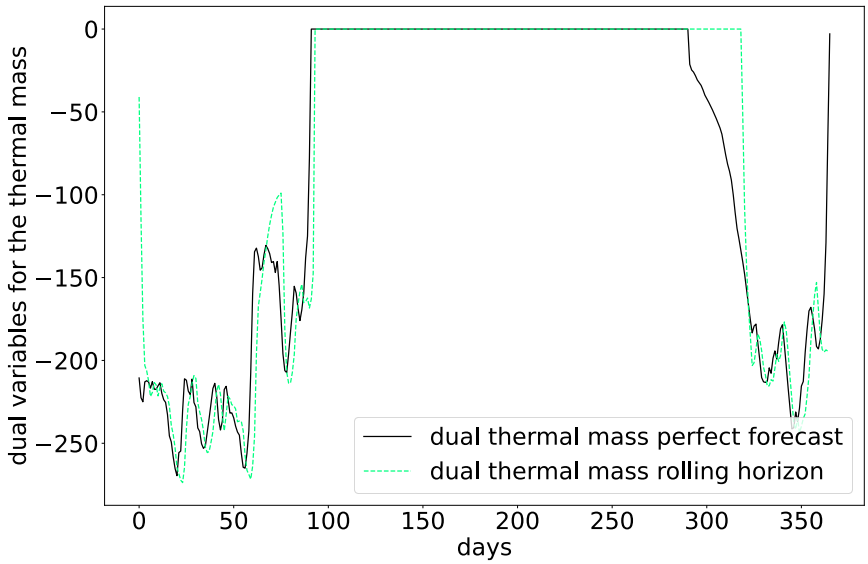

Figure A.15: Dual variable values for the thermal mass temperature constraint. Comparing the calculated daily mean duals from the rolling horizon with the values in the respective hour in the perfect foresight optimization.

By monetizing the remaining energy in the thermal mass, the rolling horizon optimization increases the shifted energy significantly compared to a rolling horizon approach where terminal costs are not evaluated (Figure A.16). The difference can also be observed in the relative cost decrease throughout the year visualized in Figure A.17. As reported in the literature (e.g., Zhang et al. (2021)), better-insulated buildings achieve a higher relative cost decrease through the optimized operation of the HP. Still, the absolute cost savings are higher for buildings with high demand (as shown in Mascherbauer et al. (2024)). By monetizing the thermal energy in the thermal mass, the relative cost decrease can be increased significantly in the rolling horizon approach. It is also visible that this approach works better for poorly insulated buildings, as the relative cost decrease is higher in those buildings compared to the maximum achievable cost reductions in the perfect foresight. The reason for this discrepancy is the increasing inaccuracy of the terminal cost for buildings with better insulation, as pre-heating them influences the heating demand for a longer, not forecastable, time. To see how a larger time horizon would impact the results, a 3-day rolling horizon approach was implemented as well. It was assumed that the weather could be forecasted sufficiently well for these 3 days. For the next three days, the day-ahead price of the next day was copied three times, implying that the day-ahead price would not change significantly. As visible in Figure A.16 and A.17, using only a 3-day forecast instead of one day did not improve the results significantly. Only by introducing the terminal cost can we see a huge improvement, and the rolling horizon optimization

achieves similar results both with a one- and three-day horizon window.

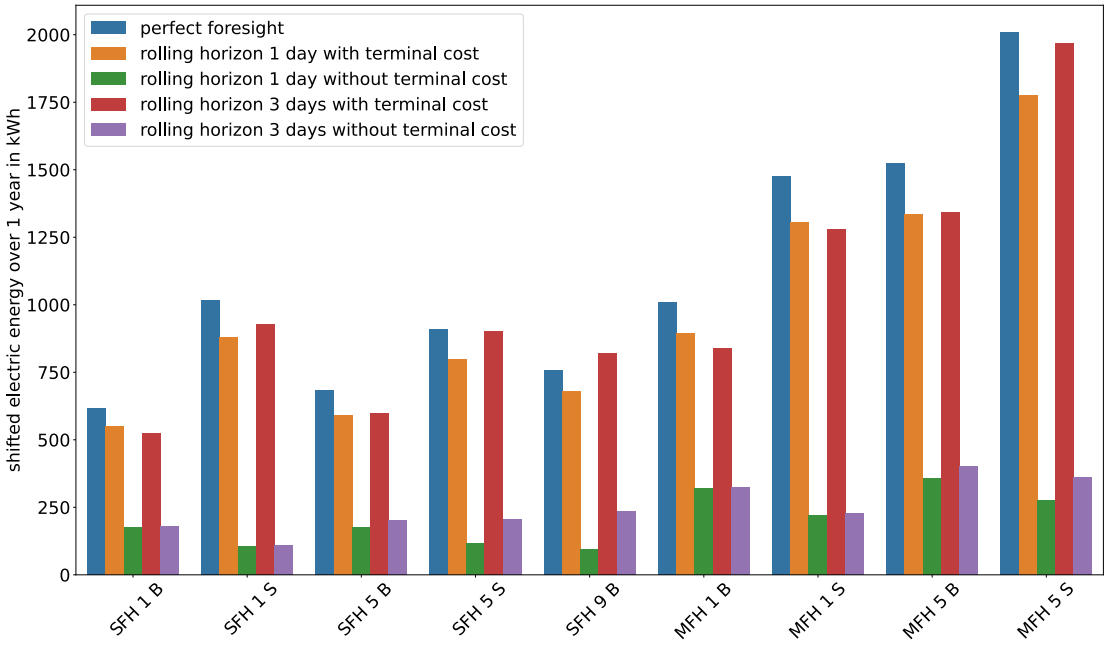

Figure A.16: Shifted energy throughout the whole year with different optimization methods for all buildings using only the thermal mass for load shifting.

These results show that the perfect foresight method applied in the FLEX model, compared to a more practical approach with a rolling horizon window, yields acceptable results for buildings that only use the thermal mass for load shifting. A rolling horizon approach can achieve similar results in regard to shifted electricity and potential cost savings when implemented correctly.

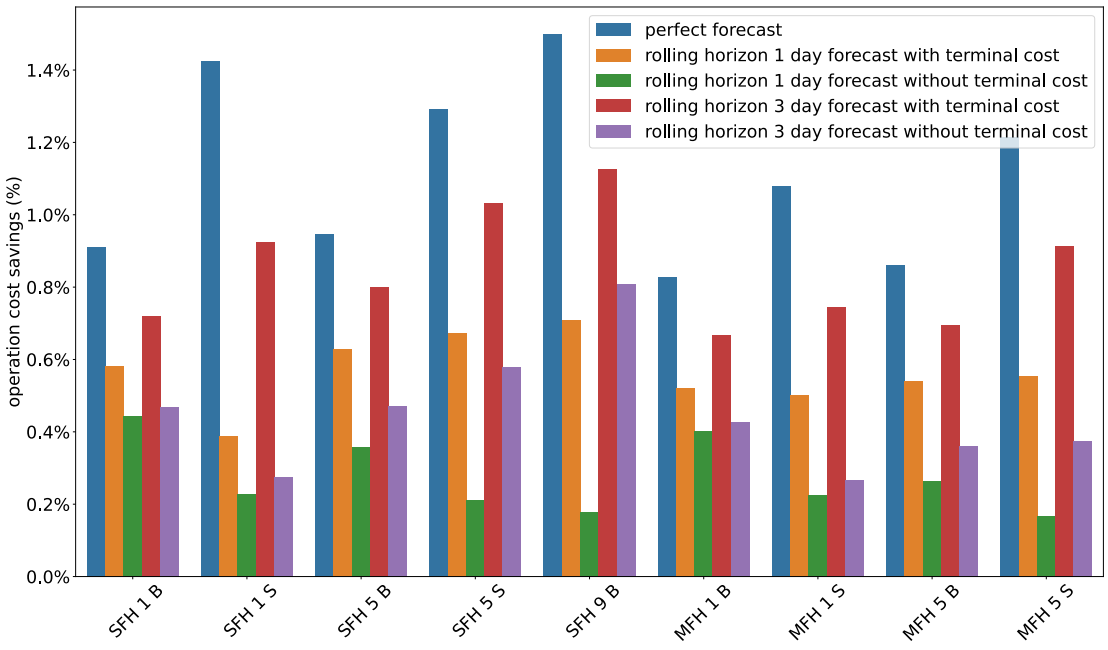

Figure A.17: Relative cost decrease for optimization with perfect foresight and rolling horizon using only the thermal mass for load shifting.

Terminal cost of storage

To find the terminal cost of both the heating-, DHW tank, and the battery, all nine buildings were equipped with either a 700 or 1500 L heating tank, a 300 or 700 L DHW tank, and a 7 kWh or 15 kWh battery, depending on if they are SFH or MFH, respectively.

At first, the terminal cost (Γ) for the battery and water tanks was estimated the same way as the thermal mass by using the dual variables of the respective constraints for the SOC. However, it turned out that the rolling horizon optimization performed worse when the thermal storage and batteries were monetized this way than when their terminal costs were not included in the objective function at all. The reason for this was the very high dependency on electricity prices, which were volatile. Compared to the thermal mass, the shadow variables for the battery, DHW, and heating tank were much more volatile. In Figure A.18, we see the comparison of the daily mean duals from the rolling horizon compared to the dual variables from the perfect forecast optimization. Especially in summer, the average of the daily dual variable is often different due to PV-generated electricity. Thus, by taking the average shadow variable from the previous day, the value of the charged storage is frequently overestimated in the rolling horizon approach, leading to a sub-optimal result. The same can be observed for the dual variables of the DHW and heating tank in Figure A.19 and A.20.

Adding all the storage and PV to the houses shows the relative cost reduction in Figure A.22. In all methods for the rolling horizon approach, the terminal cost for the building mass was included. It is visible that the achievable cost reductions through the rolling horizon approach are limited compared to the perfect foresight. Especially the costs for building SFH 9 B even increase when optimizing the operation with a one-day forecast. Including terminal costs with the above-mentioned strategy minimizes the cost increase. However, the long-term effects of charging various storage systems are too unpredictable to optimize the building correctly. A considerable improvement is achieved if the forecasting window is increased by three days. However, the total amount of shifted electricity (Figure A.21) is in all cases very close to the FLEX calculation with perfect foresight. In

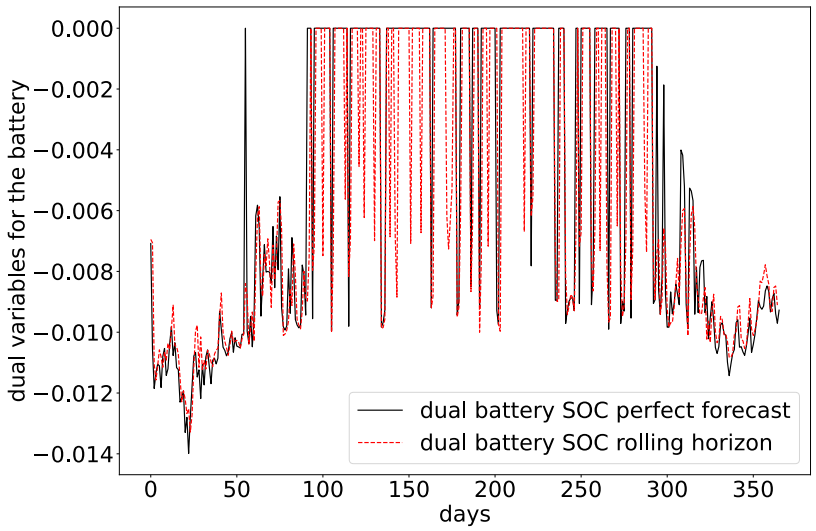

Figure A.18: Dual variables of the SOC for the battery for House SFH 9 B.

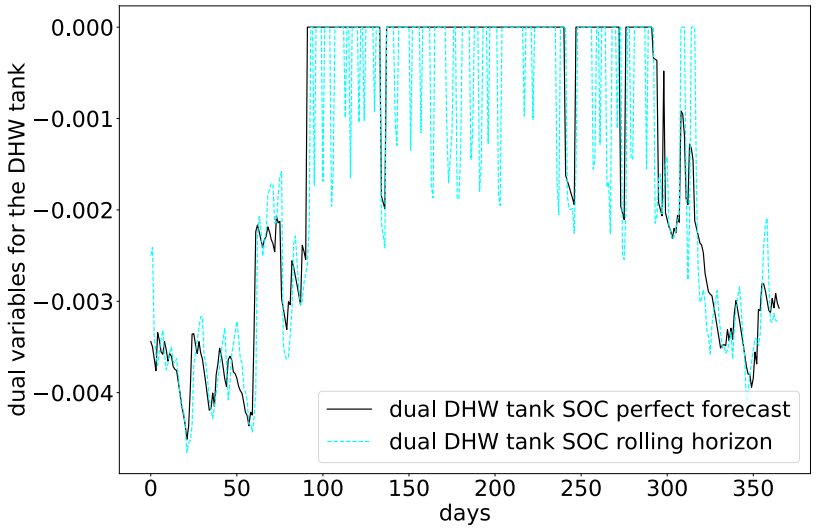

Figure A.19: Dual variables of the SOC for the DHW tank for House SFH 9 B.

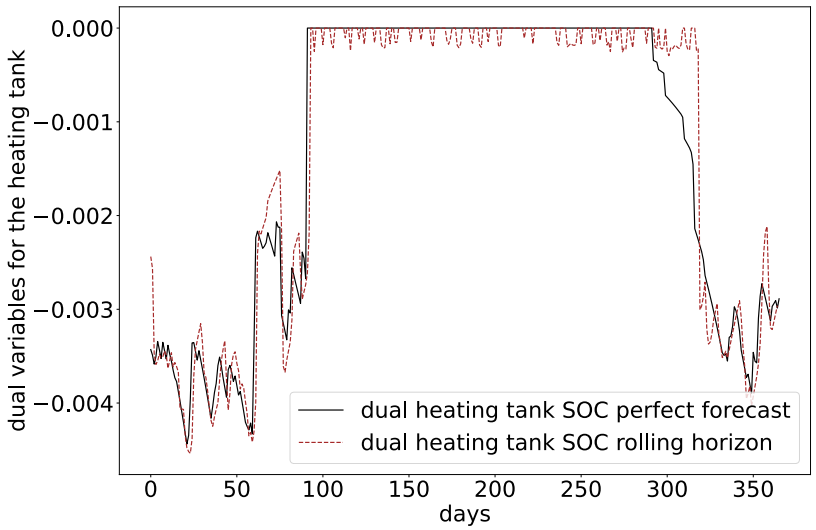

Figure A.20: Dual variables of the SOC for the heating tank for House SFH 9 B.

both Figures A.21 and A.22, a third analysis for the 3-day rolling horizon is shown, where the price for all 3 days is perfectly forecasted. This results in slightly better operation cost savings (Figure A.22), but for the sake of estimating the potential of DR, using the same day-ahead price for the next 3 days can provide a good approximation (see Figure A.21).

The previous analysis used the day-ahead price in 2019 in Austria. This begs the question of whether different prices will affect this approach, for example, if prices change drastically from one day to another, as we saw when gas prices spiked in 2021 and 2022. The impact of more volatile prices on the operation cost savings is shown in Figure A.23. In 2021, electricity prices in Austria spiked at the end of the year, and 2022 showed more volatile prices than any previous year. With more volatile prices, the optimization can increase the relative cost reduction while having a more accurate price forecast over the next 3 days instead of one, increasing the possible operation cost reduction significantly for higher volatile prices. In this figure, it is also clearly visible that the rolling horizon approach performs better if the storage is not modeled with terminal costs. This indicates that calculating the terminal costs through the shadow variables of the previous day is not a suitable method for storage that can be easily charged and discharged within the horizon window. As mentioned before, the terminal costs are often overestimated due to the PV generation, which skews the mean dual variable. Also, the different dual variables of the storage are impacted by the SOC of the other storage, which might be completely different from the day before. The volatility of the prices did not impact the performance of the different rolling horizon methods on the shifted energy. With higher price volatility, more electricity was shifted uniformly. The ratios between each method and the perfect forecast remained the same.

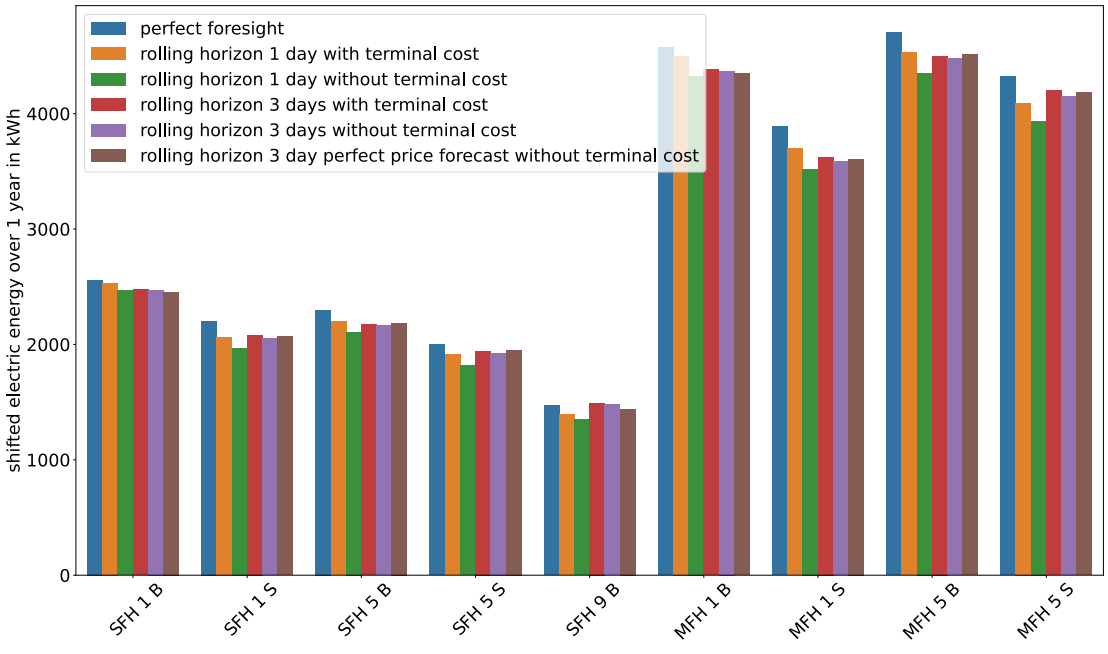

Figure A.21: Shifted energy throughout the whole year with different optimization methods for all buildings. Buildings are equipped with PV, a DHW tank, a buffer tank, and a stationary battery.

The analysis has shown that the potential to shift electricity in different buildings is not unrealistic when estimated using a perfect foresight approach. On the other hand, cost savings for single buildings can only be lower when using the rolling horizon approach. When implementing a rolling horizon approach to optimize the HP operation of a building,

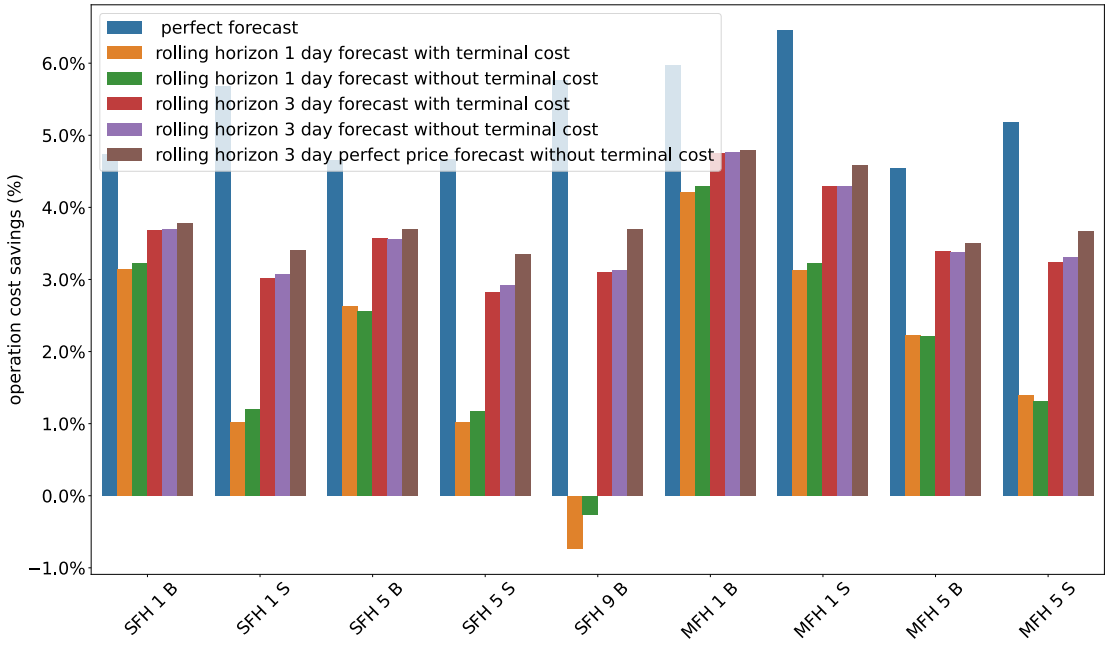

Figure A.22: Relative decrease in cost comparison for the buildings equipped with PV, Battery, DHW, and heating tank.

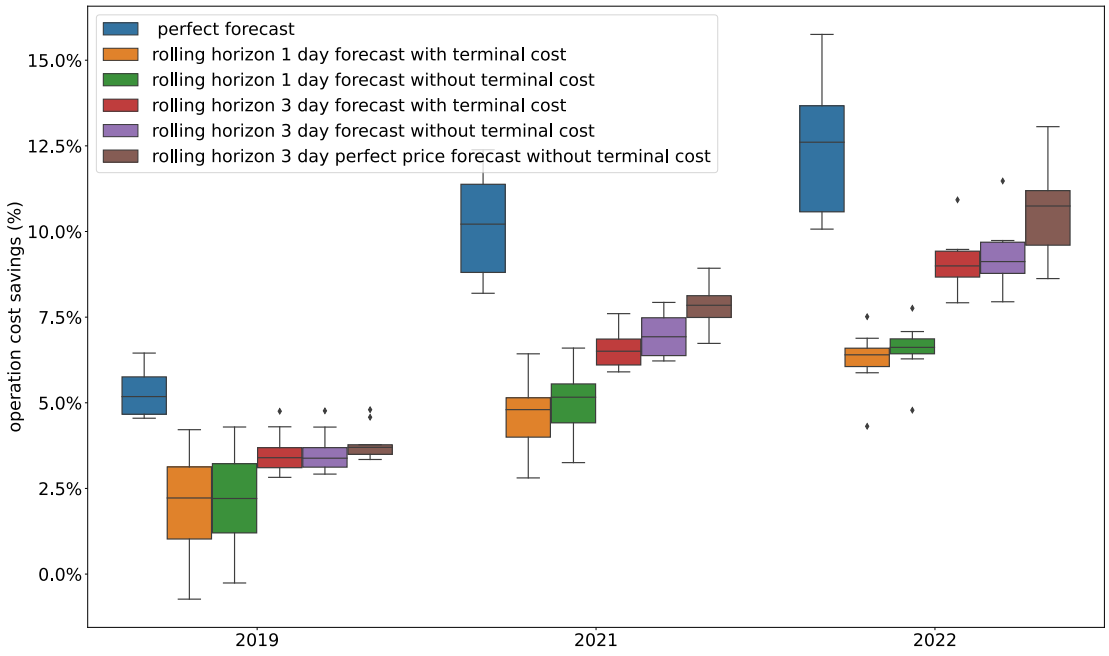

Figure A.23: Relative decrease in cost comparison for the buildings equipped with PV, Battery, DHW, and heating tank for 2019, 2021, and 2022.

the terminal cost for the building's thermal mass has to be considered to achieve better results. At the same time, the presented methodology for estimating the terminal cost of different storage appliances is not suitable if a building has multiple storage devices installed.

Table A.7: List of symbols used for the comparison between perfect forecast and rolling horizon

Character	Unit	Description
$\beta_{\text{heat demand}}$	-	binary variable stating if heat demand is greater than zero
Γ	EUR/K or EUR/kWh	terminal cost
ξ_{building}	EUR/K	dual variable of Equation 3.23
$\Delta T_{\text{building mass}}$	K	temperature difference

A.4 6R2C formulation

In this section of the appendix, the mathematical formulation of the 6R2C model is described. Figure A.24 shows the circuit representation of the 5R1C model with the extension of the floor heating node f, which is connected to the room temperature node via the resistance H_f. H_f describes the heat transfer rate between the floor heating and the indoor environment. C_f is connected to the node f and represents the thermal capacity of the floor heating system.

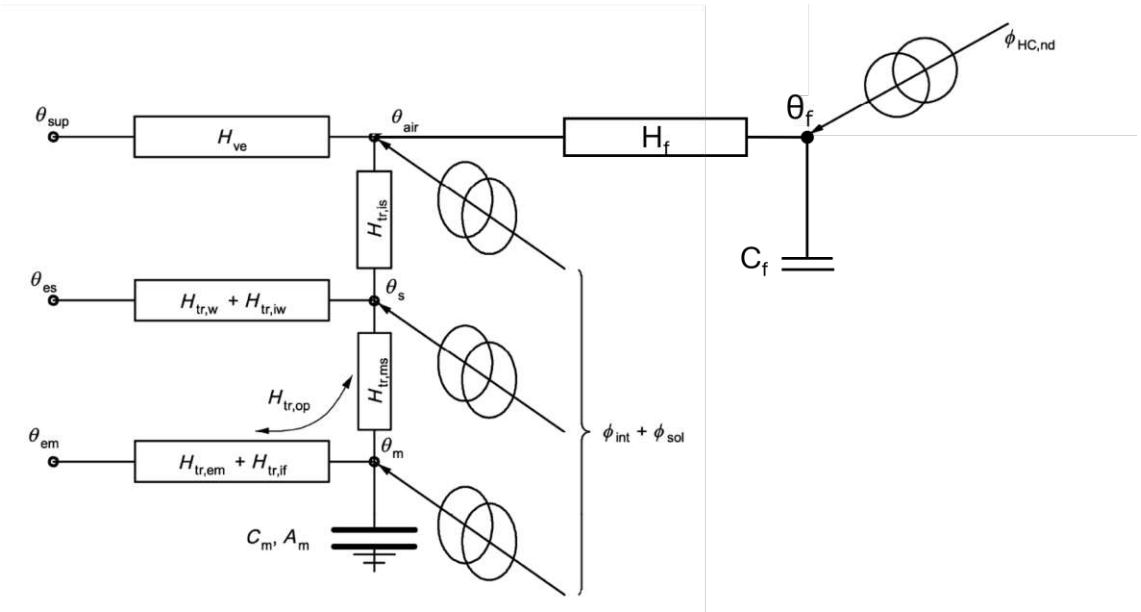

Figure A.24: 6R2C circuit representation

The 6R2C model is equivalent to the 5R1C model in its mathematical formulation for the nodes s and m. The indoor air temperature θ_{air} is calculated through:

$$\theta_{air} = \frac{\theta_s * H_{is} + H_{ve} * \theta_{outside} + \phi_{ia} + \theta_f * H_f}{H_{\text{is}} + H_{ve} + H_f} \tag{A.24}$$

The temperature of the added floor node is calculated with the following equation. The floor capacity is discretized using the Crank–Nicolson method.

$$\theta_{\text{floor, t}} = \frac{H_f * \theta_{air,t} + Q_{heating,t} + \theta_{\text{floor, t-1}} * (\frac{C_f}{3600} - 0.5 * H_f)}{\frac{C_f}{3600} + 0.5 * H_f} \tag{A.25}$$

The rest of the equations describing the heat flows in the nodes s and m are identical to the ones from the 5R1C model.

$$\theta_{m_{avg},t} = \frac{\theta_{m,t} + \theta_{m,t-1}}{2} \tag{A.26}$$

$$\phi_{st,t} = (1 - \frac{A_m}{A_t} - \frac{H_w}{9.1 \times A_t}) \times (0.5 \times \phi_{int} + \phi_{sol,t}) \tag{A.27}$$

$$\theta_{s,t} = \frac{\theta_{air,t} * H_{is} + \theta_{m_{avg},t} * H_{ms} + \theta_{outside,t} * H_w + \phi_{st,t}}{H_{is} + H_{ms} + H_w} \tag{A.28}$$

The Crank–Nicolson method is also used to discretize the equation describing the thermal mass temperature of the building, like in the DIN ISO 13790.

$$\phi_{m,t} = \frac{A_m}{A_{tot}} * (0.5 * \phi_{int} + \phi_{sol,t}) \tag{A.29}$$

$$\theta_{m,t} = \frac{\theta_{m,t-1} * (\frac{C_m}{3600} - 0.5 * (H_{ms} + H_{em})) + \phi_{m,t} + H_{ms} * \theta_{s,t} + H_{em} * \theta_{outside,t}}{\frac{C_m}{3600} + 0.5 * (H_{ms} + H_{em})} \tag{A.30}$$

A.5 Building specifics for assessing model accuracy with IDA ICE

SFH 5B	Material	Thickness [m]	Density [kg/m³]	Thermal conductivity [W/mK]	Thermal capacity [J/kgK]	Area [m²]
Ceiling	Cement screed	0.06	2000	1.33	1080	172.11
	Insulation	0.09782923	15.8	0.04	1450	172.11
	Bedding	0.05	1800	0.7	1000	172.11
	Normal reinforced concrete	0.18	2300	2.3	1000	172.11
	Standard plaster mortar	0.015	1500	0.67	1000	172.11
Wall	Standard plaster mortar	0.015	1500	0.67	1000	258.36
	Perforated bricks before 1980 + Standard brickwork mortar	0.59	800	0.42	1000	258.36
	Lightweight plaster mortar 900	0.04	900	0.27	1000	258.36
	Fine plaster mortar 1600	0.015	1600	0.78	1000	258.36
Floor	Wooden floors and parquet	0.02	675	0.16	1600	138.51
	Cement screed	0.06	2000	1.33	1080	138.51
	Footfall sound insulation 250	0.036	250	0.057	1700	138.51
	Bedding	0.05	1800	0.7	1000	138.51
	Standard reinforced concrete	0.18	2300	2.3	1000	138.51
Load- bearing interior walls	Standard plaster mortar 1500	0.025	1500	0.67	1000	129.18
	Perforated bricks before 1980 + Standard brickwork mortar	0.5	800	0.42	1000	129.18
	Standard plaster mortar 1500	0.015	1500	0.67	1000	129.18
Interior walls	Plasterboard	0.025	700	0.21	1000	129.18
	Timber	0.1	475	0.12	1600	129.18
	Plasterboard	0.025	700	0.21	1000	129.18
Interior ceiling	Coating	0.01	1300	0.19	1400	138.51
	Cement screed	0.05	2000	1.33	1080	138.51
	Standard reinforced concrete	0.14	2300	2.3	1000	138.51
	Standard plaster mortar 1500	0.015	1500	0.67	1000	138.51

SFH 5S	Material	Thickness [m]	Density kg/m^3	Thermal conductivity W/mK	Thermal capacity J/kgK	Area m^2
Ceiling	Rafter	0.12	475	0.12	1600	172.11
	Oriented Strand Board	0.02	650	0.13	1700	172.11
	Auxiliary layer	0.08	15.80	0.04	1450	172.11
	Timber	0.05	475	0.12	1600	172.11
	Plasterboard	0.02	700	0.21	1000	172.11
Wall	Standard plaster mortar	0.02	1500	0.67	1000	258.36
	Perforated brick before 1980 + standard masonry mortar	0.40	800	0.42	1000	258.36
	Lightweight plaster mortar	0.04	900	0.27	1000	258.36
	Fine plaster mortar	0.02	1600	0.78	1000	258.36
	Insulation	0.14	15.80	0.04	1450	258.36
	Fine plaster mortar	0.01	1500	0.67	1000	258.36
Floor	Wooden floors and parquet	0.01	675	0.16	1600	138.51
	Cement screed	0.06	2000	1.33	1080	138.51
	Footfall sound insulation	0.02	250	0.06	1700	138.51
	Bedding	0.05	1800	0.70	1000	138.51
	Standard reinforced concrete	0.18	2300	2.30	1000	138.51
	Insulation	0.03	15.80	0.04	1450	138.51
Load-bearing interior walls	Standard plaster mortar	0.03	1500	0.67	1000	129.18
	Perforated brick before 1980 + standard masonry mortar	0.50	800	0.42	1000	129.18
	Standard plaster mortar	0.02	1500	0.67	1000	129.18
Interior walls	Plasterboard	0.03	700	0.21	1000	129.18
	Timber	0.10	475	0.12	1600	129.18
	Plasterboard	0.03	700	0.21	1000	129.18
Interior Ceiling	Coating	0.01	1300	0.19	1400	138.51
	Cement screed	0.05	2000	1.33	1080	138.51
	Standard reinforced concrete	0.14	2300	2.30	1000	138.51
	Standard plaster mortar	0.02	1500	0.67	1000	138.51

SFH 9B	Material	Thickness [m]	Density [kg/m^3]	Thermal conductivity [W/mK]	Thermal capacity [J/kgK]	Area [m^2]
Ceiling	Rafter	0.16	475	0.12	1600	162.15
	Oriented Strand Board	0.02	650	0.13	1700	162.15
	Auxiliary layer	0.09	15.80	0.04	1450	162.15
	Timber	0.05	475	0.12	1600	162.15
	Plasterboard	0.02	700	0.21	1000	162.15
Wall	Standard plaster mortar	0.02	1400	0.57	1000	229.74
	Perforated brick	0.30	675	0.23	1000	229.74
	Insulation	0.21	15.80	0.04	1450	229.74
	Fine plaster mortar	0.01	1500	0.67	1000	229.74
Floor	Wooden floors and parquet	0.01	675	0.16	1600	124.42
	Cement screed	0.06	2000	1.33	1080	124.42
	Insulation	0.21	15.80	0.04	1450	124.42
	Standard reinforced concrete	0.15	2300	2.30	1000	124.42
Load-bearing interior walls	Standard plaster mortar	0.03	1500	0.67	1000	114.87
	Perforated brick	0.50	575	0.09	1000	114.87
	Standard plaster mortar	0.02	1500	0.67	1000	114.87
Interior walls	Plasterboard	0.03	700	0.21	1000	114.87
	Timber	0.10	475	0.12	1600	114.87
	Plasterboard	0.03	700	0.21	1000	114.87
Interior Ceiling	Coating	0.01	1300	0.19	1400	124.42
	Cement screed	0.05	2000	1.33	1080	124.42
	Standard reinforced concrete	0.14	2300	2.30	1000	124.42
	Standard plaster mortar	0.02	1500	0.67	1000	124.42

SFH 1B	Material	Thickness [m]	Density [kg/m^3]	Thermal conductivity [W/mK]	Thermal capacity [J/kgK]	Area [m^2]
Ceiling	Clay brick(Coating)	0.04	2000	1	800	167.64
	Auxiliary layer	0.05	15.80	0.04	1450	167.64
	Bedding	0.06	1800	0.70	1000	167.64
	Timber	0.20	700	0.18	1600	167.64
	Standard plaster mortar on plaster base	0.03	1800	1.05	1000	167.64
Wall	Standard plaster mortar	0.03	1800	1.05	1000	261.25
	Bricks + standard masonry mortar	0.62	2100	0.87	1000	261.25
	Standard plaster mortar	0.04	1800	1.05	1000	261.25
Floor	Wooden floors and parquet	0.03	675	0.16	1600	128.99
	BlindFloor	0.03	700	0.18	1600	128.99
	Timber	0.05	700	0.18	1600	128.99
	Bedding	0.10	1800	0.70	1000	128.99
	Auxiliary layer	0.02	15.80	0.04	1450	128.99
Load-bearing interior walls	Standard plaster mortar	0.03	1500	0.67	1000	130.63
	Bricks + standard masonry mortar	0.74	2200	0.90	1000	130.63
	Standard plaster mortar	0.02	1500	0.67	1000	130.63
Interior walls	Standard plaster mortar	0.02	1500	0.67	1000	130.63
	Bricks + standard masonry mortar	0.14	2200	0.90	1000	130.63
	Standard plaster mortar	0.02	1500	0.67	1000	130.63
Interior Ceiling	Wooden floors and parquet	0.03	675	0.16	1600	257.99
	Subfloor	0.03	700	0.18	1600	257.99
	Bedding	0.08	1800	0.70	1000	257.99
	Wooden formwork	0.03	475	0.12	1600	257.99
	Timber	0.20	700	0.18	1600	257.99
	Wooden formwork	0.02	475	0.12	1600	257.99
	Standard plaster mortar	0.03	1500	0.67	1000	257.99

SFH 1S	Material	Thickness [m]	Density [kg/m^3]	Thermal conductivity [W/mK]	Thermal capacity [J/kgK]	Area [m^2]
Ceiling	Rafter	0.12	475	0.12	1600	167.64
	Oriented Strand Board	0.02	650	0.13	1700	167.64
	Auxiliary layer	0.10	15.80	0.04	1450	167.64
	Timber	0.05	475	0.12	1600	167.64
	Plasterboard	0.02	700	0.21	1000	167.64
Wall	Standard plaster mortar	0.03	1800	1.05	1000	261.25
	Bricks + standard masonry mortar	0.44	2100	0.87	1000	261.25
	Standard plaster mortar	0.04	1800	1.05	1000	261.25
	Insulation	0.04	15.80	0.04	1450	261.25
	Fine plaster mortar	0.01	1500	0.67	1000	261.25
Floor	Wooden floors and parquet	0.01	675	0.16	1600	128.99
	Cement screed	0.06	2000	1.33	1080	128.99
	Insulation	0.07	15.80	0.04	1450	128.99
	Standard reinforced concrete	0.15	2300	2.30	1000	128.99
Load-bearing interior walls	Standard plaster mortar	0.03	1500	0.67	1000	130.63
	Bricks + standard masonry mortar	0.74	2200	0.90	1000	130.63
	Standard plaster mortar	0.02	1500	0.67	1000	130.63
Interior walls	Standard plaster mortar	0.02	1500	0.67	1000	130.63
	Bricks + standard masonry mortar	0.14	2200	0.90	1000	130.63
	Standard plaster mortar	0.02	1500	0.67	1000	130.63
Interior Ceiling	Wooden floors and parquet	0.03	675	0.16	1600	257.99
	BlindFloor	0.03	700	0.18	1600	257.99
	Bedding	0.08	1800	0.70	1000	257.99
	Wooden formwork	0.03	475	0.12	1600	257.99
	Timber	0.20	700	0.18	1600	257.99
	Wooden formwork	0.02	475	0.12	1600	257.99
	Standard plaster mortar	0.03	1500	0.67	1000	257.99

MFH 5B	Material	Thickness [m]	Density [kg/m³]	Thermal conductivity [W/mK]	Thermal capacity [J/kgK]	Area [m²]
Ceiling roof	Cement screed	0.06	2000	1.33	1080	302.11
	Insulation	0.10	15.80	0.04	1450	302.11
	Bedding	0.05	1800	0.70	1000	302.11
	Standard reinforced concrete	0.18	2300	2.30	1000	302.11
	Standard plaster mortar	0.02	1500	0.67	1000	302.11
Wall outside	Standard plaster mortar	0.02	1500	0.67	1000	432.51
	Perforated brick vor 1980 + standard masonry mortar	0.60	1200	0.50	1000	432.51
	Lightweight plaster mortar	0.04	900	0.27	1000	432.51
	Fine plaster mortar	0.02	1600	0.78	1000	432.51
Floor ground	Wooden floors and parquet	0.02	675	0.16	1600	228.78
	Cement screed	0.06	2000	1.33	1080	228.78
	Footfall sound insulation	0.04	250	0.06	1700	228.78
	Bedding	0.05	1800	0.70	1000	228.78
	Standard reinforced concrete	0.18	2300	2.30	1000	228.78
Load-bearing interior walls	Standard plaster mortar	0.03	1500	0.67	1000	216.26
	Perforated brick before 1980 + standard masonry mortar	0.50	800	0.42	1000	216.26
	Standard plaster mortar	0.02	1500	0.67	1000	216.26
Interior walls	Plasterboard	0.03	700	0.21	1000	216.26
	Timber	0.10	475	0.12	1600	216.26
	Plasterboard	0.03	700	0.21	1000	216.26
Interior Ceiling	Coating	0.01	1300	0.19	1400	457.57
	Cement screed	0.05	2000	1.33	1080	457.57
	Standard reinforced concrete	0.14	2300	2.30	1000	457.57
	Standard plaster mortar	0.02	1500	0.67	1000	457.57

MFH 5S	Material	Thickness [m]	Density [kg/m^3]	Thermal conductivity [W/mK]	Thermal capacity [J/kgK]	Area [m^2]
Ceiling roof	Insulation	0.18	15.80	0.04	1450	302.11
	Cement screed	0.06	2000	1.33	1080	302.11
	Footfall sound insulation	0.02	250	0.06	1700	302.11
	Bedding	0.05	1800	0.70	1000	302.11
	Standard reinforced concrete	0.18	2300	2.30	1000	302.11
	Standard plaster mortar	0.02	1500	0.67	1000	302.11
Wall outside	Standard plaster mortar	0.02	1500	0.67	1000	432.51
	Perforated brick vor 1980 + Normalmauermörtel (MFH)	0.44	1200	0.50	1000	432.51
	Lightweight plaster mortar	0.04	900	0.27	1000	432.51
	Fine plaster mortar	0.02	1600	0.78	1000	432.51
	Insulation	0.09	15.80	0.04	1450	432.51
	Fine plaster mortar	0.01	1500	0.67	1000	432.51
Floor	Wooden floors and parquet	0.01	675	0.16	1600	228.78
	Cement screed	0.06	2000	1.33	1080	228.78
	Footfall sound insulation	0.02	250	0.06	1700	228.78
	Bedding	0.05	1800	0.70	1000	228.78
	Standard reinforced concrete	0.18	2300	2.30	1000	228.78
	Insulation	0.03	15.80	0.04	1450	228.78
Load-bearing interior walls	Standard plaster mortar	0.03	1500	0.67	1000	216.26
	Perforated brick before 1980 + standard masonry mortar	0.50	800	0.42	1000	216.26
	Standard plaster mortar	0.02	1500	0.67	1000	216.26
Interior walls	Plasterboard	0.03	700	0.21	1000	216.26
	Timber	0.10	475	0.12	1600	216.26
	Plasterboard	0.03	700	0.21	1000	216.26
Interior Ceiling	Coating	0.01	1300	0.19	1400	457.57
	Cement screed	0.05	2000	1.33	1080	457.57
	Standard reinforced concrete	0.14	2300	2.30	1000	457.57
	Standard plaster mortar	0.02	1500	0.67	1000	457.57

MFH 1B	Material	Thickness [m]	Density [kg/m^3]	Thermal conductivity [W/mK]	Thermal capacity [J/kgK]	Area [m^2]
Ceiling	Clay brick (coating)	0.04	2000	1	800	272.59
	Auxiliary layer	0.05	15.80	0.04	1450	272.59
	Bedding	0.06	1800	0.70	1000	272.59
	Timber	0.20	700	0.18	1600	272.59
	Standard plaster mortar on plaster base	0.03	1800	1.05	1000	272.59
Wall	Standard plaster mortar	0.03	1800	1.05	1000	404.83
	Bricks + standard masonry mortar	0.62	2100	0.87	1000	404.83
	Standard plaster mortar	0.04	1800	1.05	1000	404.83
Floor	Wooden floors and parquet	0.03	675	0.16	1600	204.46
	BlindFloor	0.03	700	0.18	1600	204.46
	Timber	0.05	700	0.18	1600	204.46
	Bedding	0.10	1800	0.70	1000	204.46
	Auxiliary layer	0.02	15.80	0.04	1450	204.46
Load-bearing interior walls	Standard plaster mortar	0.03	1500	0.67	1000	202.42
	Bricks + standard masonry mortar	0.74	2200	0.90	1000	202.42
	Standard plaster mortar	0.02	1500	0.67	1000	202.42
Interior walls	Standard plaster mortar	0.02	1500	0.67	1000	202.42
	Bricks + standard masonry mortar	0.14	2200	0.90	1000	202.42
	Standard plaster mortar	0.02	1500	0.67	1000	202.42
Interior Ceiling	Wooden floors and parquet	0.03	675	0.16	1600	408.92
	BlindFloor	0.03	700	0.18	1600	408.92
	Bedding	0.08	1800	0.70	1000	408.92
	Wooden formwork	0.03	475	0.12	1600	408.92
	Timber	0.20	700	0.18	1600	408.92
	Wooden formwork	0.02	475	0.12	1600	408.92
	Standard plaster mortar	0.03	1500	0.67	1000	408.92

MFH 1S	Material	Thickness [m]	Density [kg/m^3]	Thermal conductivity [W/mK]	Thermal capacity [J/kgK]	Area [m^2]
Ceiling	Rafter	0.12	475	0.12	1600	272.59
	Oriented Strand Board	0.02	650	0.13	1700	272.59
	Auxiliary layer	0.10	15.80	0.04	1450	272.59
	Timber	0.05	475	0.12	1600	272.59
	Plasterboard	0.02	700	0.21	1000	272.59
Wall	Standard plaster mortar	0.03	1800	1.05	1000	404.83
	Bricks + standard masonry mortar	0.44	2100	0.87	1000	404.83
	Standard plaster mortar	0.04	1800	1.05	1000	404.83
	Insulation	0.04	15.80	0.04	1450	404.83
	Fine plaster mortar	0.01	1500	0.67	1000	404.83
Floor	Wooden floors and parquet	0.01	675	0.16	1600	204.46
	Cement screed	0.06	2000	1.33	1080	204.46
	Insulation	0.07	15.80	0.04	1450	204.46
	Standard reinforced concrete	0.15	2300	2.30	1000	204.46
Load-bearing interior walls	Standard plaster mortar	0.03	1500	0.67	1000	202.42
	Bricks + standard masonry mortar	0.74	2200	0.90	1000	202.42
	Standard plaster mortar	0.02	1500	0.67	1000	202.42
Interior walls	Standard plaster mortar	0.02	1500	0.67	1000	202.42
	Bricks + standard masonry mortar	0.14	2200	0.90	1000	202.42
	Standard plaster mortar	0.02	1500	0.67	1000	202.42
Interior Ceiling	Wooden floors and parquet	0.03	675	0.16	1600	408.92
	BlindFloor	0.03	700	0.18	1600	408.92
	Bedding	0.08	1800	0.70	1000	408.92
	Wooden formwork	0.03	475	0.12	1600	408.92
	Timber	0.20	700	0.18	1600	408.92
	Wooden formwork	0.02	475	0.12	1600	408.92
	Standard plaster mortar	0.03	1500	0.67	1000	408.92